

Biochemical, Structural and Functional  
Characterization of Diheme-Containing  
Quinol:Fumarate Reductases:  
the Role of Heme Propionates and  
the Enzymes from Pathogenic  $\epsilon$ -Proteobacteria

Dissertation  
zur Erlangung des Doktorgrades  
der Naturwissenschaften

Vorgelegt beim Fachbereich 14  
Chemische und Pharmazeutische Wissenschaften  
der Johann Wolfgang Goethe-Universität  
in Frankfurt am Main

von  
**Mauro Mileni**  
aus Corridonia (Italien)

Frankfurt am Main, 2005

(DF1)

vom Fachbereich Chemische und Pharmazeutische Wissenschaften der Johann  
Wolfgang Goethe-Universität als Dissertation angenommen.

Dekan: Prof. Dr. Harald Schwalbe

1. Gutachter: Prof. Dr. Bernd Ludwig

2. Gutachter: PD Dr. C. Roy D. Lancaster

Datum der Disputation: 1. August 2005

## Manuscripts to be published:

**Mauro Mileni, Fraser MacMillan, Christos Tziatzios, Klaus Zwicker, Alexander H. Haas, Werner Mäntele, Jörg Simon, and C. Roy D. Lancaster. (2005)** Heterologous production in *Wolinella succinogenes* and characterization of the quinol:fumarate reductases from *Helicobacter pylori* and *Campylobacter jejuni*. *Manuscript submitted.*

**Mauro Mileni, Alexander H. Haas, Werner Mäntele, Jörg Simon, and C. Roy D. Lancaster. (2005)** Probing heme propionate involvement in transmembrane proton transfer coupled to electron transfer in dihemic quinol:fumarate reductase by  $^{13}\text{C}$ -labeling and FTIR difference spectroscopy. *Manuscript submitted.*

**Mauro Mileni & C. Roy D. Lancaster.** The 3D-crystal structure of the quinol:fumarate reductase from the pathogenic  $\epsilon$ -proteobacterium *C. jejuni*. *Manuscript in preparation.*

**Mauro Mileni, Fraser MacMillan, C. Roy D. Lancaster.** Quinol:fumarate reductases from  $\epsilon$ -proteobacteria, new mechanistic insights from biophysical data. *Manuscript in preparation.*

# Ausführliche deutschsprachige Zusammenfassung

Die Chinol:Fumarat Reduktase (QFR) ist die terminale Reduktase der anaeroben Fumarat-Atmung, welche die häufigste Art der anaeroben Atmung darstellt. Dieser Membranprotein-komplex koppelt die Oxidation von Menachinon zu Menachinol an die Reduktion von Fumarat zu Succinat. Die dreidimensionale Kristallstruktur der QFR von *Wolinella succinogenes* wurde zuvor mit einer Auflösung von 2,2 Å gelöst.

Obwohl die dihä-m-haltige QFR von *W. succinogenes* erwiesenermaßen einen elektroneutralen Prozeß katalysiert, hat die strukturelle und funktionelle Charakterisierung des Wild-Typ-Enzyms und verschiedener Enzymvarianten ergeben, dass die Lage der aktiven Zentren auf einen über die Membran elektrogenen katalytischen Prozeß hindeutet. Der scheinbare Widerspruch konnte durch die sogenannte „E-Weg“ Hypothese überwunden werden. Sie besagt, dass der transmembrane Elektronentransfer über die Hämgruppen strikt an einen parallelen, die Ladung kompensierenden Protonentransfer gekoppelt ist, Dieser erfolgt über einen im reduzierten Zustand vorübergehend aktiven Transportweg, der im oxidierten Zustand des Enzyms blockiert ist. Als wesentliche Bestandteile dieses „E-Weges“ werden die Seitenkette von Glu C180 und das Ring-C Propionat der distalen Hämgruppe angenommen. Frühere experimentelle Ergebnisse weisen deutlich auf eine Beteiligung von Glu C180 hin. Ein Ziel der vorliegenden Arbeit war es, mit Hilfe einer Kombination aus <sup>13</sup>C-Isotopenmarkierung der Hämpropionate der QFR und anschließender FTIR-Differenzspektroskopie experimentell nachzuweisen, dass dem Ring-C Propionat der distalen Hämgruppe eine entsprechende Rolle im redox-gekoppelten Protonentransfer in der QFR von *W. succinogenes* zukommt.

Zusätzlich zu *W. succinogenes* sind auch die Primärstrukturen zweier weiterer ε-Proteobakterien, nämlich *Campylobacter jejuni* und *Helicobacter pylori*, bekannt. Beide Spezies sind im Gegensatz zu *W. succinogenes* humanpathogen und in der Lage, Schleimhäute zu kolonisieren und verschiedene Krankheiten auszulösen. Die QFR von *H. pylori* wurde schon früher als potentieller Angriffspunkt für eine medikamentöse Behandlung identifiziert. Gleiches ist auch für die QFR von *C. jejuni* wahrscheinlich. Die Möglichkeit, die beiden Chinol:Fumarat Reduktasen der genannten Bakterien zu studieren und somit möglicherweise effizientere Medikamente gegen sie zu entwickeln, hängt empfindlich davon ab, über größere Mengen qualitativ hochwertiger Proteinsubstanz zu verfügen. Weiterhin können die biochemische und strukturelle Untersuchung der QFR Enzyme anderer ε-

Proteobakterien als *W. succinogenes* hilfreich sein, neue Aspekte dieser Klasse von Membranproteinen zu beleuchten und deren allgemeines Verständnis zu vertiefen.

- 1. Heterologe Expression in *W. succinogenes*.** In dieser Arbeit wird zum ersten Mal die erfolgreiche Überproduktion von Membranproteinen in dem anaeroben Bakterium *W. succinogenes* in großem Maßstab vorgestellt. Da sich die homologe Produktion von QFR aus *C. jejuni* und *H. pylori* bis dato nur durch geringe Mengen kaum aktiven und unreinen Enzyms auszeichnete, wurde eine Methode der heterologen Produktion in *W. succinogenes* entwickelt. Zu diesem Zweck wurde das vollständige *frdCAB* Operon das die drei Untereinheiten der Chinol:Fumarat Reduktase codiert, in das Genom einer Deletionsmutante  $\Delta$ *frdCAB* von *W. succinogenes* eingefügt. Im Genom dieser Mutante wurde vorher der komplette Abschnitt, der *frdCAB* codiert, entfernt, was zu einem vollständigen Verlust der Fähigkeit der Zellen zur Fumarat-Atmung führte. Der Austausch der Gene von *W. succinogenes* durch das heterologe Gen-Cluster ergab Mutanten, die in vollem Umfang zur Fumarat-Atmung fähig waren. Die QFR der  $\epsilon$ -Proteobakterien ist eine Succinat:Chinon Oxidoreduktase (SQOR) des Typs B, welche aus drei Untereinheiten besteht: Einer hydrophoben Untereinheit (FrdC), die zwei Häm *b* Gruppen enthält, einer großen hydrophilen Untereinheit (FrdA), die ein Flavinadenindinukleotid (FAD) als prosthetische Gruppe bindet, und einer kleineren hydrophilen Untereinheit (FrdB), welche die Eisen-Schwefel-Zentren [2Fe-2S], [4Fe-4S] und [3Fe-4S] umfasst. Es konnte gezeigt werden, dass alle diese Kofaktoren korrekt in die beiden heterolog produzierten Proteine eingebaut wurden. Dank dieses neuen heterologen Expressionssystems, konnten die *frdCAB* Operons der beiden pathogenen Spezies *C. jejuni* und *H. pylori* kloniert und exprimiert werden, so dass die korrespondierenden Enzyme isoliert und charakterisiert werden konnten.
- 2. Reinigung der QFR von *H. pylori* und *C. jejuni*.** Um die QFR der beiden pathogenen Spezies zu untersuchen, sind große Mengen stabilen, reinen und aktiven Enzyms erforderlich. Eine solche Verfügbarkeit würde eine Charakterisierung und Kristallisation der beiden Enzyme im Hinblick auf Röntgenbeugungsexperimente ermöglichen. Im Vergleich zu früher publizierten Reinigungsprozeduren, wie sie für die Isolierung der *W. succinogenes* QFR etabliert wurden, und die im Wesentlichen aus Anionenaustausch-Chromatographie und isoelektrischer Fokussierung bestanden, erlaubte es die Hinzufügung einer Gel-Filtration als Reinigungsschritt

eine Proteinverunreinigung mit der ungefähren Größe von 55-60 kDa zu eliminieren. Die relativ einfache Handhabung von *W. succinogenes* und der hohe Ertrag der Proteinexpression ermöglichten es, nach dem letzten Reinigungsschritt bis zu 100 mg *C. jejuni* QFR und bis zu 150 mg *H. pylori* QFR je Proteinpräparation zu erhalten. Dennoch war im Falle der *H. pylori* QFR nach erfolgter Gelfiltration eine drastische Abnahme wenn diese durch Verfolgung der Oxidation von DMNH<sub>2</sub> durch Fumarat gemessen wurde Enzymaktivität zu verzeichnen. Daher wurden verschiedene Methoden zur Bestimmung von an die *H. pylori* QFR gebundenen Phospholipide herangezogen, die schließlich die Präsenz von Cardiolipin während der Reinigung enthüllten. Durch die Zugabe dieses Lipids konnte die enzymatische Aktivität der QFR vollständig wiederhergestellt werden. Desweiteren verbesserte die Zugabe von Cardiolipin auch die Kristallisationseigenschaften des Enzyms. Verschiedene biochemische Analysen, wie z. B. SDS-PAGE und Messungen der enzymatischen Aktivität, zeigten, dass sich die durchgeführten Proteinpräparationen durch hohe Reinheit und Homogenität auszeichnen. Der abschließende Beweis für den Erfolg des entwickelten heterologen Systems zur Proteinüberproduktion war dadurch gegeben, dass es möglich war, gut beugende dreidimensionale Proteinkristalle zu erhalten. Die Kristalle der *H. pylori* QFR beugten bis zu einer Auflösung von 8 Å und *C. jejuni* QFR Kristalle bis zu 3,1 Å.

- 3. Ausführliche Enzymcharakterisierung und Kristallisation der heterolog produzierten QFRs.** Die hohe Qualität der Präparation ermöglichte eine vollständige Charakterisierung der beiden Membranproteinkomplexe mit: i) akkurater Bestimmung der Oxidations/Reduktions-Mittelpunktpotentiale aller sechs Kofaktoren mit Hilfe von EPR-Spektroskopie und UV/VIS-Spektroskopie; ii) Bestimmung der Elektronentransportkettenaktivitäten (ETC) der beiden QFR Enzyme in Membranen gekoppelt an die Formiatdehydrogenase; iii) Berechnung der Michaelis-Konstanten und maximalen Aktivität in drei verschiedenen enzymatischen Tests; iv) Berechnung der Inhibierungskonstanten und -arten von Oxantel, Thiabendazol und Omeprazol, die zwar schon früher als QFR-Inhibitoren bekannt, jedoch kaum charakterisiert waren; v) endgültige und eindeutige Bestimmung des oligomeren Zustandes der QFR von *W. succinogenes*, *C. jejuni* und *H. pylori* mit Hilfe von analytischer Ultrazentrifugation, die bestätigte, dass die in Gegenwart von Detergenz gelösten Enzyme in einem physiologischen homodimeren Zustand

- vorliegen; vi) Identifizierung eines nativen Phospholipids das, wie früher erwähnt, mit dem Proteinkomplex zusammen gereinigt wird. Die verfeinerte Charakterisierung einiger der Eigenschaften der *W. succinogenes* QFR sowie die umfassende Charakterisierung der heterolog produzierten QFR Enzyme verbessert somit das Verständnis der physiologischen und funktionellen Eigenschaften dieser Enzymklasse.
4. **Bestimmung der dreidimensionalen Kristallstruktur der *C. jejuni* QFR.** Die 3D-Kristallstruktur der QFR der *C. jejuni* Spezies wurde mit einer Auflösung von 3,24 Å gelöst. Trotz der zufriedenstellenden Statistik der Datensammlung und der Verfeinerung des Strukturmodells konnten die Positionen einiger Aminosäuren nicht zugeordnet werden. Im Allgemeinen gab es einige Regionen, wie z. B. die Chinonbindungsstelle und die „Verschluß“-Domäne, die nur über eine schlecht definierte Elektronendichte verfügten und für welche daher kein Modell gebildet werden konnte. Dennoch erschienen andere Bereiche sehr deutlich, und die Struktur konnte in den meisten Regionen eindeutig zugeordnet werden. Obwohl sich die primärstrukturelle Identität der QFR von *W. succinogenes* und *C. jejuni* über alle drei Untereinheiten hinweg zwischen 50 % und 70 % bewegt, sind die Tertiärstrukturunterschiede nur unbedeutend.
  5. **Erzeugung einer *W. succinogenes* Mutante zur <sup>13</sup>C-Markierung der QFR Hämpropionate.** Anders als für Aminosäureseitenketten, deren Bedeutung mit ortsgerichteter Mutagenese untersucht werden kann, erfordert die Zuordnung von potentiellen Signalen, die von den Hämpropionaten ausgehen, eine andere Herangehensweise wie z. B. die selektive <sup>13</sup>C-Isotopenmarkierung der Carboxykohlenstoffpositionen der Hämpropionate. In *W. succinogenes* ist die Glutamat-1-Semialdehyd-2,1-Aminomutase (*hemL* Gen) verantwortlich für die Synthese des Hämgruppenvorläufers 5-Aminolävulinat. Die Deletion des *hemL* Gens aus dem *W. succinogenes* Genom resultierte in einer Mutante, die nur mit extern zur Verfügung gestelltem 5-Aminolävulinat wuchs. Des weiteren zeichnete sich die Mutante durch eine verzögerte Wachstumsphase aus und konnte nur nach Animpfen mit einem hochkonzentrierten Inokulum zum Wachstum gebracht werden. Die spezifische Markierung wurde durch die Erzeugung einer in Bezug auf den Hämgruppenvorläufer 5-Aminolävulinat auxotrophen *W. succinogenes* Mutante

( $\Delta hemL$ ) und durch externe Zugabe von  $[1-^{13}C]$ -5-Aminolevulinat zum Medium erreicht.

- 6. Produktion reiner *W. succinogenes* QFR mit  $^{13}C$ -markierten Hämpropionaten zur Charakterisierung durch FTIR-Differenzspektroskopie.** Die markierte QFR wurde mit Hilfe der bereits erwähnten *W. succinogenes* Mutante  $\Delta hemL$  produziert. Eine MALDI-TOF Analyse zeigte eindeutig, dass die  $^{13}C$ -Markierung der Hämgruppen dieser QFR vollständig war. Durch weitere biochemische Analysen wurden eventuell störende Unterschiede zwischen markierter und unmarkierter QFR ausgeschlossen. Da sich die Oxidations/Reduktions-Mittelpunktpotentiale der beiden Hämgruppen der QFR um fast 150 mV unterscheiden, war es möglich, die zugehörigen Signale eindeutig zu trennen, und die distale bzw. proximale Hämgruppe durch die Wahl geeigneter Referenzpotentiale im Experiment getrennt zu untersuchen. Die charakteristischen Beiträge deprotonierter Carboxylgruppen konnten im Infrarotspektrum nachgewiesen werden. Durch die  $^{13}C$ -Markierung wurde eine signifikante Verschiebung der Signale hin zu niedrigeren Wellenzahlen beobachtet. Diese FTIR-Ergebnisse konnten als (De)Protonierung, möglicherweise überlagert von einer Umgebungsänderung, mindestens einer der beiden Hämpropionate der distalen Hämgruppe interpretiert werden kann. Diese experimentelle Beobachtung steht in exzellentem Einklang mit der vorgeschlagenen „E-Weg“ Hypothese des gekoppelten transmembranen Elektronen- und Protonentransfers.



## Summary

The quinol:fumarate reductase (QFR) is the terminal reductase of anaerobic fumarate respiration, the most commonly occurring type of anaerobic respiration. This membrane protein complex couples the oxidation of menaquinol to menaquinone to the reduction of fumarate to succinate. The three-dimensional crystal structure of the QFR from *Wolinella succinogenes* has previously been solved at 2.2 Å resolution.

Although the diheme-containing QFR from *W. succinogenes* is known to catalyze an electroneutral process, structural and functional characterization of parental and variant enzymes has revealed active site locations which indicate electrogenic catalysis across the membrane. A solution to this apparent controversy was proposed with the so-called “E-pathway hypothesis”. According to this, transmembrane electron transfer via the heme groups is strictly coupled to a parallel, compensatory transfer of protons via a transiently established pathway, which is inactive in the oxidized state of the enzyme. Proposed constituents of the E-pathway are the side chain of Glu C180, and the ring C propionate of the distal heme. Previous experimental evidence strongly supports such a role for the former constituent. One aim of this thesis is to investigate by a combination of specific <sup>13</sup>C-heme propionate labeling and FTIR difference spectroscopy whether the ring C propionate of the distal heme is involved in redox-coupled proton transfer in the QFR from *W. succinogenes*.

In addition to *W. succinogenes*, the primary structures of the QFR enzymes of two other  $\epsilon$ -proteobacteria are known. These are *Campylobacter jejuni* and *Helicobacter pylori*, which unlike *W. succinogenes* are human pathogens. The QFR from *H. pylori* has previously been established to be a potential drug target, and the same is likely for the QFR from *C. jejuni*. The two pathogenic species colonize mucosal surfaces causing several diseases. The possibility of studying these QFRs from these bacteria and creating more efficient drugs specifically active for this enzyme depends substantially on the availability of large amounts of high-quality protein. Further, biochemical and structural studies on QFR enzymes from  $\epsilon$ -proteobacteria species other than *W. succinogenes* can be valuable to enlighten new aspects or corroborate the current understanding of this class of membrane proteins.

- 1. Heterologous expression in *W. succinogenes*.** In this thesis is presented, for the first time, a successful large-scale heterologous overproduction of membrane proteins in the anaerobic bacterium *W. succinogenes*. Since homologous production of the QFR from *C. jejuni* and *H. pylori* has so far only been characterized by low amounts of

scarcely pure and active enzymes, a heterologous (large-scale) production in *W. succinogenes* has been developed. To this end, the respective intact *frdCAB* operons were restored in the genome of the deletion mutant *W. succinogenes*  $\Delta$ *frdCAB*. In the genome of this mutant, the complete *frdCAB*-coding region had been deleted, resulting in the inability of the cells to grow by fumarate respiration. The replacement of the homologous enzyme from *W. succinogenes* with the heterologous enzymes yielded mutants where fumarate respiration was still fully functional. The QFR from  $\epsilon$ -proteobacteria is a B-type succinate:quinone oxidoreductase (SQOR) that is made of one hydrophobic subunit (FrdC), which contains two heme *b* groups; a large hydrophilic subunit (FrdA), which binds a flavin adenosine dinucleotide (FAD) prosthetic group; and a smaller hydrophilic subunit (FrdB), which contains the iron-sulfur clusters [2Fe-2S], [4Fe-4S], and [3Fe-4S]. It was demonstrated that all of these cofactors were correctly inserted in the two heterologously produced proteins. Thanks to this novel heterologous expression system, the *frdCAB* operons from the pathogen species *C. jejuni* and *H. pylori* were cloned and expressed under safe laboratory conditions, so that the corresponding enzymes could be isolated and characterized.

- 2. Large-scale purification of QFR from *H. pylori* and *C. jejuni*.** In order to study the QFR from these two pathogens, large amounts of stable, pure and active enzymes are required. This achievement would allow the characterization and crystallization of these two enzymes for X-ray diffraction experiments. In comparison to previously published purification procedures established for the isolation of the *W. succinogenes* QFR, which consisted of an anion exchange chromatography and isoelectric focusing, the addition of a gel filtration purification step permitted the discarding of a contaminant protein of approximately 55-60 kDa. The relative simplicity of working with *W. succinogenes* and its high yield of expression enabled to obtain, at the final stage of purification, up to 100 mg of *C. jejuni* QFR and 150 mg of *H. pylori* QFR per protein preparation. However, when the *H. pylori* QFR sample was subjected to gel filtration, the total QFR enzymatic activity, as measured by the DMNH<sub>2</sub>-to-fumarate assay, decreased drastically. For this reason, several methods were adopted for the identification of phospholipids bound to the *H. pylori* QFR complex, and revealed the loss of cardiolipin during this purification step. Strikingly, addition of this lipid allowed full recovery of the enzymatic activity of the enzyme. Moreover, addition of

cardiolipin improved the crystallization properties of the enzyme. Several biochemical analyses performed on the purified samples, like for instance SDS-PAGE and enzymatic activity, have demonstrated that these protein preparations are characterized by a high purity and a high homogeneity. The final evidence of the success of the established heterologous overproduction system is that these enzyme preparations supported the formation of well-diffracting 3D crystals. The *H. pylori* QFR crystals diffracted up to 8 Å, whereas the *C. jejuni* QFR crystals diffracted up to 3.1 Å.

- 3. Extensive enzyme characterization and crystallization of the heterologously produced QFRs.** The high quality of the preparation permitted to fully characterize these two membrane protein complexes with: i) accurate determination of the midpoint potential of all the six cofactors by EPR spectroscopy and UV/VIS-spectroscopy; ii) determination of the electron transport chain (ETC) activities of the two QFRs coupled to formate dehydrogenase in membranes; iii) calculation of the Michaelis constants and maximal activity by three different enzymatic assays; iv) calculation of the inhibition constants and types of inhibition of oxantel, thiabendazole, and omeprazole, which were previously reported as QFR-inhibitors but poorly characterized; v) final and unambiguous assignment of the oligomeric state of the QFR from *W. succinogenes*, *C. jejuni*, and *H. pylori* by analytical ultracentrifugation, which has ascertained that these detergent-solubilized enzymes are in a physiological homodimeric state; vi) identification of the native phospholipids that are co-purifying with the *H. pylori* complex (as mentioned previously). The improved characterization of some of the properties of *W. succinogenes* QFR, and the full characterization of the heterologously produced QFRs provides a better understanding of the physiological and functional properties of this class of enzymes.
- 4. Determination of the *C. jejuni* QFR three-dimensional crystal structure.** The 3D crystal structure of the QFR from the *C. jejuni* species was solved at the resolution of 3.24Å. In spite of reasonable statistics for data collection and refinement, such as low values of crystal mosaicity (0.09),  $R_{\text{sym}}$  (8.2 %) and  $R_{\text{free}}$  (25.8 %), some amino acid positions could not be assigned. In general, some important regions of the electron density maps, such as the quinone binding site and part of the capping domain, were poorly defined and model building was prevented. However, other areas of the maps

appeared very clearly defined, and the structure was unambiguously assigned in most parts of the protein. Interestingly, although the primary structure identity of the QFR from *W. succinogenes* and *C. jejuni* ranges from 50% to 70% amongst the three subunits, differences between the two quaternary structures are only minor. In other words, although slight differences between the two species cannot be ruled out at the present stage of analysis, the positions and the orientations of the cofactors, as well as numerous other features, appear to be conserved.

5. **Creation of a *W. succinogenes* mutant for  $^{13}\text{C}$ -labeling of the QFR heme propionates.** Unlike amino acid side chains, whose role can be investigated by site-directed mutagenesis, assignment of potential signals arising from heme propionates requires a different approach, such as selective  $^{13}\text{C}$  isotope labeling at the carboxy carbon positions of the heme propionates. In *W. succinogenes*, the glutamate-1-semialdehyde-2,1-amino-mutase (*hemL* gene) is responsible for the synthesis of 5-aminolevulinate, a heme precursor. The specific labeling was achieved by creating a *W. succinogenes* mutant ( $\Delta hemL$ ) that was auxotrophic for 5-aminolevulinate and by providing [1- $^{13}\text{C}$ ]-5-aminolevulinate to the medium. The deletion of the *hemL* gene from the genome of *W. succinogenes* resulted in a strain that, together with the auxotrophy for 5-aminolevulinate, was characterized by a longer lag-phase and irreproducible cell growth. In order to overcome this latter severe complication, the mutant strain required an increased ratio of inoculated cells per fresh medium volume.
  
6. **Production of pure *W. succinogenes* QFR containing  $^{13}\text{C}$ -labeled heme propionates for characterization by FTIR difference spectroscopy.** The labeled QFR was produced using the  $\Delta hemL$  mutant strain previously introduced. MALDI TOF analysis indicated that the hemes of this QFR were fully labeled, whereas other biochemical analyses excluded further differences to the unlabeled QFR enzyme. FTIR spectroscopy was adopted to analyze and compare the labeled and unlabeled enzymes when redox changes are induced. Since the midpoint potentials of the two heme groups differ by almost 150 mV, it was feasible to separate the corresponding signals and address the distal and proximal hemes individually by setting the appropriate reference potentials in the experiment. Contributions from stretching modes of deprotonated carboxyl groups can be localized at specific infrared

wavenumbers, and the  $^{13}\text{C}$ -labeling of the heme propionate carboxyl groups results in significant modifications of the corresponding bands. The interpretation of the obtained FTIR double-difference spectrum (reduced-minus-oxidized and labeled-minus-unlabeled) in terms of a (de)protonation event possibly accompanied by an environmental effect, which could well be a conformational change, agreed very well with the suggested role of this propionate in the proposed “E-pathway” hypothesis of coupled transmembrane electron and proton transfer.



Dedicated to my friend Simone





# Table of Contents

Ausführliche deutschsprachige Zusammenfassung .....	iv
Summary.....	ix
List of Tables .....	xxii
List of Equations .....	xxiii
List of Figures.....	xxiv
Symbols and Abbreviations.....	xxvi
<b>1. INTRODUCTION .....</b>	<b>1</b>
<b>1.1. Respiration and the Chemiosmotic Theory .....</b>	<b>1</b>
1.1.1. Cellular respiration and ATP creation.....	1
1.1.2. The chemiosmotic theory is at the basis of energy production.....	1
1.1.3. Aerobic respiration makes use of molecular oxygen as terminal electron acceptor.....	1
1.1.4. Anaerobic respiration makes use of other substrates as terminal electron acceptors .....	2
1.1.5. Fumarate respiration and <i>Wolinella succinogenes</i> .....	3
<b>1.2. The Quinol:Fumarate Reductase.....</b>	<b>6</b>
1.2.1. QFR is a member of the succinate:quinone oxidoreductases (SQORs) superfamily.....	6
1.2.2. The QFR cofactors are at the basis of the electron transfer mechanism .....	7
<b>1.3. The <i>Wolinella succinogenes</i> Species .....</b>	<b>9</b>
1.3.1. Phylogeny and morphology of <i>W. succinogenes</i> .....	9
1.3.2. The <i>W. succinogenes</i> QFR: operon organization, genetic manipulation and protein production.....	10
<b>1.4. Structural Properties of the QFR from <i>W. succinogenes</i> .....</b>	<b>11</b>
1.4.1. The three dimensional structure of QFR from <i>W. succinogenes</i> .....	11
1.4.2. Catalytic mechanism and electron transfer in QFR .....	12
<b>1.5. The <i>Wolinella</i> Paradox and the E-Pathway Hypothesis .....</b>	<b>13</b>
1.5.1. The <i>Wolinella</i> paradox.....	13
1.5.2. The E-pathway hypothesis of coupled transmembrane electron and proton transfer .....	14
<b>1.6. The <i>Campylobacter jejuni</i> and <i>Helicobacter pylori</i> Species .....</b>	<b>16</b>
1.6.1. <i>Campylobacter jejuni</i> : habitat and diseases .....	17
1.6.2. <i>Helicobacter pylori</i> : habitat and diseases .....	18

1.6.3.	The QFR as a potential drug target .....	19
<b>1.7.</b>	<b>Goals of this Work</b> .....	<b>20</b>
1.7.1.	Production, characterization, and crystallization of the QFR from the pathogenic bacteria <i>H. pylori</i> and <i>C. jejuni</i> .....	20
1.7.2.	Investigation of the distal heme propionate and its involvement in the E-pathway hypothesis.....	20
<b>2.</b>	<b>MATERIALS AND METHODS</b> .....	<b>23</b>
<b>2.1.</b>	<b>Materials</b> .....	<b>23</b>
2.1.1.	Suppliers.....	23
2.1.2.	Equipment.....	24
2.1.3.	Computing.....	26
2.1.3.1.	Computational equipment .....	26
2.1.3.2.	Software.....	26
2.1.4.	Chemicals .....	27
2.1.4.1.	Mediators .....	29
2.1.4.2.	Phospholipids.....	30
2.1.5.	Biological material.....	31
2.1.5.1.	Bacterial strains and genomic DNA.....	31
2.1.5.2.	Oligonucleotide Primers .....	31
2.1.5.3.	Plasmids .....	33
2.1.5.4.	Enzymes .....	34
2.1.6.	Media and growth conditions .....	34
<b>2.2.</b>	<b>Molecular Biology/Genetics</b> .....	<b>35</b>
2.2.1.	Standard methods .....	35
2.2.2.	Transformation of <i>W. succinogenes</i> .....	36
2.2.3.	Southern blotting.....	37
<b>2.3.</b>	<b><i>W. succinogenes</i> Growth Curves and Membrane Preparation</b> .....	<b>38</b>
<b>2.4.</b>	<b>Large-Scale Protein Production and Purification</b> .....	<b>38</b>
2.4.1.	Heterologous QFR production and purification .....	38
2.4.1.1.	Membrane protein solubilization .....	39
2.4.1.2.	DEAE-sepharose anion exchange.....	39
2.4.1.3.	Preparative isoelectric focusing .....	39
2.4.1.4.	Gel filtration.....	40
2.4.2.	Production of the <i>W. succinogenes</i> QFR containing <sup>13</sup> C-labeled heme propionates .....	40
<b>2.5.</b>	<b>Protein Characterization</b> .....	<b>41</b>

2.5.1.	Oxidation-reduction (“redox”) titration of FAD and iron-sulfur clusters and detection by EPR spectroscopy .....	41
2.5.2.	Electrochemistry and FTIR/VIS-spectroscopy .....	43
2.5.3.	Mass spectrometric analysis of hemes .....	43
2.5.4.	Native quinone quantification.....	44
2.5.5.	Lipid analysis .....	44
2.5.5.1.	2D thin layer chromatography (TLC) .....	44
2.5.5.2.	MALDI TOF mass spectrometry.....	45
2.5.5.2.1.	<i>Whole protein analysis</i> .....	45
2.5.5.2.2.	<i>Methanol-chloroform extraction</i> .....	45
2.5.5.2.3.	<i>Lipid isolation by TLC</i> .....	45
2.5.5.3.	High pressure liquid chromatography .....	46
2.5.6.	Analytical ultracentrifugation (AUC) .....	46
2.5.7.	Functional characterization.....	46
2.5.7.1.	Enzymatic activities.....	46
2.5.7.1.1.	<i>Quinol:fumarate reductase</i> .....	46
2.5.7.1.2.	<i>Hydrogenase</i> .....	48
2.5.7.1.3.	<i>Electron transport activity (QFR and Fdh)</i> .....	48
<b>2.6.</b>	<b>3D-Crystal Structure Determination .....</b>	<b>49</b>
2.6.1.	Crystallization .....	49
2.6.2.	Data collection.....	50
2.6.3.	Data processing and refinement .....	52
<b>3.</b>	<b>RESULTS .....</b>	<b>53</b>
<b>3.1.</b>	<b><i>H. pylori</i> and <i>C. jejuni</i> QFR Studies .....</b>	<b>53</b>
3.1.1.	Plasmid construction and insertion of the QFR operons from <i>H. pylori</i> and <i>C. jejuni</i> into the <i>W. succinogenes</i> genome.....	53
3.1.2.	Properties of <i>W. succinogenes</i> strains expressing the heterologous <i>frdCAB</i> operons .....	57
3.1.3.	Protein purification .....	58
3.1.4.	QFR enzymatic characterization .....	61
3.1.4.1.	Cofactor analysis and redox midpoint potential determination.....	61
3.1.4.2.	Analysis of native lipids co-purifying with the QFR.....	65
3.1.4.2.1.	<i>Lipid isolation by 2D thin layer chromatography</i> .....	65
3.1.4.2.2.	<i>MALDI TOF mass spectrometry assessment for lipid identification</i> .....	68
3.1.4.2.3.	<i>High-pressure liquid chromatography</i> .....	70
3.1.4.3.	Analytical ultracentrifugation.....	72
3.1.4.4.	Functional characterization .....	74

3.1.4.4.1.	<i>Electron transfer activity</i> .....	74
3.1.4.4.2.	<i>Enzymatic activity</i> .....	74
3.1.4.4.3.	<i>Effects of inhibitors</i> .....	76
3.1.5.	Crystallization and data collection.....	78
3.1.5.1.	3D-crystal structure of the <i>C. jejuni</i> QFR.....	83
<b>3.2.</b>	<b><sup>13</sup>C-Labeling of QFR Heme Propionates</b> .....	<b>90</b>
3.2.1.	Cloning and characterization of the $\Delta$ <i>hemL</i> mutant.....	90
3.2.2.	Enzymatic production and characterization.....	93
3.2.2.1.	Midpoint potentials of <sup>13</sup> C-labeled hemes at pH 7.....	95
3.2.3.	FTIR-spectroscopy analysis.....	95
3.2.3.1.	Reversible FTIR difference spectra of the “full potential” step.....	95
3.2.3.2.	Separation of redox-induced IR signals from hemes <i>b<sub>D</sub></i> and <i>b<sub>P</sub></i> .....	96
3.2.3.3.	FTIR difference spectra of the “partial potential” steps.....	98
3.2.3.4.	Tentative signals of protonated heme propionate(s) of heme <i>b<sub>D</sub></i> .....	99
3.2.3.5.	Tentative signals of deprotonated heme propionate(s) of heme <i>b<sub>D</sub></i> .....	100
<b>4.</b>	<b>DISCUSSION</b> .....	<b>103</b>
<b>4.1.</b>	<b>Quinol:Fumarate Reductase from <i>H. pylori</i> and <i>C. jejuni</i>: Production and Characterization</b> .....	<b>103</b>
4.1.1.	A novel host for heterologous expression.....	103
4.1.2.	A functional heterologous replacement of the QFR in <i>W. succinogenes</i> .....	103
4.1.3.	The first large-scale preparation of a pure and homogeneous QFR from <i>C. jejuni</i> and <i>H. pylori</i> .....	106
4.1.4.	A full protein characterization of the produced enzymes.....	107
4.1.4.1.	Redox midpoint potentials of QFR cofactors and correlation to enzymatic activities.....	108
4.1.4.2.	Identification of lipids bound to the QFR.....	111
4.1.4.3.	Ultracentrifugation experiments identify a homogeneous and homodimeric form of the QFR in other two $\epsilon$ -proteobacteria.....	114
4.1.5.	Enzyme preparations producing X-ray diffracting 3D-crystals.....	115
4.1.5.1.	The 3D-crystal structure of the <i>C. jejuni</i> QFR.....	115
4.1.6.	Functional characterization.....	116
4.1.6.1.	An accurate inhibitor characterization.....	117
<b>4.2.</b>	<b><sup>13</sup>C-Labeling of QFR Heme Propionates</b> .....	<b>119</b>
4.2.1.	Construction of the $\Delta$ <i>hemL</i> deletion strain.....	119
4.2.2.	A <sup>13</sup> C-labeled QFR suitable for FTIR spectroscopy analysis and comparison.....	119
4.2.3.	FTIR Spectroscopy analysis of the labeled and unlabeled enzymes.....	121

4.2.3.1.	Tentative vibrations of protonated heme propionates .....	121
4.2.3.2.	Tentative anti- and symmetric vibrations of deprotonated heme propionates .....	122
4.2.3.3.	Differences between the full and partial potential steps at the distal heme.....	122
<b>4.3.</b>	<b>Concluding remarks and perspectives .....</b>	<b>124</b>
<b>5.</b>	<b>REFERENCES .....</b>	<b>127</b>
	Appendixes .....	137
	Acknowledgements .....	169
	Curriculum Vitae .....	173

# List of Tables

Table 1-I: Redox midpoint potential ( $E_m$ ) of the cofactors from the <i>W. succinogenes</i> QFR.....	8
Table 2-I: Supplier list.....	23
Table 2-II: Equipment list.....	24
Table 2-III: Chemicals list.....	27
Table 2-IV: List of mediators for enzymatic titrations.....	30
Table 2-V: Synthetic phospholipids.....	30
Table 2-VI: Oligonucleotide primers used for preparative and analytic PCR.....	31
Table 2-VII: Oligonucleotide primers used for sequencing.....	32
Table 2-VIII: Oligonucleotide primers used for site-directed mutagenesis.....	32
Table 2-IX: Site-directed mutagenesis performed on the <i>C. jejuni</i> and <i>H. pylori</i> <i>frdCAB</i> operons.....	33
Table 2-X: Plasmids used.....	33
Table 2-XI: Formate – fumarate 10x (A) and formate – nitrate pre-medium 20x (B).....	34
Table 2-XII: Formate – fumarate (A) and formate – nitrate medium (B).....	35
Table 2-XIII: Trace elements solution 500x (A); cysteine – glutamate (cys-glu) solution 100x (B); calcium – magnesium solution 1000x (C).....	35
Table 2-XIV: Southern blotting buffers and instructions.....	38
Table 2-XV: EPR spectroscopy parameters used for the measurement of the QFR cofactor’s radical species.....	42
Table 2-XVI: Crystallization conditions that lead to the 3D-crystal structure determination of the <i>C. jejuni</i> QFR.....	50
Table 2-XVII: Data set collection parameters at the beamline ID14-EH1.....	52
Table 3-I: Doubling times and specific fumarate reductase activities of <i>W. succinogenes</i> strains.....	58
Table 3-II: Purification profile based on total specific activity (“DT-DMNH <sub>2</sub> assay”).....	60
Table 3-III: Redox midpoint potentials of all QFR cofactors from <i>W. succinogenes</i> (W.s.), <i>C. jejuni</i> (C.j.), and <i>H. pylori</i> (H.p.).....	65
Table 3-IV: List of retention times obtained from the standard calibration curve.....	70
Table 3-V: Recovery of the <i>H. pylori</i> QFR enzymatic activity upon treatment with lipids at the stoichiometric ratio of 5 molecules per monomer.....	72
Table 3-VI: Electron transfer activities (Sp. activity) and turnover numbers (TN or $K_{cat}$ ) performed on <i>W. succinogenes</i> re-suspended membranes containing the homologous QFR (A), the <i>C. jejuni</i> QFR (B) and the <i>H. pylori</i> QFR (C).....	74
Table 3-VII: Enzymatic activity, Michaelis constant, and inhibitor constant values of the isolated QFR from <i>W. succinogenes</i> (A), <i>C. jejuni</i> (B), and <i>H. pylori</i> (C) after IEF.....	76
Table 3-VIII: Crystallization conditions which have been used for the achievement of the <i>C. jejuni</i> and <i>H. pylori</i> QFR crystals shown in Figure 3-25.....	82
Table 3-IX: Unassigned amino acids and side chains.....	83
Table 3-X: Crystallographic table: data processing and refinement statistics of the <i>C. jejuni</i> QFR structure.....	84
Table 3-XI: Purification profile based on partial specific activity (“MB assay”) of the <sup>13</sup> C-labeled QFR from <i>W. succinogenes</i> .....	93
Table 4-I: Amino acidic sequence identities between the QFR from <i>W. succinogenes</i> DSM 1740 strain, the <i>C. jejuni</i> clinical isolate strain, and the <i>H. pylori</i> 26695 strain.....	105

## List of Equations

Equation 2-1: Double Nernst equation for the calculation of the oxidation-reduction (redox) midpoint potential values of the FAD.....	42
Equation 2-2: Nernst equation for the calculation of the redox midpoint potential values of the iron-sulfur clusters.....	43
Equation 2-3: Double Nernst equation for the calculation of the heme redox midpoint potentials.....	43
Equation 2-4: Kröger-Klingenberg equation (Kröger & Klingenberg, 1973).....	48

# List of Figures

Figure 1-1: Cartoon representation of fumarate respiration. ....	3
Figure 1-2: Chemical structure of menaquinone (A), 5-methyl-menaquinone (B), and ubiquinone (C). ....	5
Figure 1-3: The succinate:quinone oxidoreductase (SQOR) superfamily and its classification. ....	7
Figure 1-4: Electron transfer rate constants between cofactors of the QFR from <i>W. succinogenes</i> . ....	8
Figure 1-5: Phylogenetic tree of <i>Wolinella succinogenes</i> and its closest neighbors. ....	9
Figure 1-6: A transmission electron microscopy (TEM) picture of the <i>W. succinogenes</i> . ....	9
Figure 1-7: X-ray crystal structure of the <i>W. succinogenes</i> QFR. ....	11
Figure 1-8: Catalytic sites and electron transfer pathway of the <i>W. succinogenes</i> QFR. ....	13
Figure 1-9: Electron and proton transfer in the <i>W. succinogenes</i> QFR and the E-pathway hypothesis. ....	16
Figure 1-10: Transmission electron micrographs of <i>Campylobacter jejuni</i> (A) and <i>Helicobacter pylori</i> species (B). ....	17
Figure 2-1: Chemical structure of the 1- <sup>13</sup> C-5-aminolevulinate. ....	35
Figure 2-2: Graphical representation of the three different enzymatic assays on the QFR. ....	47
Figure 2-3: The beamline ID14-EH1 at the ESRF. ....	51
Figure 2-4: Crystal transportation and mounting. ....	51
Figure 3-1: Maps of the PCR-amplified DNA fragments used for cloning. ....	53
Figure 3-2: Map of the constructed plasmids containing the <i>H. pylori</i> and <i>C. jejuni</i> QFR operons. ....	54
Figure 3-3: Illustration of the integration of the plasmid constructs into the genome of <i>W. succinogenes</i> . ....	55
Figure 3-4: Maps of the genomic QFR locus after integration. ....	56
Figure 3-5: Southern blot analysis. ....	57
Figure 3-6: The QFR purification procedure: anion exchange chromatography (A), and preparative isoelectric focusing (B). ....	59
Figure 3-7: Chromatogram of the gel filtration purification. ....	59
Figure 3-8: SDS-PAGE of samples during purification. ....	61
Figure 3-9: FAD fluorescence under UV-light exposure (A) after running an SDS-PAGE (B). ....	61
Figure 3-10: Determination of the redox midpoint potential of the prosthetic group FAD by EPR. ....	62
Figure 3-11: Determination of the redox midpoint potential of the iron-sulfur clusters [2Fe-2S] (or S1), [4Fe-4S] (or S2) and [3Fe-4S] (or S3). ....	63
Figure 3-12: Fitting of the titration curves for the determination of the heme redox midpoint potentials from the <i>C. jejuni</i> (A) and <i>H. pylori</i> (B) QFRs. ....	64
Figure 3-13: TLC trials of the <i>C. jejuni</i> (A) and <i>H. pylori</i> (B) QFRs after IEF. ....	66
Figure 3-14: TLC lipid standard. ....	67
Figure 3-15: Portions of TLC trials of the <i>C. jejuni</i> (A) and <i>H. pylori</i> (B) QFRs after gel filtration. ....	68
Figure 3-16: MALDI TOF measurement of the extracted spots labeled “detergent” (A) and n° 5 (B). ....	69
Figure 3-17: Tandem MS-MS of the peak 817 m/z. ....	70
Figure 3-18: HPLC chromatogram of the <i>H. pylori</i> QFR after extraction. ....	71



Figure 3-19: Sedimentation velocity analysis on QFR from <i>C. jejuni</i> (A,B), <i>H. pylori</i> (C) and <i>W. succinogenes</i> (D).....	73
Figure 3-20: Typical “DT-DMNH <sub>2</sub> assay” course. ....	75
Figure 3-21: Lineweaver-Burk plots of <i>C. jejuni</i> QFR (A) and <i>H. pylori</i> QFR (B) activity.....	77
Figure 3-22: Chemical structure of tested inhibitors: oxantel (A), thiabendazole (B) and omeprazole (C). ....	77
Figure 3-23: Phase diagram of the <i>C. jejuni</i> QFR.....	79
Figure 3-24: Co-crystallization of the <i>H. pylori</i> QFR with cardiolipin (CA 18:1) (B), and comparison to a crystallization trial without cardiolipin (A). ....	80
Figure 3-25: Crystals of <i>C. jejuni</i> (A, E-S) and <i>H. pylori</i> QFRs (B, C, D). The respective crystallization conditions have been displayed in Table 3-VIII.....	81
Figure 3-26: Crystal packing (top) of the <i>C. jejuni</i> QFR structure and a snapshot (bottom) of one crystal contact as indicated by the blue box. ....	85
Figure 3-27: The crystal structure of the <i>C. jejuni</i> QFR.....	86
Figure 3-28: Arrangement of the prosthetic groups in the fumarate reductase from <i>C. jejuni</i> . ....	87
Figure 3-29: Electron density and model of the FAD prosthetic group (A) and the S1 and S2 iron-sulfur clusters (B, cross-eye stereo view). ....	88
Figure 3-30: Electron density and model of the distal heme (A), and the region between the hemes containing the FrdCE180 residue (B, cross-eye stereo view). ....	89
Figure 3-31: Plasmid maps of the pBR322 and the recombinant pBRH1. ....	90
Figure 3-32: Plasmid map of the recombinant pBRAH1. ....	91
Figure 3-33: One-step gene disruption of the <i>hemL</i> gene from the <i>W. succinogenes</i> genome. ....	92
Figure 3-34: SDS-PAGE of samples during purification.....	93
Figure 3-35: MALDI TOF analysis of the extracted hemes.....	94
Figure 3-36: Heme <i>b</i> titration curve of the <sup>13</sup> C-labeled QFR WT at pH 7. ....	95
Figure 3-37: Electrochemically-induced FTIR difference spectra of unlabeled and <sup>13</sup> C-labeled QFR.....	96
Figure 3-38: Electrochemically induced FTIR difference spectra of unlabeled QFR at pH 7 with intermediate step.....	97
Figure 3-39: Electrochemically induced FTIR difference spectra of <sup>13</sup> C-labeled QFR at pH 7 with intermediate step.....	98
Figure 3-40: Schematic view of the three relevant heme propionate vibrations. ....	99
Figure 3-41: Detail of FTIR difference spectra of unlabeled and <sup>13</sup> C-labeled QFR at pH 7.....	100
Figure 3-42: FTIR double-difference spectra of “unlabeled-minus- <sup>13</sup> C-labeled” QFR at pH 7. ....	101
Figure 4-1: Redox midpoint potentials of the QFR cofactors from <i>C. jejuni</i> (black), <i>H. pylori</i> (red) and <i>W. succinogenes</i> (blue).....	108
Figure 4-2: The chemical structure of a heme <i>b</i> group and indication of the isotopically labeled propionates (magenta).....	120
Figure 4-3: A representation of the E-pathway hypothesis. ....	124

# Symbols and Abbreviations

2D, bi-dimensional	DM, decyl maltoside
3D, tri-dimensional	DMN, 2,3-dimethyl-1,4-naphthoquinone
°C, Celsius degrees	DMNH <sub>2</sub> , 2,3-dimethyl-1,4-naphthoquinol
A(r,t), experimentally observed sedimentation data	DNA, deoxyribonucleic acid
ACN, acetonitrile	dNTP, deoxyribonucleotide triphosphate
ADP, adenosine diphosphate	DTT, dithiothreitol
Amp, ampicillin	$\epsilon_x$ , extinction coefficient at the wavelength $x$
Å, angstrom(s)	$E'_{\theta}$ , standard redox potential
AP, alkaline phosphatase	$E_{\text{H}}$ , environmental redox potential
ATP, adenosine triphosphate	$E_m$ , redox midpoint potentials
ALA, 5-aminolevulinate	EPR, electron paramagnetic resonance
AUC, analytical ultracentrifugation	ESRF, European Synchrotron Radiation Facility
BA, benzamidine	ETC, electron transfer chain
BLM, black lipid membrane	F, Faraday
bp, base pairs	FAD, flavin-adenine dinucleotide
BSA, bovine serum albumin	FTIR, Fourier transformed infrared
BV, benzyl viologen	Fdh, formate dehydrogenase
c(s), sedimentation coefficient distribution	Frd, fumarate reductase
CA, cardiolipin	g, force of gravity
<i>cat</i> , chloramphenicol acetyltransferase (chl resistance)	G, Gauss (magnetic field)
chl, chloramphenicol	Gpp, Gauss, peak-to-peak
cyt. <i>b</i> , cytochrome <i>b</i>	h, hours
$\Delta E$ , redox difference potential	Heme $b_D$ (or $H_D$ ), distal heme <i>b</i>
$\Delta E'_{\theta}$ , standard redox different potential	Heme $b_P$ (or $H_P$ ), proximal heme <i>b</i>
$\Delta G$ , free energy (Gibbs)	Heme $b_H$ , high potential heme <i>b</i>
$\Delta p$ , electrochemical proton potential	Heme $b_L$ , low potential heme <i>b</i>
D-value, diffusion coefficient	HPLC, high pressure liquid chromatography
Da, Dalton	HT, heptane-1,2,3-triol
dB, decibel	Hz, Herz
DEAE, diethylaminoethyl	$I/\sigma(I)$ , signal over noise intensities ratio
DESY, Deutsches Elektronen-Synchrotron	$I_{\text{max}}$ , max absorbance intensity
DHB, dihydroxybenzoic acid	$IC_{50}$ , concentration of inhibitor that reduces activity to 50 %
DIG, digoxigenin	IEF, isoelectric focusing

JWGU, Johan Wolfgang Goethe University	PE, phosphatidylethanolamine
K, Kelvin degrees	PG, phosphatidylglycerol
$K_i$ , inhibition constant	PI, phosphatidylinositol
$K_M$ , Michaelis constant	PL, phospholipid
Kan, kanamycin	PS, phosphatidylserine
$KP_i$ , potassium phosphate	Q, occupancy
LDAO, lauryl dimethylamine oxide	QFR, quinol:fumarate reductase
LM, dodecyl maltoside	RF, retention factor
$M_{eff,c}$ , effective molar mass	RNA, ribonucleic acid
MALDI TOF, matrix-assisted laser desorption ionization time of flight	rpm, rounds per minute
MB, methylene blue	RT, room temperature
min, minute(s)	s-value, sedimentation coefficient
MK, menaquinone	S, Svedberg
$MKH_2$ , menaquinol	S1, iron-sulfur cluster [2Fe-2S]
mM, millimolar	S2, iron-sulfur cluster [4Fe-4S]
MMK, 8-methyl menaquinone	S3, iron-sulfur cluster [3Fe-4S]
Mpa, megaPascal	SB, Southern blotting
MPIBP, Max Planck Institute of Biophysics	SDS, sodium dodecyl sulfate
MS, mass spectrometry	SHE, standard hydrogen electrode
mV, millivolt(s)	SQORs, succinate:quinone oxidoreductases
MW, molecular weight	SQR, succinate:quinone reductase
mW, milli watts	SSM, solid supported membranes
m/z, mass/ionic charge	TEM, transmission electron microscopy
$\nu$ , vibrations	Tet, tetracycline
$\nu_{as}$ or $\nu_s$ , asymmetrical or symmetrical vibrations	TFA, trifluoroacetic acid
n=1, one electron involved	TLC, thin layer chromatography
nm, nanometers	TN, turnover number
$OD_x$ , optical density at the waveleght x	Tris, tris-(hydroxymethyl)-aminomethane
OG, octyl glucopyranoside	tRNA, transfer ribonucleic acid
ORF, open reading frame	U, enzymatic unit
ori, plasmid replication initiation site	UM, undecyl maltoside
PA, phosphatidic acid	UV, ultraviolet
PAGE, polyacrylamide gel electrophoresis	$\bar{v}$ , partial specific volume
PC, phosphatidylcholine	V, volt
PCR, polymerase chain reaction	$V_{MAX}$ , maximal velocity
PDB, protein data bank	vitK <sub>2</sub> , vitamin K <sub>2</sub>
	WT, wild type



# 1. INTRODUCTION

## 1.1. Respiration and the Chemiosmotic Theory

### 1.1.1. Cellular respiration and ATP creation

Cellular respiration is the process that exploits the energetic content of “food” molecules (nutrients) to produce forms of readily available energy to be used in all the non-spontaneous/endergonic activities of the cell. These molecules, for example glucose, are oxidized to carbon dioxide and water, and the released energy is stored in the form of ATP (Lodish, *et al.*, 1999).

The process occurs in two phases: glycolysis, where the glucose is converted to pyruvic acid, and the oxidative phosphorylation, where pyruvic acid is completely oxidized to carbon dioxide and water. This latter process is the main one responsible for the production of ATP from ADP and inorganic phosphate, using energy derived from the transfer of electrons in an electron transport system (the respiratory chain), and is driven by chemiosmosis.

### 1.1.2. The chemiosmotic theory is at the basis of energy production

Peter Mitchell, who formulated the chemiosmotic theory (Mitchell, 1979), postulated that a proton electrochemical gradient is produced by a sequential transfer of electrons through a series of membrane-bound proteins, and that the flow of protons back across the membrane in the energetically favorable direction is then coupled to ATP synthesis. Thus, the intermediate stage that couples electron transport to ATP synthesis is a proton electrochemical gradient across the membrane. The chemiosmotic theory is the basis for the generation of ATP during oxidative phosphorylation and photosynthesis in bacteria, mitochondria, and chloroplasts, and also for the energy-requiring secondary transport of a variety of molecules across cell membranes.

### 1.1.3. Aerobic respiration makes use of molecular oxygen as terminal electron acceptor

Aerobic respiration is so named because the molecular oxygen (O<sub>2</sub>) contained in air is used as a terminal electron acceptor in the electron transport system. In eukaryotic cells, oxidative phosphorylation occurs entirely within the mitochondria. In prokaryotes, the enzymes and

carrier molecules involved in the aerobic pathways are embedded in the plasma membrane, and the reactions occur at the surfaces of the membrane. The electron transport machinery of aerobic respiration consists of five complexes of transmembrane enzymes: complex I, or NADH quinone oxidoreductase; complex II, or succinate:quinone reductase; complex III, or ubiquinol:cytochrome *c* oxidoreductase; complex IV, or cytochrome *c* oxidase; and complex V, or ATP synthase. The complex IV is also referred to as terminal oxidase, since it catalyses the last substrate (cytochrome *c*) oxidation in order to reduce oxygen to water. Complexes I, III, and IV pump protons out of the cytoplasm (or mitochondrial matrix), building a proton gradient. Then, the energetically favorable flow of protons back to the cytoplasm is mediated by complex V, which generates ATP.

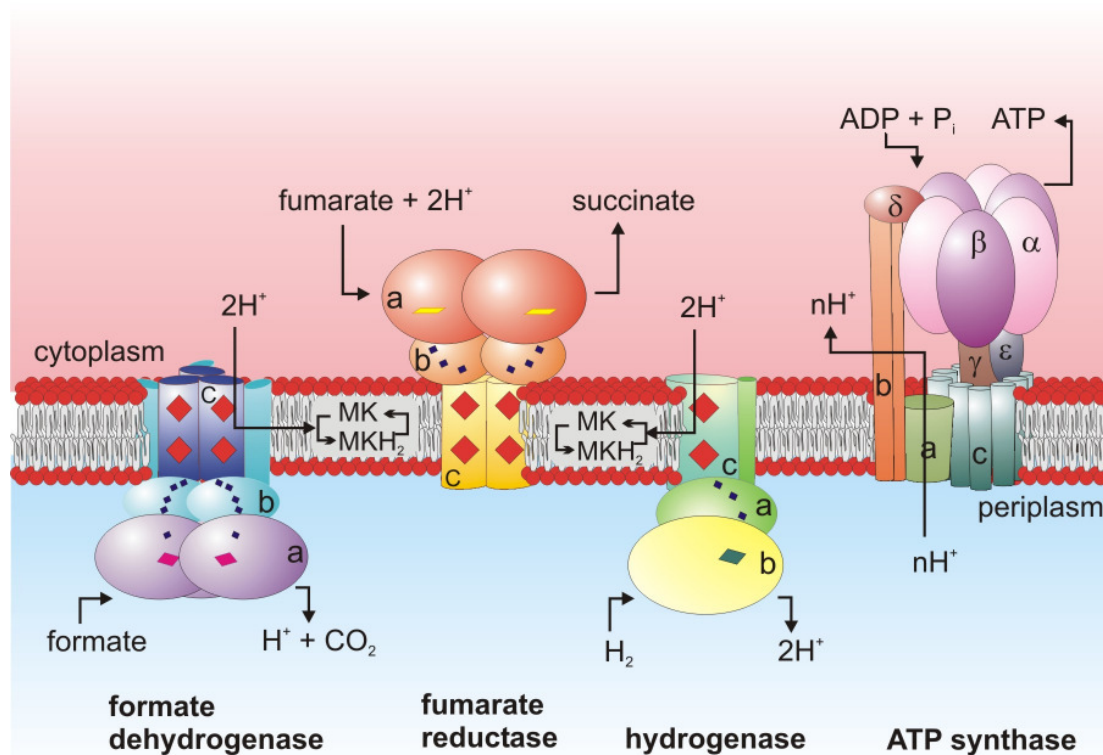
#### **1.1.4. Anaerobic respiration makes use of other substrates as terminal electron acceptors**

Most of the anaerobic or facultative bacteria perform ATP synthesis not only by the substrate level phosphorylation described above, but also by electron transport coupled phosphorylation (ETP) (Thauer, *et al.*, 1977, Thauer & Morris, 1984, Kröger, *et al.*, 1992). This process, generally performed during anaerobic respiration, is also termed the 'redox loop mechanism' (Berks, *et al.*, 1995). It resembles oxidative phosphorylation with respect to the mechanism of energy transduction, but differs by the terminal electron acceptor used. Indeed, in anaerobic respiration, oxygen is replaced by other substrates - organic or inorganic compounds, or certain heavy metal ions. In turn, the terminal oxidase of the respiratory chain, thus the enzyme that catalyzes the oxidation of the terminal electron donor (by the reduction of the terminal electron acceptor), varies with the variation of the type of substrate.

Depending on the species and on the environmental situation, bacteria can perform respiration with a variety of redox reactions involving different electron donors, such as molecular hydrogen (H<sub>2</sub>), formate or sulfide, and different electron acceptors, such as fumarate, nitrate, nitrite, nitrous oxide, polysulfide ([S]), and dimethyl sulfoxide. As a consequence, the composition of the respiratory chains and the mechanism of electrochemical proton gradient generation may vary greatly (Kröger, *et al.*, 2002). Anaerobic respiration with fumarate (Kröger, 1978, Lancaster, 2004a) is called "fumarate respiration" (see Figure 1-1).

### 1.1.5. Fumarate respiration in *Wolinella succinogenes*

In analogy to aerobic respiration, the energy released in fumarate respiration is transiently stored in the form of an electrochemical proton potential across the membrane. Probably because fumarate can be formed via two different metabolic pathways, this kind of respiration is the most widespread kind of anaerobic respiration (Kröger, *et al.*, 1992). Besides, other membrane proteins are indirectly involved in this energy production system, such as  $C_4$ -dicarboxylate carriers, which are essential for functions like transport or uptake of  $C_4$ -dicarboxylates (i.e. fumarate and succinate) across the membrane (Janausch, *et al.*, 2002). *Wolinella succinogenes*, a member of the  $\epsilon$ -subclass of the proteobacteria, has been adopted as a model system to study fumarate respiration at the physiological and structural level. Since the objects of this thesis studies are the QFRs from  $\epsilon$ -proteobacteria, next paragraphs will specifically focus on aspects concerning this subclass of proteobacteria.



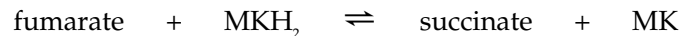
**Figure 1-1: Cartoon representation of fumarate respiration.** MK and MKH<sub>2</sub> stand for menaquinone and menaquinol, respectively. The little parallelograms represent cofactors associated with the enzymes. Color codes are: red squares, hemes; blue squares, iron-sulfur clusters; yellow squares, flavin groups; green squares, [NiFe] or [FeFe] groups; purple squares, molybdopterin guanine dinucleotide. The fading red and blue colors in the background represent the negative and positive environmental redox potentials, respectively. (Figure was modified from Lancaster, 2002b)

Figure 1-1 depicts fumarate respiration, consisting of three electron transport enzymes coupled to the complex V (ATP synthase), which generates ATP. The redox couples here involved are:  $H^+/H_2$ , with a standard (pH 7, 25°C) reduction-oxidation (redox) potential of  $-420$  mV (Kröger, 1978); menaquinone/menaquinol, with a standard redox potential of  $-75$  mV (Wagner, *et al.*, 1974, Kröger & Innerhofer, 1976a); fumarate/succinate, with a standard redox potential of  $+30$  mV (Clark, 1960); carbonate/formate, with a standard redox potential of  $-420$  mV (Ljungdahl & Wood, 1969, Kröger, 1978, Jormakka, *et al.*, 2002).

As indicated in the reaction legends and in Figure 1-1, the reactions are catalyzed by the formate dehydrogenase (Fdh, Reaction 1-1), the quinol:fumarate reductase (QFR, Reaction 1-2), the hydrogenase (Reaction 1-3), and ATP synthase (Reaction 1-4).



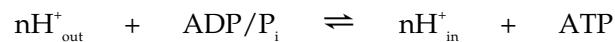
**Reaction 1-1:** Molecular hydrogen ( $H_2$ ) is oxidized and two electrons are released and transported to the menaquinone (MK) to form menaquinol ( $MKH_2$ ). The hydrogenase catalyzes this reaction, whose total standard redox different potential ( $\Delta E'_0$ ) is:  $-345$  mV.



**Reaction 1-2:** The two electrons released from menaquinol are transported to the fumarate, which is thereby reduced to succinate. The quinol:fumarate reductase catalyzes this reaction, whose  $\Delta E'_0$  is:  $-105$  mV.



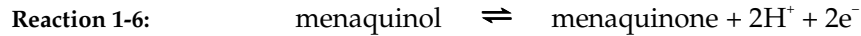
**Reaction 1-3:** Formate is oxidized and two electrons are released and transferred to the menaquinone (MK) to form menaquinol ( $MKH_2$ ). The formate dehydrogenase catalyzes this reaction, whose  $\Delta E'_0$  is:  $-341$  mV.



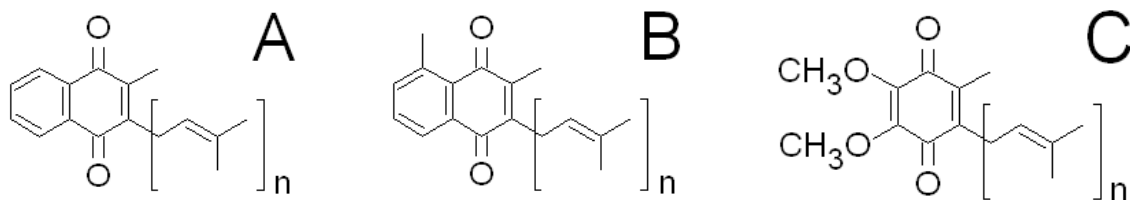
**Reaction 1-4:** The flow of protons across the electrochemical proton gradient leads to ADP phosphorylation for the formation of ATP. The ATP synthase catalyzes this reaction.

The overall reaction catalyzed by the QFR (Reaction 1-2) implies the exchange of two protons and two electrons, and can be divided in two half-reactions, as shown in Reaction 1-5 and Reaction 1-6.





The electron transport chain is at the basis of respiration, and involves the connection of two enzymes, such as hydrogenase and QFR or formate dehydrogenase and QFR. The presence of low-potential quinones, i.e. menaquinone (Figure 1-2-A) and 8-methyl-menaquinone (Figure 1-2-B) (Dietrich & Klimmek, 2002, MacMillan F. & Klimmek O., unpublished), whose molar amount in the cellular membrane is at least 10-fold more abundant than the enzymes (Kröger & Innerhofer, 1976b, Uden, *et al.*, 1983), is the link between all the respiratory components (Lemma, *et al.*, 1990). Because the high-potential quinones that are normally operating in aerobic respiration (e.g. ubiquinone, Figure 1-2-C) have higher redox midpoint potentials than the terminal electron acceptor (i.e. fumarate), in anaerobic respiration they have been replaced by low-potential quinones<sup>a</sup>.



**Figure 1-2: Chemical structure of menaquinone (A), 8-methyl-menaquinone (B), and ubiquinone (C).**

Hydrogenase (Gross, *et al.*, 1998) and formate dehydrogenase (Kröger, *et al.*, 1979, Jormakka, *et al.*, 2003b) are large membrane protein complexes, which use of the exergonic hydrogen or formate oxidation reaction, to generate an electrochemical proton gradient across the membrane. ATP synthase is a large protein complex (Bokranz, *et al.*, 1985) that consists of two subcomplexes of several protein subunits, named F<sub>0</sub>- (the membrane integral base-piece)

<sup>a</sup> The fumarate/succinate and ubiquinone/ubiquinol redox couples have a standard redox potential of +30 mV and +100 mV, respectively, therefore the reaction catalyzed by the QFR would be endergonic (hence energetically unfavorable).

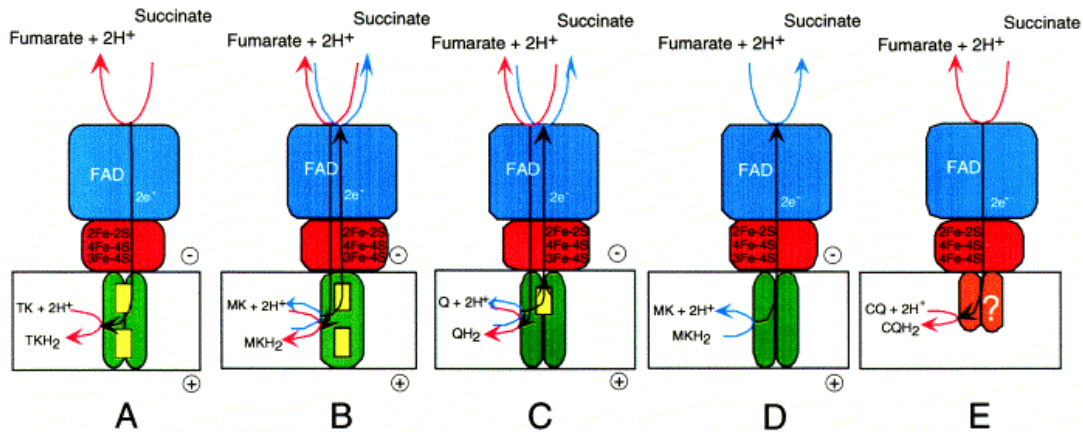
and F<sub>1</sub>-ATPase (the soluble domain). This enzyme couples the vectorial proton transport across a membrane with the synthesis (or cleavage) of the energy rich compound ATP. The QFR is the terminal electron transport component (or terminal reductase) of fumarate respiration, as it uses fumarate instead of oxygen as the terminal electron acceptor (Lancaster, 2004a).

## 1.2. The Quinol:Fumarate Reductase

The QFR catalyzes the reaction that couples the two-electron reduction of fumarate to succinate to the oxidation of the low-potential menaquinol to menaquinone (Reaction 1-2-C), as well as the reverse reaction. The overall reaction implies the exchange of two protons and two electrons, and can be divided in two half-reactions, as shown in Reaction 1-2-A and -B. The major quinone species (Lancaster & Simon, 2002) used from this enzyme are menaquinone-6 and methyl-menaquinone-6 (Figure 1-2-A and -B), both derivatives of 1,4-naphthoquinone with a chain of six isoprenyl units.

### 1.2.1. QFR is a member of the succinate:quinone oxidoreductases (SQORs) superfamily

QFR is the physiological antagonist of succinate:quinone reductase (SQR), which is the complex II of cellular aerobic respiration and a component of the Krebs cycle (for recent reviews on complex II see (Lancaster, , Cecchini, 2003, Cecchini, *et al.*, 2003, and Lancaster, 2004b). The SQR and QFR complexes together are referred to as succinate:quinone oxidoreductases (SQORs, Lancaster, 2002a), a membrane protein superfamily which consists of two hydrophilic subunits and one or two hydrophobic subunits. The hydrophobic milieu can carry either one, two, or no heme groups. Depending on the hydrophobic domain and heme content, the SQORs can be divided into five different classes (type-A to type-E, Figure 1-3). They are classified as EC 1.3.5.1 (international union of biochemistry and molecular biology –or IUBMB- enzyme nomenclature), and since they catalyze Reaction 1-2 in both directions, the distinction between SQR and QFR depends only on the direction of the reaction catalyzed *in vivo*.



**Figure 1-3: The succinate:quinone oxidoreductase (SQOR) superfamily and its classification.** The integral transmembrane subunits (in green) can contain heme groups (yellow rectangles). The hydrophilic subunits are drawn in red (subunit B) and blue (subunit A) (modified from Lancaster, 2002a).

In recent years, the three-dimensional crystal structures of three different SQORs, such as type-D QFR from *E. coli* (Iverson, *et al.*, 1999), type-B QFR from *W. succinogenes* (Lancaster, *et al.*, 1999), and type-C SQR from *E. coli* (Yankovskaya, *et al.*, 2003), have been solved. A detailed analysis of the QFR structure from *W. succinogenes* is presented in chapter 1.4.

### 1.2.2. The QFR cofactors are at the basis of the electron transfer mechanism

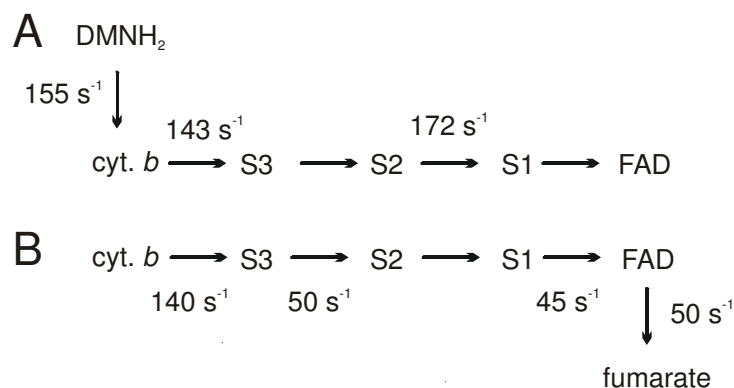
The QFR from *W. succinogenes* is a membrane protein complex containing one hydrophobic subunit and several cofactors (Lancaster, 2001b) including two heme *b* groups, a flavin adenine dinucleotide (FAD) prosthetic group, and the iron sulfur clusters [2Fe-2S], [4Fe-4S], and [4Fe-4S]. The UV/VIS absorbance spectrum of this enzyme is dominated by the  $\alpha$ ,  $\beta$ , and  $\gamma$  (or Soret) bands, which arise from the two heme groups. The iron-sulfur cluster can be better monitored with the use of EPR (Albracht, *et al.*, 1981, Uden, *et al.*, 1984, Maguire, *et al.*, 1985), linear electric field effect (LEFE) EPR (Ackrell, *et al.*, 1984), and magnetic circular dichroism (MCD, Johnson, *et al.*, 1985) spectroscopy.

In the last decades, the use of these various spectroscopic methods allowed characterization of some of these cofactors (Beinert, 2002). The redox midpoint potentials ( $E_m$ ) of the cofactors are summarized in Table 1-I and taken from the references Lancaster, *et al.*, 2000, Lancaster, 2001b, Haas & Lancaster, 2004. Furthermore, calculation of the electron transfer rate

constants between cofactors has allowed identification of the rate-limiting steps of the catalytic reaction (Figure 1-4).

**Table 1-I: Redox midpoint potential ( $E_m$ ) of the cofactors from the *W. succinogenes* QFR.**

Cofactor type	$E_m$ (mV)
FAD	- 20
S1	- 59
S2	< - 250
S3	- 24
Proximal heme	- 9
Distal heme	- 152



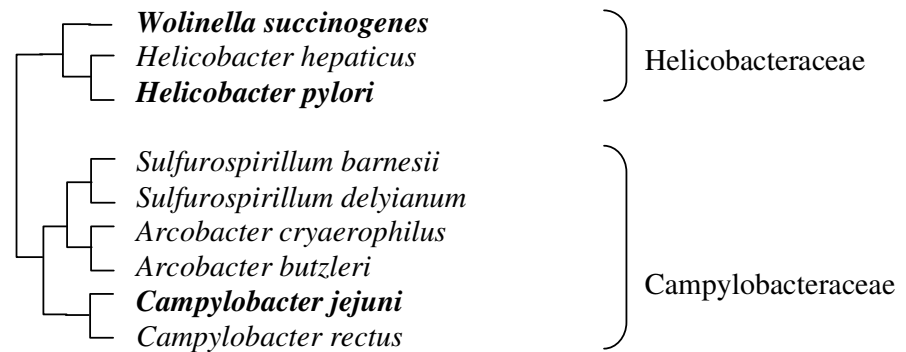
**Figure 1-4: Electron transfer rate constants between cofactors of the QFR from *W. succinogenes*.** (Kröger, *et al.*, 2002) The rate constants refer to the reduction of components in the fully oxidized enzyme upon the addition of  $\text{DMNH}_2$  (A), and their oxidation in the fully reduced enzyme by fumarate (B) at  $20^\circ\text{C}$ . The arrows indicate an electron transfer. S3, S2 and S1 designate the [3Fe-4S], [4Fe-4S] and [2Fe-2S] iron-sulfur clusters, respectively.

The establishment of various enzymatic activity assays on QFR (Lancaster, 2001b) has provided powerful methods for its functional study. The QFR from *W. succinogenes* is a highly active membrane protein complex with turnover times (i.e. the inverse of turnover rates) in the range of tens of milliseconds (calculated from a specific activity of  $7.4 \text{ U mg}^{-1}$ , Lancaster, *et al.*, 2000).

### 1.3. The *Wolinella succinogenes* Species

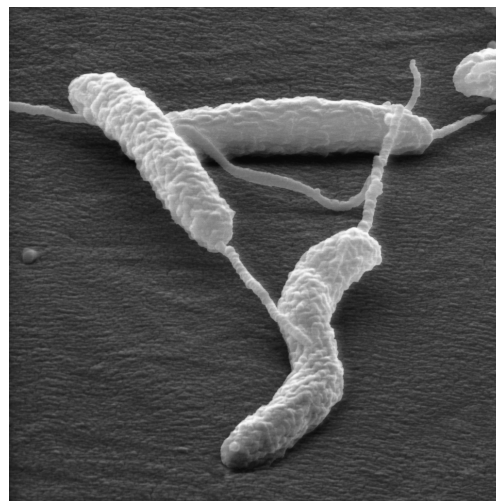
#### 1.3.1. Phylogeny and morphology of *W. succinogenes*

*W. succinogenes* is a member of the helicobacteraceae, a family belonging to the  $\epsilon$ -subclass of the proteobacteria. The typical habitat of this bacterium is the rumen of cattle.



**Figure 1-5: Phylogenetic tree of *Wolinella succinogenes* and its closest neighbors.** (Simon, *et al.*, 2000a)

*W. succinogenes* is Gram-negative, and it was originally classified with the name *Vibrio succinogenes*. It is an anaerobic, non-spore-forming, rod-shaped bacterium that possesses a single polar flagellum able to confer a rapid, darting motility.



**Figure 1-6: A transmission electron microscopy (TEM) picture of the *W. succinogenes*.** (Picture kindly provided by Dr. S. Schuster)

The cells are helical, curved or straight, with a diameter of 0.5-1.0  $\mu\text{m}$  and a length of 2-6  $\mu\text{m}$  (Simon, *et al.*, 2000a). They do not ferment carbohydrates, but can grow only by anaerobic respiration in liquid and in solid media. Fumarate respiration (Figure 1-1) of *W. succinogenes* is the best investigated system of this type.

### **1.3.2. The *W. succinogenes* QFR: operon organization, genetic manipulation and protein production**

The open reading frames (ORF) coding for the QFR of *W. succinogenes*, as well as all other proteobacteria, are organized in one operon. Thus, the three structural genes, in the order *frdC*, *frdA*, *frdB*, are concatenated and preceded by a common promoter and followed by a common terminator of transcription (Kortner, *et al.*, 1990).

The development of some genetic manipulation tools suitable for *W. succinogenes* (Simon, *et al.*, 2000a) allowed the generation of a QFR deletion mutant ( $\Delta\text{frdCAB}$ ) of this species (Simon, *et al.*, 1998) In the genome of this mutant, the complete *frdCAB* coding region was replaced by the kanamycin resistance gene resulting in the inability of the cells to grow by fumarate respiration. This strain does not induce an alternative fumarate reductase and cannot grow in media containing fumarate as a unique source of terminal electron acceptor. Instead, this deletion strain can be grown on media containing nitrate as a terminal electron acceptor, implying that fumarate respiration was impaired. The homologous *frdCAB* operon was restored at its genomic locus in *W. succinogenes*  $\Delta\text{frdCAB}$  by integration of plasmid pFrdcat2 via homologous recombination between the *frd* promoter present both on the plasmid and on the genome of the deletion mutant (Simon, *et al.*, 1998). The resulting strain (named K4) showed wild type properties in terms of fumarate respiration and fumarate reductase activity.

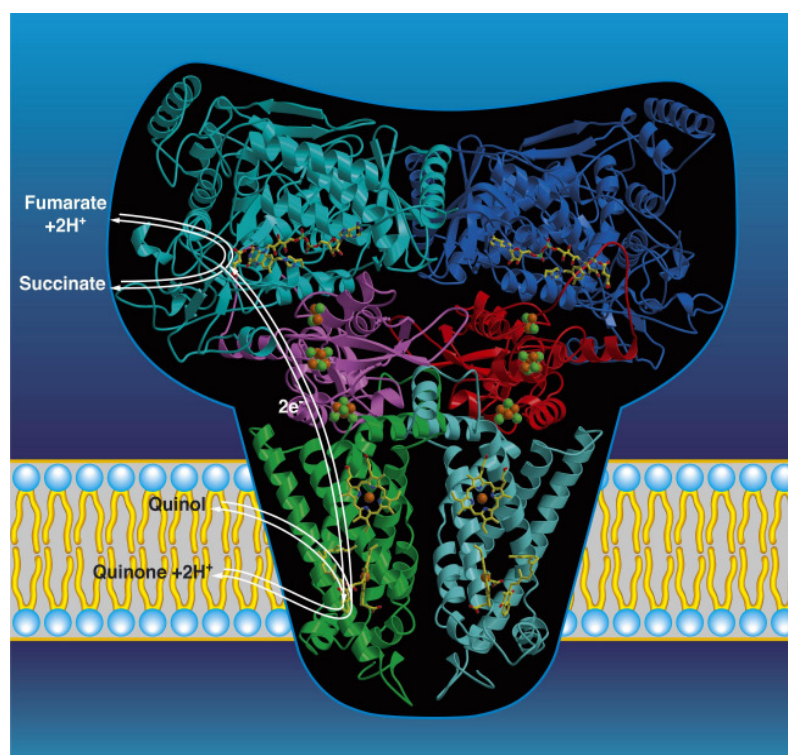
The previous expression of *W. succinogenes* QFR from the native source and the established purification procedure consisting of anion exchange chromatography and isoelectric focusing, demonstrated that this bacterium is able to yield high amounts of stable and pure material, which was also suitable for crystallization purposes (Lancaster, 2003b).

## 1.4. Structural Properties of the QFR from *W. succinogenes*

### 1.4.1. The three dimensional structure of QFR from *W. succinogenes*

The 3D-crystal structures of the QFR from *W. succinogenes* (Figure 1-7) were solved from three different crystal forms, named A, B (2.20 and 2.33 Å resolution, respectively, Lancaster, *et al.*, 1999) and C (3.10 Å resolution, Lancaster, *et al.*, 2001). Very recently, a further crystal structure of this enzyme has been solved even at higher resolution (Lancaster, C.R.D., unpublished).

The complex is a type-B member of the SQORs, and consists of the hydrophilic subunits FrdA and FrdB, and a transmembrane subunit FrdC. This latter subunit, which contains the domain where the menaquinol oxidation takes place (Reaction 1-6), binds the two heme *b* groups.



**Figure 1-7: X-ray crystal structure of the *W. succinogenes* QFR.** (Lancaster, 2001a) The enzyme consists of a homodimer of a heterotrimer, consisting of flavoprotein subunit A, iron-sulfur protein subunit B, and the transmembrane diheme-containing subunit C. The C $\alpha$  traces of the two A subunits are shown in turquoise and blue, those of the two B subunits in purple and red, and those of the two C subunits in green and light blue. The atomic structures of the six prosthetic groups per heterotrimer are superimposed for better visibility. From top to bottom, there are the covalently bound FAD, the [2Fe-2S], the [4Fe-4S], the [3Fe-4S] iron-sulfur clusters, the proximal and the distal heme *b* groups. The position of the bound quinone was determined crystallographically (PDB entry code 2BS2, Lancaster, C.R.D., unpublished).

The position of the cofactors, which were previously identified by biochemical and spectroscopical techniques and then clearly resolved in the crystal structure, contributed enormously to the understanding of the catalytic mechanism of this enzyme. Based on their relative distance to the hydrophilic subunits, the heme *b* groups are referred to as the “proximal” heme  $b_p$  and the “distal” heme  $b_d$ , respectively. Thanks to the structural information available, the location of the high and low potential hemes of the *W. succinogenes* QFR have been assigned to the proximal and distal heme, respectively (Haas & Lancaster, 2004).

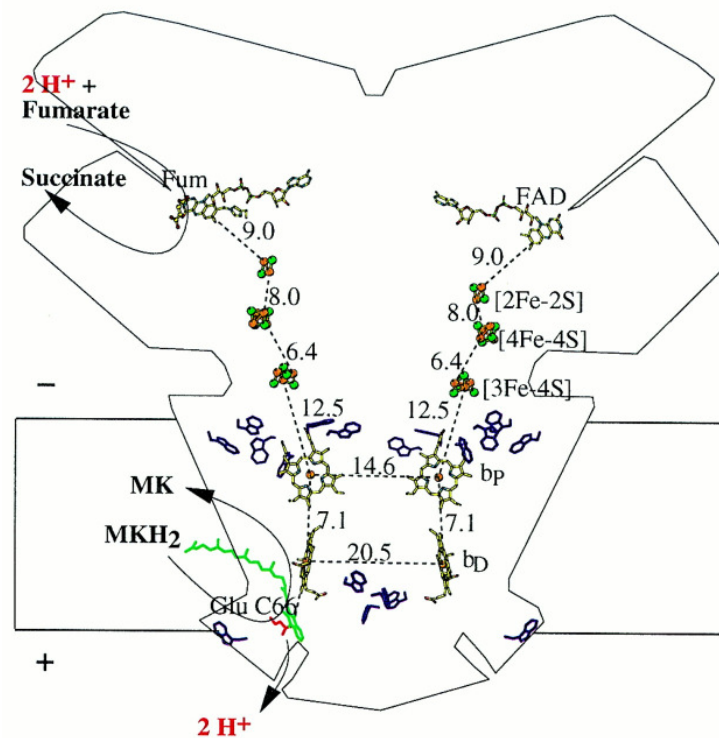
#### 1.4.2. Catalytic mechanism and electron transfer in QFR

The availability of high-resolution X-ray structures of this enzyme has contributed significantly to the understanding of the mechanism of fumarate reduction by the Sdh/Frd family of flavoproteins. The polar nature of the hydrogen bonding environment around the carboxylic groups has been suggested to polarize the fumarate. The combined effect of twisting of the substrate and electronic effects generates a positive charge at the C2 position of the fumarate, making it a candidate for nucleophilic attack from the flavin cofactor. The hydride transfer from the FAD group is compensated by protonation at the C3 position by an arginine lining the opposite side of the fumarate catalytic site.

By a combination of site-directed mutagenesis (Lancaster, *et al.*, 2000) and crystal structure analysis (Lancaster, C.R.D., unpublished) it was concluded that quinol oxidation relies on the distal heme of the *W. succinogenes* QFR, where the electrons enter the electron transfer pathway. A glutamate residue (FrdC-E66) lines a cavity which extends from the hydrophobic phase of the membrane to the periplasmic aqueous phase, and could be involved in the acceptance of the protons liberated upon oxidation of the menaquinol.

For the function of QFR, electrons have to be transferred from the quinol-oxidizing site in the membrane to the fumarate-reducing site, protruding into the cytoplasm. The linear arrangement of the cofactors in the complex (Figure 1-8) provides a straightforward pathway by which electrons could be transferred efficiently between the two sites of catalysis (Lancaster, 2004b). In accordance to what has been postulated by Page, *et al.*, 1999, the edge-to-edge distances between cofactors of each heterotrimer is sufficiently short to allow an efficient electron tunneling. However, a physiological electron tunneling between cofactors belonging to different homomers cannot be supported due to the prohibitive edge-to-edge distances (>14Å).





**Figure 1-8: Catalytic sites and electron transfer pathway of the *W. succinogenes* QFR.** (Lancaster, *et al.*, 2000) The cofactors of the QFR dimer are displayed (coordinates retrieved from the PDB entry 1QLA). Distances between prosthetic groups are edge-to-edge distances in Å. Also drawn are the side chains of Glu-C66 (in red) and of the subunit C Trp residues (violet), which are used as markers for the hydrophobic surface-to-polar transition zone of the membrane. The position of bound fumarate (Fum) is taken from PDB entry 1QLB and the tentative model of menaquinol (in green) binding was proposed in Lancaster, *et al.*, 2000. The positive (+) and negative (-) sides of the membrane are indicated.

## 1.5. The *Wolinella* Paradox and the E-Pathway Hypothesis

### 1.5.1. The *Wolinella* paradox

If menaquinol oxidation by fumarate would be coupled to the generation of an electrochemical proton gradient, the theoretical ratio of transferred protons per electron ( $H^+/e^-$ ) in physiological conditions should be far below 1, as calculated by the available free energy of the reaction<sup>b</sup> catalyzed by the QFR (Kröger, *et al.*, 2002). Accordingly, a number of

<sup>b</sup> The standard redox difference potential ( $\Delta E'_0$ ) is only -105 mV.

experiments on QFR from *W. succinogenes* in inverted vesicles (Kröger & Innerhofer, 1976a, Kröger & Innerhofer, 1976b, Kröger, 1978, Kröger, *et al.*, 1980, Mell, *et al.*, 1986, Geisler, *et al.*, 1994,) or in reconstituted proteoliposomes have permitted the examination of QFR's physiological properties and the coupling of this enzyme with the hydrogenase (Graf, *et al.*, 1985, Biel, *et al.*, 2002) or formate dehydrogenase enzymes (Uden & Kröger, 1982, Uden, *et al.*, 1983, Uden & Kröger, 1986). These electrophysiological experiments indicated that whereas the hydrogenase and formate dehydrogenase are generating a transmembrane electrochemical proton potential ( $\Delta p$ ) by a scalar proton transfer across the plasma membrane (see also ref. Jormakka, *et al.*, 2003a), the reaction catalyzed by the diheme-containing QFR from *W. succinogenes* is not directly associated with the generation of  $\Delta p$  (i.e. is an electroneutral process) (Biel, *et al.*, 2002, Kröger, *et al.*, 2002).

Nevertheless, the three-dimensional structure of this membrane protein complex (Lancaster, *et al.*, 1999) and the characterization of variant enzymes (Lancaster, *et al.*, 2000), point towards a model for quinone/quinol binding in which the redox-active Q-site is located towards the periplasmic side of the membrane anchor domain. Thus, the quinol oxidation site, where two protons are released, and the fumarate oxidation site, where two protons are consumed, are oriented towards opposite sides of the membrane (Figure 1-7). This arrangement of catalytic sites suggests that menaquinol oxidation by fumarate, as catalyzed by *W. succinogenes* QFR, is associated directly with the establishment of an electrochemical proton potential across the membrane, which is in contrast to the directly measured evidences found previously (Kröger, *et al.*, 2002, Lancaster, 2002b).

Similar structural properties have been assigned to the SQR complex from the Gram-positive bacterium *Bacillus subtilis*, whose quinol oxidizing site is also occurring at the periplasmic site of the membrane (Matsson, *et al.*, 2000). Indeed, this enzyme has been demonstrated to generate a proton potential when forced to operate as a quinol:fumarate reductase (Schnorpfeil, *et al.*, 2001).

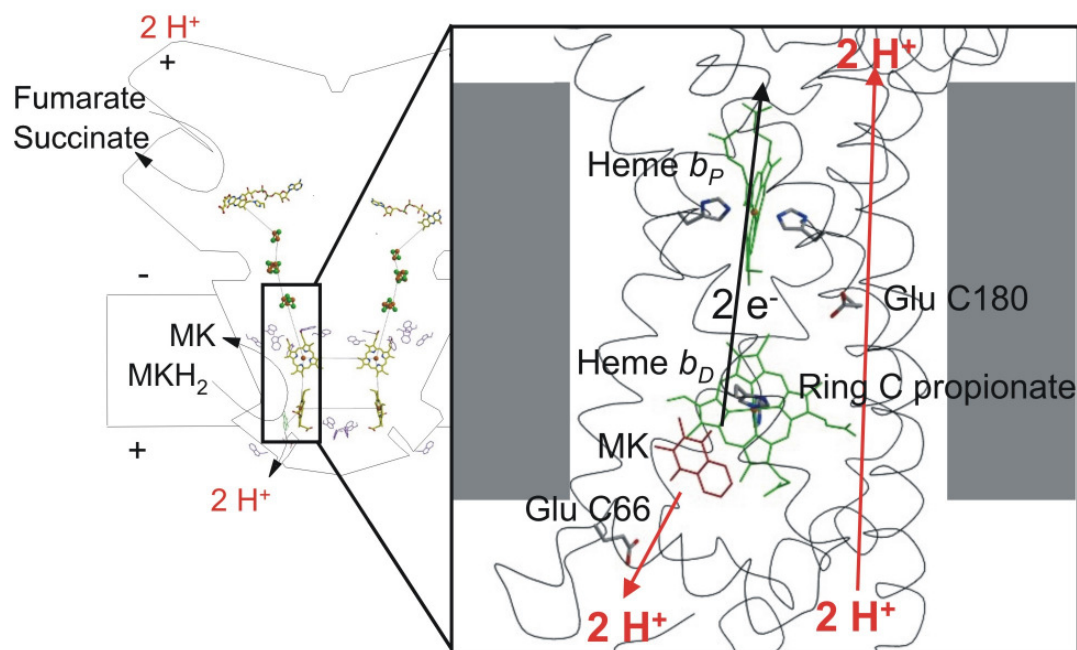
### **1.5.2. The E-pathway hypothesis of coupled transmembrane electron and proton transfer**

Prior to the "E-pathway hypothesis", proposed in a seminal article by C. Roy D. Lancaster in 2002 (Lancaster, 2002b), there was no satisfactory explanation for the apparent discrepancies stated above. According to this hypothesis, the transfer of two electrons via the two QFR heme groups is strictly coupled to a compensatory, parallel transfer of two protons across

the membrane via a proton transfer pathway (Figure 1-9), which is transiently open upon reduction of the two hemes and closed in the oxidized state of the enzyme. The most prominent constituents of the proposed pathway were suggested to be the ring C propionate of the distal heme  $b_d$  and amino acid residue Glu C180, which are both not in direct association with the quinol binding site.

The role of Glu C180 in this context is supported by two previous reports involving a combination of site-directed mutagenesis and structural and functional characterization of the enzyme (Lancaster, *et al.*, 2005) as well as electrochemically-induced FTIR difference spectroscopy (Haas, *et al.*, 2005). Moreover, in accordance with the proposed proton pathway, the FrdC-E180 residue of the *W. succinogenes* QFR is not conserved in the *Bacillus subtilis* SQR complex, which indeed catalyzes an electrogenic reaction and it is not supposed to host any compensatory proton transfer similar to the E-pathway.

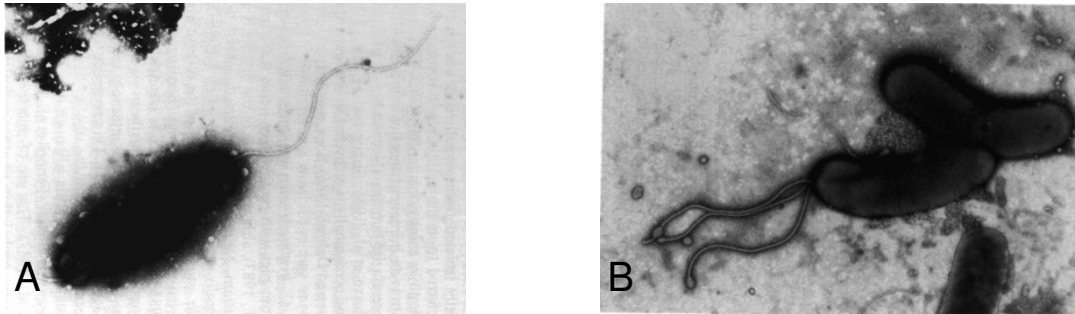
The involvement of heme propionates in a proton transfer pathway has already been proposed for the respiratory protein cytochrome *c* oxidase (Behr, *et al.*, 2000, Richter & Ludwig, 2003). Unlike most of the heme propionates found in heme *b*-containing protein structures solved so far (QFR, PDB entry 1QLA, Lancaster, 2003a; SQR, PDB entry 1NEK Yankovskaya, *et al.*, 2003; chicken  $bc_1$  complex, PDB entry 1BCC, Zhang, *et al.*, 1998; yeast  $bc_1$  complex, PDB entry 1KB9, Lange, *et al.*, 2001; nitrate reductase, PDB entry 1Q16, Bertero, *et al.*, 2003; formate dehydrogenase, PDB entry 1KQF, Jormakka, *et al.*, 2002; etc.), the ring C propionate of the *W. succinogenes* QFR distal heme does not point towards the membrane surface, but displays a peculiar conformation that points towards a region that was proposed to host the E-pathway. Furthermore, as calculated by multiconformation continuum electrostatics (MCCE), this propionate was the only one that was protonated in all simulated heme protonation states, indicating a possible role as a transient proton donor/acceptor in the E-pathway (Haas & Lancaster, 2004).



**Figure 1-9: Electron and proton transfer in the *W. succinogenes* QFR and the E-pathway hypothesis.** (Lancaster, 2002b) The prosthetic groups of the *W. succinogenes* QFR dimer are displayed (coordinate set 1QLA; Lancaster, *et al.*, 1999). Also indicated are the side chain of Glu C66 and a tentative model of menaquinol (MKH<sub>2</sub>) binding. The hypothetical transfer of one proton (H<sup>+</sup>) per electron (e<sup>-</sup>) across the membrane is shown in red. The two protons that are liberated upon oxidation of menaquinol (MKH<sub>2</sub>) are released to the periplasm (bottom) via the residue Glu C66. In compensation, coupled to electron transfer via the two heme groups, protons are transferred from the periplasm via the ring C propionate of the distal heme (heme b<sub>D</sub>) and the residue Glu C180 to the cytoplasm (top), where they replace those protons which are bound during fumarate reduction. In the oxidized state of the enzyme, the “E-pathway” is blocked. Positive and negative sides of the membrane are indicated.

## 1.6. The *Campylobacter jejuni* and *Helicobacter pylori* Species

*Campylobacter jejuni* (Wassenaar & Newell, 2001) and *Helicobacter pylori* (Dunn, *et al.*, 1997, Solnick, *et al.*, 2003) are human pathogens and are members of the  $\epsilon$ -subclass of the proteobacteria. These two bacteria are microaerophilic, Gram-negative, and flagellate species that colonize the mucous overlying the mucosal surfaces in humans and animals, and their genomic sequence is known (Parkhill, *et al.*, 2000, Tomb, *et al.*, 1997). These organisms are 2 to 5  $\mu\text{m}$  long and 0.5 to 1  $\mu\text{m}$  wide, and they typically assume a spiral or rod-like shape (Figure 1-10).



**Figure 1-10: Transmission electron micrographs of *Campylobacter jejuni* (A) and *Helicobacter pylori* species (B).** The polar flagella conferring motility are visible. (Pictures taken from Wassenaar & Newell, 2001 and Solnick, *et al.*, 2003).

### 1.6.1. *Campylobacter jejuni*: habitat and diseases

*C. jejuni* belongs to the family of the Campylobacteraceae and can colonize the mucosal surfaces of the intestinal tracts, oral cavities, or urogenital tracts of humans. It is a thermophilic organism that is also typically found in birds, whose body temperature is 42°C. In this habitat, the organism appears to act as a commensal. The microaerophilic nature and temperature dependence of this organism precludes growth outside the mucosal niches. Nevertheless, this species can be isolated from fecally contaminated environmental sources, such as surface water and animal products, including meat and milk (Wassenaar & Newell, 2001).

*C. jejuni* is very common throughout the world as it is the etiological factor for the bacterial food-borne diarrhoeal disease (Butzler, 2004, Mead, *et al.*, 1999), known as “traveler disease”. This bacterium is also responsible for gastroenteritis and a very severe disease called Guillain-Barré syndrome (GBS) (Chowdhury & Arora, 2001, (Blaser, 1997), which is an acute type of nerve inflammation involving progressive muscle weakness or paralysis. Recently, *C. jejuni* has also been found to be associated with the immunoproliferative small intestinal disease (IPSID) (Lecuit, *et al.*, 2004), a mucosa-associated lymphoid tissue (MALT) lymphoma.

### 1.6.2. *Helicobacter pylori*: habitat and diseases

The typical *H. pylori*'s niche is the mucus-lined surface of the antrum of the human stomach. Despite being able to colonize this extreme environment, where the luminal pH is around 1-2, *H. pylori* is not acidophilic, and must therefore rapidly gain access to the mucous layer where the pH is closer to neutrality (Kelly, 1998). The bacterium is most probably a neutrophile that has adapted itself to the acidic environment of the stomach and can be classified as an acid-tolerant neutrophile. The physiological strategies used to survive this environment are mainly a strong production of urease, which induces the accumulation of ammonia and carbon dioxide, providing an acid-neutralizing cloud around the cells, and production of basic amines from amino acid decarboxylates (Marais, *et al.*, 1999a). Moreover, together with a special ability in regulating the proton motive force (PMF), this bacterium adopts a mechanism that consents to mitigate the force against which protons must be extruded by concentrating cations at the cytoplasmic side. In this way, the membrane potential is inverted to a positive-inside mode (Matin, *et al.*, 1996, Marais, *et al.*, 1999a).

*H. pylori* inhabits approximately 50% of the world human population (Covacci, *et al.*, 1999, (Bardhan, 1997). After colonization of the mammalian stomach it may cause peptic ulcers, gastric atrophy, gastric MALT lymphoma (Cover & Blaser, 1999, Parsonnet, *et al.*, 1994, Hussell, *et al.*, 1993, Wotherspoon, *et al.*, 1993, Fujimori, *et al.*, 2005) and, importantly, it is associated with the development of gastric adenocarcinoma, the world's second leading cause of cancer-related death (Peek & Blaser, 2002, Uemura, *et al.*, 2001, Kuniyasu, *et al.*, 2000, Hansson, 2000, Correa, 1996, Correa, 2003a, Correa, 2003b). Finally, *H. pylori* was proposed to be weakly correlated with an increased risk of coronary heart disease (CHD), even though current results are controversial (Gaby, 2001).

Although chemotherapies for the eradication of these species are currently available, the development of more efficient, economic, and adequate drugs is needed in order to cope with the drawbacks of the therapies, especially the for the treatment of *H. pylori* infection, and with the continuous emergence of antibiotic resistance (Ge, 2002).

### 1.6.3. The QFR as a potential drug target

The quinol:fumarate reductase (QFR) has been considered a potential drug target for *H. pylori* eradication (Mendz, *et al.*, 1995). More recently, this consideration has been highly enforced by the finding that the QFR from *H. pylori* is essential for the colonization of the mouse stomach (Ge, *et al.*, 2000). In parallel, strains of *Salmonella typhimurium* lacking a functional QFR have also lost the ability to colonize murine intestine (Antje Kahnert, unpublished).

The QFR from *C. jejuni* and *H. pylori* have an identical subunit composition and operon organization compared to the *W. succinogenes* species, consisting of three concatenated open reading frames in the order *frdC*, *-A* and *-B* (Ge, *et al.*, 1997, Parkhill, *et al.*, 2000).

Although culturing these two pathogenic species is quite demanding (Kelly, 2001), homologous production of the *H. pylori* QFR has been attempted, resulting in a very low yield and minimal enzymatic activity (Birkholz, *et al.*, 1994). First attempts at heterologous production in *Escherichia coli* of the FrdA and FrdB subunits from an  $\epsilon$ -proteobacterium like *W. succinogenes* (Lauterbach, *et al.*, 1987, Lauterbach, *et al.*, 1990) achieved EPR signals of the bi- and trinuclear iron-sulfur centers of the enzyme, but did not result in the synthesis of functional proteins. Later, Ge and co-workers (Ge, *et al.*, 1997) attempted to express the entire *frdCAB* operon from *H. pylori* in *E. coli*. Nevertheless, no documentation of successful heterologous expression of a functional QFR from *H. pylori* or *C. jejuni* is available at present.

In the past it has been reported that *in vitro* treatment with some antihelmintics such as morantel, oxantel, thiabendazole (Mendz, *et al.*, 1995), and other compounds like nizatidine, omeprazole (Chen, *et al.*, 2002), metronidazole (Hoffman, *et al.*, 1996), levamisole (Smith, *et al.*, 1999), and TTFA (Grivennikova & Vinogradov, 1982) were found to have an effect on QFR enzymes from *C. jejuni* or *H. pylori*. The antihelmintics impaired cell growth in liquid cultures but the minimal inhibitory and minimal bactericidal concentrations were in the millimolar range, which is not suited for therapeutic treatment. In fact, since the succinate:quinone oxidoreductase is assumed not to be essential for growth under the conditions used for the inhibitor studies, it is likely that these antiparasitics affected other targets besides fumarate reduction (Lancaster & Simon, 2002).

## 1.7. Goals of this Work

### 1.7.1. Production, characterization, and crystallization of the QFR from the pathogenic bacteria *H. pylori* and *C. jejuni*

The QFR membrane protein complexes from the pathogens *C. jejuni* and *H. pylori* can be considered potential drug targets for the eradication of these  $\epsilon$ -proteobacteria (Ge, 2002). The development of novel chemotherapies for the eradication of these species based on drugs with new active principles is strongly needed (Ge, 2002). The possibility of creating new drugs active on the QFR from these bacteria is substantially depending on the availability of high-quality protein.

Well diffracting crystals, leading to a high-resolution crystal structure, would be helpful for a better understanding of the structure-function relationships of this protein superfamily, and for obtaining highly efficient inhibitors, for example by structure-based drug design.

Up to now, the lack of large amounts of highly pure and active QFR enzymes from *H. pylori* and *C. jejuni* (Lancaster & Simon, 2002) makes their characterization and crystallization very difficult if not impossible. Therefore, the first aim of this thesis work was to establish the successful large-scale heterologous overproduction of these enzymes.

Further, biochemical and structural studies on QFR enzymes from species other than *W. succinogenes* will be valuable for a complete understanding of this class of membrane proteins.

### 1.7.2. Investigation of the distal heme propionate and its involvement in the E-pathway hypothesis

Another aim of this study was to clarify the possible heme propionate involvement in the coupling of transmembrane electron and proton transfer as it has been suggested for *W. succinogenes* QFR in the context of the E-pathway hypothesis. The orientation of the ring C propionate (Lancaster, *et al.*, 1999) together with the results from electrostatic calculations concerning its protonation state (Haas & Lancaster, 2004) indicated that this propionate might act as a proton donor/acceptor in the proposed “E-pathway” (Lancaster, 2002b).

In principle, electrochemically induced FTIR difference spectroscopy is the appropriate method for detecting reaction-induced protonation and/or environmental changes of the heme propionates experimentally. However, unlike amino acid side chains, whose role can be investigated by site-directed mutagenesis (Haas, *et al.*, 2005), assignment of potential signals arising from heme propionates requires a different approach, such as selective  $^{13}\text{C}$



isotope labeling at the carboxy carbon positions of the heme propionates, which is expected to result in the downshift of the corresponding bands to smaller wavenumbers in the FTIR difference spectra.

Heme is composed of porphyrin, a large circular molecule made from four pyrrole rings (tetrapyrrole), whose electron pairs derived from the nitrogen atoms are coordinating an iron atom, which sits at its center. The first committed precursor in the tetrapyrrole biosynthetic pathway is 5-aminolevulinic acid (ALA). Two different routes for ALA biosynthesis are found in nature: the succinyl-coenzyme-A pathway, and the glutamate (C5) pathway (Michal, 1999). In the  $\alpha$ -group of the proteobacteria, in yeast and in mammalian cells, ALA is synthesized by a one-step condensation of succinyl-CoA and glycine along the 'Shemin' route mediated by the *hemA* gene, encoding for the ALA synthase (Warren & Scott, 1990). In higher plants, algae and many prokaryotic systems, this aminoketo acid is synthesized from the intact carbon skeleton of glutamate using the C5 pathway. This pathway involves an unusual activation of the carboxyl group by formation of Glu-tRNA<sup>Glu</sup> for the subsequent reduction to glutamate-1-semialdehyde (Kannangara, *et al.*, 1988). In a third step, 5-aminolevulinate is formed by an 'internal transaminase reaction', which transfers the amino group from the C-1 to the C-2 position. This reaction is catalyzed by the glutamate-1-semialdehyde 2,1-amino-mutase, which is encoded by the *hemL* gene. In the genome sequence of *W. succinogenes*, the *hemL* gene of the C5 pathway is readily identified, but there is no evidence for a *hemA* gene of the 'Shemin route'.

The combined approach of <sup>13</sup>C heme propionate labeling and electrochemically induced FTIR difference spectroscopy has previously been successfully employed to investigate the role of heme propionates in *Paracoccus denitrificans* cytochrome *c* oxidase (Behr, *et al.*, 1998). However, this approach involved disruption of the *hemA* gene of the 'Shemin route' rather than the disruption of the *hemL* gene of the C5 pathway as performed in the work described here.



## 2. MATERIALS AND METHODS

### 2.1. Materials

#### 2.1.1. Suppliers

Table 2-I: Supplier list.

Company	Location	Web address
Agilent Technologies	Böblingen, DE	<a href="http://www.agilent.com">http://www.agilent.com</a>
Aldrich, Sigma-Aldrich Laborchemik. GmbH	Seelze, DE	<a href="http://www.sigmaaldrich.com">http://www.sigmaaldrich.com</a>
Amersham Biosciences / Pharmacia Biotech	Freiburg, DE	<a href="http://www.amersham.com/">http://www.amersham.com/</a>
Applied Biosystems	Framingham, MA, US	<a href="http://www.appliedbiosystems.com/">http://www.appliedbiosystems.com/</a>
Avanti Polar Lipids Inc.	Alabaster, AL, US	<a href="http://www.avantilipids.com/">http://www.avantilipids.com/</a>
Beckman Coulter	Krefeld, DE	<a href="http://www.beckman.com/">http://www.beckman.com/</a>
Biometra	Goettingen, DE	<a href="http://www.biometra.de/">http://www.biometra.de/</a>
Bio-Tek Instruments GmbH	Bad Friedrichshall, DE	<a href="http://www.biotek.com/">http://www.biotek.com/</a>
Bio-Rad Laboratories GmbH	Muenchen, DE	<a href="http://www.bio-rad.com/">http://www.bio-rad.com/</a>
Biozym Scientific GmbH	Hess. Oldendorf, DE	<a href="http://www.biozym.com/">http://www.biozym.com/</a>
Branson	Danbury, CT, US	<a href="http://www.bransonultrasonics.com/">http://www.bransonultrasonics.com/</a>
Bruker	Rheinstetten, DE	<a href="http://www.bruker.de/">http://www.bruker.de/</a>
Cartesian Dispensing Systems,	Huntingdon, UK	<a href="http://www.cartesiantech.com/">http://www.cartesiantech.com/</a>
Genomic Solutions Ltd		<a href="http://www.genomicsolutions.com/">http://www.genomicsolutions.com/</a>
C/D/N Isotopes	Pointe Claire, CA	<a href="http://www.cdniso.com/">http://www.cdniso.com/</a>
DIFCO (provider: Merck)	Kansas City, KS, US	<a href="http://service.merck.de/microbiology">http://service.merck.de/microbiology</a>
Dr. Ehrenstorfer GmbH	Augsburg, DE	<a href="http://www.analytical-standards.com/">http://www.analytical-standards.com/</a>
Eppendorf	Hamburg, DE	<a href="http://www.eppendorf.com/">http://www.eppendorf.com/</a>
Eurogentec	Seraing, BE	<a href="http://www.eurogentec.com/">http://www.eurogentec.com/</a>
Fermentas	St. Leon-Rot, DE	<a href="http://www.fermentas.de/">http://www.fermentas.de/</a>
Fluka, Sigma-Aldrich	Seelze, DE	<a href="http://www.sigmaaldrich.com">http://www.sigmaaldrich.com</a>
Laborchemikalien GmbH		
GERBU Biochemical Mart	Gaiberg, DE	<a href="http://www.gerbu.de/">http://www.gerbu.de/</a>
Gilson / ABIMED, Gilson International B.V.	Bad Camberg, DE	<a href="http://www.gilson.com/">http://www.gilson.com/</a>
Glycon Biochemicals	Luckenwalde, DE	<a href="http://www.glycon.de/">http://www.glycon.de/</a>
GMI, Inc.	Ramsey, MN, US	<a href="http://www.gmi-inc.com/">http://www.gmi-inc.com/</a>
Hampton Research	Aliso Viejo, CA, US	<a href="http://www.hamptonresearch.com/">http://www.hamptonresearch.com/</a>
Hellma	Muellheim, DE	<a href="http://www.hellma-worldwide.de/">http://www.hellma-worldwide.de/</a>
Heraeus	Hanau, DE	<a href="http://www.wc-heraeus.com/">http://www.wc-heraeus.com/</a>
HI-TECH Scientific	Salisbury, UK	<a href="http://www.hi-techsci.com/">http://www.hi-techsci.com/</a>
Holzner GmbH	Nussloch, Heidelberg, DE	<a href="http://www.holzner.net/2.htm">http://www.holzner.net/2.htm</a>
H+P Labortechnik	Oberschleissheim, DE	<a href="http://www.hp-lab.de/">http://www.hp-lab.de/</a>
Jena Bioscience GmbH	Jena, DE	<a href="http://www.jenabioscience.com/">http://www.jenabioscience.com/</a>
Infors AG	Bottmingen-Basel, CH	<a href="http://www.infors-ht.com/">http://www.infors-ht.com/</a>
IKA Labortechnik	Staufen, DE	<a href="http://www.ika.de/">http://www.ika.de/</a>
Lambda Physik	Goettingen, DE	<a href="http://www.lambdaphysik.com/">http://www.lambdaphysik.com/</a>
Maag Technic AG	Duebendorf, CH	<a href="http://www.maagtechnic.ch/">http://www.maagtechnic.ch/</a>
MAGV	Rabenau, DE	<a href="http://www.magv-gmbh.de/">http://www.magv-gmbh.de/</a>
MEMMERT	Schwabach, DE	<a href="http://www.memmert.com/">http://www.memmert.com/</a>
Merck / VWR International	Darmstadt, DE	<a href="http://de.vwr.com/app/Home">http://de.vwr.com/app/Home</a>
Merck-Hitachi Ltd.	Tokyo, JP	
Mettler-Toledo GmbH	Giessen, DE	<a href="http://www.mt.com/">http://www.mt.com/</a>
Millipore	Schwalbach, DE	<a href="http://www.millipore.com">www.millipore.com</a>
Molecular Dimensions Ltd.	Soham, UK, DE	<a href="http://www.moleculardimensions.com/">http://www.moleculardimensions.com/</a>

New England Biolabs GmbH	Frankfurt/Main, DE	<a href="http://www.neb.com/">http://www.neb.com/</a>
NUNC GmbH	Wiesbaden, DE	<a href="http://www.nunc.de/">www.nunc.de/</a>
Olympus	Hamburg, DE	<a href="http://www.olympus.de/">http://www.olympus.de/</a>
Oxford Instruments	Wiesbaden, DE	<a href="http://www.oxford.de/">http://www.oxford.de/</a>
Pall	Dreieich, DE	<a href="http://www.pall.com/">http://www.pall.com/</a>
Pierce Biotechnology (Perbio Science D. GmbH)	Bonn, DE	<a href="http://www.piercenet.com/">http://www.piercenet.com/</a> <a href="http://www.perbio.com/">http://www.perbio.com/</a>
Qiagen	Hilden, DE	<a href="http://www1.qiagen.com/">http://www1.qiagen.com/</a>
Rainin Instrument LLC (Mettler-Toledo)	Giessen, DE	<a href="http://www.rainin.com/">http://www.rainin.com/</a>
Roche Diagnostics GmbH, Roche Applied Science	Mannheim, DE	<a href="http://www.roche.de/">http://www.roche.de/</a>
Riedel De Haen AG	Hannover, DE	<a href="http://www.riedeldehaen.com/">http://www.riedeldehaen.com/</a>
Roth, Carl Roth GmbH + Co. KG	Karlsruhe, DE	<a href="http://www.carl-roth.de/">http://www.carl-roth.de/</a>
SANOclav	Bad Überkingen-Hausen, DE	<a href="mailto:wolf-sanoclav-macryl@t-online.de">wolf-sanoclav-macryl@t-online.de</a>
Sartorius AG	Goettingen, DE	<a href="http://www.sartorius.de/">http://www.sartorius.de/</a>
Scientific & Educational Software	Cary, US	<a href="http://www.scied.com/">http://www.scied.com/</a>
SeqLab	Goettingen, DE	<a href="http://www.seqlab.de/">http://www.seqlab.de/</a>
Sedere (ERC)	Riemerling, DE	<a href="http://www.erc-hplc.de/">http://www.erc-hplc.de/</a>
SERVA Electrophoresis GmbH	Heidelberg	<a href="http://www.serva.de/">http://www.serva.de/</a>
Sigma-Aldrich Laborchemikalien GmbH	Seelze, DE	<a href="http://www.sigmaaldrich.com">http://www.sigmaaldrich.com</a>
SLM-Instruments, Inc.	Rochester, NY, US	
Stratagene	La Jolla, CA, US	<a href="http://www.stratagene.com/">http://www.stratagene.com/</a>
Systemec	Wettenberg, DE	<a href="http://www.systemec-lab.de/">http://www.systemec-lab.de/</a>
ThermoHybaid	Ulm, DE	<a href="http://www.thermo.com/">http://www.thermo.com/</a>
Toepffer Lab Systems	Göppingen, DE	<a href="http://www.glovebox.de/english.htm">http://www.glovebox.de/english.htm</a>
TOSOH Bioscience	Stuttgart, DE	<a href="http://www.tosohbioscience.com/">http://www.tosohbioscience.com/</a>
Vivascience	Hannover, DE	<a href="http://www.vivascience.com/">http://www.vivascience.com/</a>
Zeiss, Carl Zeiss AG	Oberkochen, DE	<a href="http://www.zeiss.de/">http://www.zeiss.de/</a>

### 2.1.2. Equipment

The equipment that have been used for the accomplishment of the experiments presented in the thesis are listed and described in more details in the following table.

**Table 2-II: Equipment list.**

Device	Type	Supplier
Äkta	Äkta Purifier 10	Amersham Biosciences
Anaerobic tent	Anaerobic glove box (Coy Laboratory Products Inc.)	Toepffer
Autoclave	V150	Systemec
Autoclave	La-VA-MCS	SANOclav
Autoclave	DSL 676-1-FD	Holzner
Centrifuge	Sigma 4K10	Sigma
Centrifuge (6x1 liter)	Avanti J20 XPI	Beckman
Centrifuge	Centrifuge 5415 D	Eppendorf
Chromatography column	LiChroCART 250-4 (LiCroSphere Si60, 5 µm, for HPLC)	Merck
Chromatography column	LiChroCART 250-10 (LiCrosorb RP-18, for HPLC)	Merck
Chromatography column	PD-10 columns, Sephadex G-25 (gel filtration)	Amersham

Chromatography columns	Plastic columns for ion exchange chromatography	Biosciences
Chromatography column	TSK-GEL G4000SW 60 cm x 21.5 mm (gel filtration)	home-made, MPIBP
Concentrators	Amicon cells, 50 ml and 250 ml capacity	TOSOH
Concentrators	centrisart I filtration, 2.5 ml tube	Millipore
Concentrators	Microcon filtration cell (Amicon)	Sartorius
Concentrators	Vivaspin, 500 µl tube	Millipore
Crystallization Robot	Synquad Dispensing System	Vivascience
		Cartesian Technologies
Cuvettes	114 QS, 5mm path (quartz)	Hellma
Degassing station		home-made, MPIBP
Digital camera	C3030 zoom	Olympus
Agarose gel imaging station	DNA gel documentation system (UV) (+ PC maxdata)	Bio-Rad
Electroporation device	Gene Pulser	Bio-Rad
Elisa reader	PowerWave X	Bio-Tek Instruments
French-press (+ chamber)	SLM-AMINCO	SLM Instrum., Inc.
HPLC instrument	LaChrom D-7000 HPLC System	Merck-Hitachi
HPLC detector	Sedex 75 ELS	Sedere
Glassware and stoppers	Anaerobic glassware and equipment	Maag Technic
IEF	ECPS 3000/150	Amersham Pharmacia
		MEMMERT
Incubator		Heraeus
Incubator	BK-600	Infors
Incubators		NUNC GmbH
Laminar flow bench	Microflow / Laminar Flow	H+P Labortechnik
Magnetic stirrer	VARIOMAG (10 lit. flasks)	IKA Labortechnik
Magnetic stirrer	RET IKAMAG	H+P Labortechnik
Magnetic stirrer	Multipoint HP VARIOMAG (multiple stirrer)	Rainin
Multipipette	(for greiner 96-well plates)	Zeiss
Optical microscope	Axiovert 35 (for cells)	Olympus
Optical microscope	SZ40 (for crystals)	Gilson / ABIMED
Peristaltic pump	Miniplus 3	Roth
pH meter	SevenEasy Mettler Toledo (for buffer)	Gilson
Pipettes	P10- P5000	Mettler-Toledo
Redox micro-electrode		Vivascience
Resin for protein washing	vivapure Q resin maxi	Beckman
Rotors	70Ti, 60Ti, 45Ti	Sorvall (GMI, Inc)
Rotors	SLA3000, GS3	Sartorius
Scaler	BL1500S	Sartorius
Scaler	R180D	Branson
Sonifier	SONIFIER 250	Kröger's lab, JWGU
Souther blotting device	Vacuum chamber + porous carrier	Agilent
Spectrophotometer	Agilent 8453 UV-visible Spectroscopy System (diode array)	Amersham Pharmacia
Spectrophotometer	Ultrospec 2100 pro (UV-VIS)	Bio-Tek Instrum., Inc.
Spectrophotometer	Power wave X (for 96-wells plates)	Bruker
Spectrometer (EPR)	Bruker spectrometer E500 or ESP300	

Speedvacuum	Concentrator 5301	Eppendorf
Thermostatic room 18°		
Thermostatic room 4°		
Thermocycler (x PCR)	T3 Thermocycler	Biometra
Ultracentrifuge	L8-60M	Beckman
Ultracentrifuge	Optima MAX UC (Benchtop)	Beckman
Vacuum blotting device	Vacugene Apparatus 2016 (Pharmacia LBK)	Amersham Pharmacia
Vacuum pumps		Biometra
Water bath	(60L culture)	home-made, MPIBP
Water bath	Julabo 5	MAGV
Water	Destamat (bi-distilled)	Heraeus
Water	Milli-Q plus	Millipore

### 2.1.3. Computing

#### 2.1.3.1. Computational equipment

The hardware that have been used for computational activities are:

- Alpha server ES40 system (Hewlett-Packard)
- Thin Client, ezConnect Connection Management Tool, version 2.0 (Neoware Systems, Inc.)
- Silicon Graphics (SGI) workstation Octane MIPS R10000 (Silicon Graphics, Inc.)
- PC computers

#### 2.1.3.2. Software

The software that have been used for computational activities are:

- Compaq Tru64 UNIX V5.1B (for the Alpha server), Linux Suse, SGI platform (IRIX64-6.5), and Windows as operative systems
- SECentral (Scientific & Educational Software), for molecular biology
- Unicorn v3.20 control system, for the control of the Äkta chromatography system (Amersham Biosciences)
- VMD 1.8.2 (University of Illinois) and PyMOL 0.96 (DeLano Scientific), for protein structure drawings
- ProDC, for hardware control and data set collection at the ESRF synchrotron
- HKL package (XDISPLAY, DENZO, and SCALEPACK, HKL research, Charlottesville, NC), for data set processing

- O, for model building: Origin 7 and KaleidaGraph 3.52, for curve fitting and graphs
- CNS (Crystallography and NMR Software) version 1.0, for refinement
- Moleman (by Gerard J. Kleywegt, Uppsala Software Factory), for manipulation of PDB-files
- Molscrip (by Per Kralius, Avatar Software AB), Bobscrip (by Robert Esnouf, Oxford University), and Raster3D (by Ethan A. Merritt, University of Washington, US) for generating high quality images of protein structures
- Other softwares: Office 2000 (Microsoft), Corel draw 10 (Corel Corporation), GIMP (GNU Image Manipulation Program, Free Software Foundation), Photoshop 6.0 (Adobe), WinDrawChem 1.6.2 (by Brian Herger), Acrobat (Adobe), EndNote 6.0 (Thomson ISI ResearchSoft), Mozilla Firefox 1.0.3 (Mozilla Foundation), Sophos Anti-Virus (Sophos Plc), SSH secure shell 2.1.0 (SSH Communication Security Ltd.)

The web-based software that have been used for the work are:

EMBL-EBI (<http://www.ebi.ac.uk/services/>)

ExPASy (<http://www.expasy.org/tools/peptide-mass.html>)

Blast (NCBI) (<http://www.ncbi.nlm.nih.gov/BLAST/>)

WebCutter 2.0 (<http://rna.lundberg.gu.se/cutter2/>)

Ovid (<http://ovid1.gwdg.de/>)

PubMed (<http://www.ncbi.nlm.nih.gov/entrez/query.fcgi>)

#### 2.1.4. Chemicals

The chemicals that have been used for the accomplishment of the experiments presented in the thesis are listed and described in more details in the following table.

**Table 2-III: Chemicals list.**

Name	Supplier
Acetonitrile, HPLC UGG	Roth
Agarose (LE)	Cambrex (Biozym)
1- <sup>13</sup> C-ALA hydrochloride (99 % purity)	(C/D/N Isotopes)
ALA (non-labeled)	Fluka
Al's oil	Hampton
Ammonium chloride (NH <sub>4</sub> Cl)	Roth

## Section 2.1: Materials

Ammonium sulfate ((NH <sub>4</sub> ) <sub>2</sub> SO <sub>4</sub> )	Roth
Anti-DIG-AP antibody	Roche
Antifoam 204	Sigma
benzamidine hydrochloride hydrate	Fluka
Bio-Beads SM-2 Adsorbent	Bio-Rad
Brain Heart Infusion	Difco
boric acid (H <sub>3</sub> BO <sub>3</sub> )	Merck
calcium chloride (CaCl <sub>2</sub> )	Merck
chloramphenicol	GERBU
chloroform, 99%	Roth
di-chloro di-methylsilane	Aldrich
cobalt chloride (CoCl <sub>2</sub> *6H <sub>2</sub> O)	Riedel De Haen
copper chloride (CuCl <sub>2</sub> *2H <sub>2</sub> O)	Riedel De Haen
CSPD kit, di-sodium 3-(4-methoxyspiro{1,2-dioxetane-3,2'-(5'chloro) tricyclo [3.3.1.1 <sup>3,7</sup> ] decan}-4-yl) phenyl phosphate	Roche
L-(+)-cysteine	Merck
DEAE-sepharose chromatography medium	Amersham Biosciences
DM, <i>n</i> -decyl-β-D-maltoside	Glycon
DMF, dimethyl formamide	Merck
DMSO, dimethylsulfoxide	Merck
EDTA, ethylene diamine tetra-acetic acid, di-sodium salt	GERBU
Ethyl acetate	Aldrich
ferrous chloride (FeCl <sub>2</sub> *4H <sub>2</sub> O)	Riedel De Haen
formic acid, sodium salt (HCOONa)	Sigma
fumaric acid	Roth
fumaric acid, disodium salt	Fluka
L-(+)-glutamic acid hydrochloride	Roth
glycerol (99.5 %)	GERBU
HEPES, 4-(2-Hydroxyethyl)piperazine-1-ethanesulfonic acid	GERBU
heptane-1,2,3-triol (>98 %)	Fluka
hydrochloridric acid (HCl)	Roth
Isopropanol (p.a.)	Roth
kanamycin	GERBU
LDAO, N-lauryl-N,N-dimethylamine-N-oxide	Fluka
lipids (synthetic lipids, see the lipid analysis chapter)	Avanti Polar Lipids
lithium chloride (LiCl)	Merck
LM, <i>n</i> -dodecyl-β-D-maltoside (cmc = 0.17 mM, Vanaken, <i>et al.</i> , 1986)	Glycon
magnesium chloride hexahydrate (MgCl <sub>2</sub> *6 H <sub>2</sub> O)	Merck
manganese chloride tetrahydrate (MnCl <sub>2</sub> *4H <sub>2</sub> O)	Merck
mediators: see mediators list, next chapter	Sigma/Aldrich/Fluka
Menaquinone-4 (MK <sub>4</sub> or VitK <sub>2</sub> )	Sigma
methanol, 99.9%	Roth
metronidazole	Sigma
morantel	Sigma
nichel chloride (NiCl <sub>2</sub> *6H <sub>2</sub> O)	Riedel De Haen
OG, <i>n</i> -octyl-β-D-glucopyranoside	Glycon
omeprazole	Sigma
oxantel	Sigma
maleic acid	Sigma



nizatidine	Sigma
PCR DIG Probe Synthesis Kit	Roche
PEG, polyethylene glycol (MME)	Hampton Research
phosphatidic acid	Fluka
orto-phosphoric acid ( $H_3PO_4$ )	Fluka
potassium hexacyanoferrate (III), $K_3Fe(CN)_6$	Sigma
di-potassium hydrogenphosphate trihydrate ( $K_2HPO_4 \cdot 3H_2O$ )	Roth
potassium di-hydrogenphosphate trihydrate ( $KH_2PO_4 \cdot 3H_2O$ )	Roth
potassium hydroxide (KOH)	Roth
potassium nitrate ( $KNO_3$ )	Roth or Merck
potassium sulfate ( $K_2SO_4$ )	Merck
Servalyt 5-8	SERVA
sodium acetate ( $CH_3COONa$ )	Roth
sodium azide ( $NaN_3$ )	Merck
sodium borohydride ( $NaBH_4$ )	Sigma
sodium chloride (NaCl)	GERBU
tri-sodium citrate dihydrate	Merck
sodium dithionite ( $Na_2S_2O_4$ )	Sigma
SDS, sodium dodecyl sulfate	GERBU
sodium hydroxide (NaOH)	GERBU
sodium molybdate ( $Na_2MoO_4 \cdot 2H_2O$ )	Riedel De Haen
sulfuric acid ( $H_2SO_4$ )	Roth
Thesit, polyoxyethylene 9-dodecyl	Boehringer Mannheim (Roche)
Thiabendazole (99 %)	Sigma
1,1,1-tri-chloroethane	Merck
Tris, tris-hydroxymethyl-9-aminomethane (99.9 %)	Roth
Triton-X 100	GERBU or Sigma
TTFA, 2-thenoyltrifluoroacetone	Fluka
Tween 20	GERBU
UM, <i>n</i> -undecyl- $\beta$ -D-maltoside	Glycon
Vitamin K1, 2-Methyl-3-phytyl-1,4-naphthoquinone (phylloquinone)	Sigma
zinc chloride ( $ZnCl_2$ )	Roth

#### 2.1.4.1. Mediators

The mediators that have been used for the titration of cofactors are listed and described in more details in the following table. The standard (pH 7.0, 25°C) redox midpoint potential ( $E_m$ ) and the solvent used for solubilization are also indicated.

**Table 2-IV: List of mediators for enzymatic titrations.** All listed mediators were purchased from Sigma/Aldrich/Fluka.

Mediator	$E_{m,7}$ vs. $H_2/H^+$	Solvent
tetrachlorobenzoquinone	+ 280	diethyl ether
N,N,N',N'-tetramethyl-phenylene-diamine	+ 270	water
2,6-dichlorophenolindophenol	+ 217	ethanol
ruthenium hexaminchloride	+ 200	water
anthraquinone-2,6-disulphonate	+ 185	water
1,2-naphtoquinone	+ 145	ethanol
anthraquinone	+ 100	ethanol
trimethylhydroquinone	+ 100	ethanol
phenazine-methosulfate,	+ 80	DMSO
5-hydroxy-1,4-naphtoquinone	+ 50	ethanol
methylene blue	+ 11	DMSO
duroquinone	+ 10	ethanol
menadione	-12	acetone
resorufin	-50	DMSO
indigotrisulfonate	-70	water
2-hydroxy-1,4-naphtoquinone	- 125	ethanol
anthraquinone-2-sulphonate	- 225	ethanol
phenosafranine	-239	DMSO
neutral red	- 307	ethanol
benzyl viologen	- 360	water
methyl viologen	- 420	water

#### 2.1.4.2. Phospholipids

The phospholipids that have been used in this work are listed in the following table. Their.

**Table 2-V: Synthetic phospholipids.** All lipids were purchased from Avanti Polar Lipids. Abbreviation name, chemical formula, composition of the fatty acid (FA) chains, and molecular weight (MW; *m*:: mostly) are also indicated.

Name	Chemical formula	MW	FA chains
1,2-di-oleoyl- <i>sn</i> -glycero-3-phosphoethanolamine (DOPE)	$C_{41}H_{78}NO_8P$	744.05	18:1, 18:1
1,2-di-palmitelaidoyl- <i>sn</i> -glycero-3-phosphocholine (PC)	$C_{40}H_{76}NO_8P$	730.02	16:1, 16:1
1,1',2,2'-tetra-oleoyl-cardiolipin (CA)	$C_{81}H_{148}O_{17}P_2Na_2$	1,502.0	18:1, 18:1
1,2-di-oleoyl- <i>sn</i> -glycero-3-[phospho- <i>rac</i> -(1-glycerol)] (DOPG)	$C_{42}H_{78}O_{10}PNa$	797.04	18:1, 18:1
1,2-di-palmitelaidoyl- <i>sn</i> -glycero-3-phosphoethanolamine (PE)	$C_{37}H_{70}NO_8P$	687.93	16:1, 16:1
1,2-di-oleoyl- <i>sn</i> -glycero-3-phosphocholine (DOPC)	$C_{44}H_{84}NO_8P$	786.15	18:1, 18:1
1,2-dipalmitoyl- <i>sn</i> -glycero-3-phosphoethanolamine (DPPE)	$C_{37}H_{74}NO_8P$	691.97	16:0, 16:0
1,2-dipalmitoyl- <i>sn</i> -glycero-3-[phospho- <i>rac</i> -(1-glycerol)] (DPPG)	$C_{38}H_{74}O_{10}PNa$	744.96	16:0, 16:0
1,2-dipalmitoyl- <i>sn</i> - glycero-3-phosphocholine (DPPC)	$C_{40}H_{80}NO_8P$	734.05	16:0, 16:0
Brain L- $\alpha$ -phosphatidylserine (Brain PS, Porcine)	$C_{42}H_{79}NO_{10}PNa$	812.05	<i>m</i> . 18:0, 18:1
L- $\alpha$ -Phosphatidylinositol (PI, Soy)	$C_{43}H_{78}O_{13}PNa$	857.05	<i>m</i> . 18:2, 16:0
1,2-di-phytanoyl- <i>sn</i> -glycero-3-phosphocholine (PC)	$C_{48}H_{96}NO_8P$	846.27	16:0, 16:0

## 2.1.5. Biological material

### 2.1.5.1. Bacterial strains and genomic DNA

*Helicobacter pylori* 26695 genomic DNA and a clinical isolated strain of *Campylobacter jejuni* were kindly provided by Dr. Stefan Bereswill. The sequence of the *frdCAB* operon from this *C. jejuni* strain was determined (double-strand) and deposited (EMBL nucleotide sequence accession number AJ628040) using the primers Cat2Cj\_seq1-20. *Wolinella succinogenes* wild type (WT) DSM 1740 (genome accession number EMBL BX571656) was employed to produce WT QFR and to create the *AhemL* mutant strain. For the production of the heterologous enzymes, a *W. succinogenes*  $\Delta$ *frdCAB* deletion mutant strain (Simon, *et al.*, 1998) ( $\Delta$ *frdCAB*) was used. All cloning steps were performed in *E. coli* JM110 and XL1-blue MRF' Kan supercompetent cells (Stratagene).

### 2.1.5.2. Oligonucleotide Primers

The oligonucleotide primers that were used for preparative PCR, analytic PCR, sequencing, and site-directed mutagenesis were synthesized by ThermoHybaid and are listed in the following tables. Table 2-IX shows the homology between the residues previously exchanged in the *W. succinogenes* QFR and those that have been here exchanged in the *C. jejuni* and *H. pylori* QFRs by using the primers listed in Table 2-XIV.

**Table 2-VI: Oligonucleotide primers used for preparative and analytic PCR.** The inserted restriction sites are indicated as underlined nucleotides. Start and stop codons are indicated as bold nucleotides.

Name	Sequence
<i>C. jejuni</i> _Fw	5'- <u>CCA TCG ATC</u> GTG AGC TTA TCG AAG GTT ATT TGG G-3'
<i>C. jejuni</i> _Rv	5'- <u>CCC CTA GGT</u> TTA TTT CTT TGA GCG ACA AGT TGT C-3'
<i>H. pylori</i> _Fw	5'- <u>CCA TCG ATC</u> AAC AAG AAG AGA TTA TAG AGG GT-3'
<i>H. pylori</i> _Rv	5'- <u>CCC CTA GGG</u> CGG CTT TTA CCC ACT TTC AAC ATC C-3'
pFrdcat2_Fw	5'- <u>CCC CTA GGT</u> <b>AAA</b> TCT CCT TGG AGC GGG GTC TCC C-3'
pFrdcat2_Rv	5'- <u>CCA TCG ATC</u> <b>ATC</b> TGT TTC CCC TGT GCA GTA TT-3'
HemL1_Fw	5'- <u>CCG GAT CCG</u> CAT CAC CCC CGA AGC CTT GGC TGT C-3'
HemL1_Rv	5'- <u>CCG AAT TCG</u> GTT AAA CGC CCA AAG TGC CAC GCC C-3'
KanM_Fw	5'-CCC CGG GCC CGG AAA GCC ACG TTG TGT CTC AAA ATC TC-3'
KanM_Rv	5'-CCC CCC ATG GGG CGC TGA GGT CTG CCT CGT GAA GAA GG-3'
HpG_probe_Rv	5'- CCT TAA CCC AGC TAG TCC GC -3'
2_Integr.check	5'-GAT TGC ACC CTC ACG CTC ATC C-3'

**Table 2-VII: Oligonucleotide primers used for sequencing.**

Name	Sequence
Cat2_seq1	5'-CTC TTA CAG TTC CAA ACT ACC-3'
Cat2_seq11	5'-CCT TTA ACA GGG GAT TCT CTA G-3'
Cat2Cj_seq2	5'-GCT TCA GGG CTT TTT TTA GG-3'
Cat2Cj_seq3	5'-GGT TGT AAG TCA TTT TAT GTG GC-3'
Cat2Cj_seq4	5'-GTG AAG CGT TCT CAC TCT GC-3'
Cat2Cj_seq5	5'-TAT TGA TAG AAT GGA AGC AG-3'
Cat2Cj_seq6	5'-ATG GAG CAT ATT CGT AAA GG-3'
Cat2Cj_seq7	5'-GAC ACA AAT GTA GTA AAA GAC-3'
Cat2Cj_seq8	5'-AGA AGG CGA AAC TTT GCC AC-3'
Cat2Cj_seq9	5'-GGA TGC AGA TCT GAG TTT TG-3'
Cat2Cj_seq10	5'-CTA GAT ATT TAC AAG ATC CGC-3'
Cat2Cj_seq12	5'-GCG GAT CTT GTA AAT ATC TAG-3'
Cat2Cj_seq13	5'-CAA AAC TCA GAT CCG CAT CC-3'
Cat2Cj_seq14	5'-GTG GCA AAG TTT CGC CTT CTA C-3'
Cat2Cj_seq15	5'-GTC TTT TAC TAC ATT TGT ATC-3'
Cat2Cj_seq16	5'-CCT TTA CGA ATA TGC TCC ATC-3'
Cat2Cj_seq17	5'-CTG CTT CCA TTC TAT CAA TG-3'
Cat2Cj_seq18	5'-GCA GAG TGA GAA CGC TTC AC-3'
Cat2Cj_seq19	5'-GCC ACA TAA AAT GAC TTA CAA CC-3'
Cat2Cj_seq20	5'-CCT AAA AAA AGC CCT GAG GC-3'
Cat2Hp_seq2	5'-CGG GCT TGA TTT TAG CGC TC-3'
Cat2Hp_seq3	5'-CTT ATT GTT TGC CGT AGA ATT GC-3'
Cat2Hp_seq4	5'-CAA GCG AGC CTT GCG AAC GC-3'
Cat2Hp_seq5	5'-ATA AAT GCT ATG GGG CGG TG-3'
Cat2Hp_seq6	5'-GAT ATT GCT ATT TTA GGG CG-3'
Cat2Hp_seq7	5'-CAA CAC GCA AAA AGT TGA AG-3'
Cat2Hp_seq8	5'-CTG AGC AAG ACA TGC CCA CG-3'
Cat2Hp_seq9	5'-AAG CGC GGT GAG TAA GCC GC-3'
Cat2Hp_seq10	5'-TGC GGG TGT TGT ATC GCT TC-3'

**Table 2-VIII: Oligonucleotide primers used for site-directed mutagenesis.** The underlined-bold triplets indicate the mutagenized amino acids (see also Table 2-IX).

Name	Sequence
Cj E64Q_Fw	5'-CTG TGG TAC ATT TTT <u>TAC</u> <b><u>AA</u></b> T TAA AAT TTG TTT ACG ATA ATC CTG-3'
Cj E64Q_Rv	5'-CAG GAT TAT CGT AAA CAA ATT TTA <u>ATT</u> <b><u>GT</u></b> A AAA AAT GTA CCA CAG-3'
Cj V162K_Fw	5'-CGG CGA TAT GTC AGG AGA TAG <u>GAA</u> <b><u>AG</u></b> T AAG TCA TTT TAT GTG GC-3'
Cj V162K_Rv	5'-GCC ACA TAA AAT GAC TTA <u>CTT</u> <b><u>TCC</u></b> TAT CTC CTG ACA TAT CGC CG-3'
Cj V162R_Fw	5'-CGG CGA TAT GTC AGG AGA TAG <u>GCG</u> <b><u>CG</u></b> T AAG TCA TTT TAT GTG GC-3'
Cj V162R_Rv	5'-GCC ACA TAA AAT GAC TTA <u>CGC</u> <b><u>GCC</u></b> TAT CTC CTG ACA TAT CGC CG-3'

Cj E179Q_Fw	5'-CTT TTA GTC TGT GTT <u>CAA</u> CTT CAT GGA AGT ATA GGG C-3'
Cj E179Q_Rv	5'-GCC CTA TAC TTC CAT GAA <u>GTT</u> GAA CAC AGA CTA AAA G-3'
Hp E66Q_Fw	5'-GTG GCG AAA TTT TTT <u>CAA</u> GGG AGC TTG TTT TTA AAA GCG G-3'
Hp E66Q_Rv	5'-CCG CTT TTA AAA ACA AGC TCC <u>CTT</u> GAA AAA ATT TCG CCA C-3'
Hp F163K_Fw	5'-GGC CTC ATG GTT CAA GCT ATC <u>GTA</u> <u>AAG</u> TAA CGC AAA ACT TTT GGC-3'
Hp F163K_Rv	5'-GCC AAA AGT TTT GCG TTA <u>CTT</u> <u>TAC</u> GAT AGC TTG AAC CAT GAG GCC-3'
Hp F163R_Fw	5'-GGC CTC ATG GTT CAA GCT ATC <u>GTC</u> <u>GCG</u> TAA CGC AAA ACT TTT GGC-3'
Hp F163R_Rv	5'-GCC AAA AGT TTT GCG TTA <u>CGC</u> <u>GAC</u> GAT AGC TTG AAC CAT GAG GCC-3'
Hp E180Q_Fw	5'-CTT ATT GTT TGC CGT <u>ACA</u> <u>ATT</u> GCA TGG CTC TAT TGG G-3'
Hp E180Q_Rv	5'-CCC AAT AGA GCC ATG CAA <u>TTG</u> TAC GGC AAA CAA TAA G-3'

**Table 2-IX: Site-directed mutagenesis performed on the *C. jejuni* and *H. pylori* *frdCAB* operons.** The residues exchanged in this thesis work are homologous to those indicated in the *W. succinogenes* QFR column.

<i>W. succinogenes</i> QFR	<i>C. jejuni</i> QFR substitution	<i>H. pylori</i> QFR substitution
FrdC-E66	FrdC-E64Q	FrdC-E66Q
FrdC-M163	FrdC-V162L	FrdC-F163L
FrdC-M163	FrdC-V162R	FrdC-F163R
FrdC-E180	FrdC-E179Q	FrdC-E180Q

### 2.1.5.3. Plasmids

The characteristics of the plasmids used and constructed in this thesis are summarized in the following table.

**Table 2-X: Plasmids used.**

Name	Characteristics	Reference
pFrdcat2	Derivative of pSC101. <i>E. coli</i> low copy number vector. Contains the chloramphenicol resistance ( <i>cat</i> ), a truncated kan resistance, <i>lacZ'</i> , SC101 replicon, <i>W. succinogenes</i> wild type <i>frdCAB</i> operon including promoter and terminator sequences.	Simon, <i>et al.</i> , 1998
pCatCj4	Derivative of pFrdcat2. The <i>W. succinogenes</i> wild type <i>frdCAB</i> operon is replaced by the <i>C. jejuni</i> <i>frdCAB</i> operon.	This work
pCatHpG8	Derivative of pFrdcat2. The <i>W. succinogenes</i> wild type <i>frdCAB</i> operon is replaced by the <i>H. pylori</i> <i>frdCAB</i> operon.	This work
pBR322	Contains the tetracycline resistance, ampicillin resistance.	Bolivar, <i>et al.</i> , 1977
pBRH01	Derivative of pBR322, contains the <i>W. succinogenes</i> <i>hemL</i> gene.	This work
pBRΔH01	Derivative of pBR322, contains the <i>W. succinogenes</i> disrupted <i>hemL</i> gene.	This work

### 2.1.5.4. Enzymes

Taq polymerase 'Expand Long Template PCR System' (Roche) was used for long-template preparative PCR, whereas Taq polymerase GoldStar (Eurogentec) was used for analytical short template PCR. Restriction and modification enzymes were obtained from Fermentas.

### 2.1.6. Media and growth conditions

*W. succinogenes* was grown in minimal or rich medium (addition to the minimal medium of Brain Heart Infusion, Difco) with formate, as electron donor, and fumarate or nitrate as electron acceptors (Table 2-XI, Table 2-XII and Table 2-XIII) (Bronder, *et al.*, 1982, Lorenzen, *et al.*, 1993). The media were made anaerobic in gastight bottles by repeated vacuum-nitrogen cycles. Large-scale protein production was performed in 60 liters anaerobic medium containing the required additives and 200 µl antifoam. Maintenance of *W. succinogenes* strains was accomplished in 10 ml culture gastight vials that were stored at 4°C up to 1-2 months. For the aminolevulinate-auxotrophic strain, 1 mM ALA or 0.2-0.4 mM 1-<sup>13</sup>C-ALA (Figure 2-1) was supplied. *W. succinogenes* cultures contained, when required, kanamycin and chloramphenicol at a concentration of 25 and 12.5 mg/l, respectively. These concentrations were doubled (50 and 25 mg/l) in *E. coli* Luria-Bertani cultures.

**Table 2-XI: Formate – fumarate 10x (A) and formate – nitrate pre-medium 20x (B).**

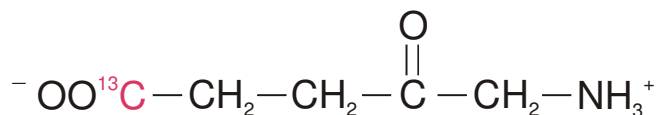
A		B	
Tris	0.5 M	Tris	1 M
KOH	2 M	Sodium formate	1.6 M
Fumaric acid	0.9 M	KNO <sub>3</sub>	0.8 M
Sodium formate	1 M	K <sub>2</sub> HPO <sub>4</sub>	20 mM
K <sub>2</sub> HPO <sub>4</sub>	200 mM	K <sub>2</sub> SO <sub>4</sub>	100 mM
(NH <sub>4</sub> ) <sub>2</sub> SO <sub>4</sub>	50 mM	Fumaric acid	100 mM
NH <sub>4</sub> Cl	50 mM	Adjust pH	7.5
CH <sub>3</sub> COONa x 3H <sub>2</sub> O	200 mM	Trace elements	2x
Glutamic acid	10 mM		
Adjust pH	7.9-8.0		
Trace elements	1x		

**Table 2-XII: Formate – fumarate (A) and formate – nitrate medium (B).**

A		B	
Pre-medium	1x	Pre-medium	1x
Ca-Mg solution	1x	Ca-Mg solution	4x
Brain Heart Infusion	13 g/l	Brain Heart Infusion	13 g/l
Adjust pH	7.9-8	Adjust pH	7.5
Degas and autoclave		Degas and autoclave	
		Add cys-glu solution prior to inoculation	

**Table 2-XIII: Trace elements solution 500x (A); cysteine – glutamate (cys-glu) solution 100x (B); calcium – magnesium solution 1000x (C).**

A		B		C	
Na <sub>2</sub> EDTA x 2H <sub>2</sub> O	5.2 g/l	Glutamic acid	10 g/l	CaCl <sub>2</sub> x 2H <sub>2</sub> O	7.4 g/l
FeCl <sub>2</sub> x 4H <sub>2</sub> O	1.5 g/l	L-cysteine x HCl	10 g/l	MgCl <sub>2</sub> x 6H <sub>2</sub> O	51 g/l
ZnCl <sub>2</sub>	0.07 g/l	Adjust pH	7.0		
MnCl <sub>2</sub> x 2H <sub>2</sub> O	0.1 g/l	Degas and autoclave			
H <sub>3</sub> BO <sub>3</sub>	0.062 g/l				
CoCl <sub>2</sub> x 6H <sub>2</sub> O	0.190 g/l				
CuCl <sub>2</sub> x 2H <sub>2</sub> O	0.017 g/l				
NiCl <sub>2</sub> x 6H <sub>2</sub> O	0.024 g/l				
Na <sub>2</sub> MoO <sub>4</sub> x 2H <sub>2</sub> O	0.036 g/l				

**Figure 2-1: Chemical structure of the 1-<sup>13</sup>C-5-aminolevulinate.** The isotopically labeled carbon (<sup>13</sup>C) is indicated in red.

## 2.2. Molecular Biology/Genetics

### 2.2.1. Standard methods

Agarose gels for DNA gel electrophoresis were prepared using LE agarose. Plasmid extractions from *E. coli* (maxi- and mini-prep) and DNA extraction from agarose gels were carried out using Qiagen kits. The DNA ligations were performed with T4 DNA Ligase overnight at 16°C. Genomic DNA preparation from *W. succinogenes* was performed using the

DNeasy Tissue Kit (Qiagen). DNA sequencing was performed according to Sanger *et al.* (Sanger, *et al.*, 1977) and provided by SeqLab. DNA quantification was accomplished spectrophotometrically and by agarose gel electrophoresis with the help of a calibrated molecular mass standard (1 kb DNA molecular mass standard, New England Biolabs). *E. coli* supercompetent cells were transformed as indicated in the kit (Stratagene). The DNA manipulations not described here were performed using standard protocols, as described by Sambrook *et al.* (Sambrook, *et al.*, 1989). Site-directed mutagenesis on the FrdC subunit was performed with the use of one of the oligonucleotide primer couples Cj E64Q, Cj V162K, Cj V162R, Cj E179Q for the mutation of the pCatCj4 construct, and Hp E66Q, Hp F163K, Hp F163R, Hp E180Q for the mutation of the pCatHpG8 construct. The method (QuickChange II site-directed mutagenesis kit, Stratagene) is based on PCR-based amplification of the mutated plasmids and digestion by the *DpnI* restriction enzyme, which digests the parental methylated and hemimethylated DNA strands. Subsequently, transformation of *E. coli* will repair the nick and clone the new plasmid with the desired mutation(s).

### **2.2.2. Transformation of *W. succinogenes***

Transformation of *W. succinogenes* (Simon, *et al.*, 1998) was carried out by electroporation in an anaerobic tent. A fresh 10 ml formate/nitrate rich medium was inoculated and incubated at 37°C until an OD<sub>578</sub> of ~0.3 was reached. The cells were then spun down and resuspended in 10 ml sterile sucrose (0.3 M). After a second centrifugation, the sucrose solution was decanted until ~50 µl were left. The cells were then resuspended, mixed with 5-10 µg of dialyzed ("V" Series Membranes, Millipore) plasmid and set on ice. Five minutes later, the mixture was placed in an electroporation cuvette and pulsed (800 ohm, 25 µFD, 1.25 kV, time constant). Immediately after the pulse, 1 ml of cold fresh medium without antibiotic was added. The culture was transferred into a new tube together with 9 ml of fresh medium and incubated at 37°C for ~10 hours. The longer incubation and the larger volume of fresh medium are modifications from the method established by Simon, *et al.*, 1998. The cells were finally spun down and plated on Petri dishes with an agar formate/nitrate rich medium containing the required selective antibiotics. The growing colonies (usually in 2-3 days) were isolated and inoculated in a fresh formate-nitrate liquid medium without any antibiotic, and screened for the right genomic insertion by PCR. Oligonucleotide primers were designed so that only a locus-specific genome insertion could give a signal by using 2\_Integr.check



primer and a specific reverse primer (CatCj\_seq19 or HpG\_probe\_Rv). PCR-positive clones were re-inoculated in a rich formate-fumarate medium and stored at 4°C.

### 2.2.3. Southern blotting

Southern blotting was performed as described (Southern, 1975, Simon, *et al.*, 1998). The genomic DNA (2 µg) of *W. succinogenes* was digested with the restriction enzyme HindIII and run into an agarose gel. The gel was then placed on a nylon membrane (Biodyne B transfer membrane, Pall) and laid on a porous carrier of an aspirating vacuum-blotting device. The digested DNA was transferred to the nitrocellulose by adding i) SB buffer 1 (depurination step); ii) SB buffer 2 (denaturation step); iii) SB buffer 3 (neutralization step); iv) SB SSC (1x) buffer. The DNA was then fixed to the membrane by incubation at 121°C for 30 minutes. Rinsing of the membrane with SB SSC buffer was followed by a pre-hybridization at 68°C with the hybridization buffer for one hour. Previously, digoxigenin-labeled probes were made for the upstream (QFR locus) and downstream region (*cat* locus) using the PCR DIG Probe Synthesis Kit and the primers CatCj\_seq8 and CatCj\_seq12 (800 bp fragment) for the *C. jejuni frdCAB* and *H. pylori\_Fw* and HpG\_probe\_Rv (500 bp fragment) for the *H. pylori frdCAB*. The probe was added to the hybridization buffer, boiled for 10 min, shock-frozen in liquid N<sub>2</sub> and finally thawed on ice. The membrane underwent hybridization in an oven at 68°C overnight by mixing it with the prepared digoxigenin-labeled probe inside a rolling tube. After hybridization, the membrane was washed twice with 2x SSC + 0.1 % SDS at RT, and subsequently twice with 0.1x SSC + 0.1 % SDS at 68°C for 15 min. The membrane was then washed with the SB detection wash buffer for 5 min and with SB detection 2 buffer for 30 min. The anti-DIG-AP was mixed with the SB detection 2 buffer and left binding to the membrane. The membrane was washed with SB detection 3 buffer and the CSPD solution was added. After washing off the CSPD solution with water and with the stripping solution, the labeled DNA fragments were detected with a radiography film (Kodak).

**Table 2-XIV: Southern blotting buffers and instructions.**

Buffer name	Ingredients
SB buffer 1	0.25 M HCl
SB buffer 2	1.5 M NaCl, 0.5 M NaOH
SB buffer 3	1 M Tris, 2 M NaCl, pH 5.0
SB SSC (20x)	3 M NaCl, 0.3 M sodium citrate*2H <sub>2</sub> O, pH 7.0
SB hybridisation	5x SSC, 1 % blocking reagent, 0.1 % <i>n</i> -lauryl sarkosin (Na), 0.02 % SDS
SB detection 1	100 mM maleic acid, NaCl 150 mM, NaOH to pH 7.0 (autoclave)
SB detection wash	SB detection 1 + 0.3 % Tween 20
SB detection 2	SB det. 1 + Blocking Reagent (Roche), dissolve at 68°C, autoclave, store at 4°C
SB detection 3	100 mM Tris, 100 mM NaCl, HCl to pH 9.5
Stripping solution	0.2 M NaOH, 0.1 % SDS

### 2.3. *W. succinogenes* Growth Curves and Membrane Preparation

Growth of *W. succinogenes* strains was tested in triple-trial in rich and minimal media (50 or 250 ml) and doubling times were calculated by measuring absorbance at 578 nm every one or two hours until the stationary phase was reached. Membranes of *W. succinogenes* were prepared by harvesting the cells by centrifugation at late-exponential phase and resuspending in a buffer containing 50 mM Tris (pH 7.8), 2 mM malonate, 1 mM EDTA. The cells were then resuspended using a grinder and physically disrupted by a French press at 130 MPa. Afterwards, the membranes were isolated by ultracentrifugation (100'000 g, 45 min, 4°C).

### 2.4. Large-Scale Protein Production and Purification

#### 2.4.1. Heterologous QFR production and purification

The expression of QFR for large-scale preparation consisted of a culture of *W. succinogenes* in 60 liters formate/fumarate anaerobic rich medium containing 12.5mg/l chloramphenicol. After inoculation (with a 240 ml preculture), the culture was incubated for approximately 12-15 hours at 37°C until late exponential phase. As described earlier, the cells were harvested by centrifugation (with a centrifuge Avanti J20 XPI), homogenized, disrupted, and the membranes were isolated by ultracentrifugation (see previous section).

#### 2.4.1.1. Membrane protein solubilization

The pelleted membranes were resuspended in Tris-acetate (50 mM, pH 7.8), 1 mM DTT, and 2 mM malonate buffer with Triton X-100 at a detergent:membrane protein ratio of 1:1 (w/w)<sup>c</sup>. After stirring for one hour in anaerobic conditions at room temperature (RT), the solubilized membrane proteins were isolated by a second step of ultracentrifugation (100'000 g, 45 min, 4°C). The supernatant, containing the solubilized membrane proteins, was collected and kept on ice.

#### 2.4.1.2. DEAE-sepharose anion exchange

The solubilized membrane proteins were loaded into a DEAE-sepharose column (~400 ml bed volume), which was previously equilibrated with the Tris-malonate buffer plus 0.05 % Triton X-100, and washed with two bed volumes of equilibration buffer. A linear NaCl gradient (0-300 mM) in this buffer was applied to the column and the eluate was collected in ~10 ml fractions. QFR eluted at a NaCl concentration of about 100-120 mM. A first indication of the presence of QFR was obtained by observing the color of the eluted fractions. The amount of fumarate reductase activity present in each fraction was then precisely calculated via the "MB assay" (see below section 2.5.7.1). The salt concentration present in the protein sample after elution was halved using a pressure dialysis concentrator (Amicon) with a membrane cut-off of 100 kDa. Subsequently, the protein solution was re-loaded into a smaller (~60 ml capacity) DEAE-sepharose column in order to exchange the detergent from TritonX100 to a mixture of 0.05 % decyl- $\beta$ -D-maltoside (DM) and 0.05 % dodecyl- $\beta$ -D-maltoside (LM). The enzyme was eluted from this second anion exchange chromatography column with a NaCl-containing (200 mM) Tris-malonate buffer. The high salt concentration of the sample was diluted to 10-14 mM with the use of a second smaller pressure dialysis concentrator (Amicon) with a membrane cut-off of 100 kDa.

#### 2.4.1.3. Preparative isoelectric focusing

The isoelectric focusing gel was prepared by mixing 0.01% (w/v) LM, 0.1% (w/v) DM, 2 % ampholyte solution with a pH range 5-8 (servalyt, SERVA), and 8 g of Ultrodex (Amersham Pharmacia) in 200 ml water, poured onto the electrofocusing flatbed and dried at 60°C until

---

<sup>c</sup> As a rule of thumb, the amount of membrane proteins was estimated to be one twentieth of the cell mass weight.

30 % water evaporation was reached. A maximum of 200 mg of highly concentrated protein (>20 mg/ml) was loaded onto the gel, which was situated on a thermostatic plate at 4°C. A power of 16 W was applied to the gel for at least 8 hours. After isoelectric focusing, the protein was extracted from the gel with a buffer containing 20 mM HEPES (pH 7.3), 1 mM EDTA, 0.01% (w/v) LM, 0.1% (w/v) DM and either 2 mM malonate or 20 mM fumarate in those samples subjected to crystallization trials and concentrated with Centriscart I micro-concentrators (100 kDa cut-off) up to 20 mg/ml. In order to remove the ampholytes, the sample was subjected to a gel filtration step on PD-10 columns. The re-concentrated samples were either further purified by gel filtration or shock frozen with liquid N<sub>2</sub> and stored at -77°C.

#### **2.4.1.4. Gel filtration**

In order to improve the purity and homogeneity of the sample, a further purification step was introduced by performing gel filtration at 4°C on a TSK-GEL G4000SW column 60 cm x 21.5 mm (200 ml bed volume, TOSOH Bioscience) on an Äkta Purifier 10. After equilibration with at least one bed-volume of the previously used buffer, the protein was loaded into the column at a flow speed of 3 ml/min, and the QFR eluted at a volume equal to ¾ of the bed volume. Due to the capacity of this column (up to 20 mg of protein), multiple cycles were consecutively performed by washing with two bed volumes between one cycle and the next. Only the fractions (0.8 ml volume each) that appeared to contain pure QFR were collected. Subsequently, the pooled fractions underwent concentration by Centriscart I (cut-off 100 kDa), shock freezing with liquid N<sub>2</sub> and storage at -77°C. These samples were used for crystallization and analytical ultracentrifugation analysis.

#### **2.4.2. Production of the *W. succinogenes* QFR containing <sup>13</sup>C-labeled heme propionates**

A mutant strain of *W. succinogenes* lacking the *hemL* gene (N2 strain, see work in section 3.2.1) was pre-inoculated overnight in minimal medium supplemented with 0.4 mM <sup>13</sup>C-labeled ALA. Using this pre-culture the 60 liters minimal medium containing 0.2 mM <sup>13</sup>C-labeled ALA were subsequently re-inoculated at an inoculum to fresh medium volume ratio of 1:50. Cells were harvested by centrifugation at late exponential phase after 24 to 30 hours. QFR isolation (up to isoelectric focusing) was performed as described above. The samples subjected to FTIR spectroscopy analysis were washed and concentrated to 1.0-1.5 mM in 100

mM potassium phosphate (KP) buffer at pH 7 containing 100 mM KCl as supporting electrolyte and 1 mM DM as detergent. The final sample concentration was adjusted in Vivaspin concentrators (500  $\mu$ l capacity, 100 kDa cut-off).

## 2.5. Protein Characterization

Detection of covalently bound FAD was carried out on SDS-polyacrylamide gels containing 5-10  $\mu$ g protein. After electrophoresis, the gel was treated for 10 min with 10 % acetic acid, washed with water, and irradiated with UV light (Uندن, *et al.*, 1980).

The concentration of heme *b* in the sample was determined by looking at the difference spectrum “reduced-minus-oxidized” redox states derived from spectra of the enzyme treated respectively with dithionite or  $K_3Fe(CN)_6$  ( $\Delta\text{Abs}_{563-575}$ ,  $\epsilon = 23.4 \text{ mM}^{-1} \text{ cm}^{-1}$  (Kröger & Innerhofer, 1976a). Alternatively, determination of heme *b* concentration was calculated from the absorbance at 415 nm (Soret-band), using an extinction coefficient of  $139.1 \text{ mM}^{-1} \text{ cm}^{-1}$  each heme. An Agilent 8453 spectrophotometer was used for spectrophotometric measurements.

The total protein concentration was measured using BSA as a standard with the bicinchoninic acid assay (BCA assay, Pierce) (Smith, *et al.*, 1985) in a multi-well reader Power-wave-X spectrophotometer.

SDS polyacrylamide gel electrophoresis (12.5% w/v acrylamide) was carried out as described (Laemmli, 1970), using Coomassie blue for staining and Prestained Protein Marker (6-175 kDa, New England Biolabs) as a molecular mass standard.

### 2.5.1. Oxidation-reduction (“redox”) titration of FAD and iron-sulfur clusters and detection by EPR spectroscopy

The experimental work of FAD and iron-sulfur cluster titration and detection by EPR spectroscopy was carried out in collaboration with Dr. Fraser MacMillan and Dr. Klaus Zwicker. The titration of the redox states of the QFR's FAD and iron-sulfur clusters from *W. succinogenes*, *C. jejuni* and *H. pylori* was performed essentially as described by Dutton (Dutton, 1978). A solution of purified protein (60-75  $\mu$ M) was stirred at 298K in an anaerobic reaction vessel. The following redox mediators were added to the protein solutions: tetramethyl-phenylene-diamine, phenazine-methosulfate, methylene blue, menadione, resorufin, indigotrisulfonate, 1,2-naphthoquinone, 2-hydroxy-1,4-naphthoquinone,

phenosafranine, benzyl viologen, and methyl viologen, resulting in a final concentration of 35  $\mu\text{M}$  each. The redox potential of the solution was monitored by a redox micro-electrode and adjusted to selected values by addition of small aliquots of a 50 mM sodium dithionite solution. At appropriate redox potentials, 80  $\mu\text{l}$  aliquots of protein sample were anaerobically transferred into an argon flushed EPR tube, frozen at  $\sim 120\text{K}$  in a cold isopentane/methylcyclohexane mixture (5:1) and stored in liquid nitrogen. The degree of reduction of individual redox centers was monitored by cw-EPR spectroscopy under non-powersaturating conditions, using a Bruker spectrometer E500 or ESP300 (Bruker) equipped with a continuous flow liquid helium cryostat (Oxford Instruments) set at 50K and 10K for the FAD and iron-sulfur clusters, respectively. The conditions adopted are listed in Table 2-XV. Due to overlapping signals arising from FAD and mediators, the FAD titration data were normalized by subtracting the EPR intensities generated by titration of a protein-free solution of buffer and mediators. FAD redox midpoint potentials were calculated by fitting with a double Nernst equation (Equation 2-1, Hägerhall, *et al.*, 1999, Sato-Watanabe, *et al.*, 1995). From the experimental conditions, an error/approximation of about  $\pm 10$  mV can be considered. Radical formation of FAD was quantified by calculating the ratio of the integrated areas of the maximum intensity peak obtained from FAD and the iron-sulfur cluster S1 (fully reduced). The titrations of the iron-sulfur clusters were fitted with the Nernst equation (Equation 2-2).

**Table 2-XV: EPR spectroscopy parameters used for the measurement of the QFR cofactor's radical species.**

Radical species:	FAD	S1 and S3	S2
Temperature (K)	50	10	10
Microwave power (dB/mW)	20/2	20/2	3/100
Amplitude (Gpp)	2	2	10
Modulation frequency (kHz)	100	100	100

$$Abs = I_{\max} \times \left\{ 1 + 10^{[(E_h - E_{m1}) \times 16.89]} + 10^{[(E_{m2} - E_h) \times 16.89]} \right\}^{-1}$$

**Equation 2-1: Double Nernst equation for the calculation of the oxidation-reduction (redox) midpoint potential values of the FAD.** Parameters: Abs, absorbance;  $I_{\max}$ , max absorbance intensity;  $E_h$ , redox potential (V);  $E_{m1}$ , redox midpoint potential of the first electron reduction;  $E_{m2}$ , redox midpoint potential of the second electron reduction.

$$Abs = I_{\max} \times \left\{ 1 + 10^{[(E_h - E_m) \times 16.89]} \right\}^{-1}$$

**Equation 2-2: Nernst equation for the calculation of the redox midpoint potential values of the iron-sulfur clusters.** Abs, absorbance;  $I_{\max}$ , max absorbance intensity;  $E_h$ , redox potential;  $E_m$ , redox midpoint potential.

### 2.5.2. Electrochemistry and FTIR/VIS-spectroscopy

For both FTIR and vis-spectroscopy, the QFR sample in phosphate buffer (100 mM, pH 7), containing 100 mM KCl and 1.0 mM LM was concentrated to approximately 1.0 mM by using a 100 kDa Microcon filtration cell. The experimental work of heme titration by vis-spectroscopy (Lancaster, *et al.*, 2000) and the FTIR-spectroscopy analysis (Haas, *et al.*, 2005) was carried out in an ultra-thin-layer spectroelectrochemical cell by Alexander Haas (Haas, 2004).

The redox midpoint potentials of heme  $b_H$  (high potential) and heme  $b_L$  (low potential) were obtained using a double Nernst equation (Equation 2-3). The error in the determination of the midpoint potentials can be estimated to be  $\pm 10$  mV.

$$Abs = I_{\max L} \times \left\{ 1 + 10^{[(E_h - E_{mL}) \times 41.72]} \right\}^{-1} + I_{\max H} \times \left\{ 1 + 10^{[(E_h - E_{mH}) \times 41.72]} \right\}^{-1}$$

**Equation 2-3: Double Nernst equation for the calculation of the heme redox midpoint potentials.** Absorbance intensities are always referred to a reference spectrum (see text). Abs, absorbance;  $E_h$ , redox potential; L, low potential (distal) heme; H, high potential (proximal) heme;  $I_{\max}$ : max absorbance intensity;  $E_m$ , redox midpoint potential.

### 2.5.3. Mass spectrometric analysis of hemes

The heme  $b$  cofactors were extracted (Lubben & Morand, 1994) from the purified labeled and unlabeled QFR. A volume of 50  $\mu$ l of QFR sample at a concentration of about 20 mg/ml was thoroughly mixed with 0.45 ml of an acetone/HCl mixture (19:1, v/v) in clean glass tubes (washed with acetone, or chromic mix etc.), kept at RT for 20 min, and centrifuged (5000 g, 2 min). The supernatant was treated with 1 ml of ice-cold water and 0.3 ml of ethyl acetate.

After thoroughly vortexing and centrifuging, the supernatant underwent another cycle of extraction with 0.3 ml of ethyl acetate. After solvent evaporation in a speed-vacuum, the extracted hemes were re-dissolved in 50  $\mu$ l acetonitrile. The measurements at the MALDI TOF mass spectrometer were carried out by Dr. Ute Bahr, in the department of Prof. Michael Karas, and described in Mileni, *et al.*, 2005a.

#### **2.5.4. Native quinone quantification**

The native quinone quantification was performed as described (Unden, 1988). The menaquinone (MK<sub>6</sub>) and methyl-menaquinone (MMK<sub>6</sub>) were extracted by adding the protein (1 volume, aqueous solution) to a solvent mixture 1:1 of methanol and petroleum benzine (2 volumes + 2 volumes), and vigorously shaking at 37°C for 15 min. After adding acetone (2 volumes), the shaking step was repeated. The two phases were then left for 10 min on ice and subsequently centrifuged (3000 g, 5-10 min). The organic solvent, which contained the dissolved quinones was then evaporated and replaced by a mixture of acetonitrile/isopropanol in a ratio of 6.5:3.5 and loaded into a HPLC column (LiChroCART 250-10, LiChrosorb RP-18 column, Merck) for separation and quantification with a UV detector. The standard curve was derived from a commercially available menaquinone MK<sub>4</sub> (Vitamin K<sub>2</sub>).

#### **2.5.5. Lipid analysis**

##### **2.5.5.1. 2D thin layer chromatography (TLC)**

Approximately 3  $\mu$ l of enzyme sample (15-20 mg/ml) after IEF or after gel filtration was applied to thin layer silica plates (Kieselgel 60, Merck). The mobile phase of the first-dimension migration was a mixture of 13 ml chloroform, 5 ml methanol and 0.8 ml water. The mobile phase of the second-dimension migration was a mixture of chloroform, methanol, and 25 % ammonia (13:7:1 v/v/v). A non-specific staining was carried out at first with iodine vapor and the developed smears were marked with a pencil. Subsequently, the TLC plates underwent specific staining by spraying either with a solution 1.3 % molybdenum oxide in 4.2 M sulfuric acid, for staining of phosphorous-containing compounds; or with  $\alpha$ -naphthol (0.05 g dissolved in 10 ml methanol-water 1:1) for glycolipid staining; or with ninhydrin (1 g dissolved in 100 ml acetone), for the staining of nitrogen-containing compounds. Up to 5  $\mu$ mol of synthetic lipids (sodium salts, Avanti Polar Lipids,



Table 2-V) were applied on the standard TLC plates. In the case of the standard calibration assay, the 2 dimensions were tested separately in two different plates.

#### **2.5.5.2. MALDI TOF mass spectrometry**

Analysis of lipids by mass spectrometry (MS) was attempted on IEF-purified QFR samples adopting three different approaches depending on the level of lipid isolation. The measurements were performed by Dr. Ute Bahr and Prof. Michael Karas.

##### **2.5.5.2.1. Whole protein analysis**

The protein sample was diluted in a buffer (pH 7.4) containing 10 mM Tris-HCl, 2 mM fumarate and 0.03 % LM. Up to 10 pmol of protein were loaded into the mass spectrometer, either directly after dilution or mixed with acetonitrile to a ratio of 1:1 (Distler, *et al.*, 2004).

##### **2.5.5.2.2. Methanol-chloroform extraction**

In this procedure (Patton & Robins, 1998, Folch, *et al.*, 1957) one volume of the protein sample (10-20 mg/ml) was treated with 19 volumes of a chloroform/methanol (2:1 v/v) mixture, saturated with nitrogen, shaken vigorously and sonified. After adding 0.2 volumes of 0.9 % NaCl and shaking, the biphasic mixture was centrifuged (2000 g, 10 min). The upper phase (methanol/water) was discarded and the lower phase (chloroform) was transferred by a glass Pasteur pipette into a new tube, concentrated (speed-vacuum) and used for MS, or stored at -20°C. Every step was carried out with glass tools and in glass tubes.

##### **2.5.5.2.3. Lipid isolation by TLC**

The hydrophobic substances isolated by TLC and appearing as smears in the TLC plate were removed by selectively scraping these silica patches and collecting the material in a glass tube. The lipids contained in the collected silica gel were separated by extraction with a chloroform/methanol (2:1 v/v) mixture. This sample was concentrated by evaporation (speed-vacuum) and used for MS analysis. Tandem MS-MS was performed on the prominent peaks appearing in the 600-1700 Da range.

### 2.5.5.3. High pressure liquid chromatography

The protein sample underwent methanol-chloroform extraction as described above. The automatic sampler loaded 15  $\mu$ l of the extracted portion into a LaChrome HPLC coupled to a Sedex 75 ELS detector. The HPLC chromatography column (LiCroSphere Si60) could separate lipids with different polar head groups using a gradient of two solvent mixtures of chloroform, methanol and 32 % ammonium hydroxide (90:10:1 and 20:80:1, respectively). Typical operating pressures ranged from 80 to 95 bars (1 ml/min flow). Prior to every experiment, standard calibration was accomplished by making a pair of runs with a chloroform-dissolved standard mixture of cardiolipin, phosphatidylethanolamine, phosphatidylinositol, phosphatidic acid, phosphatidylcholine, phosphatidylserine and DM.

### 2.5.6. Analytical ultracentrifugation (AUC)

The QFRs from *C. jejuni*, *H. pylori* and *W. succinogenes* that were used in analytical ultracentrifugation experiments were prepared as described above. For sedimentation velocity experiments, the samples were diluted to a final concentration of 0.35 mg/ml using a buffer containing 20 mM HEPES, 1 mM EDTA, 20 mM fumarate, 0.1% DM and 0.01% LM). The AUC experiments were carried out by Dr. Christos Tziatzios and are described in Mileni, *et al.*, 2005b.

### 2.5.7. Functional characterization

#### 2.5.7.1. Enzymatic activities

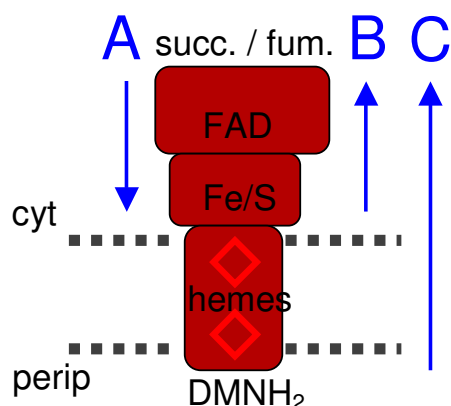
All spectrophotometer measurements were performed with an Agilent Spectrophotometer. The enzymatic velocity was calculated using the slope calculated by the Agilent software imposing a zero-order reaction. The activity units are defined as equivalent to  $\mu$ moles of product produced per minute.

##### 2.5.7.1.1. *Quinol:fumarate reductase*

The samples containing isolated QFR were diluted to a concentration of 0.5-1.0 mg/ml in a nitrogen-saturated buffer containing 20mM HEPES, 1mM EDTA, 2 mM malonate, 0.01% LM and 0.1% DM, and subsequently incubated at 37°C for 30 minutes. Volumes of 4-8 $\mu$ l were added to the assay mixture. All enzymatic assays were performed in nitrogen saturated 25

mM potassium phosphate buffer at pH 7.3. Three different kinds of enzymatic assays were performed using photometric recording at 37°C in 0.5-cm-path-length degassed quartz cuvettes:

- A. "MB assay", radical methylene blue (0.2 mM,  $\epsilon_{578}$ : 17.5 mM<sup>-1</sup> cm<sup>-1</sup>) reduction by succinate (10 mM) (Kröger, *et al.*, 1979, Kröger, *et al.*, 1980)
- B. "BV assay", dithionite-reduced (radical) benzyl viologen (1 mM,  $\epsilon_{546}$ : 19.5 mM<sup>-1</sup> cm<sup>-1</sup>) oxidation by fumarate (10 mM) (Kröger & Innerhofer, 1976b, Uden & Kröger, 1986)
- C. "DMNH<sub>2</sub> assay", 2,3-dimethyl-1,4-naphthoquinol (DMNH<sub>2</sub>, 0.2 mM) oxidation by fumarate (1 mM)



**Figure 2-2: Graphical representation of the three different enzymatic assays on the QFR.** The blue arrow represents the electron direction during catalytic activity. The membrane limits are shown as gray dotted lines; cyt, cytoplasm; perip, periplasm; succ., succinate; fum., fumarate.

Whereas the first two assays (A and B) are independent of the membrane-integral subunit C, the third (C) represents a total activity assay, and is subunit C-dependent. The different kinds of enzymatic activity assays can also be classified as succinate-oxidizing (Figure 2-2-A) or fumarate-reducing (Figure 2-3-B and -C) depending on the direction of the electrons within the complex.

Reduction of DMN was performed either by NaBH<sub>4</sub> ("BH<sub>4</sub>-DMNH<sub>2</sub> assay") (Lancaster, 2003b, Uden, *et al.*, 1980), or by a coupled reaction with DT-diaphorase and NADH ("DT-DMNH<sub>2</sub> assay") (Grivennikova, *et al.*, 1993). In the former method, the enzymatic reaction was monitored by measuring the DMNH<sub>2</sub> (re-)oxidation as the absorbance difference of 270-minus-290 nm ( $\Delta\epsilon_{270-290}$ : 15.0 mM<sup>-1</sup> cm<sup>-1</sup>). Alternatively, the catalytic reaction can be measured with the "low-sensitivity-BH<sub>4</sub> assay", which consists of monitoring the fumarate reduction at the same wavelengths (270-290 nm) after adding an excess of NaBH<sub>4</sub> ( $\epsilon_{270-290}$ : 0.45 mM<sup>-1</sup> cm<sup>-1</sup>).

Although this last procedure was 33.3 times less sensitive than monitoring the DMNH<sub>2</sub> oxidation, the reaction course was linear over far longer periods of time. The “DT-DMNH<sub>2</sub> assay” was instead used for the calculation of QFR maximum velocities, Michaelis constants ( $K_M$ ) and inhibitor constants ( $K_I$ ). Here, the enzymatic activity was indirectly determined by adding to the assay mixture ~400  $\mu$ M NADH ( $\epsilon_{340}$ : 6.29 mM<sup>-1</sup> cm<sup>-1</sup>) and rat liver DT-diaphorase (20  $\mu$ g/ml), and by measuring NADH disappearance at 340 nm.

#### 2.5.7.1.2. Hydrogenase

D. “hydrogenase assay”, DMN reduction by oxidation of H<sub>2</sub>

The activity of the hydrogenase (HydCAB, EC 1.12.5.1) from *W. succinogenes* was measured using the same conditions as described for the “BH<sub>4</sub>-DMNH<sub>2</sub> assay”, except that the electron donor substrate was added by saturating the buffer with H<sub>2</sub> instead of adding NaBH<sub>4</sub>.

#### 2.5.7.1.3. Electron transport activity (QFR and Fdh)

This assay measured the respiratory chain activity that leads to the reduction of fumarate by the oxidation of formate (Uندن & Kröger, 1986). The *W. succinogenes* WT and the strains expressing the *frdCAB* operons from *C. jejuni* and *H. pylori* were grown in one liter cultures until late exponential phase, and harvested. The membranes were prepared as described earlier (chapter 0) and resuspended in HEPES buffer (50 mM, pH 7.5).

E. “ETC assay”, formate (10 mM) oxidation by fumarate (2 mM) reduction ( $\epsilon_{270-290}$ : 0.45 mM<sup>-1</sup> cm<sup>-1</sup>) The fumarate disappearance was recorded identically to the “BH<sub>4</sub>-DMNH<sub>2</sub> assay”, but using an extinction coefficient of  $\Delta\epsilon_{270-290}$ : 0.45 mM<sup>-1</sup> cm<sup>-1</sup>

F. “Fdh assay”, formate (10 mM) oxidation by DMN ( $\epsilon_{270-290}$ : 15.0 mM<sup>-1</sup> cm<sup>-1</sup>) reduction

“DT-DMNH<sub>2</sub> assay” was used to measure the QFR activities directly on the membrane preparations. The theoretical electron-transport activities of the formate-fumarate respiratory chain were also calculated following the two independent catalytic activities using the Kröger-Klingenberg equation:

$$V_{ET} = V_{Fdh} V_{QFR} (V_{Fdh} + V_{QFR})^{-1}$$

**Equation 2-4: Kröger-Klingenberg equation (Kröger & Klingenberg, 1973).**  $V_{ET}$ , electron transport activity;  $V_{Fdh}$ , Fdh activity;  $V_{QFR}$ , QFR activity.

## 2.6. 3D-Crystal Structure Determination

### 2.6.1. Crystallization

After purification, the enzyme at a concentration of 20 mg/ml or higher was in a buffer at pH 7.4 containing 20 mM HEPES, 1 mM EDTA and 20 mM fumarate, 0.1 % DM and 0.01 % LM. The sample was then supplied with some additives: an oxidant (2 mM  $K_3Fe(CN)_6$ ), the quinone substrate (2 mM vitamin  $K_2$ ), and a small amphiphile (2.4-4.8 % benzamidine or 3.0-6.0 % heptane-1,2,3-triol). After mixing of such prepared enzyme with the reservoir solution, the crystallization mix underwent a centrifugation step (15'000 g, 2 min). The crystals were mainly obtained by vapor diffusion (sitting drops and hanging drops). Only the phase diagrams were obtained from micro-batch trials. Crystallization screenings were performed using a crystallization robot in Greiner sitting drop plates (CrystalQuick 96-well standard profile - round bottom), where the overall protein droplet volume was of 1  $\mu$ l (500 nl enzyme sample + 500 nl reservoir). The screening reservoir solutions were purchased either from Hampton Research, or Jena Bioscience, or Sigma, or Molecular Dimensions Ltd. When needed, larger amounts of reservoir solutions were self-prepared using bi-distilled water and filtered (0.2  $\mu$ m cut-off). The hanging drop technique consisted of 1  $\mu$ l of the reservoir mixed with 1-1.5  $\mu$ l of the protein solution on silanized cover slides (2 % dichlorodimethylsilane in trichloroethane and washed in ethanol 100 %). Sitting-drop trials were also carried out in 24-well plates equipped with micro-bridges (round bottom, 12 $\mu$ l capacity) or boxes equipped with 1 or 2 bridges with 3-drop positions (50  $\mu$ l capacity each). The bridges were glued to plastic boxes or 24-wells plates with ethyl acetate. When required, crystal nucleation was triggered by the microseeding or streaking techniques. For the micro-batch crystallization, the reservoir was mixed with the protein sample under a layer of Al's oil (paraffin oil and silicon oil, 1:1) in 72-well microbatch plates. Ultracentrifugation of the crystallization sample prior to incubation was carried out in an Optima MAX UC (~170'000 g, 30 min, 4°C). The protein detergents LM and DM were exchanged with either 0.1 % LDAO, or 0.04 % UM, or 0.015 % Thesit, or 0.01 % LM, or 0.1 % DM, or 0.6 % OG. Small-scale detergent exchange was performed by Vivapure Q (quaternary ammonium) resin maxi (60-80 mg capacity). This procedure did not have any effect on the enzymatic activity of the enzymes. The presented X-ray crystal structure was obtained using from a crystal of about 4 x 1.5 x 0.1-0.2 mm size and grown with the following conditions (Table 2-XVI):

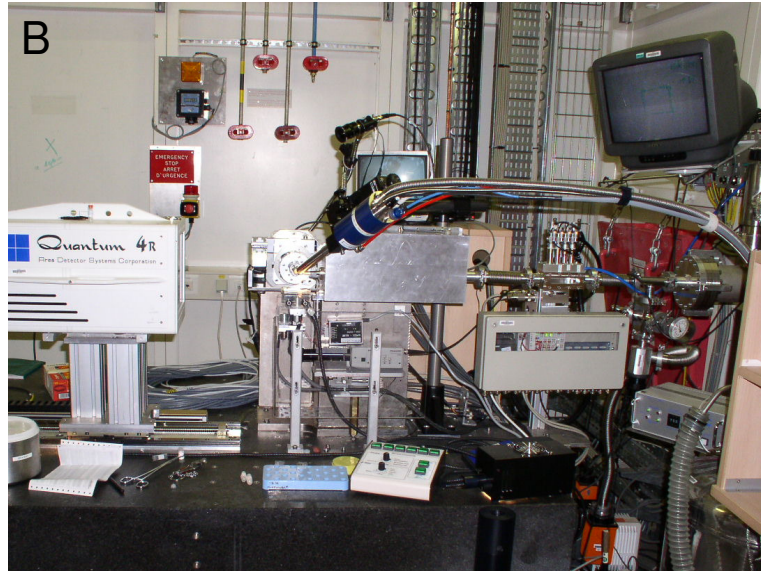
**Table 2-XVI: Crystallization conditions that lead to the 3D-crystal structure determination of the *C. jejuni* QFR.**

<b>Protein concentration:</b>	28 mg/ml
<b>Purification grade</b>	Gel purification
<b>Protein buffer</b>	HEPES, EDTA, fumarate, LM, DM (see above)
<b>Oxidizing agent</b>	1 mM $K_3Fe(CN)_6$
<b>Substrate</b>	Vitamin $K_2$ ( $MK_4$ )
<b>Buffer, pH</b>	0.1 M ADA/NaOH, pH 6.5
<b>Precipitant</b>	12 % PEG 4000
<b>Salt</b>	0.1 M $LiSO_4 \cdot x H_2O$
<b>Small amphiphile</b>	Heptane-1,2,3-triol
<b>Seeding</b>	No
<b>Drop volume</b>	50 $\mu$ l
<b>Reservoir volume</b>	8 ml
<b>Temperature</b>	18°C
<b>Incubation time</b>	~6 weeks

### 2.6.2. Data collection

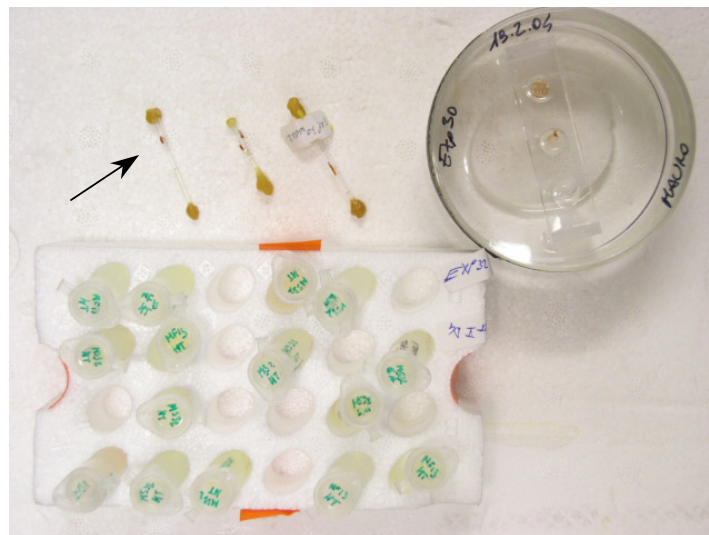
Data sets from the *C. jejuni* QFR crystals were collected at 4°C in the beamline ID14-EH1 of the ESRF synchrotron light source (Figure 2-3, [www.esrf.fr](http://www.esrf.fr), Grenoble, France) and in the beamline X11 of the DESY synchrotron light source ([www.desy.de/html/home/](http://www.desy.de/html/home/), Hamburg, Germany).





**Figure 2-3:** The beamline ID14-EH1 at the ESRF. The control room (A) and the hutch (B) are shown.

For transportation, the crystals were harvested from the crystallization drop and placed in eppendorf tubes containing the soaking buffer (i.e. in a solution equivalent to the mother liquor). Just prior to x-ray exposure, the crystals were extracted from the soaking buffers, placed in glass capillary tubes partially filled with the soaking buffer and sealed with wax.



**Figure 2-4: Crystal transportation and mounting.** Crystals (indicated by the arrow) were transferred from the crystallization plate (7.5-cm-diameter round box at the right-top of the picture) to eppendorf tubes containing soak buffer (bottom) and transported to the synchrotron location. The crystals were then transferred into glass capillary tubes and sealed with wax (left-top).

The capillaries were then mounted on a goniometer with plasticine and aligned to the x-ray beam. Due to radiation damage, and thus diffraction decay, crystal translations equal to the beam size (0.08 mm) through the x-axis were generally executed every 10 images. The back up of data sets was carried out on DLT tapes and laptop PCs.

The dataset that produced the crystal structure presented here was collected at the beamline ID14-EH1. The parameters under which the data set has been collected are summarized in Table 2-XVII.

**Table 2-XVII: Data set collection parameters at the beamline ID14-EH1.**

<b>N° of images</b>	195
<b>Oscillation angle</b>	1°
<b>Exposure time (no attenuation)</b>	6 seconds
<b>Number of passes per frame</b>	2
<b>Detector distance</b>	300.00 mm
<b>Max resolution</b>	3.14 Å
<b>Vertical slit aperture</b>	0.08 mm
<b>Horizontal slit aperture</b>	0.08 mm
<b>Wavelength (fix)</b>	0.934 Å (13.270 keV)

### 2.6.3. Data processing and refinement

HKL package, which includes the software XdisplayF, Denzo, and Scalepack (Otwinowski & Minor, 1997), was used for viewing the diffraction patterns, indexing and processing the data set. The phases were calculated by PD Dr. C. Roy D. Lancaster by molecular replacement using the *W. succinogenes* QFR (PDB entry code 2BS2, Lancaster, C.R.D., unpublished) as a search model.

The atomic model of the QFR from *C. jejuni* was built using the program O (Jones, *et al.*, 1991). Model refinement, including simulated annealing and grouped<sup>d</sup> B-factor refinement, was performed using the “Crystallography & NMR system” (CNS) package (Brunger, *et al.*, 1998).

<sup>d</sup> Single amino acids were divided in two groups, i.e. main chain and side chain.

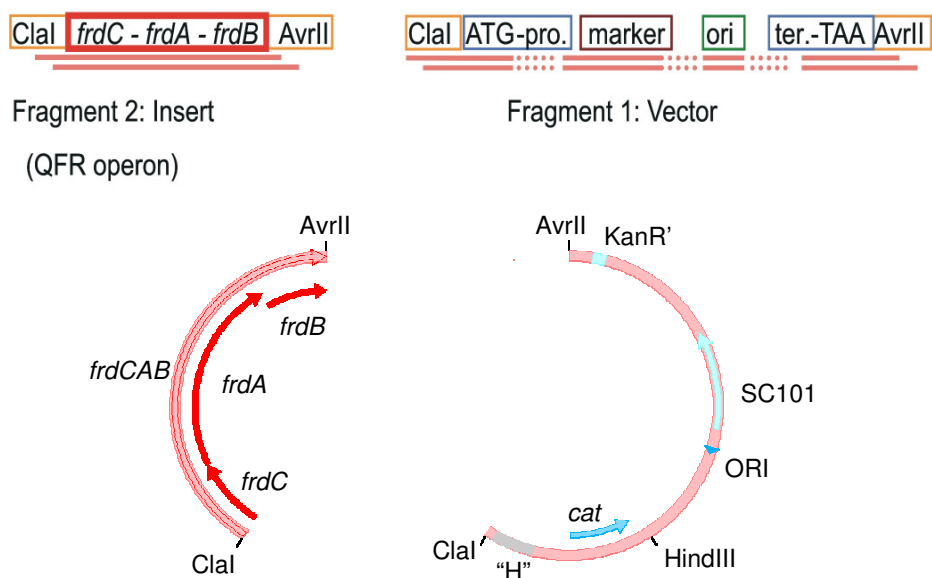


### 3. RESULTS

#### 3.1. *H. pylori* and *C. jejuni* QFR Studies

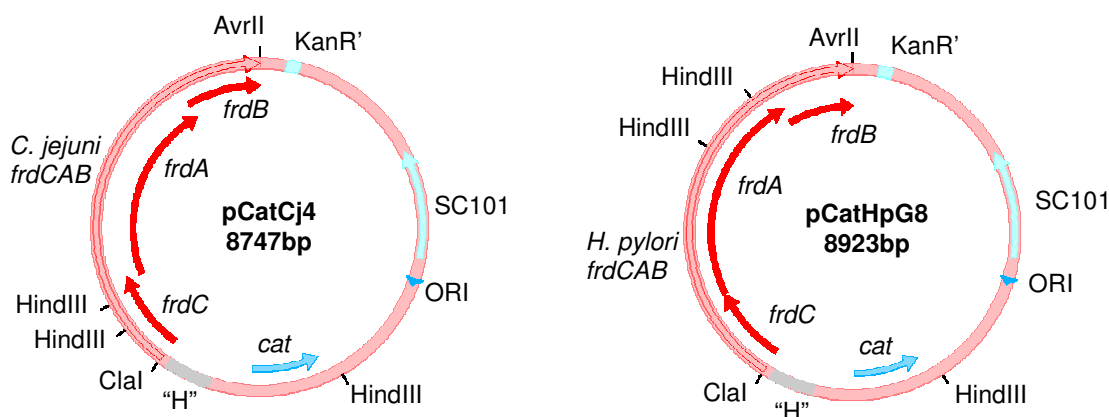
##### 3.1.1. Plasmid construction and insertion of the QFR operons from *H. pylori* and *C. jejuni* into the *W. succinogenes* genome

The heterologous expression of *frdCAB* loci from *C. jejuni* or *H. pylori* in *W. succinogenes* is based on the restoration of an intact *frdCAB* operon in the genome of the deletion mutant *W. succinogenes*  $\Delta$ *frdCAB* (see section 1.3.2). The strategy for plasmid construction consisted of ligating a vector derived from pFrdcat2 (Simon, *et al.*, 1998) to the PCR-amplified *frdCAB* operon from *H. pylori* or *C. jejuni*. The *frdCAB* operons were amplified using *H. pylori* genomic DNA and whole *C. jejuni* cells (colony-PCR) and the oligonucleotide primers *C. jejuni*\_Fw/Rv or *H. pylori*\_Fw/Rv, respectively. The PCR products contained the entire *frdC*, -A and -B genes excluding the *frdC* start codon and the *frdB* stop codon. The vector was also amplified by PCR, using the synthesized pFrdcat2 Fw/Rv oligonucleotide primers and the pFrdcat2 (Simon, *et al.*, 1998) as template. The amplified vector contains the chloramphenicol resistance gene (*cat*), the origin of replication site for *E. coli*, the promoter and terminator regions including start and stop codons of the homologous *W. succinogenes* QFR operon, and a region (named "H") for homologous recombination in the genome of the  $\Delta$ *frdCAB* deletion strain (Figure 3-1).



**Figure 3-1: Maps of the PCR-amplified DNA fragments used for cloning.** Markers, restriction sites and coding regions are indicated. The terms "pro." and "ter." stand for promoter and terminator, respectively.

The primer pairs used for amplification contained suitable restriction sites at their 5'-ends (Table 2-VI): the restriction sites *Cla*I and *Avr*II were added after the start codon "ATG" and before the stop codon "TAA", respectively, to clone the heterologous operons in frame with the expression vector. Therefore, due to the cloning procedure four amino acids (Ile-Asp at the amino terminus of *FrdC*, and Pro-Arg at the carboxy terminus of *FrdB*) were inserted into the WT enzymes. The *C. jejuni* and *H. pylori* *frdCAB* operons contained in the plasmids pCatCj4 and pCatHpG8 (Figure 3-2), respectively, were sequenced. Whereas the *H. pylori* QFR operon did not undergo any undesired mutation, it was found that the *FrdCAB* of the *C. jejuni* clinical isolate differs from the *FrdCAB* of the *C. jejuni* NCTC11168 (Parkhill, *et al.*, 2000) by 84 nucleotides (see appendix). Interestingly, nearly all of these operon mutations were silent, since there were only five amino acid changes after translation. The determined *frdCAB* sequence from pCatCj4 was deposited in the databank under accession no. AJ628040.



**Figure 3-2: Map of the constructed plasmids containing the *H. pylori* and *C. jejuni* QFR operons.** Restriction sites, coding regions and relevant regions are indicated.

The  $\Delta$ *frdCAB* deletion mutant strain of *W. succinogenes* was transformed by electroporation with the constructed plasmids described above. The homologous non-reciprocal recombination occurring by a single crossing-over is graphically illustrated in Figure 3-3. A few hundred clones grew in the selection agar medium plates containing chloramphenicol at concentrations of 12.5 and 25.0 mg/l<sup>e</sup>. Approximately 35 clones were analyzed by PCR using the primers 2\_Integr.check and CatCj\_seq19 or HpG\_probe\_Rv: three clones contained a *C. jejuni* QFR operon whereas ten clones contained a *H. pylori* QFR operon. In order to verify

<sup>e</sup> The amount of antibiotic was increased to minimize false positive clones (see section 2.1.6).

the insertion of the appropriate operon, the species-specificity of the primers was demonstrated, as PCR cross-reaction did not occur. In contrast to the starting *W. succinogenes* deletion mutant strain  $\Delta frdCAB$ , these clones were all capable of growth on a rich medium with fumarate as a sole terminal electron acceptor. After determination of the doubling times by growth cultures, three clones were selected<sup>f</sup> for expression and named WsHpGM31 and WsHpGM33, containing the *H. pylori* QFR operon, and WsCjM11, containing the *C. jejuni* QFR operon.

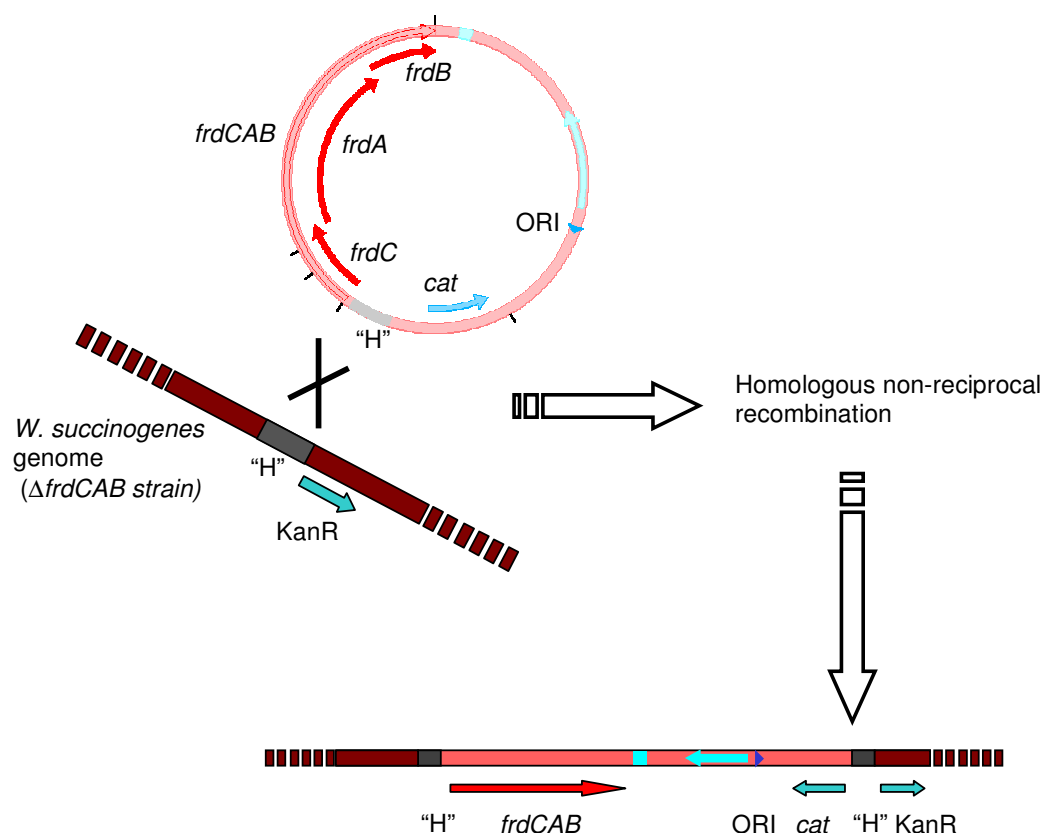
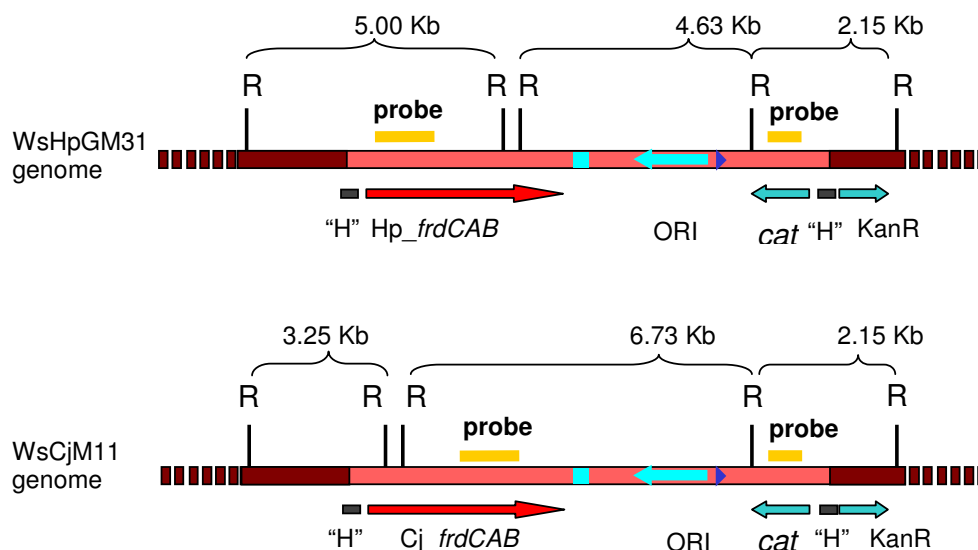


Figure 3-3: Illustration of the integration of the plasmid constructs into the genome of *W. succinogenes*.

After genomic extraction of the recombinant clones, plasmid integration into the correct genomic locus was further verified by Southern blotting analysis of the *Hind*III-digested genome, using two PCR-synthesized labeled probes complementary to the upstream region,

<sup>f</sup> The isolated clones characterized by lower doubling times were discarded.

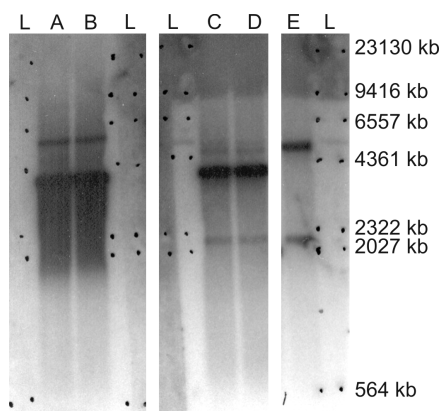
inside the QFR operon, and to the downstream region of recombination, at the *cat* locus (Figure 3-4): the two different labeled probes appear to bind to DNA fragments of the expected size.



**Figure 3-4: Maps of the genomic QFR locus after integration.** WsHpGM31 and WsCjM11 are the recombinant strains of *W. succinogenes* that have been transformed with the plasmid pCatHpG8 and pCatCj4, respectively. R, restriction sites (HindIII), "H", homology regions for recombination.

Unfortunately, the upstream region of integration for the *C. jejuni* QFR-containing plasmid could not be verified as the Hind III restriction sites were too close to the upstream integration site for an efficient pairing of the labeled probe. For this reason, only the results from the WsHpGM31 and WsHpGM33 strains are shown (Figure 3-5). Cross-reactions between labeled probes was tested as a negative control, and again ensured correct species-identification of the inserted heterologous QFR. Together with the expected bands at about 5.0 kb (upstream integration) and 2.2 kb (downstream integration), two other prominent bands appeared at 4.2 kb<sup>§</sup>.

<sup>§</sup> This size corresponds to the DNA fragments containing the *H. pylori* QFR operon or the *cat* gene after digestion of the pCatCj4 plasmid with the restriction enzyme HindIII.



**Figure 3-5: Southern blot analysis.** L, molecular mass standard; A and C, WsHpGM31; B and D, WsHpGM33; A and B, hybridization with the upstream (QFR) labeled probe; C and D, hybridization with the downstream (*cat*) labeled probe; E, positive control made with the recombinant K4 QFR (Simon, *et al.*, 1998).

### 3.1.2. Properties of *W. succinogenes* strains expressing the heterologous *frdCAB* operons

The mutants *W. succinogenes* CjM11 and HpGM31/33 express the respective *frdCAB* operons from *C. jejuni* and *H. pylori* under the control of the *W. succinogenes* *frd* promoter and terminator. These mutants contain a single copy of the *frdCAB* locus on the genome that replaces the genuine *frdCAB* operon of *W. succinogenes* WT cells. In contrast to the parental strain *W. succinogenes*  $\Delta$ *frdCAB*, the CjM11 and HpGM31/33 strains grow by fumarate respiration, albeit at slightly longer doubling times compared to the WT (Table 3-I). The cell yield for growth by fumarate respiration was found to be identical in the three strains (not shown). Light microscopy (400x) observation of the two strains grown in rich medium did not reveal any difference in motility or cell morphology as compared to the WT *W. succinogenes*. Table 3-I shows the specific fumarate reductase activities measured in cell fractions of the strains using various enzyme activity assays.

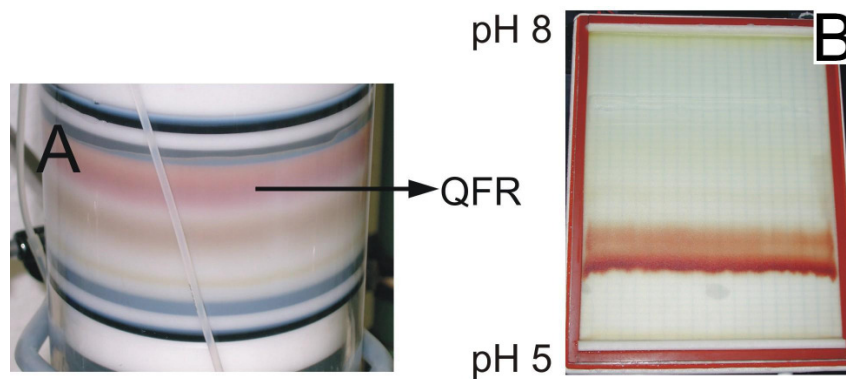
In order to examine the possibility that this longer doubling time in the HpGM31/33 strains corresponded to a lower efficiency of the respiratory chain, the electron transfer activity between Fdh and QFR of cell membranes was measured and is presented in section 3.1.4.4.1.

**Table 3-I: Doubling times and specific fumarate reductase activities of *W. succinogenes* strains.** The cells were grown by fumarate respiration either in minimal or rich medium. The specific activities were based on cells grown in rich medium.

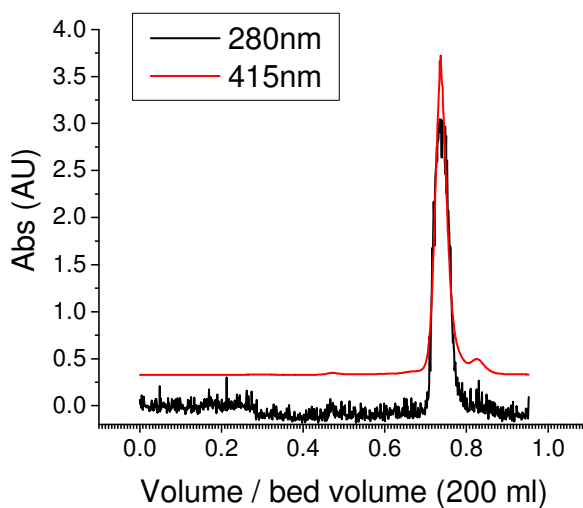
	DSMZ 1740	WsCjM11	WsHpGM31
<b>Doubling time (h)</b>			
<i>in rich medium</i>	1.0	1.2	1.9
<i>in minimal medium</i>	2.0	2.3	3.0
<b>Specific fumarate reductase activity (U mg<sup>-1</sup>)</b>			
Succinate → methylene blue			
<i>Cell homogenate</i>	0.7	0.2	0.8
<i>Membrane fraction</i>	1.4	0.4	1.1
<i>Soluble fraction</i>	≤0.03	≤0.02	≤0.02
DMNH <sub>2</sub> → fumarate			
<i>Cell homogenate</i>	2.3	1.2	2.4
<i>Membrane fraction</i>	3.2	2.1	3.4
<i>Soluble fraction</i>	≤0.05	≤0.04	≤0.05

### 3.1.3. Protein purification

The two heterologous *frdCAB* operons inserted in *W. succinogenes* were expressed for large-scale membrane protein preparation. As monitored with the “MB assay”, the specific activity of cell homogenates was about 0.2-0.3 U mg<sup>-1</sup> (total volume 233 ml, 72 g cells) for CjM11 and 0.7-0.8 U mg<sup>-1</sup> (255 ml, 105 g cells) for HpGM31. The same assay performed on the cytosolic fraction after the first ultracentrifugation of the membranes was found to give negligible values (see Table 3-I). After anion exchange chromatography, about 14 to 18 fractions were pooled, usually consisting of fractions with an “MB assay” specific activity above ~4 U ml<sup>-1</sup>. An SDS-PAGE of the fractions confirmed the activity results (not shown). Further purification steps yielded a remarkable increase in the specific partial activity (“MB assay”) of the protein sample up to 12.3 U mg<sup>-1</sup> for *H. pylori* QFR and 7.3 U mg<sup>-1</sup> for *C. jejuni* QFR. However, a more relevant determination of the purification profile was accomplished by monitoring the specific activity of DMNH<sub>2</sub> oxidation by fumarate (Table 3-II).



**Figure 3-6: The QFR purification procedure: anion exchange chromatography (A), and preparative isoelectric focusing (B).** The fumarate reductase (reddish band) was separated during elution from other membrane proteins (A). In the IEF gel, the theoretical pH established by the electric field is shown (B).



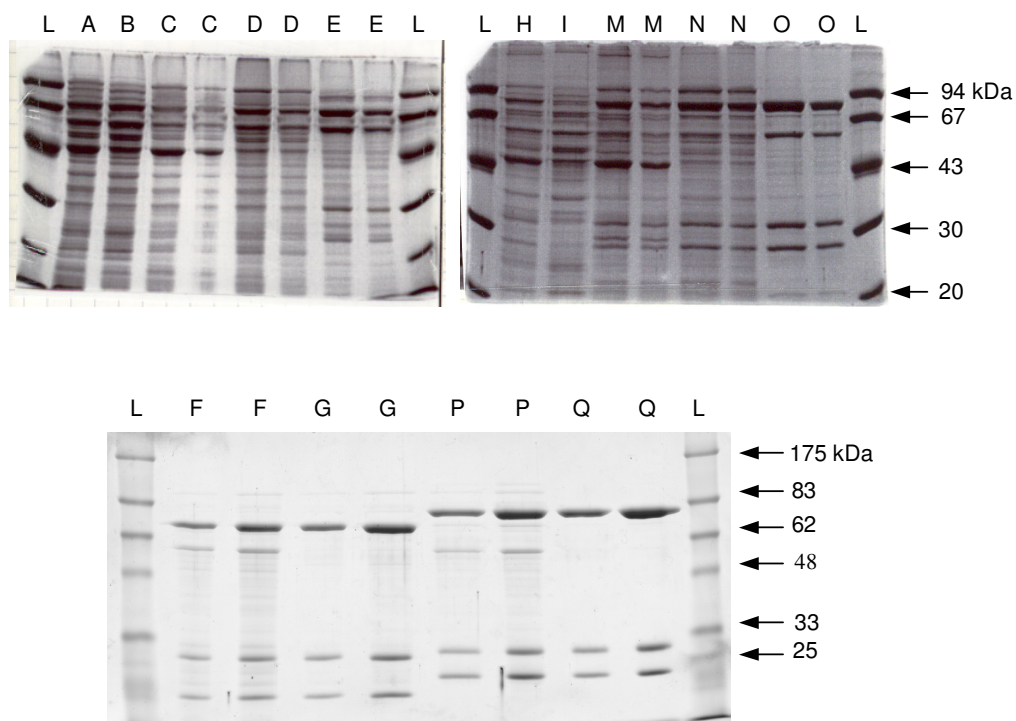
**Figure 3-7: Chromatogram of the gel filtration purification.** The curves show the absorbance course at 415 nm (Soret band, red line) and 280 nm (black line). The bed volume of the chromatography column was 200 ml. The minor ticks on the abscissa display the fraction volume, which corresponds to 0.8 ml.

**Table 3-II: Purification profile based on total specific activity (“DT-DMNH<sub>2</sub> assay”).**

		<b>Total activity (U)</b>	<b>Specific activity (U mg<sup>-1</sup>)</b>	<b>Protein yield (%)</b>	<b>Purification factor</b>
<i>C. jejuni</i>	Cell Homogenate	12.9 × 10 <sup>3</sup>	1.2	100	1.0
	Triton X-100 Homogenate	16.3 × 10 <sup>3</sup>	2.0	126	1.7
	Triton X-100 Extract	14.3 × 10 <sup>3</sup>	3.4	111	2.8
	Anion Exchange Chromatography	4.2 × 10 <sup>3</sup>	7.3	33	6.1
	Isoelectric Focusing	1.6 × 10 <sup>3</sup>	9.3	12.4	7.8
	Gel Filtration	0.78 × 10 <sup>3</sup>	9.7	6.0	8.1
<i>H. pylori</i>	Cell Homogenate	40.9 × 10 <sup>3</sup>	2.4	100	1.0
	Triton X-100 Homogenate	43.8 × 10 <sup>3</sup>	3.8	107	1.6
	Triton X-100 Extract	43.0 × 10 <sup>3</sup>	6.0	105	2.5
	Anion Exchange Chromatography	11.7 × 10 <sup>3</sup>	10.4	29	4.3
	Isoelectric Focusing	3.9 × 10 <sup>3</sup>	12.2	10	5.1
	Gel Filtration	0.5 × 10 <sup>3</sup>	2-3	~1.3	~1

Although a drastic decrease in enzymatic activity of the *H. pylori* QFR after the gel purification (nearly 80 %) was observed, this purification procedure resulted in a purity factor of 8.1 and 5.1 for the *C. jejuni* and *H. pylori* QFR, respectively, with a final specific activity of 9.7 U mg<sup>-1</sup> for *C. jejuni* and 12.2 U mg<sup>-1</sup> for *H. pylori* QFR (see Table 3-II). Nevertheless, as will be shown in chapter 3.1.4.2, the addition of certain lipids did have a striking effect on the enzymatic activity of the *H. pylori* QFR after gel filtration (Table 3-V). Alongside the purification profile based on enzymatic activity, protein purity was assessed by SDS-PAGE (Figure 3-8). Three bands represent the three subunits FrdA, B and C from the two QFRs with no major contamination and appropriate stoichiometric ratios, as inferred from the respective band intensities. Based on the amino acid sequences, the molecular weights of the *H. pylori* QFR subunits A, B, and C are 80.2 kDa, 27.6 kDa, and 28.8 kDa, respectively. The corresponding values for *C. jejuni* QFR subunits are 73.8 kDa, 27.5 kDa, 30.3 kDa. As demonstrated by (Unden, *et al.*, 1980), the QFR hydrophobic subunit C appears smallest in the SDS-PAGE experiment. Together with a general improvement in purity, the gel filtration step eliminated a contaminant protein of approximately 55-60 kDa.



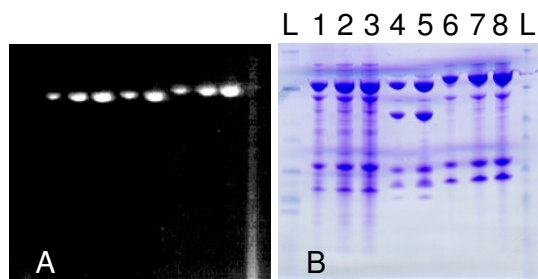


**Figure 3-8: SDS-PAGE of samples during purification.** A-G, *C. jejuni* QFR samples; H-Q, *H. pylori* QFR samples. L, molecular mass standard (or "ladder"); A and H, cell homogenate; B and I, supernatant; C and M, Triton homogenate; D and N, Triton extract; E and O, anion exchange; F and P, isoelectric focusing; G and Q, gel filtration.

### 3.1.4. QFR enzymatic characterization

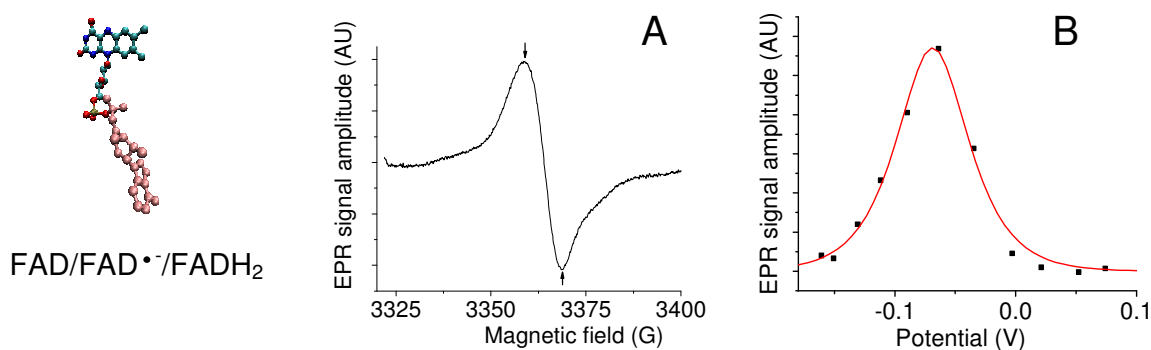
#### 3.1.4.1. Cofactor analysis and redox midpoint potential determination

**FAD:** Fluorescence associated with the A subunit band in an SDS polyacrylamide gel after electrophoresis illuminated with UV-light (Figure 3-9) demonstrated that the FAD prosthetic group is covalently bound to the respective A subunits of the *H. pylori* and *C. jejuni* enzymes.



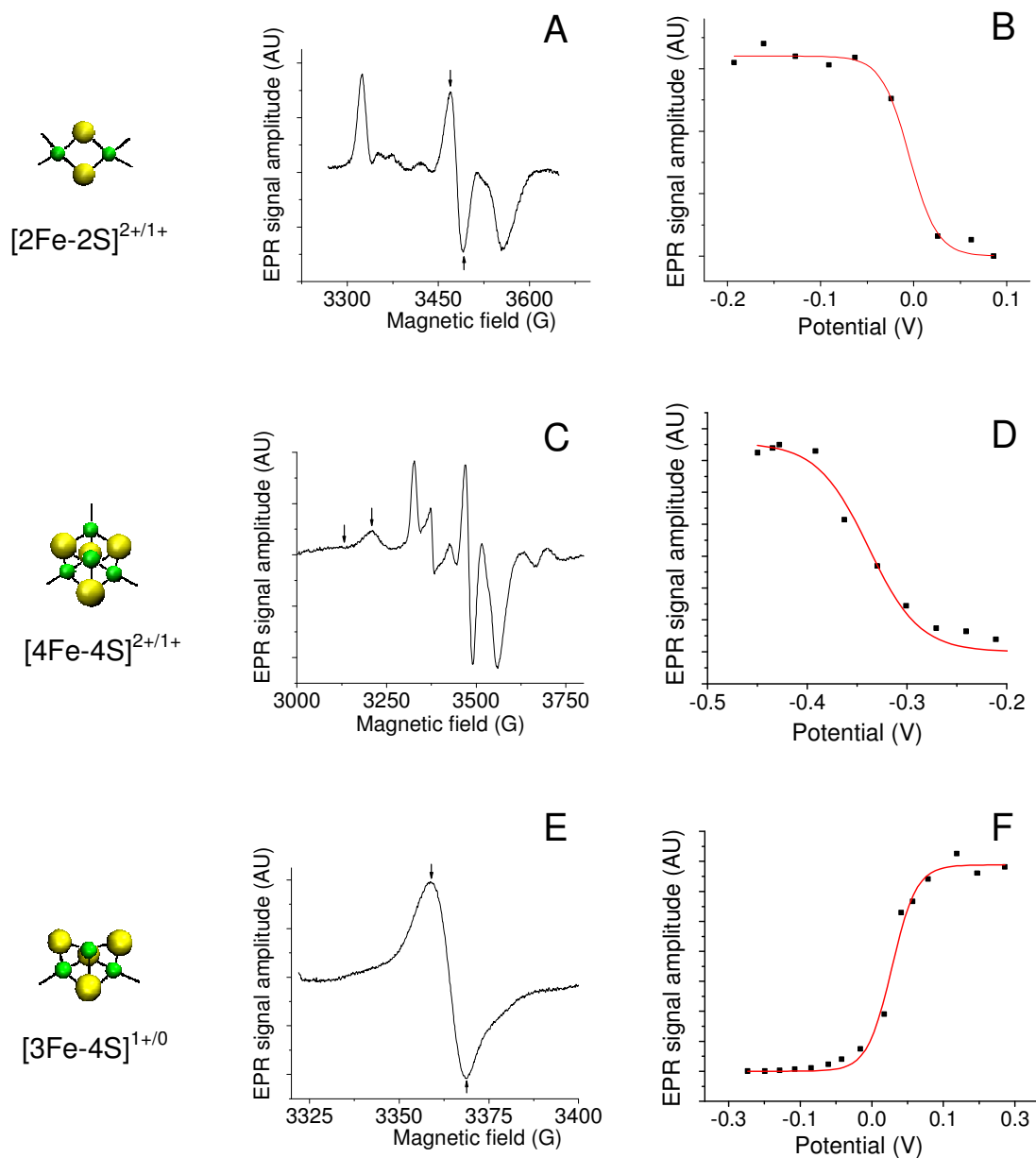
**Figure 3-9: FAD fluorescence under UV-light exposure (A) after running an SDS-PAGE (B).** L, molecular mass standard; 1-3, *C. jejuni* QFR; 4-5, *W. succinogenes* QFR; 6-8, *H. pylori* QFR.

Although redox characterization of flavin prosthetic groups can be accomplished by UV/VIS spectrophotometry, in this case the determination of the redox properties by this method was not feasible since its absorption spectrum was obscured by intense transitions from the heme *b* groups, which have far higher extinction coefficients. Therefore, the FAD (n=2) redox midpoint potential at pH 7.3 was determined by measuring the cw-EPR (X-band) signal of the flavin semiquinone (radical  $\text{FAD}^{\bullet-}$  state) as a function of the environmental potential. The potential was adjusted by performing a dithionite titration in the presence of redox mediators (see Materials and Methods). An FAD prosthetic group can exist in three redox active states: the fully oxidized form, which is diamagnetic and hence EPR silent; the semiquinone (or one-electron reduced) form, which is paramagnetic and has a characteristic EPR spectrum; and the hydroquinone (or fully -two-electron- reduced) form, which is again diamagnetic and EPR silent. The peak intensity values at different potentials were plotted and the curve was fitted with a double Nernst function. Typical bell-shaped curves were obtained for this prosthetic group (Figure 3-10-B). In order to determine the two half-wave potentials, the signal yield of the FAD semiquinone state was required. Taking the fully reduced iron-sulfur cluster S1 as a reference, the signal yield values obtained for the FAD radicals were 9 %, 12 % and 7 % for *W. succinogenes*, *C. jejuni* and *H. pylori* QFR, respectively. These ratios did not change when the titration was repeated in the presence of 10-fold vitamin  $\text{K}_2$  ( $\text{MK}_4$ ).



**Figure 3-10: Determination of the redox midpoint potential of the prosthetic group FAD by EPR.** A typical EPR spectrum at 50K is shown (A). The intensity amplitudes were measured as indicated by the arrows. The double Nernst equation was used for fitting the data points (B). The three oxidation states and the structure of FAD are shown (left side). The magnetic field is measured in Gauss (G). The potential is always referred to the standard hydrogen electrode (SHE).

**Iron-sulfur clusters:** Redox midpoint potentials at pH 7.3 of the three iron-sulfur clusters S1, S2 and S3 ( $n=1$ ) were also determined in the presence of mediators. A plot of the EPR signal against the potential was fitted with the standard Nernst function revealing a typical sigmoidal shape (Figure 3-11).



**Figure 3-11: Determination of the redox midpoint potential of the iron-sulfur clusters [2Fe-2S] (or S1), [4Fe-4S] (or S2) and [3Fe-4S] (or S3).** EPR spectra at 10K (A, C, E) and fitting of the respective data points with the Nernst equation (B, D, F) are illustrated. Intensity amplitudes were measured as indicated by the arrows. The oxidation states and the structures of these coenzymes are shown (left side).

**Heme groups:** Spectroscopic determination of the heme *b* content consisted of quantifying the absorption difference ( $\Delta\text{Abs}$ ) at 565-minus-575 nm of the difference spectrum derived from the protein reduced-minus-oxidized redox states. These measurements have verified a heme to protein (monomer) stoichiometric ratio of 2:1. The redox midpoint potential of the heme *b* groups were determined by analyzing electrochemically induced absorbance difference spectra by monitoring at the wavelengths of 428 nm (Soret-band) and 561 nm ( $\alpha$ -band). Two titrating groups, i.e. heme  $b_{\text{H}}$  and heme  $b_{\text{L}}$ , can be perfectly fitted with a double Nernst function in each of the curves. Within an error of 5%, the two hemes contributed equally to the total change in absorbance. Taking the average value of reductive and oxidative titrations, the fitted curves yielded midpoint potentials of -129 mV and +1 mV for the low potential and high potential hemes of the *C. jejuni* QFR, and -106 mV and +8 mV for the low potential and high potential hemes of the *H. pylori* QFR. Monitoring the  $\alpha$ -band and Soret-band yielded analogous titration curves and very similar redox midpoint potentials. As determined for the *W. succinogenes* QFR (Lancaster, *et al.*, 2000), high potential values can be assigned to the proximal hemes, and the low potential values can be assigned to the distal hemes (Haas & Lancaster, 2004). As is known for *W. succinogenes* QFR (see e.g. Lancaster, *et al.*, 2000), the interaction of the  $\text{NaBH}_4$ -poised DMN with the enzymes<sup>h</sup> showed that *C. jejuni* and *H. pylori* QFRs sustain a reduction of only one heme out of two. This behavior is interpreted as a release of one electron from the quinol via the distal heme, whose midpoint potential was -129/-106 mV, to the proximal heme, whose midpoint potential was +1/+8 mV, confirming that an intramolecular electron transfer between the hemes is possible.

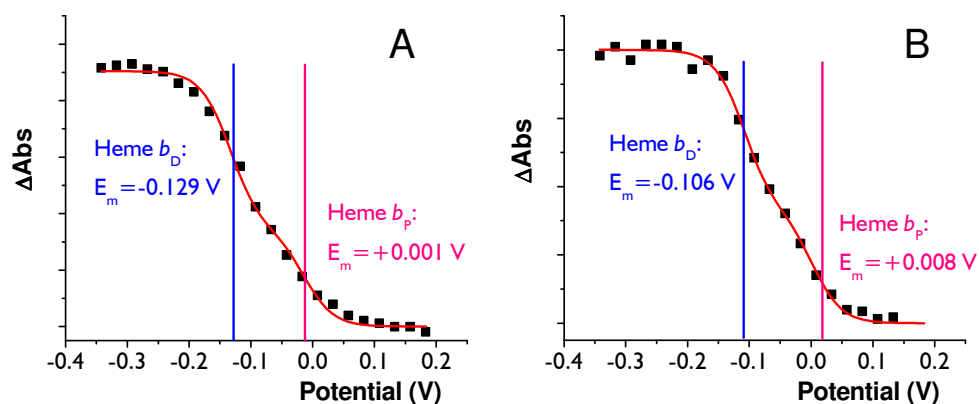
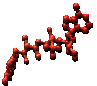



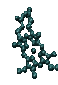



Figure 3-12: Fitting of the titration curves for the determination of the heme redox midpoint potentials from the *C. jejuni* (A) and *H. pylori* (B) QFRs. The intersection points of the blue and pink lines with the fitting curves represent the heme redox midpoint potentials.

<sup>h</sup>  $\text{NaBH}_4$  reduces the DMN to  $\text{DMNH}_2$  but not the enzyme.

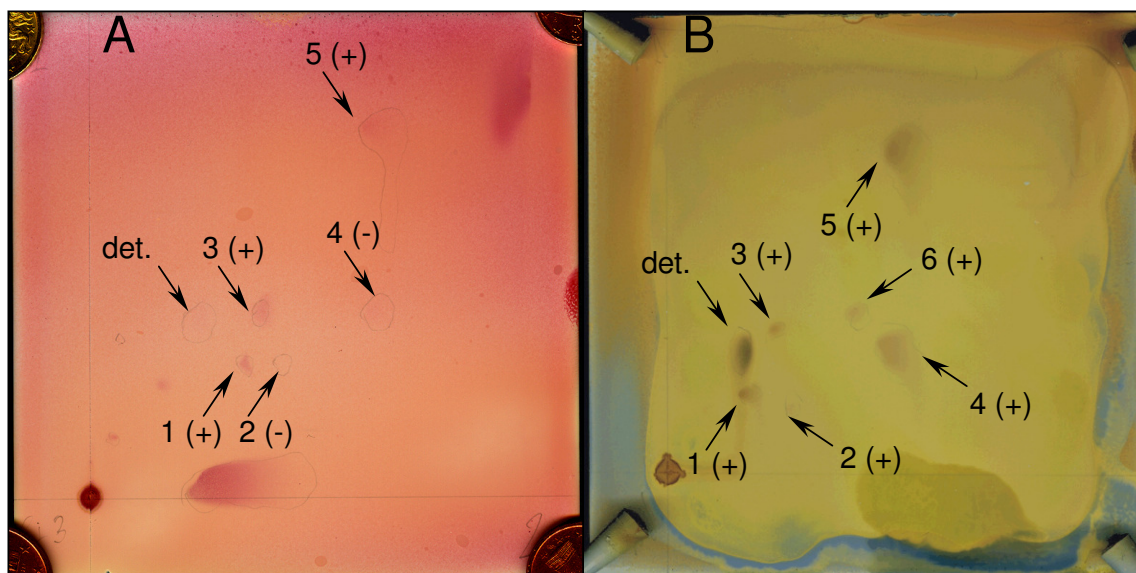
**Table 3-III: Redox midpoint potentials of all QFR cofactors from *W. succinogenes* (W.s.), *C. jejuni* (C.j.), and *H. pylori* (H.p.).** The structures and the arrangement of the cofactors shown on the left side of the table are based on the *W. succinogenes* QFR structure (Lancaster, *et al.*, 1999).

Cofactor		W.s. QFR (mV)	C.j. QFR (mV)	H.p. QFR (mV)
	FAD	-125	-101	-70
	[2Fe-2S]	-112	-5	+26
	[4Fe-4S]	-340	-235	-260
	[3Fe-4S]	-61	+42	+33
	Proximal heme <i>b</i>	-9	+1	+8
	Distal heme <i>b</i>	-152	-129	-106

### 3.1.4.2. Analysis of native lipids co-purifying with the QFR

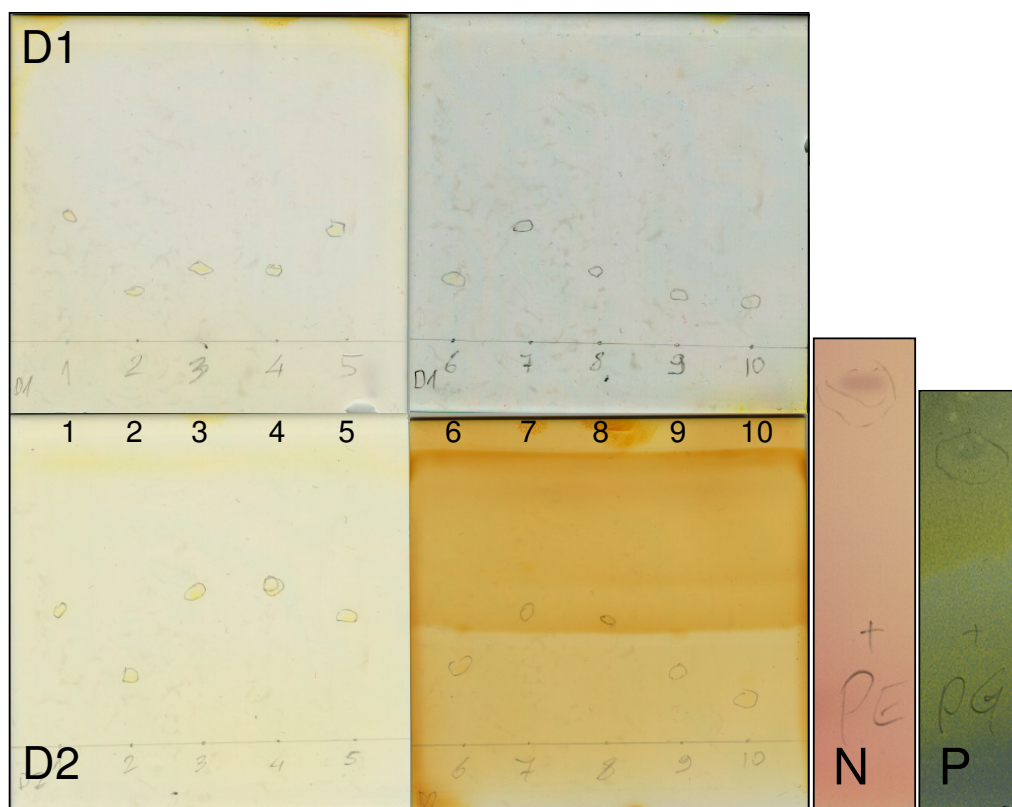
#### 3.1.4.2.1. Lipid isolation by 2D thin layer chromatography

An attempt was made to isolate and identify lipids co-purifying with the proteins on 2D TLC plates. Staining procedures allowed detection either of nitrogen, phosphorous, or glycolipid containing compounds. While the outcome of the latter staining procedure was always negative, except for the case of the detergents which appear as black spots, staining for nitrogen and phosphorous allowed detection of several positive signals (Figure 3-13 A and B, respectively).



**Figure 3-13:** TLC trials of the *C. jejuni* (A) and *H. pylori* (B) QFRs after IEF. Spots appearing after iodine vapor staining are pencil-encircled. Nitrogen staining (A) and phosphorous staining (B) are shown. Symbols and abbreviations: +, staining-positive; -, staining-negative; det., detergents.

All spots appeared to be positive in the phosphorous staining. Comparing the experiments shown above, although the migration of the spots was slightly different, the overall patterns, e.g. number of spots and staining results, were very similar. The only exception is spot n° 6, which was present only in the *H. pylori* QFR and turned out to be positive for both phosphorous and nitrogen staining. Spots no. 1, 3, and 5 were also positive for the nitrogen staining. The spots appearing black after applying the staining for glycolipids were classified as “detergents”. As will be shown below, this prediction was confirmed with the MS analysis. In order to identify the lipidic head-groups of the migrated spots, most of the common lipids found in prokaryotic membranes were run in the TLC plate for standard calibration (Figure 3-14). However, because of the poor accuracy of migration, the precise identification of the isolated lipids/compounds was not possible.



**Figure 3-14: TLC lipid standard.** D1, first dimension; D2, second dimension; 1, DOPE; 2, 16:1 PC; 3, 18:1 CA; 4, DOPG; 5, 16:1 PE; 6, DOPC; 7, DPPE; 8, DPPG; 9, DPPC; 10, Brain PS. As expected, lipids with the same head group have very similar retention factors. The two columns on the right represent phosphatidyl phosphoethanolamine (PE) and phosphatidylglycerol (PG) treated with the nitrogen staining (N) and phosphorous staining (P).

Thanks to the standard calibration, it was possible to infer that only the compounds localized close to the detergent spots are possible lipidic compounds and to exclude those with very high retention factor.

The 2D TLC was also performed on QFR samples after gel filtration purification. Interestingly, in the *H. pylori* QFR sample almost every smear was either lost or too weak to be detected (Figure 3-15).



**Figure 3-15:** Portions of TLC trials of the *C. jejuni* (A) and *H. pylori* (B) QFRs after gel filtration. Det., detergents; the arrows are indicating detected smears. The dashed arrow indicates a weakly visible smear.

#### 3.1.4.2.2. MALDI TOF mass spectrometry assessment for lipid identification

The MALDI TOF mass spectrometry method was chosen for the identification of lipids bound to the *C. jejuni* and *H. pylori* QFR purified samples. Three approaches were undertaken for the preparation of the analyzed samples (see Materials and Methods).

##### 1<sup>st</sup> approach: whole protein analysis

As a positive control for the instrument, approximately two molecules per monomer of a synthetic lipid (DPPC) were added to the protein solution and analyzed. The presence of this phospholipid was confirmed with the appearance of two peaks at the correct masses of 734.4 m/z (proton adduct) and 756.4 m/z (sodium adduct). Unfortunately, apart from the detergents DM and LM, which were identified as two peaks corresponding to 505.3 m/z and 533.3 m/z (sodium adducts), respectively, it was not possible to assign any of the peaks obtained. In other words, none of the peaks found in the expected mass (m/z) range of 500-1800 kDa were sufficiently strong to be investigated further. This negative result was also due to the persistence of a mild unpredictable contamination background.

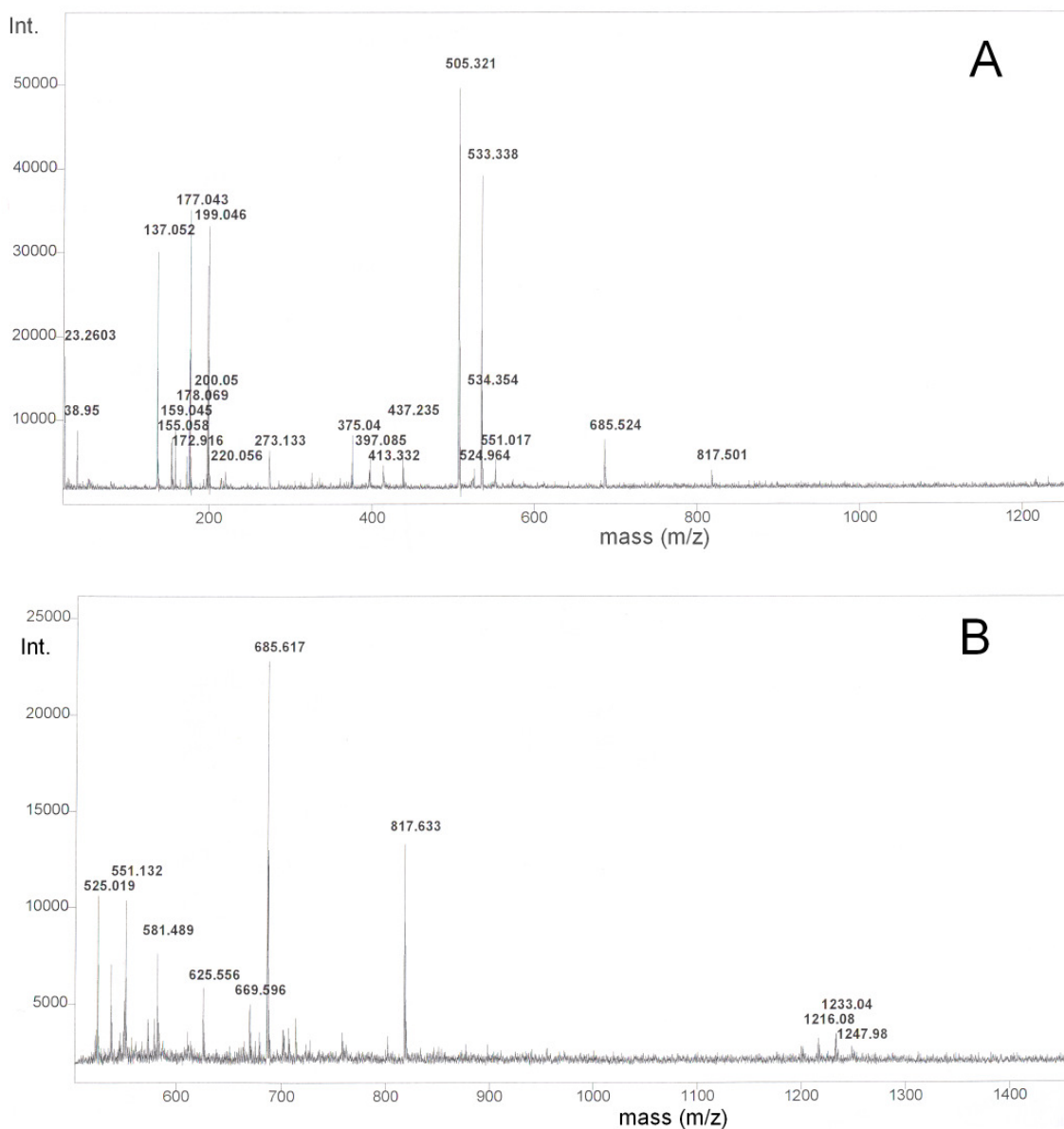
##### 2<sup>nd</sup> approach: analysis of the methanol-chloroform extract

Similar to the previous approach, the identification of compounds was impossible.

##### 3<sup>rd</sup> approach: analysis of the isolated compounds from 2D TLC

The identification of the detergent spots in the TLC plates by glycolipid staining was confirmed by mass spectrometry (Figure 3-16-A). In this third approach, apart from the detergents, only spot n° 5 (in Figure 3-13) resulted in two strong peaks at 817.6 m/z and 685.6 m/z (Figure 3-16-B).





**Figure 3-16: MALDI TOF measurement of the extracted spots labeled “detergent” (A) and n° 5 (B).**

These specific target peaks underwent fragmentation by MALDI TOF tandem MS-MS, and, whereas the 685.6 m/z peak was readily recognized as polymeric dihydroxybenzoic acid (DHB) molecules (not shown), the second peak presented a fragmentation pattern that could not be interpreted (Figure 3-17). Moreover, many of the samples were contaminated with a polymeric substance having a molecular weight of 44 m/z, most likely consisting of polyethylene glycol. The origin of this contamination was not clear.

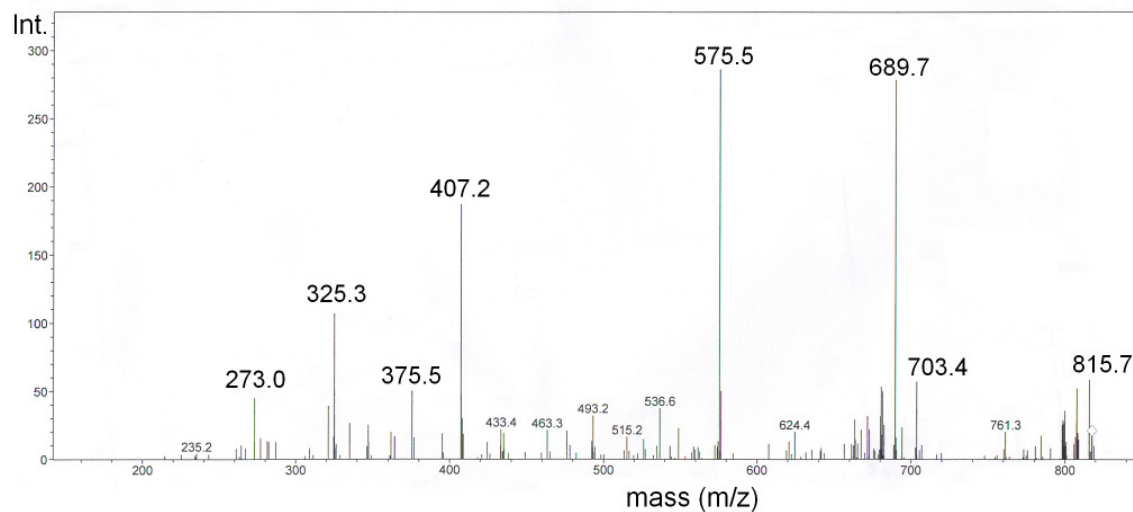


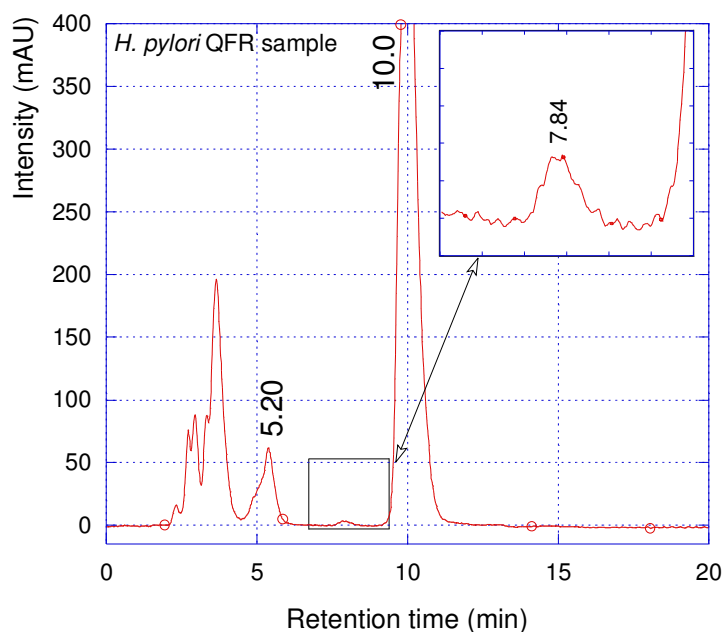
Figure 3-17: Tandem MS-MS of the peak 817 m/z.

### 3.1.4.2.3. High-pressure liquid chromatography

A further attempt to identify the lipidic species co-purifying with the *H. pylori* QFR consisted of an HPLC analysis of the purified sample after methanol-chloroform extraction. After a standard calibration, the peak retention times of the lipids added to the standard mixture (Table 3-IV) were annotated and compared to those obtained with the QFR sample extracts.

**Table 3-IV: List of retention times obtained from the standard calibration curve.** CA, cardiolipin; PE, phosphatidylethanolamine; PI, phosphatidylinositol; LM / DM, lauryl- and decyl-maltoside; PS, phosphatidylserine; PA, phosphatidic acid; PC, phosphatidylcholine.

Lipid/Detergent	Retention Time
Polar Head	(min)
CA	5.11
PE	7.72
PI	8.87
LM / DM	9.68
PS	~10-11 (weak)
PA	12.55
PC	16.55



**Figure 3-18: HPLC chromatogram of the *H. pylori* QFR after extraction.** The upright inset represents a magnification of the square highlighted in black. Retention times of the significant peaks are indicated.

The strongest peak observed in the HPLC chromatogram (Figure 3-18) has a retention time of 10.0 min, and corresponds to maltoside detergents. A second prominent signal appears at a retention time of 5.20 min. Although this latter peak is somewhat broadened at its base, its retention time strongly suggests that this compound is cardiolipin. The presence of cardiolipin confirms the results obtained with the enzymatic assays (Table 3-V). Indeed, addition of cardiolipin to the *H. pylori* QFR after gel filtration increased its enzymatic activity more than lipids like PG and PC, which had less effect on the *H. pylori* QFR enzymatic activity, or like PE, which had no effect at all (Table 3-V). Furthermore, addition of cardiolipin to the *H. pylori* QFR crystallization mixture had a beneficial effect in crystallization trials (see crystallization section). The last peak detected is characterized by a very low intensity, and might correspond to phosphatidylethanolamine (7.84 min retention time).

**Table 3-V: Recovery of the *H. pylori* QFR enzymatic activity upon treatment with lipids at the stoichiometric ratio of 5 molecules per monomer.** The results are shown in percentages and are referred to QFR sample after IEF purification.

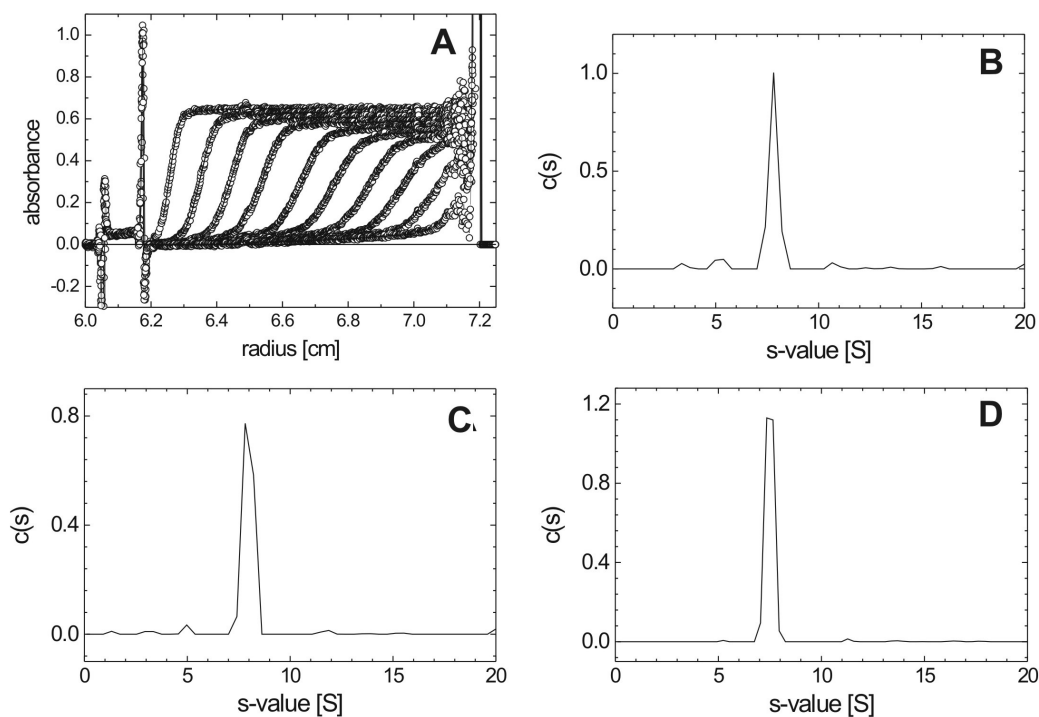
Added Lipid	Recovered Enzymatic Activity (%)
None	20
CA	154
DPPE	22
DPPG	70
DOFC	147

### 3.1.4.3. Analytical ultracentrifugation

The oligomeric state of QFR from all three organisms, *C. jejuni*, *H. pylori* and *W. succinogenes*, was studied by sedimentation velocity experiments in combination with Lamm equation fitting. Figure 3-19 shows the analyses of sedimentation velocity experiments on the three QFR species, based on a continuous distribution model for  $s$ -values in the range between 0.5 and 20 S. The partial specific volume,  $\bar{v}$ , of QFR in aqueous buffers, corrected for protein-bound prosthetic groups, was calculated from its amino acid composition as 0.730 ml/g. The corresponding  $\bar{v}$ -value for the mixed decylmaltoside/dodecylmaltoside micelles was calculated assuming a weight ratio of the two detergents of 10/1. This led to  $\bar{v} = 0.794$  ml/g. All  $c(s)$ -distributions gave an excellent fit to the experimental data, exhibiting the presence of a well-defined sharp peak at approximately 8 S. In addition, the presence of small amounts of material with higher and lower sedimentation coefficients was suggested (Figure 3-19-B, C and-D). Since the relative area under a peak in the  $c(s)$ -distribution corresponds to the relative loading concentration of the respective species, it is concluded that the majority of the material is in the single peak at  $\sim 8$  S. The area under this peak accounts for approx. 90 % of the total amount of protein in the sample for QFR from *C. jejuni* and from *H. pylori*, and for approximately 97 % for QFR from *W. succinogenes*.

The peak at  $\sim 8$  S is clearly resolved, which suggests homogeneity of the respective component. The experimental  $A(r,t)$  data were therefore analyzed using solutions of the Lamm equation for a small number of discrete non-interacting species (Schuck, 2000). For QFR from the first two bacteria, terms for four discrete components were used for the calculation of sedimentation and diffusion coefficient of the  $\sim 8$  S-peak, with starting  $s$ -values identical to those found by the  $c(s)$ -method. In the case of QFR from *W. succinogenes* the experimental sedimentation velocity data were fitted assuming the presence of a single

component. The fits were of very good quality. The results found for the main component of QFR from all three organisms were similar: the  $s$ - and  $D$ -values found for QFR from *C. jejuni* were 7.82 S and  $2.15 \cdot 10^{-7} \text{ cm}^2/\text{s}$ , respectively, those for QFR from *H. pylori* were 7.97 S and  $2.14 \cdot 10^{-7} \text{ cm}^2/\text{s}$ , respectively, and those for QFR from *W. succinogenes* 7.50 S and  $1.93 \cdot 10^{-7} \text{ cm}^2/\text{s}$ , respectively. The effective molar mass,  $M_{\text{eff,c}} = M_c(1 - \bar{v}_c \cdot \rho_0)^i$ , of the protein/detergent complexes was calculated from their  $s$ - and  $D$ -values using the Svedberg equation (Cantor & Schimmel, 1980). It was obtained  $(83,000 \pm 9,000) \text{ g/mol}$  for the first complex,  $(85,000 \pm 9,000) \text{ g/mol}$  for the second and  $(88,000 \pm 7,000) \text{ g/mol}$  for the last one. It should be noted that the relatively large uncertainty of approx. 10 % in determining  $M_{\text{eff,c}}$  has its origin mainly in the uncertainty of the  $D$ -value, which could be varied in the analysis by approx. 10% without significant increase of the rms error of the fit (Schuck, 1998). These results clearly indicate that the  $\sim 8 \text{ S}$ -component represents the same state of association of QFR from either organism.



**Figure 3-19: Sedimentation velocity analysis on QFR from *C. jejuni* (A,B), *H. pylori* (C) and *W. succinogenes* (D).** Experimental sedimentation velocity distributions (A) of the enzyme at different times (symbols) and best fit- distributions calculated using solutions of the Lamm equation based on the model of continuous size-distribution (solid lines). For clarity only every fourth data set is shown. Best fit-sedimentation coefficient distribution  $c(s)$  (B, C, D).

<sup>i</sup> Where  $\rho$  is the density of the solvent;  $\bar{v}$  is the partial specific volume

### 3.1.4.4. Functional characterization

#### 3.1.4.4.1. Electron transfer activity

The specific electron transfer activity between the formate dehydrogenase and fumarate reductase was tested on membranes of *W. succinogenes* expressing the QFR operon from *W. succinogenes*, *C. jejuni* and *H. pylori* by the establishment of an electron transfer chain supported by native menaquinone (MK<sub>6</sub> and MMK<sub>6</sub>). As controls, the single relative activities, i.e. formate dehydrogenase and fumarate reductase activities, were measured. These results together with the absolute theoretical electron transport activities calculated using the Kröger-Klingenberg equation (Equation 2-4) are listed in Table 3-VI.

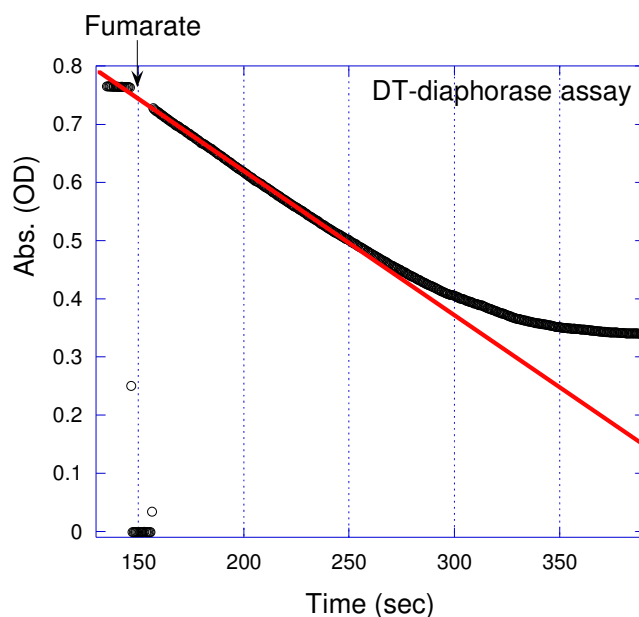
Table 3-VI: Electron transfer activities (Sp. activity) and turnover numbers (TN or K<sub>cat</sub>) performed on *W. succinogenes* re-suspended membranes containing the homologous QFR (A), the *C. jejuni* QFR (B) and the *H. pylori* QFR (C).

Activity assay	A		B		C	
	Sp. activity (U mg <sup>-1</sup> )	TN (min <sup>-1</sup> )	Sp. activity (U mg <sup>-1</sup> )	TN (min <sup>-1</sup> )	Sp. activity (U mg <sup>-1</sup> )	TN (min <sup>-1</sup> )
Formate to quinone	0.07	8	0.19	24	0.04	5
Quinol to fumarate	3.24	421	1.40	182	3.52	458
Formate to fumarate	0.48	154	1.43	458	0.23	74
Theoretical electron transport	63.7 × 10 <sup>-3</sup>	7.9	164.2 × 10 <sup>-3</sup>	21.2	38.6 × 10 <sup>-3</sup>	4.9

#### 3.1.4.4.2. Enzymatic activity

Total and partial activities of the isolated QFRs belonging to the three different  $\epsilon$ -proteobacteria were calculated and are listed in Table 3-VII. These enzymatic assays involve either the whole complex (Unden, *et al.*, 1980, Grivennikova & Vinogradov, 1982, Cecchini, *et al.*, 1986, Westenberg, *et al.*, 1990, Grivennikova, *et al.*, 1993, Maklashina & Cecchini, 1999) or only the hydrophilic subunits (Kröger, *et al.*, 1980, Unden & Kröger, 1986). The partial enzymatic assays can be usefully exploited when assessing enzyme stability or searching for some indications upon inhibitor-binding regions. Whereas the partial activity measured with the “BV assay” in the *W. succinogenes* and *C. jejuni* QFRs is far higher than the one measured with the “MB assay”, this phenomenon is not observed in the *H. pylori* QFR. Moreover, although these two different types of partial activities show that the *W. succinogenes* QFR is

apparently more active, the “DT-DMNH<sub>2</sub> assay” (Figure 3-20) proves that its total activity is similar to the two heterologous QFRs. For comparison reasons, the total enzymatic activities were also performed with the “BH<sub>4</sub>-DMNH<sub>2</sub> assay”: despite the fact that the calculated specific activity of this latter method was generally two-fold lower than the “DT-DMNH<sub>2</sub> assay”, the activity proportions amongst the three QFR species did not change. The calculated Michaelis constants ( $K_M$ ) for the quinone substrate (DMN) were found to be of the order of 0.05-0.10 mM, thus similar to what was previously determined for the *W. succinogenes* QFR (Lancaster, *et al.*, 2005). To assess the enzymatic stability, activity assays were performed after ten days of incubation at 4°C of the detergent solubilized QFRs, and showed a decrease up to 20%.



**Figure 3-20: Typical “DT-DMNH<sub>2</sub> assay” course.** The red line represents a zero order fitting of the first 100 seconds of the reaction time. The activity course is linear, and thus stable, for approximately 2/3 of the entire absorbance interval from 0.34 to 0.78 OD<sub>340</sub>.

**Table 3-VII: Enzymatic activity, Michaelis constant, and inhibitor constant values of the isolated QFR from *W. succinogenes* (A), *C. jejuni* (B), and *H. pylori* (C) after IEF.** The Michaelis constant ( $K_M$ ) values for menaquinone and fumarate, max velocities ( $V_{max}$ ), and inhibition constants ( $K_i$ ) values for the indicated inhibitors were calculated based on the “DT-DMNH<sub>2</sub> assay”.

	A		B		C	
	Sp. act. (U mg <sup>-1</sup> )	TN (sec <sup>-1</sup> )	Sp. act. (U mg <sup>-1</sup> )	TN (sec <sup>-1</sup> )	Sp. act. (U mg <sup>-1</sup> )	TN (sec <sup>-1</sup> )
“MB assay”	22.5	50	7.3	9	12.3	29
“BV assay”	154	340	41	91	15	35
$V_{max}$	14.7	32	9.3	21	12.2	28
Quinone $K_M$ (mM)	0.08		0.06		0.05	
Fumarate $K_M$ (mM)	0.35 <sup>j</sup>		0.1		0.1	
Oxantel $K_i$ (mM)	-		0.38		0.42	
Thiabendazole $K_i$ (mM)	-		0.96		1.35	
Omeprazole $K_i$ (mM)	-		1.96		-	

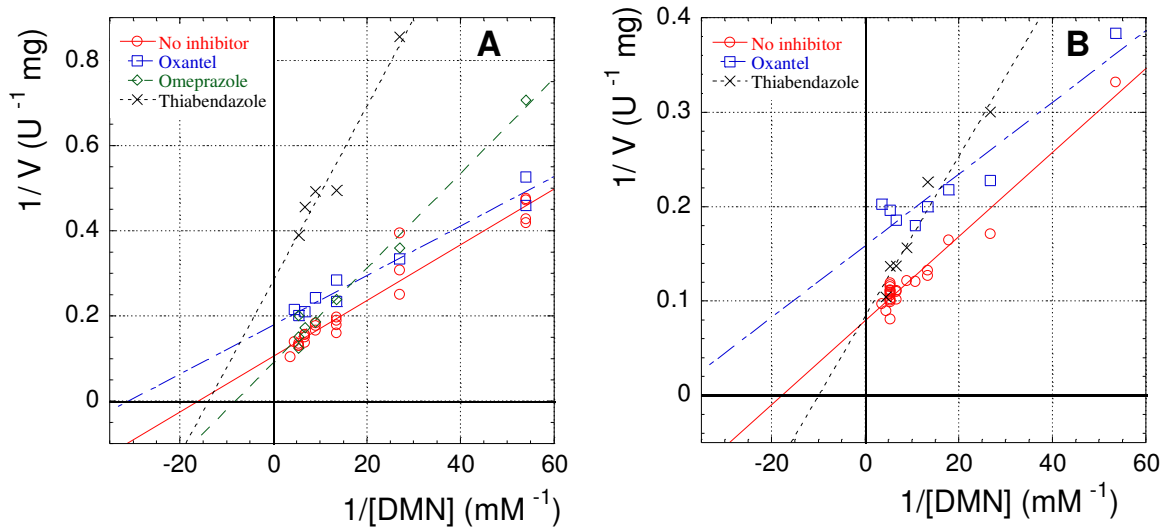
#### 3.1.4.4.3. Effects of inhibitors

Effects of inhibitors like oxantel, thiabendazole and omeprazole on QFR were finely measured using the quinol-regenerating coupled reaction with DT-diaphorase, so that long and stable enzyme kinetics could be measured (Figure 3-20). With this method, the inhibitor was added 20-30 seconds after the catalytic reaction was started, so that the pre-inhibition activity value could be used as an internal control for each trial. The enzymatic assay in the presence of the inhibitor was carried out with a minimum of six different substrate (DMN) concentrations. The rate of DMNH<sub>2</sub> regeneration by DT-diaphorase was measured, and proved to be faster than the QFR enzymatic activity at any time and condition. As a further experimental control, the DT-diaphorase enzymatic activity was measured in the presence of the inhibitors, so that any unforeseen inhibition effect was prevented. The inhibition constant ( $K_i$ ) values of these compounds are listed in Table 3-VII. The Lineweaver-Burk plots (Figure 3-21) show that whereas oxantel has an un-competitive effect on both enzymes,

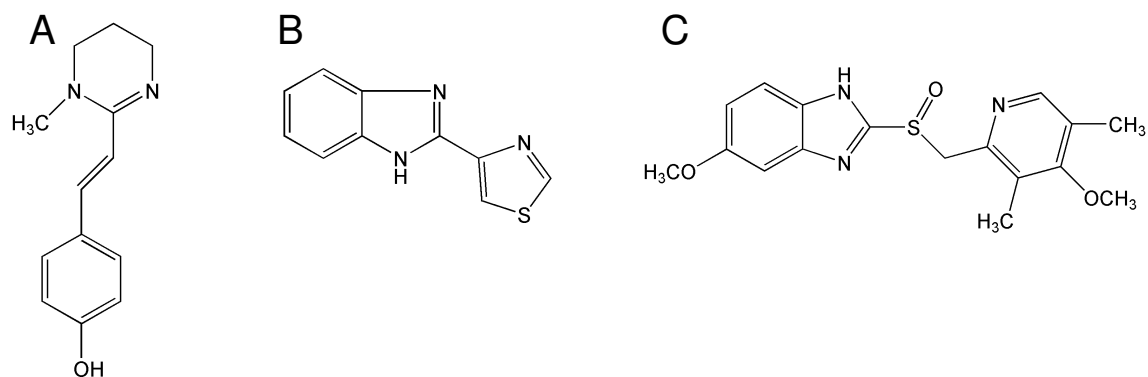
<sup>j</sup> From Lancaster & Simon, 2002.



thiabendazole affects QFR activity as a competitive inhibitor in the *H. pylori* QFR and as a non-competitive inhibitor in the *C. jejuni* enzyme. Omeprazole show only a competitive effect in the *C. jejuni* QFR.



**Figure 3-21: Lineweaver-Burk plots of *C. jejuni* QFR (A) and *H. pylori* QFR (B) activity.** The red empty circles (•) and the solid line (linear regression) represent QFR activity without inhibitors. The blue empty squares (•) and the dashed line represent QFR activity in presence of 300 $\mu\text{M}$  oxantel. The black crosses (×) and the dashed line represent QFR activity in presence of 2mM thiabendazole. The green empty squares (◇) and the dashed line represent QFR activity in presence of 2mM omeprazole.



**Figure 3-22: Chemical structure of tested inhibitors: oxantel (A), thiabendazole (B) and omeprazole (C).**

The effects of these three inhibitors, whose chemical structures are shown in Figure 3-22, were also tested on partial activities (“BV assay” and “MB assay”) of the *C. jejuni* and *H. pylori* QFR. Based on results obtained with the former enzymatic assay, oxantel was the only inhibitor affecting the hydrophilic subunits of the two enzymes ( $IC_{50} \sim 0.2-0.3$  mM). The “MB assay” was rather sensitive to the addition of DMSO (the inhibitor solvent) and, except for the oxantel, where inhibition was rather unequivocal ( $IC_{50} \sim 0.1$  mM), thiabendazole and omeprazole showed questionable effects.

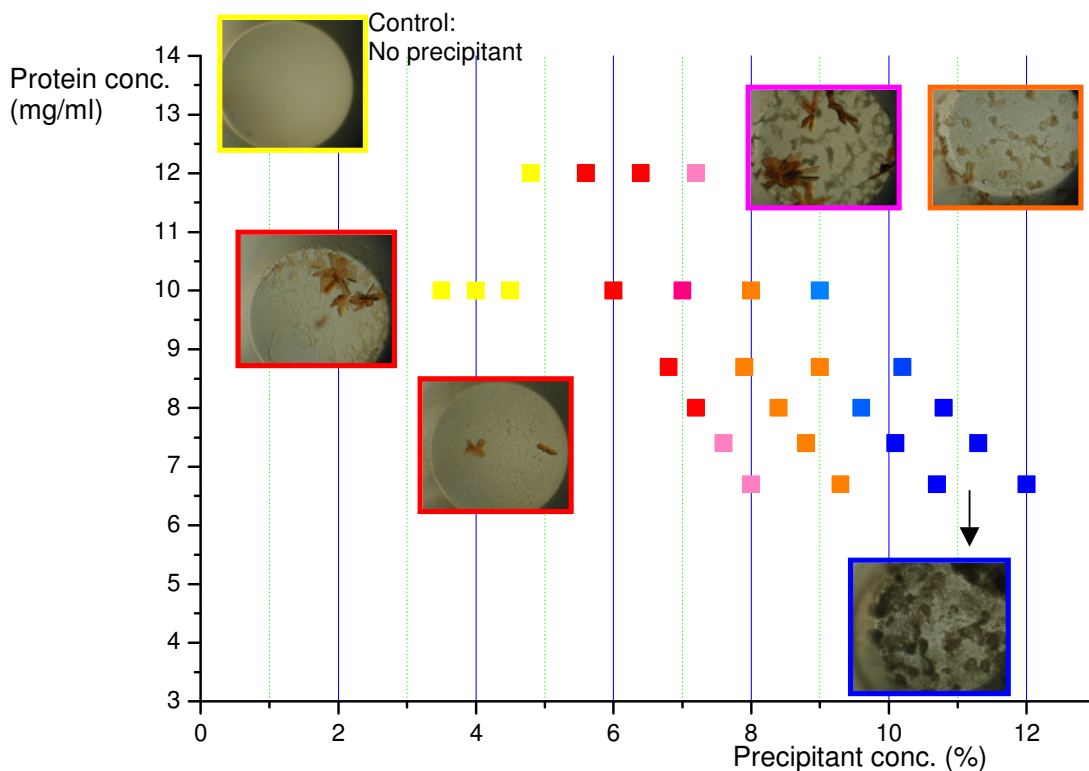
Others inhibitors such as metronidazole, nizatidine, morantel, and TTFA had very high extinction coefficients at the wavelength used for NADH or DMN detection, and hence they could not be characterized with the available enzymatic assays.

### 3.1.5. Crystallization and data collection

Firstly, crystallization attempts using conditions equal to those producing well-diffracting *W. succinogenes* QFR crystals were made. However, these conditions were not optimal for the *H. pylori* and *C. jejuni* QFRs, therefore, extensive crystallization screening of these enzyme samples after IEF or gel filtration purification has been carried out. Phase diagrams are important to monitor the precipitation tendency of the protein during crystallization attempts. The phase diagrams for *H. pylori* QFR (not shown) and *C. jejuni* QFR (Figure 3-23) after IEF were plotted based on results obtained from micro-batch crystallization at 18°C using the conditions indicated in the figure legend. As observed in Figure 3-23, the tolerance<sup>k</sup> to polyethylene glycol (precipitant) observed for the *C. jejuni* QFR was up to 7 %. Strikingly, the tolerance to the same precipitant for the *H. pylori* QFR was far higher, reaching even 10 %. Moreover, up to 7-8 % precipitant, the crystallization drop was perfectly clear and no phase changes were observed. Between 8 % and 10 % of precipitant the *H. pylori* QFR formed crystalline precipitate or gelatinous phases. Thus, though the protein did not form any proper crystal, it demonstrated to be very stable in this crystallization conditions.

---

<sup>k</sup> Intolerance is defined as formation of an amorphous precipitate where the protein assumes a dark-brownish color.

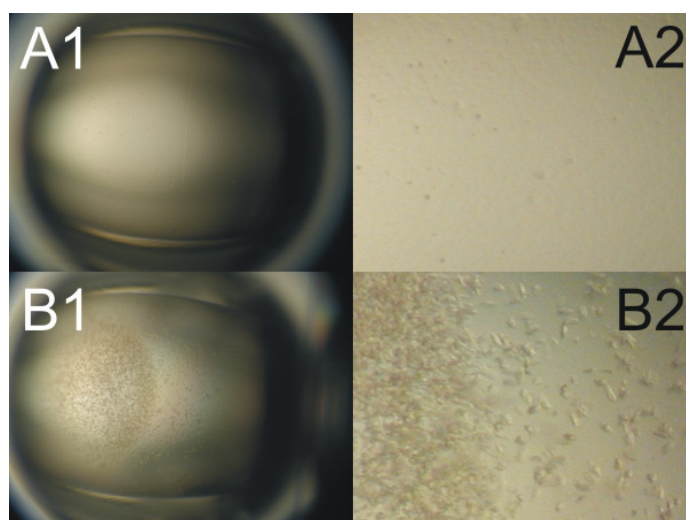


**Figure 3-23: Phase diagram of the *C. jejuni* QFR.** The diagram color code for the phases is clarified with the support of the pictures (see pictures frame). The reservoir consisted of 0.1 M LiSO<sub>4</sub>, 0.1 ADA (pH 6.5), 2 % isopropanol, and different concentrations of PEG 4000.

Preliminary three-dimensional (3D) crystallization attempts of the *C. jejuni* QFR and *H. pylori* QFR after IEF generally produced large ultra-thin layer crystals (Figure 3-25-D), and little-squared layer crystals (Figure 3-25-A), respectively. The *H. pylori* QFR clearly resulted to be less prone to crystallize, as the best achievement obtained was rod shaped crystals with size of ~0.2 mm (Figure 3-25-B) that diffracted up to 8 Å. However, results obtained in many crystallization conditions showed that both QFR samples maintained even after several weeks or months a vivid orange color, sign that the heterologous QFR preparations were highly stable and did not undergo denaturation. Whereas the size and the shape of crystals of the *C. jejuni* QFR strikingly improved after gel filtration, the *H. pylori* QFR crystals were replaced from orange jelly/amorphous phases (Figure 3-25-C).

To remove any undesired micro-precipitation and protein aggregates from the protein-reservoir crystallization mixture, an ultracentrifugation cycle (Horsefield, *et al.*, 2003) was performed on the *H. pylori* QFR sample prior to incubation, but did not lead to particular

improvements. Crystallization of the same protein in the presence of lipids (CA 18:1, DPPE, DOPC, DPPG) at the stoichiometric ratio of five lipid molecules per monomer of QFR, has also been attempted. As it was seen for the enzymatic activity, this protein seems to be far more stable and less prone to the formation of the gelly phases when lipids were added. Most importantly, the addition of cardiolipin has improved the crystallization properties of the *H. pylori* QFR (Figure 3-24). Crystallization trials with this enzyme at the last stage of purification (gel filtration) were not able to produce any crystal, whereas after addition of CA 18:1 some tiny crystals were appearing in the drop. The protein-lipid co-crystallization experiments are however at a preliminary stage, and further studies are necessary.



**Figure 3-24: Co-crystallization of the *H. pylori* QFR with cardiolipin (B), and comparison to a crystallization trial without cardiolipin (A).** The crystallization setup, photographed at two different magnifications (1 and 2), consists of 1  $\mu$ l drop volume with conditions similar to those indicated in Table 2-XVI.

Efforts aimed at the 3D crystallization of the two heterologously produced QFRs have included a large variety of crystallization methods and conditions (e.g. seeding, streaking, change of incubation temperature, screening of other additives, freezing in liquid N<sub>2</sub>, etc.). The use of cryo-compatible reservoirs (hence containing cryo-protectant) or crystal soaking in paraffin, silicon oil or Al's oil was helpful in the procedure of freezing but fruitless in terms of resolution improvement. Furthermore, the crystallization of the two enzymes did not show any improvement when the detergents LM and DM present in the QFR sample have been exchanged with other detergents like LDAO, Thesit, LM, DM, OG, UM. During

the crystal development of the *C. jejuni* QFR, several crystal forms were obtained: diamond-like (Figure 3-25-E), triangular (-F), needle-like (-G), arch-like (-H), “rugby ball”-like (-I), broom-like (-L), trapezoidal (-M, -N), crystals agglomerates (mainly at the interface between different phases) (-O), small layers (-P), large layers (-Q, -R). This latter crystal form resulted to be a high-resolution diffracting crystal (see Material and Methods for conditions), albeit some other crystal forms were larger in size (e.g. trapezoidal shape). The Figure 3-25-S shows the previous crystal (picture -R) mounted in the glass capillary.

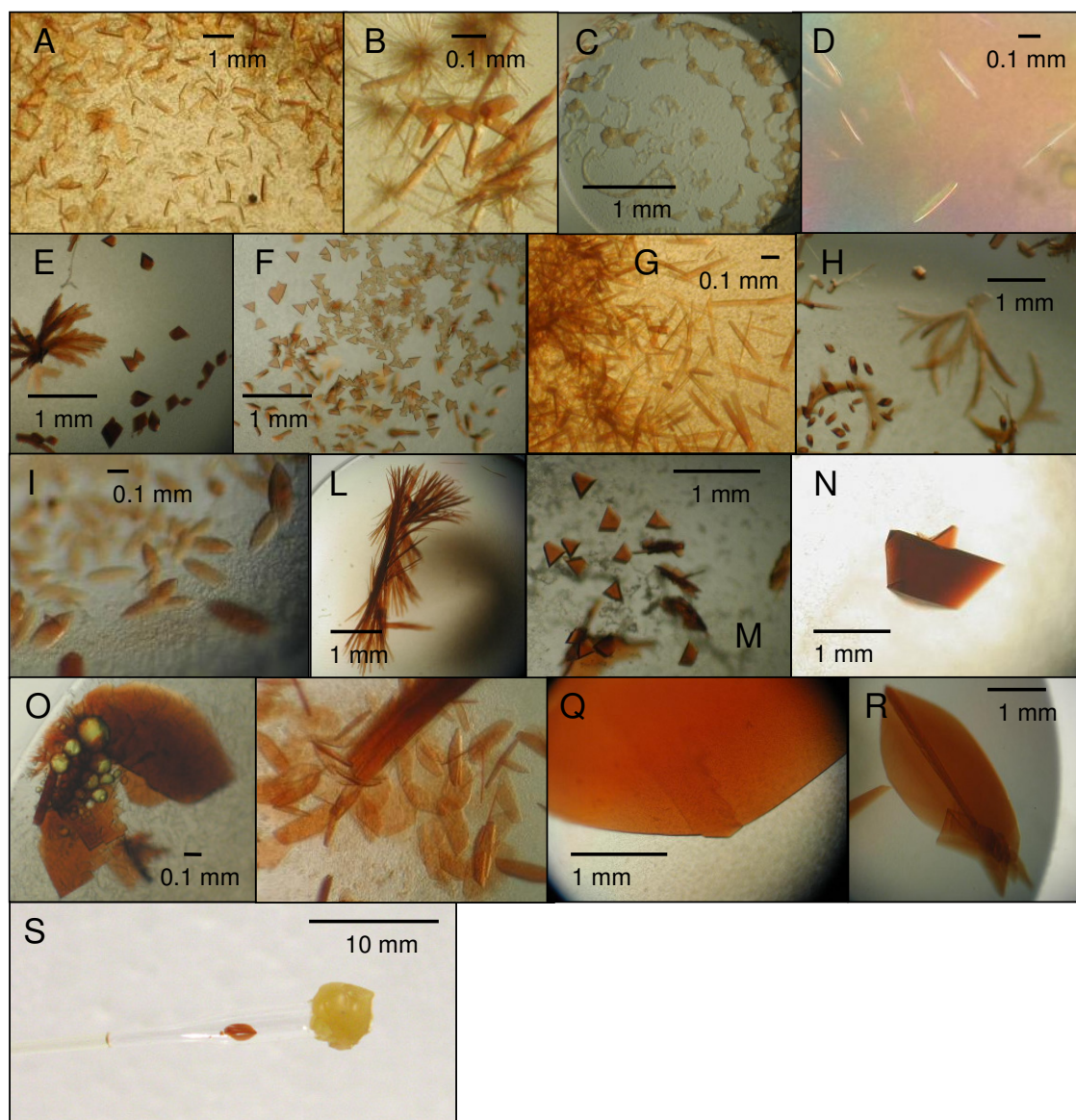


Figure 3-25: Crystals of *C. jejuni* (D-S) and *H. pylori* QFRs (A-C). The respective crystallization conditions have been displayed in Table 3-VIII.

**Table 3-VIII: Crystallization conditions which have been used for the achievement of the *C. jejuni* and *H. pylori* QFR crystals shown in Figure 3-25.** The protein buffer was containing of 0.1 % DM, 0.01 % LM, 20mM fumarate, 1mM EDTA, 20mM HEPES at pH 7.3. The protein concentration was 20mg/ml unless indicated. In order to maintain the protein oxidized, 1mM  $K_3Fe(CN)_6$  was added to every crystallization mixture. Crystallization setups were incubated at 18°C.

Pic.	Prot. Prep.	Add.	Add.	S.A.	Precip.	Salt	Buffer (mM) pH	Remarks
A	HpQFR IEF	vitK <sub>2</sub> 1 mM	DMF 5.5 %	BA 1.2 %	PEG3350 10 %	NaCl 150 mM	NaCit. 20mM pH 5.6	seeding
B	HpQFR IEF	vitK <sub>2</sub> 1 mM	DMF 5.5 %	BA 1.2 %	PEG3350 10 %	NaCl 150 mM	NaCit. 20mM pH 5.6	seeding
C	HpQFR GF	vitK <sub>2</sub> 1 mM	isop. 2 %	BA 1.2 %	PEG4000 14 %	LiSO <sub>4</sub> 0.1 M	ADA 0.1 M PH 6.5	-
D	CjQFR IEF	vitK <sub>2</sub> 1 mM	DMF 5.0 %	BA 1.2 %	PEG3350 10 %	NaCl 150mM	NaCit. 20mM pH 5.6	-
E	CjQFR GF	vitK <sub>2</sub> 1 mM	isop. 2 %	BA 2.4 %	PEG4000 10 %	LiSO <sub>4</sub> 80 mM	ADA 0.1 M PH 6.5	+ oxantel 1mM
F	CjQFR GF	vitK <sub>2</sub> 1 mM	-	BA 2.4 %	PEG8000 10 %	-	MgAc. 0.2 M	-
G	CjQFR GF	vitK <sub>2</sub> 1 mM	DMF 5.5 %	BA 1.2 %	PEG3350 10%	NaCl 150 mM	NaCit. 20mM pH5.6	-
H	CjQFR GF	vitK <sub>2</sub> 1 mM	-	-	PEG4000 12 %	LiSO <sub>4</sub> 100 mM	ADA 0.1 M PH 6.5	silicon oil
I	CjQFR GF	vitK <sub>2</sub> 1 mM	-	HT 2 %	PEG4000 15 %	AmmSO <sub>4</sub> 0.2 M	NaCit. 0.1 M PH 5.6	-
L	CjQFR GF	vitK <sub>2</sub> 2 mM	OG 0.3%	HT 1.5 %	PEG4000 16 %	LiSO <sub>4</sub> 0.2 M	TRIS-HCl 0.1 M pH 8.5	prot. conc. 28.5 mg/ml
M	CjQFR GF	vitK <sub>2</sub> 1 mM	isop. 2 %	BA 2.4 %	PEG4000 12 %	LiSO <sub>4</sub> 100 mM	ADA 0.1 M PH 6.0	-
N	CjQFR GF	vitK <sub>2</sub> 2 mM	isop. 2 %	BA 2.4 %	PEG4000 10 %	LiSO <sub>4</sub> 80 mM	ADA 0.1 M PH 6.5	+ oxantel 1mM
O	CjQFR IEF	vitK <sub>2</sub> 2 mM	DMF 5.0 %	BA 2.4%	PEG3350 10 %	NaCl 150 mM	NaCit. 20mM pH5.6	-
P	CjQFR GF	vitK <sub>2</sub> 1 mM	OG 0.6%	-	PEG4000 16 %	LiSO <sub>4</sub> 0.2 M	TRIS-HCl 0.1 M pH 8.5	+ oxantel 1 mM
Q	CjQFR GF	vitK <sub>2</sub> 2 mM	-	HT 2 %	PEG4000 12 %	LiSO <sub>4</sub> 100 mM	NaCit. 0.1 M pH5.6	prot. conc. 28.5 mg/ml
R, S	CjQFR GF	vitK <sub>2</sub> 2 mM	-	HT 2 %	PEG4000 12 %	LiSO <sub>4</sub> 100 mM	ADA 0.1 M PH 6.5	prot. conc. 28.5 mg/ml

### 3.1.5.1. 3D-crystal structure of the *C. jejuni* QFR

Data collection was accomplished as described in Materials and Methods. Data processing has established that the unit cell symmetry of the crystal form used for solving the *C. jejuni* QFR structure belong to the space group P2<sub>1</sub> (primitive monoclinic). The unit cell parameters as well as data processing statistics are listed in Table 3-X.

The three-dimensional crystal structure of the QFR from *C. jejuni* in the fully oxidized state (Figure 3-27) has been solved by molecular replacement using as a search model the *W. succinogenes* QFR, solved at 1.8 Å resolution (PDB entry code 2BS2, Lancaster, C.R.D., unpublished). In order to reduce to minimum the bias deriving from the search model, which was solved at much higher resolution, a composite omit map has been calculated and used for model building. The recombinant *C. jejuni* QFR that was heterologously produced and crystallized is composed of 1166 amino acids, and is divided in the three subunits FrdA, FrdB, and FrdC, with 663, 243, and 262 amino acids, respectively. In the structure presented here, the electron density for 1051 amino acids is defined. The main chain of other 45 amino acids have been included in the structure<sup>1</sup>, however the low quality of the electron density hindered any possibility to model their side chains. Unfortunately, other regions of the protein were not identifiable in the electron density maps, and the respective amino acids had to be deleted from the structure produced. The list of unassigned amino acids or residues and the refinement statistics are summarized in Table 3-IX and Table 3-X, respectively.

**Table 3-IX: Unassigned amino acids and side chains.** List of amino acids that have not been assigned and hence deleted from the modeled structure. List of amino acid side chains that could not be assigned and whose occupancies (Q) have been set to zero.

	Missing residues	Missing side chains
<b>Subunit A</b>	(41 aa): 271-274, 277-279, 295-297, 330-340, 349-351, 353-359, 361-368, 662-663	(29 aa): 121-123, 128-132, 267, 276, 285, 289-290, 301, 307, 342, 346-348, 500-501, 516-517, 602, 609-611, 633-634
<b>Subunit B</b>	none	none
<b>Subunit C</b>	(31 aa): 62-75, 246-262	(16 aa): 3-4, 111, 152, 199, 202-203, 205-207, 209, 212, 227-228, 231-232

<sup>1</sup> The occupancy of these 45 amino acid side chains has been set to zero in the PDB file.

**Table 3-X: Crystallographic table: data processing and refinement statistics of the *C. jejuni* QFR structure.** In brackets are showed the respective outer shell values; R.M.S.D., root mean square deviations; the  $R_{\text{free}}$  was calculated with 1.6 % of the total reflections;  $n_{\text{obs}}/n_{\text{par}}$  ratio of the number of observed unique reflections used in the working set over the number of parameters necessary to define the model.

<i>Data collection</i>		<i>Refinement</i>			
<b>Space group</b>	P2 <sub>1</sub>	<b>R<sub>cryst</sub> (%)</b>	24.4 (33.4)		
<b>Unit cell size (Å)</b>	<b>a:</b> 117.176	<b>R<sub>free</sub> (%)</b>	25.8 (39.3)		
	<b>b:</b> 130.653	<b>Average B-factor (Å<sup>2</sup>)</b>	62.1		
	<b>c:</b> 132.941	<b>n<sub>obs</sub>/n<sub>par</sub></b>	2.15		
<b>Unit cell angle β (°)</b>	107.969	<i>R.M.S.D. from ideal values</i>			
<b>Mosaicity</b>	0.090	<b>Bond lengths (Å)</b>	0.0089		
<b>Resolution range (Å)</b>	70.0-3.24 (3.36-3.24)	<b>Bond angles (°)</b>	1.461		
<b>Measured reflections</b>	241,397 (23,433)	<i>Structure validation</i>			
<b>Redundancy</b>	3.9 (3.8)	<b>Subunit</b>	<b>FrdA</b>	<b>FrdB</b>	<b>FrdC</b>
<b>Unique reflections</b>	61,387 (6,090)	<b>Amino acids n°</b>	622	243	231
<b>Completeness (%)</b>	99.2 (98.8)	<b>Most favored regions (%)</b>	82.8	83.0	81.9
<b>R<sub>sym</sub> (%)</b>	8.2 (34.3)	<b>Additional allowed (%)</b>	14.5	15.1	15.3
<b>I/σ(I)</b>	5.2 (2.2)	<b>Generously allowed (%)</b>	2.1	0.5	2.3
		<b>Disallowed (%)</b>	0.6	1.4	0.6

The asymmetric unit contains two heterotrimeric molecules of the quinol:fumarate reductase complex formed by the three subunits A, B, and C associated in an identical fashion and arranged as a homodimer with a high degree of buried surfaces. The crystal packing found in this structure (Figure 3-26-A) has likely been influenced by the presence of an unusual loop involving the last 15 assigned residues of the FrdC subunit and probably the following 17 amino acids of the same subunit (FrdC-246 to -262) that are not identified in the structure, which depart from subunit C of one asymmetric unit and reaches the subunit A of the adjacent asymmetric unit (Figure 3-26-B).



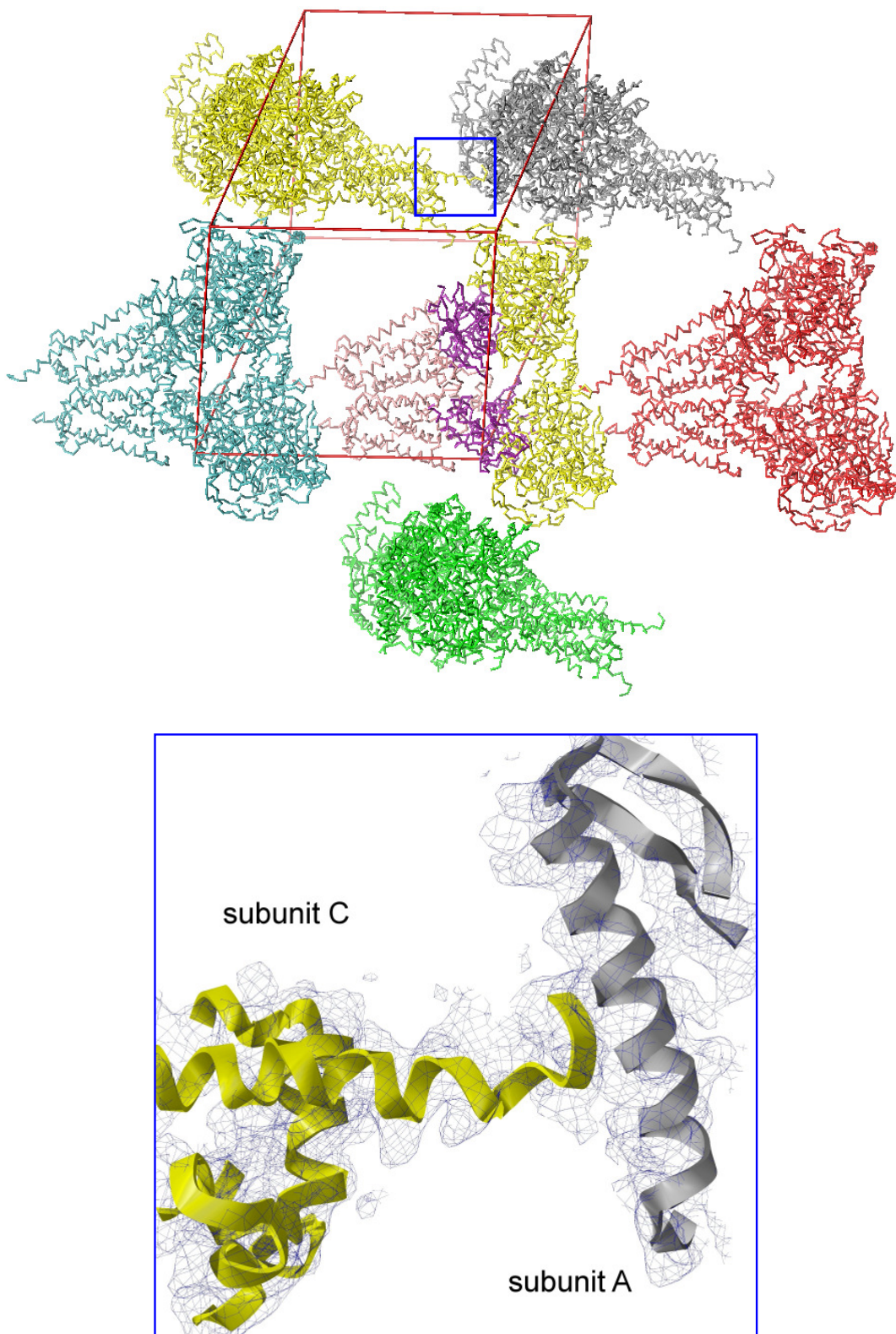
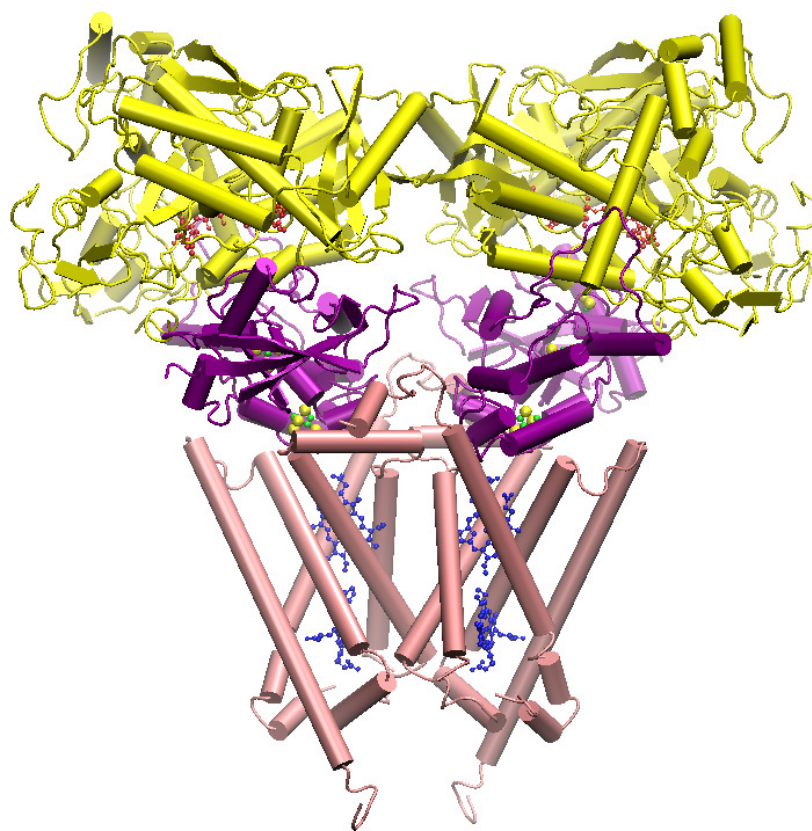


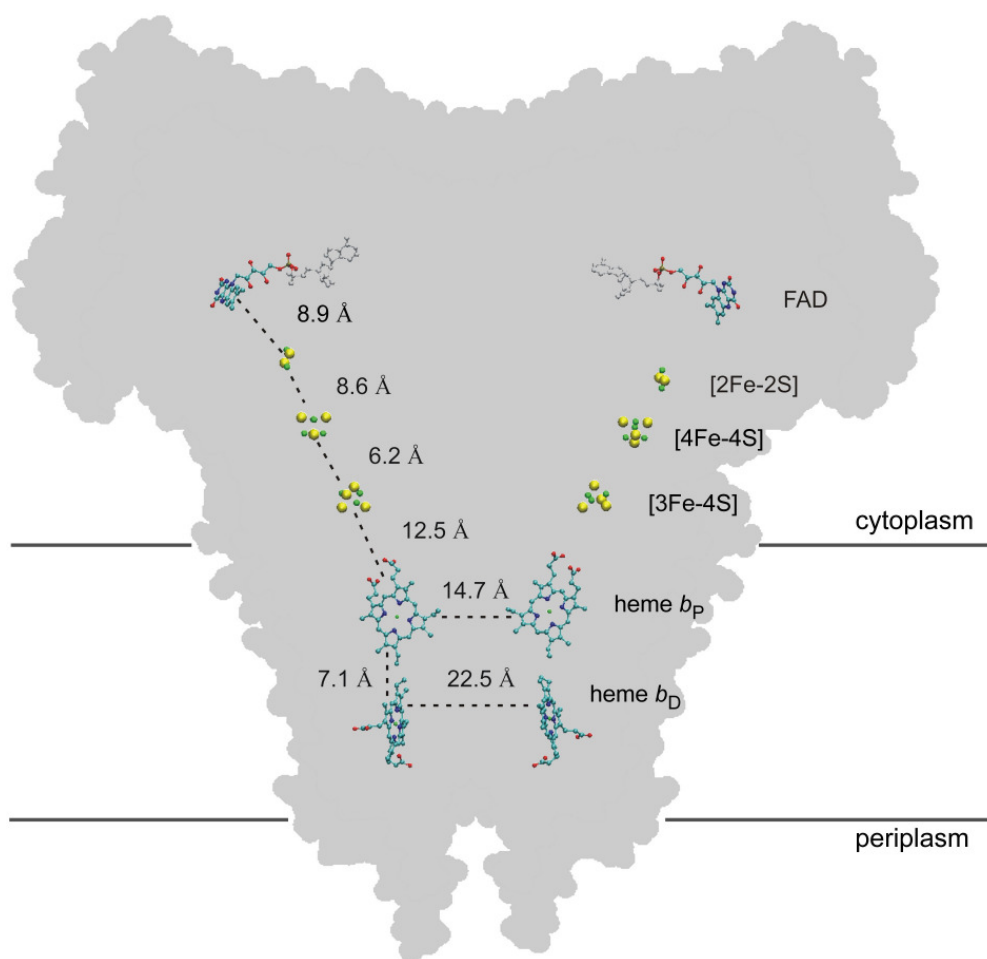
Figure 3-26: Crystal packing (top) of the *C. jejuni* QFR structure and a snapshot (bottom) of one crystal contact as indicated by the blue box. The red cube in the top figure represent the crystallographic unit cell.

Figure 3-27 shows the overall crystal structure of the *C. jejuni* QFR. Attached to subunit C, which is formed by five membrane-spanning helices and contains the site of menaquinol oxidation (Reaction 1-6), is subunit B, which is oriented towards the cytoplasmic side of the membrane and contains in the following order the [3Fe-4S], [4Fe-4S], and [2Fe-2S] iron-sulfur clusters. Attached to subunit B, and not in contact with subunit C, is subunit A, which is the largest subunit and which incorporates the covalently bound flavin adenine dinucleotide (FAD) prosthetic group and the site of fumarate reduction (Reaction 1-5). A relevant domain amongst those composing subunit A is the capping domain, which undergoes a large movement upon binding of the substrate in order to close the active site to solvent (Lancaster, *et al.*, 2001). It likely due to its high mobility that this latter domain and the nearby regions are characterized by poor electron density.



**Figure 3-27: The crystal structure of the *C. jejuni* QFR.** The subunit A (in yellow) contains the FAD prosthetic group (red sticks); the subunit B (in purple) contains from top to bottom the S1, S3, and S2 iron-sulfur clusters (the yellow and green spheres correspond to sulfur and iron atoms, respectively); the transmembrane subunit C (in pink) contains from top to bottom the proximal and the distal hemes (blue sticks).

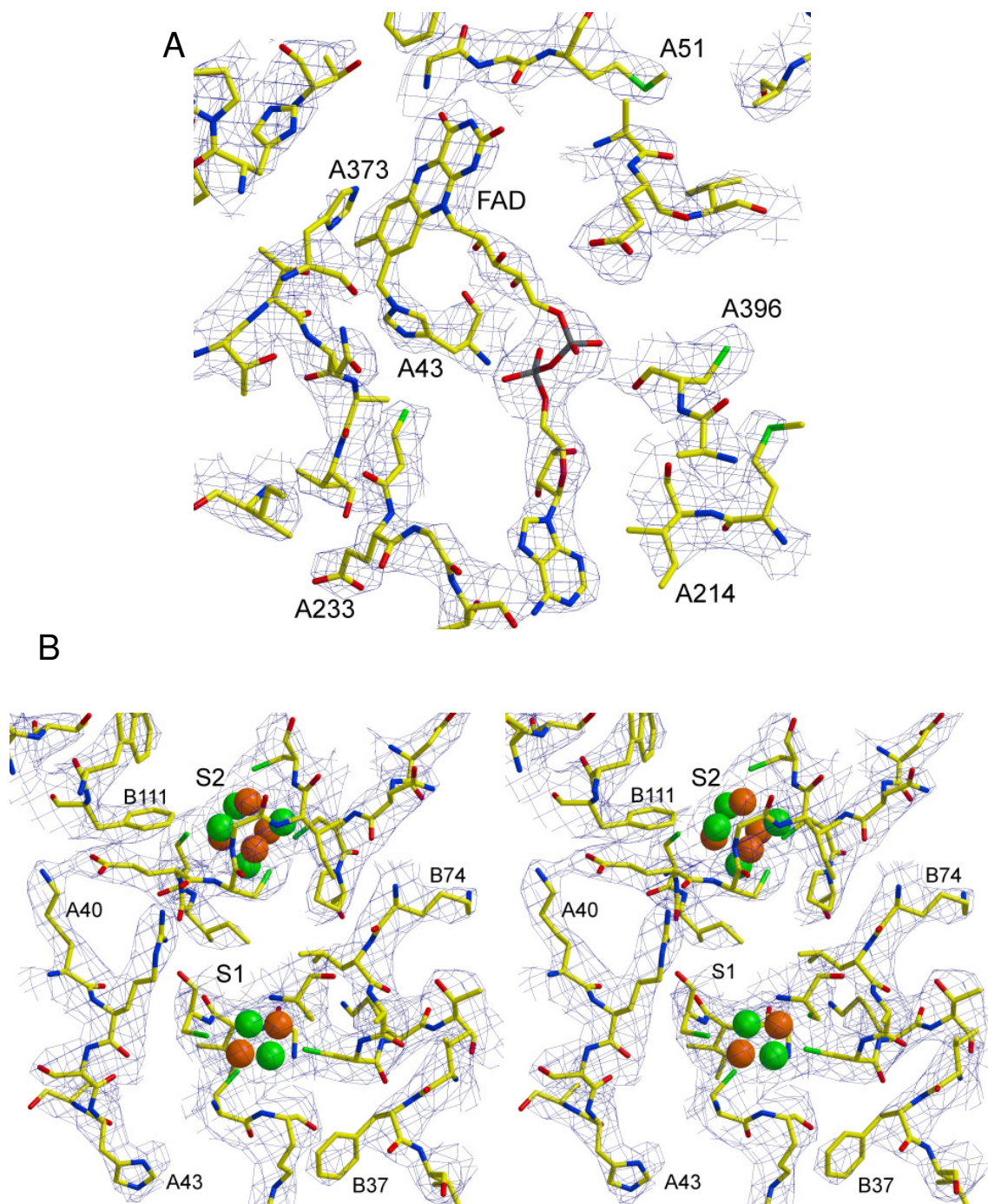
Figure 3-28 shows the location of all cofactor centers of this enzyme in the structure. Distances between centers located within one heterotrimer lie well within the so-called “Moser-Dutton limit” for physiological electron transfer of 14 Å (Page, *et al.*, 1999). Since the distances between hemes belonging to two different homomers in the dimer exceed this limit, no relevant electron transfer is to be expected between the two monomers.



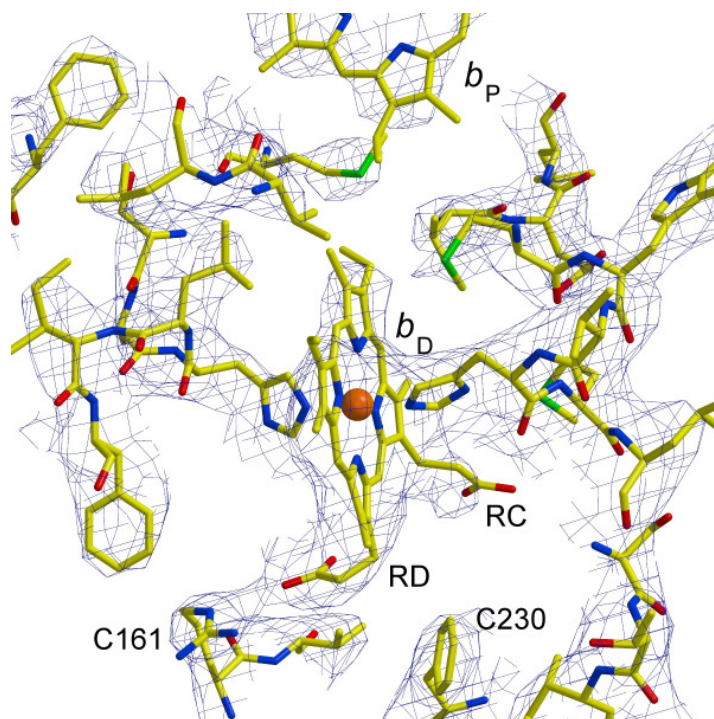
**Figure 3-28: Arrangement of the prosthetic groups in the fumarate reductase from *C. jejuni*.** At the right of the figure the names of the cofactors are provided. Numbers refer to edge-to-edge distances, which were measured as defined by Page, *et al.*, 1999. Color codes of the atoms are as follows: yellow, sulfur; green, iron; cyan, carbon; red, oxygen; blue, nitrogen. The adenosine dinucleotide group is drawn in light grey.

The goodness of the composite omit maps in the regions of the iron-sulfur clusters S1 and S2 with their cysteine ligands and some surrounding amino acids are shown in Figure 3-29-B. In addition, the electron density and the structure of the FAD group and its ligand FrdA-H43

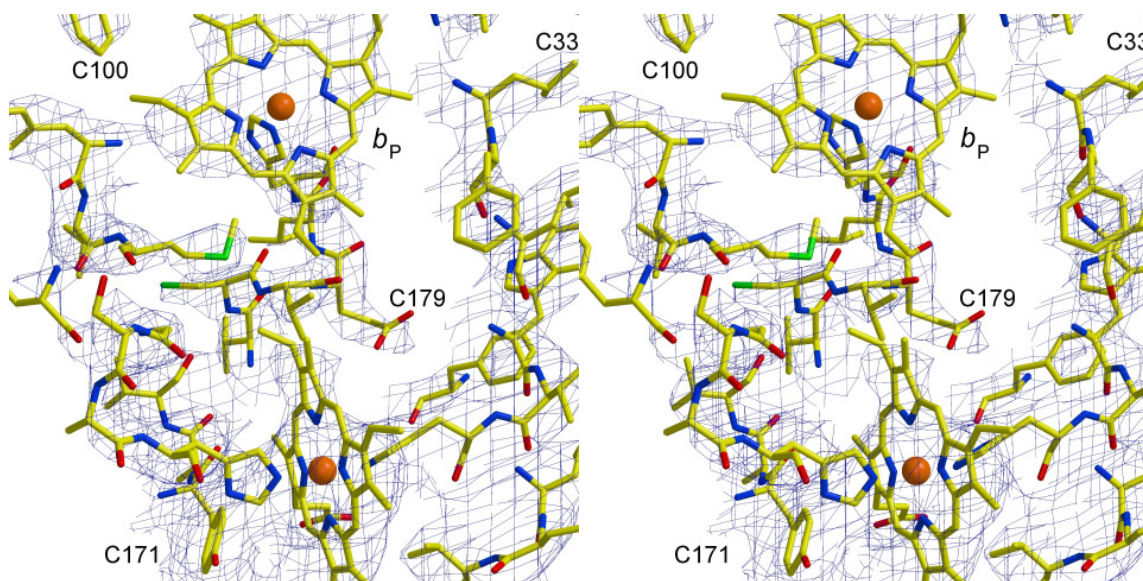
(Figure 3-29-A) are confirming the  $8\alpha$ -[N $\epsilon$ -histidyl]-linkage to the isoalloxazine ring, as determined previously by Kenney & Kroger, 1977 and Lancaster, *et al.*, 1999.



**Figure 3-29: Electron density and model of the FAD prosthetic group (A) and the S1 and S2 iron-sulfur clusters (B, cross-eye stereo view).** The  $|2F_o - F_c|$  composite omit maps (Hodel, *et al.*, 1992) are contoured at 0.8 standard deviations ( $\sigma$ ) above the mean density of the maps.



B



**Figure 3-30: Electron density and model of the distal heme (A), and the region between the hemes containing the FrdCE180 residue (B, cross-eye stereo view).** The composite omip maps are contoured at  $0.8 \sigma$ . RC and RD correspond to the ring C and ring D propionates, respectively.

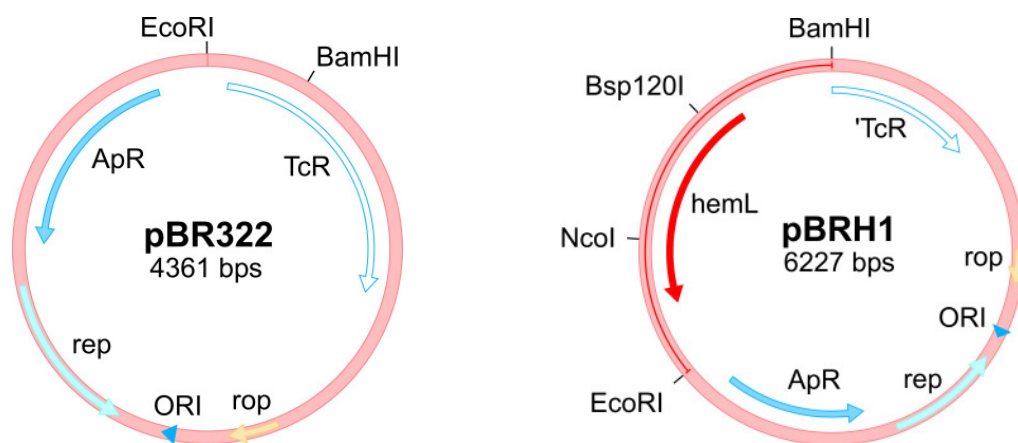
Interestingly, the feature observed in the *W. succinogenes* QFR structure concerning the structural positions of the heme<sub>D</sub> ring C propionate and the residue FrdC-E180 are here

conserved in the structure (Figure 3-30-A and -B). The conserved orientation of these two latter components is coherent with the view that also the QFRs from the  $\epsilon$ -proteobacterium *C. jejuni*, like the one from *W. succinogenes*, could make use of the coupled transmembrane proton and electron transfer as suggested by the E-pathway hypothesis. However, as it is discussed below in section 4.1.5.1, the structure here presented is characterized by low resolution, low structure factor intensities, and rather high B-factor values, which do not permit a definitive discussion at the present stage.

## 3.2. $^{13}\text{C}$ -Labeling of QFR Heme Propionates

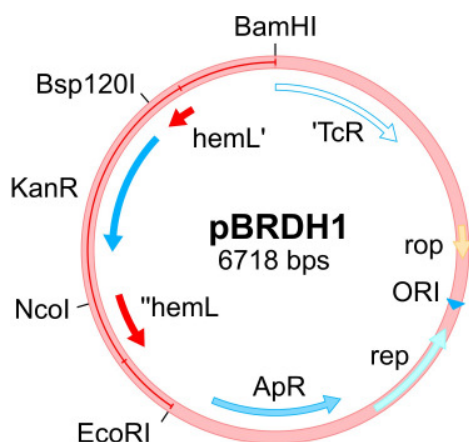
### 3.2.1. Cloning and characterization of the $\Delta hemL$ mutant

The following cloning procedure was carried out to construct a plasmid suitable for homologous reciprocal recombination with the genome of the WT *W. succinogenes* in order to carry out a one-step gene disruption of the *hemL* gene. The gene glutamate-1-semialdehyde 2,1-aminomutase (*hemL*), including 570 bp from the upstream region and 360 bp from the downstream region, was amplified by PCR using as template the genomic DNA from the WT strain. The amplification was carried out using the two synthesized oligonucleotide primers HemL1\_Fw and HemL1\_Rv (see Table 2-VI). In order to insert the fragment into the vector pBR322 by ligation, the restriction sites EcoRI (in the HemL1\_Rv primer) and BamHI (in the HemL1\_Fw primer) were introduced at the 5'-ends of these primers.



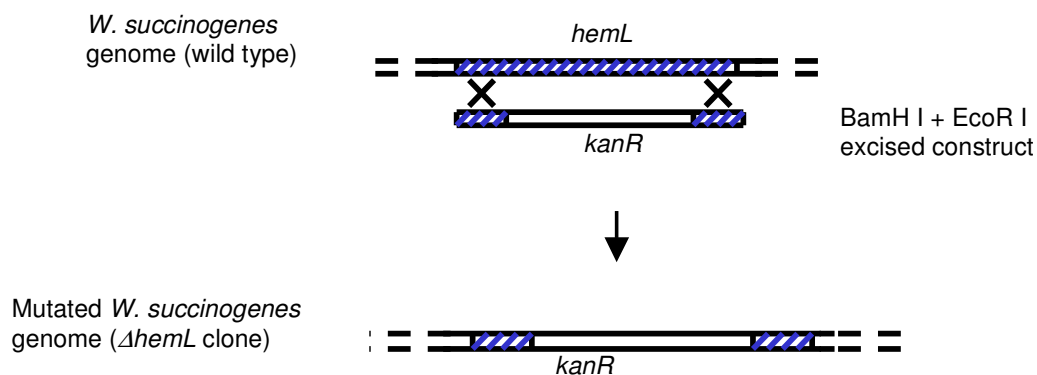
**Figure 3-31: Plasmid maps of the pBR322 and the recombinant pBRH1.** Restriction sites, plasmid size, genes, and markers are indicated.

The new recombinant plasmid (pBRH01) was then digested with NcoI and Bsp120I, generating a deletion of 740bp into the 1.3 kbp *hemL* gene. A 1.21 kbp DNA fragment containing the kanamycin resistance cassette (*kan*) was amplified by PCR using two newly synthesized primers (KanM\_Fw and KanM\_Rv), flanked by two inserted Bsp120I and NcoI restriction sites inserted at the 5'-ends. This latter amplified DNA fragment was digested with Bsp120I and NcoI restriction enzymes and ligated with the *hemL*-deleted plasmid pBRH1, maintaining the same direction of the *hemL* promoter.



**Figure 3-32: Plasmid map of the recombinant pBRΔH1.** Restriction sites, plasmid size, genes, and markers are indicated. The construction procedure is described in the text.

Analytical digestion on this new plasmid, named pBRΔH01, was performed with the four restriction enzymes used for cloning and BssSI to ensure the correct insertions and directions in the construct. As expected, double digestion with BamHI and EcoRI showed that the DNA fragment containing the  $\Delta$ *hemL* gene was about 500 bp larger respect to the fragment produced by the previous pBRH01, which was used as a control. Only the BamHI/EcoRI excised plasmidic fragment was used for integration. *W. succinogenes* WT strain was hence transformed by electroporation, and the recombinant cells were collected from rich medium agar plates containing kanamycin (25 mg/l) and 1 mM ALA.



**Figure 3-33: One-step gene disruption of the *hemL* gene from the *W. succinogenes* genome.** The double crossing-over (black crosses) is occurring at the homology regions (obliquely striped areas).

A few hundred colonies were obtained in the selective agar rich medium and screened by PCR in order to verify the homologous recombination event. The primers synthesized for the *hemL* amplification have been used to perform the PCR on the isolated colonies. The clones that underwent a genome recombination in the correct locus yielded an amplified DNA fragment that was unequivocally 500 bp larger than the WT, which was used as a control. The presence of only the target amplified DNA band ruled out the possibility of a non-homologous recombination, which would be characterized by two DNA fragments of both sizes, instead. Out of twelve colonies screened, ten (N1 to N10) showed the correct *hemL* deletion. The growth yield and doubling times of these ten mutants were determined by following growth curves in minimal medium containing 1 mM ALA. The best candidate (mutant strain N2) was then selected for large-scale protein production. The deletion strains were also inoculated in rich and minimal media containing different concentrations of ALA. In rich medium, growth was obtained in every circumstance, though final cell density decreased towards lower concentration of ALA. In minimal medium, growth was experienced only in media containing ALA at a concentration equal to or above 0.2 mM. Due to the high cost of the labeled compound, the large-scale growth medium was supplemented with a concentration of 0.2 mM ALA. At this concentration, it was found that several cultures failed to start growing, thus the cell growth was irreproducible, especially upon up-scaling to larger culture volumes. This problem was overcome by increasing the ratio of inoculum to fresh medium from 1:200 to 1:50. At this latter ratio, the growth was fully recovered and comparable to higher concentrations of ALA. Furthermore, observation of the



cells in the late exponential phase with a light microscope (400x) did not show any optical difference between mutant and WT cells.

### 3.2.2. Enzymatic production and characterization

The large-scale preparation yielded about 64 grams of cells, hence about half of the usual yield for the WT strain in rich medium. Processing of the cells and isolation of the  $^{13}\text{C}$ -labeled QFR was performed in a procedure identical to that described already (see Materials and Methods). The purification profile based on the “MB assay” activity exhibits a usual enzymatic behavior of the QFR. SDS-PAGE analysis of the IEF purified QFR presents three characteristic bands of the subunits A, B, C, and very weak contaminant bands, comparable to typical WT QFR preparations.

Table 3-XI: Purification profile based on partial specific activity (“MB assay”) of the  $^{13}\text{C}$ -labeled QFR from *W. succinogenes*.

	Total activity (U)	Specific activity (U mg <sup>-1</sup> )	Enzyme yield (%)	Purification factor
Cell homogenate	5150	0.6	100	1.0
TritonX100 homogenate	5660	1.3	110	2.2
TritonX100 extract	5700	2.8	111	4.7
Anion exchange	2394	12.0	46	20
Isoelectric focusing	1744	17.4	34	29

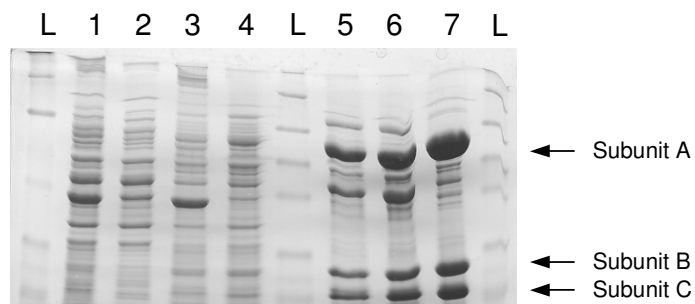
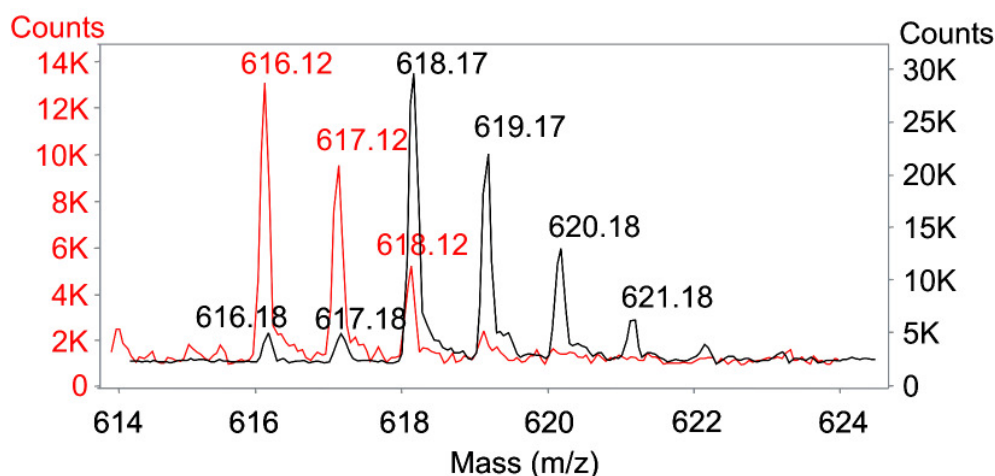


Figure 3-34: SDS-PAGE of samples during purification. L, molecular mass standard; 1 and 2 cell homogenate; 3, supernatant; 4, Triton homogenate; 5, Triton extract; 6, anion exchange; 7, isoelectric focusing.

The heme *b* concentration was also calculated spectrophotometrically at the Soret-band and proved a molar “heme to protein” ratio of about 2:1. Both enzymatic assays, “MB assay” and “ $\text{BH}_4$ -DMNH<sub>2</sub> assay” ( $\sim 6 \text{ U mg}^{-1}$ ), performed on the purified protein produced results that are comparable to the unlabeled WT QFR enzymatic activity. Mass spectrometric measurements by MALDI TOF of the hemes extracted from the labeled and unlabeled samples (Figure 3-35) yield clear signals at 616 atomic mass units ( $m/z$ ) for unlabeled hemes and 618 atomic mass units ( $m/z$ ) for labeled hemes. The examination of all the peaks obtained from the labeled sample show that only a negligible percentage of the propionates were not isotopically labeled.

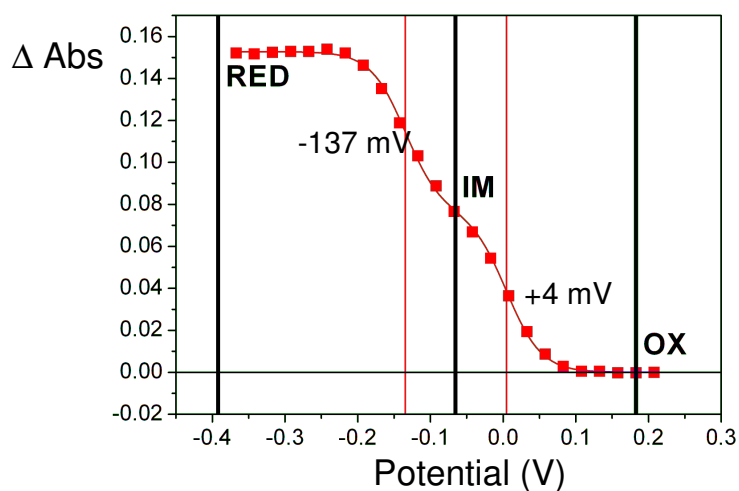


**Figure 3-35: MALDI TOF analysis of the extracted hemes.** Data for the unlabeled and  $^{13}\text{C}$ -labeled hemes are shown in red and black, respectively. The molecular masses ( $m/z$ ) are indicated above the individual peaks.

Quinones give characteristic signals at certain wavelengths during redox changes around  $-70 \text{ mV}$  (potential referred to the standard hydrogen electrode, SHE) that may be interfering with the FTIR spectra analysis. In order to exclude any significant difference concerning the quinones between unlabeled and labeled QFR preparations, bound native quinone-like species (methyl-menaquinone and menaquinone) were extracted from the same protein samples used for FTIR spectroscopy experiments and their concentration was measured. Separation and quantification were carried out by HPLC, giving a quinone-to-monomer ratio of 0.21 and 0.26 for the unlabeled and labeled sample, respectively.

### 3.2.2.1. Midpoint potentials of $^{13}\text{C}$ -labeled hemes at pH 7

The midpoint potentials of the  $^{13}\text{C}$ -labeled heme  $b$  groups of QFR were determined at pH 7 by monitoring the absorption changes in the visible spectral range at the positions of the Soret- and  $\alpha$ -bands of the hemes during a potential change. The observed midpoint potentials for the high- and low-potential hemes were +4 mV and -137 mV, respectively (Figure 3-36). Thus, the values are approximately 10 to 15 mV higher than the average midpoints measured in the unlabeled WT (Lancaster, *et al.*, 2000). For the latter, the statistical basis was broader since more independent data were collected, and an experimental error of  $\pm 10$  mV was estimated from the data scattering at pH 7. For the  $^{13}\text{C}$ -labeled enzyme, the value obtained for the high-potential proximal heme  $b_p$  lies within the error, and the value for the low potential distal heme  $b_d$  exceeds it by +5 mV. Thus, the influence of the  $^{13}\text{C}$ -label on the heme midpoint potentials, if any, is minor.



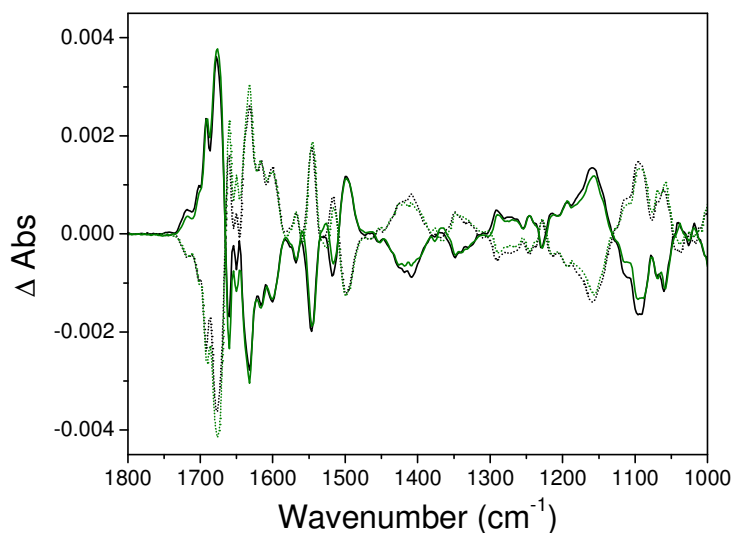
**Figure 3-36: Heme  $b$  titration curve of the  $^{13}\text{C}$ -labeled QFR WT at pH 7.** The data points were fitted with a two-step Nernst equation. The black vertical bars indicate the reference potentials (RED: reduced, IM: intermediate and OX: oxidized) chosen for the FTIR experiment, the red bars indicate the positions of the high and low midpoint potentials of the heme  $b$  groups.

## 3.2.3. FTIR-spectroscopy analysis

### 3.2.3.1. Reversible FTIR difference spectra of the “full potential” step

Figure 3-37 shows the reversible electrochemically-induced FTIR difference spectra of the unlabeled and labeled QFR WT enzyme at pH 7.0, respectively, for the “full potential” step,

i.e., with an initial reference potential at which all cofactors were fully reduced and a final potential at which all were fully oxidized (and *vice versa*). The FTIR difference spectra obtained for the QFR containing the  $^{13}\text{C}$ -labeled heme propionates are very similar to those for the unlabeled WT, which were discussed in ref. (Haas, *et al.*, 2005). This indicates that the possible heme propionate contributions in the full potential step are of small amplitude. Thus, it was advisable to compute double-difference spectra in order to better resolve any smaller signals (see chapter 3.2.3.5).

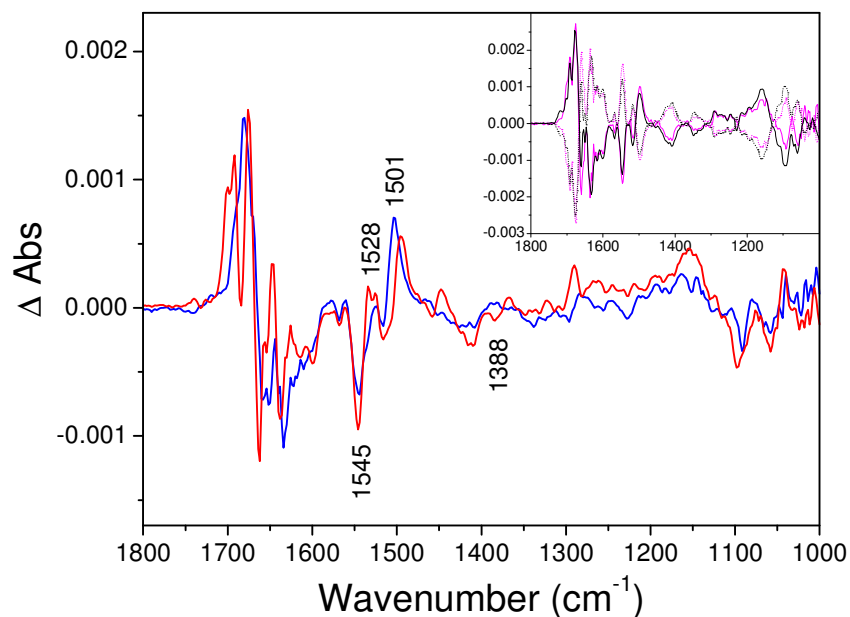


**Figure 3-37: Electrochemically-induced FTIR difference spectra of unlabeled and  $^{13}\text{C}$ -labeled QFR.** Reversible full potential steps “oxidized-minus-reduced” (solid line) and “reduced-minus-oxidized” (dotted line) FTIR difference spectra of the unlabeled QFR WT (in black), and  $^{13}\text{C}$ -labeled enzyme (in olive) at pH 7. The reference electrode potentials (vs. SHE') for the shown FTIR difference spectra were +0.21 V (full oxidative potential) and -0.37 V (full reductive potential).

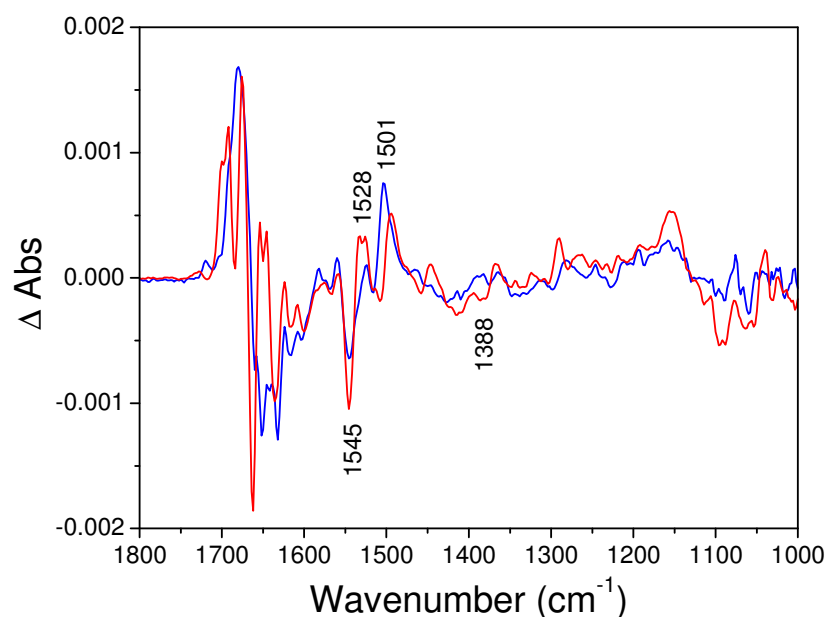
### 3.2.3.2. Separation of redox-induced IR signals from hemes $b_D$ and $b_P$

Since the midpoint potentials of the two QFR heme groups differ by almost 150 mV, it was feasible to separate the corresponding signals and address the low- and high-potential hemes individually by setting the appropriate reference potentials in the experiment. The best separation was achieved at an “intermediate” potential, which corresponds to the average of the two midpoints at -81 mV. At this intermediate potential, about 95 % of the high-potential hemes are reduced, and 95 % of the low-potential hemes are oxidized. Thus,

the separation of the two heme midpoint potentials is wide enough to guarantee negligible contributions (max. 5 %) of the respective other heme in the two partial potential steps “reduced-minus-intermediate” and “intermediate-minus-oxidized” (and *vice versa*). The corresponding spectra are shown in Figure 3-38-A and -B. Because of the small amplitude of investigated signals that and due to the occurrence of noticeable baseline instabilities in the respective experiments, the spectra corresponding to the partial potential steps had to be baseline-corrected. In other words, the respective pairs of difference spectra, e.g. “reduced-minus-intermediate” and “intermediate-minus-reduced”, were summed to determine the baseline drift. This did not seem to have a disturbing impact on the quality of the data, since independently baseline-corrected difference-spectra are practically identical. In addition, the inset of Figure 3-38-A shows how well the full potential step, i.e. the electrochemically induced redox reaction, can be subdivided in two halves. This addition of difference spectra can equally be performed for the labeled enzyme.



**Figure 3-38: Electrochemically induced FTIR difference spectra of unlabeled QFR at pH 7 with intermediate step.** Reversible “oxidized-minus-intermediate” (solid blue line), and reversible “intermediate-minus-reduced” (solid red line) FTIR difference spectra. The reference electrode potentials for the shown FTIR difference spectra were +0.21 V (full oxidative potential), -0.08 V (intermediate potential), and -0.37 V (full reductive potential). The inset shows a comparison of the difference spectra of the measured full potential step (in black, same data as in Figure 3-37) with computed “full potential step” difference spectra (in magenta), which are based on the sum of the respective pairs of spectra.



**Figure 3-39: Electrochemically induced FTIR difference spectra of  $^{13}\text{C}$ -labeled QFR at pH 7 with intermediate step.** Reversible “oxidized-minus-intermediate” (solid blue line), and reversible “intermediate-minus-reduced” (solid red line) FTIR difference spectra. The reference electrode potentials for the shown FTIR difference spectra were +0.21 V (full oxidative potential), -0.07 V (intermediate potential), and -0.37 V (full reductive potential).

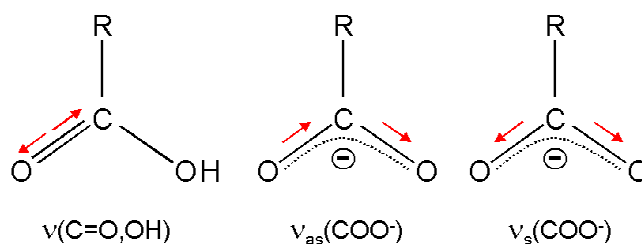
### 3.2.3.3. FTIR difference spectra of the “partial potential” steps

The FTIR difference spectra of the two potential steps, which include the intermediate potential, reflect the redox transitions of the two heme groups  $b_D$  and  $b_P$  and contributions from other cofactors and prosthetic groups, which are inevitable. Although the difference spectra reveal clear deviations, the positions and proportions of the main spectral features are similar for both partial potential steps, and comparable for the unlabeled and  $^{13}\text{C}$ -labeled QFR enzyme (see Figure 3-38 and Figure 3-39). The differences between the two steps in the amide I range of the spectra could arise from distinct sets of amino acid residues that may be altered in the course of one or the other individual potential step. Moreover, they could indicate redox-induced structural changes of the polypeptide backbone of QFR, which are either related to the redox transition of the high- or the low-potential heme.

The sharp peak at  $1545\text{ cm}^{-1}$ , which was observed in the full potential step has tentatively been assigned to heme porphyrin  $\nu(\text{C}_b\text{C}_b)$  and/or  $\nu_{\text{as}}(\text{C}_a\text{C}_m)$  vibrations (Figure 4-2, Haas, *et al.*, 2005). An analogous signal was present in both partial potential steps (with lower intensity than in the full potential step), which is in line with the performed assignment. The PO modes from the potassium phosphate buffer below  $1200\text{ cm}^{-1}$  reflect proton exchange of the enzyme and the mediators with the buffer (Hellwig, *et al.*, 1996) (Hellwig, *et al.*, 1999) (Baymann, *et al.*, 1999). The spectra for the two partial potential steps showed that this effect was more pronounced in the low-potential partial step (Figure 3-38 and Figure 3-39) since the amplitude of the respective bands was stronger in this step.

#### 3.2.3.4. Tentative signals of protonated heme propionate(s) of heme $b_b$

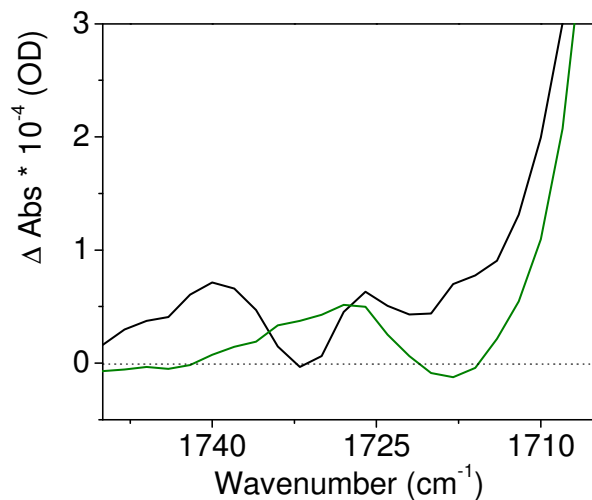
The range of Asp or Glu  $\nu(\text{COOH})$  modes above approximately  $1710\text{ cm}^{-1}$  (Venjaminov & Kalnin, 1990) is of particular interest with respect to a possible coupling of proton transfer via acidic groups to the redox transition of the high- and low-potential heme.



**Figure 3-40: Schematic view of the three relevant heme propionate vibrations.** On the left, the carbonyl stretching vibration of the protonated carboxyl group (which absorbs between approximately  $1700\text{ cm}^{-1}$  and  $1665\text{ cm}^{-1}$ ) is shown; in the middle, the antisymmetric vibration of the deprotonated form (between  $1620\text{ cm}^{-1}$  and  $1540\text{ cm}^{-1}$ ); and on the right, the corresponding symmetric vibration (between  $1420\text{ cm}^{-1}$  and  $1300\text{ cm}^{-1}$ ). The arrows indicate the stretching of the individual bonds. All of these vibrations are sensitive to  $^{13}\text{C}$  isotope exchange and a maximal downshift of 30 to 40 wavenumbers upon isotopic labeling of the heme propionate group is expected (Behr, *et al.*, 1998).

At  $1718\text{ cm}^{-1}$ , a signal in the full potential step of the unlabeled QFR WT enzyme has tentatively been assigned to a FAD  $\nu(\text{C4}=\text{O})$  vibration in the oxidized state (Haas, *et al.*, 2005). The difference spectra of the  $^{13}\text{C}$ -labeled and unlabeled QFR associated with the low-potential step and thus with heme  $b_b$  differ considerably above  $1710\text{ cm}^{-1}$  (Figure 3-41). In the unlabeled WT, two separated positive contributions associated with the intermediate state are centered at  $1740\text{ cm}^{-1}$  and  $1726\text{ cm}^{-1}$ . In opposition, the  $^{13}\text{C}$ -labeled enzyme reveals one

broad contribution in the intermediate state around  $1728\text{ cm}^{-1}$ . Hence, it has to be concluded that at least one propionate of  $b_D$  contributes in this high frequency range, and that the vibration was downshifted by 15 to 20 wavenumbers upon  $^{13}\text{C}$ -labeling (Figure 3-41).

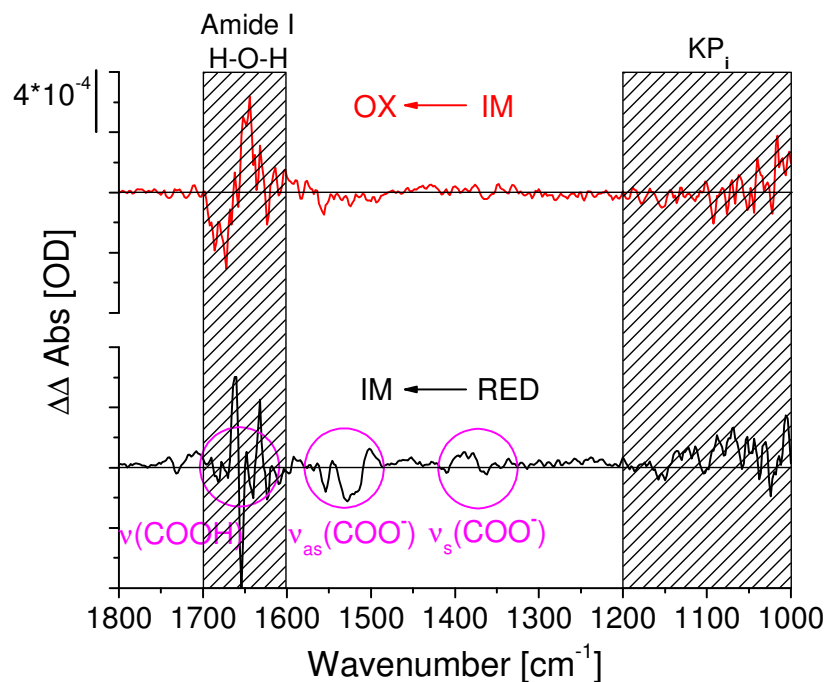


**Figure 3-41: Detail of FTIR difference spectra of unlabeled and  $^{13}\text{C}$ -labeled QFR at pH 7.** FTIR difference spectra of the partial potential step “intermediate-minus-reduced” for the unlabeled QFR (black line) and for the  $^{13}\text{C}$ -labeled QFR (olive line). The reference electrode potentials are the same as indicated above.

### 3.2.3.5. Tentative signals of deprotonated heme propionate(s) of heme $b_D$

The “single-difference” spectra of labeled and unlabeled QFR are very similar, as can be seen by comparing the corresponding spectra in Figure 3-38; therefore, it is necessary to look at “double-difference” spectra (Figure 3-42). The computed double-difference spectra are rather noisy, which is almost inevitable since independent experiments always differ slightly from each other; in addition, the spectra have to be scaled for comparison. The double-difference spectra allow the assignment of the observed contributions to the low-potential redox transition related to the distal heme.





**Figure 3-42:** FTIR double-difference spectra of “unlabeled-minus- $^{13}\text{C}$ -labeled” QFR at pH 7. The upper traces show the data for the potential step “oxidized-minus-intermediate” (red line); the lower for “intermediate-minus-reduced” (black line). The magenta circles point out the frequency ranges in which the contributions of the heme propionates are observed. The obliquely striped areas correspond to regions of elevated noise level (in the amide I region,  $1700\text{ cm}^{-1}$  to  $1600\text{ cm}^{-1}$ , due to the strong  $\text{H}_2\text{O}$  and amide I absorbance, and below  $1200\text{ cm}^{-1}$  due to the absorbance of  $\text{KP}_i$ -buffer modes), which are difficult to handle in double-difference spectra and should thus be excluded from the analysis.

As can be seen in Figure 3-42 for the low potential step, the positions of the obtained FTIR double-difference bands of “unlabeled-minus- $^{13}\text{C}$ -labeled” QFR in the IR-spectrum coincide very well with the expected ranges (Behr, *et al.*, 1998). The series of difference-signals at  $1553$ ,  $1528$ , and  $1501\text{ cm}^{-1}$  can be attributed to anti-symmetric vibrations of at least one deprotonated heme propionate of  $b_{\nu}$ , and the signal around  $1388\text{ cm}^{-1}$  to the corresponding symmetric modes, respectively (Figure 3-40). Only residual contributions of very small amplitude (as mentioned above, an overlap of 5 % at the intermediate potential was estimated for the contributions of the two hemes) plus noise are seen at the corresponding wavenumbers in the “oxidized-minus-intermediate” potential step. Additional discrepancies between the double-difference spectra of the full and the “reduced-minus-intermediate” potential step might arise due to conformational changes or environmental differences, which could affect the heme propionate vibrations, and which are specifically related to the intermediate potential, as this state does not contribute to the full potential step.



## 4. DISCUSSION

### 4.1. Quinol:Fumarate Reductase from *H. pylori* and *C. jejuni*: Production and Characterization

#### 4.1.1. A novel host for heterologous expression

The results demonstrate for the first time that the  $\epsilon$ -proteobacterium *W. succinogenes* is a well-suited host for heterologous membrane protein production. Beside the fact that *H. pylori* and *C. jejuni* must be handled with high safety standards (e.g. in a high safety level laboratory), culturing of these bacteria is a rather demanding task (Marais, *et al.*, 1999b) (Kelly, 2001). Due to the difficulty and risks of producing these enzymes from their natural, pathogenic sources, these protein complexes have been heterologously produced in the non-pathogenic host *W. succinogenes*. A well-established transformation method, the strong homologous *frdCAB* operon promoter and terminator, efficient selective markers such as like kanamycin and chloramphenicol with their own bacterial promoters are previously established genetic tools (Simon, *et al.*, 1998) that have been useful for expressing genes or operons in this novel host. Further advantages of using *W. succinogenes* are its known genome sequence (Baar, *et al.*, 2003), especially for homologous gene amplification and homologous recombination, and its rapid growth to high cell densities in minimal media, which enables fast and cost-effective production of cell quantities sufficient for large-scale protein purification. Considering that the purification factor values of the QFR from *H. pylori* and *C. jejuni* preparations are not markedly large notwithstanding the high purity, it is inferred that the level of protein production in the expression host is extremely high. Taken together, the results presented above and discussed below demonstrate *W. succinogenes* to be a useful and efficient expression system.

#### 4.1.2. A functional heterologous replacement of the QFR in *W. succinogenes*

The pCatCj4 and pCatHpG8 plasmids contain the *frdCAB* operons from *C. jejuni* and *H. pylori* QFR, respectively. Locus-specific PCR and Southern blotting analysis permitted to confirm that the recombinant HpGM and CjM strains possess the plasmid pCatHpG8 and pCatCj4, respectively, integrated into the genomic QFR-locus of the deletion mutant  $\Delta$ *frdCAB* of *W. succinogenes* (Simon, *et al.*, 1998). Indeed, although integration at the upstream

recombination region of the *C. jejuni* QFR operon could not be tested by Southern blotting analysis, the obtained results from the Southern blotting at the downstream recombination region and the locus-specific PCR (which is associated with the upstream recombination region) can undoubtedly rule out any misinterpretation. The appearance of prominent bands of the size of about 4.2 kb in the Southern blot radiography film (Figure 3-5) are most likely demonstrating that the antibiotic resistance was due to plasmid replication inside the host and not (only) to plasmid integration. This phenomenon might account for the difficulties encountered in the antibiotic selection method, which was too often affected by the appearance of too many false-positive clones. However, this last obstacle has apparently been overcome by increasing the volume of fresh medium added after electroporation and the subsequent incubation time (see Materials and Methods).

Prior to genome integration of the plasmids pCatCj4 or pCatHpG8, the deletion mutant *W. succinogenes*  $\Delta$ *frdCAB* was unable to grow on a medium containing fumarate as a sole electron acceptor. The recombinant strains of *W. succinogenes* CjM and HpGM were able to overexpress the respective *frdCAB* operons from *C. jejuni* and *H. pylori*. Growth curves of these strains cultivated on minimal and rich media containing fumarate as a sole terminal electron acceptor revealed that fumarate respiration was recovered. Moreover, even though strains carrying the *H. pylori* QFR (WsHpGM31/33) were slightly slower in growth, the doubling time and cell mass yield of these two transgenic strains are rather similar to the *W. succinogenes* WT (Table 3-I).

These observations demonstrate that the *W. succinogenes*  $\Delta$ *frdCAB* strain could efficiently restore fumarate respiration using the fully functional *H. pylori* or *C. jejuni* QFR membrane protein complex. Hence, it is possible to infer that, after a correct transcription and translation of the heterologous operon, the protein complex could be correctly folded and delivered into the plasma membrane. Furthermore, all of the six cofactors, i.e. two heme *b* groups, three iron-sulfur clusters (S1, S2, S3), and an FAD prosthetic group were correctly assembled into the enzyme. Even though these three  $\epsilon$ -proteobacteria species are all phylogenetically rather close, their QFR amino acid sequence homology is not very high (the membrane anchors show only about 50 % identity, Table 4-I). Strikingly, the respective QFRs can be efficiently interchangeable, implying also an efficient interplay between the heterologous enzymes and the contingent associated (homologous) chaperons.

**Table 4-I: Amino acidic sequence identities between the QFR from *W. succinogenes* DSM 1740 strain, the *C. jejuni* clinical isolate strain, and the *H. pylori* 26695 strain.** Values are given in percentages (%). The alignments have been performed using the scoring matrix BLOSUM 62 (by the SECentral software package).

	<b>FrdC</b>	<b>FrdA</b>	<b>FrdB</b>
<i>C. jejuni</i> vs. <i>W. succinogenes</i>	49	69	66
<i>H. pylori</i> vs. <i>W. succinogenes</i>	55	63	68
<i>C. jejuni</i> vs. <i>H. pylori</i>	45	57	64

In order to investigate the longer doubling time observed for the *W. succinogenes* strain expressing the *H. pylori* QFR operon, the electron transport activity between Fdh and QFR membrane protein complexes on *W. succinogenes* cell membranes containing the QFR from either *W. succinogenes* (DSM 1740, WT strain), or *C. jejuni* (WsCjM11 strain), or *H. pylori* (WsHpGM31 strain) have been measured and compared. A very important observation is that the Fdh activity was, as expected (Kröger & Innerhofer, 1976b, Kröger, *et al.*, 1980), several times slower than the QFR activity, and even slower than the formate to fumarate (Fdh-QFR) activity. This latter finding is perhaps due to the fact that the Fdh enzymatic activity had to be measured after several days; therefore the samples were shock-frozen and thawed, and thus part of the activity was lost due to deterioration of the enzymes. The drawback of this issue does not prevent to compare the activities among the three strains, as they were all treated exactly in the same manner. Given that the reaction catalyzed by the Fdh was by far the rate limiting reaction, both the directly measured and indirectly calculated (theoretical, see Equation 2-4) electron transfer activities were strongly influenced. Accordingly, the theoretical electron transport activities were from 6 to 8 times smaller than the values measured directly as formate to fumarate activity. In this view, a direct comparison between electron transport activities occurring in the three different strains would lead to a wrong interpretation of the values. Instead, the bias imposed by the very low Fdh activity should be eliminated. If the ratio between the individual Fdh-QFR activity and the Fdh activity is calculated, it is obtained that whereas the WsCjM11 strain and the DSM 1740 strain had similar values (7.7 and 7.4, respectively), the WsHpGM31 strain had a significantly lower value (5.9). Similarly, the ratio between the Fdh activities in different species and their respective Fdh-QFR activities were corresponding to 2.9/3.0, between the DSM 1740 and WsCjM11 strains; to 6.2/4.8 between the WsCjM11 and WsHpGM31 strains; and 2.1/1.7 between the DSM 1740 and WsHpGM31 strains. Thus, it is possible to conclude

that the only disproportion between the Fdh and the Fdh-QFR activities is tangible in the WsHpGM31 strain. In other words, the electron transport activity appears to be less efficient only in the strain containing the *H. pylori* QFR, and this is perfectly in accordance with the observed difference in cellular doubling times. Although a supramolecular organization of the aerobic respiratory systems in the mitochondrial inner-membrane (super-complexes or 'respirasome') is already known and described (Schägger & Pfeiffer, 2000), the formation of similar super-complexes in the anaerobic respiratory systems of bacteria (like fumarate respiration) has never been demonstrated. Thus, even though this eventuality cannot be completely ruled out, the effect noticed in the WsHpGM31 is not justifiable with a super-complex formation.

Carefully looking at the specific QFR activities (Table 3-I) and electron transport activities (Table 3-VI) in cell homogenates and membrane fractions, it is noticeable that the expression level of *H. pylori* QFR was higher than the *C. jejuni* QFR and slightly higher than the *W. succinogenes* QFR. On an inversely proportional logic, the respective Fdh activities were lower in the strains with higher QFR activity. It may be speculated that this phenomenon is not accidental, but the expression level of the QFR operon may affect the cellular production of Fdh in the membrane (and possibly even of membrane proteins in general), and even interfere with the production or distribution of menaquinol throughout the membrane. Since all the strains had the same QFR promoter/terminator, the higher production of *H. pylori* QFR could be explained by a longer half-life of the messenger RNA (mRNA), or a *per se* higher resistance of the protein to degradation. However, since WT *W. succinogenes* cells were also characterized by a high QFR production, one would assume that in this case the presence of QFR was finely tuned with the metabolic needs and setup of the cell.

#### **4.1.3. The first large-scale preparation of a pure and homogeneous QFR from *C. jejuni* and *H. pylori***

This novel heterologous expression system allowed to establish a large-scale preparation set up for the production of an active QFR from the pathogenic species *C. jejuni* and *H. pylori*. Previous enzymatic isolation from these two species was characterized by low yields of a QFR of comparatively low purity and stability (Birkholz, *et al.*, 1994, Ge, *et al.*, 1997, Lancaster & Simon, 2002). On the contrary, protein characterization and crystallization require large amounts of a highly pure and stable enzyme. The relative simplicity of working with *W. succinogenes* and its high yield of expression enabled to achieve, after full

purification, up to 100 mg of *C. jejuni* QFR and 150 mg of *H. pylori* QFR. The SDS-PAGE (Figure 3-8) and the gel filtration chromatogram (Figure 3-7) prove that these enzyme preparations are characterized by a high purity and a high homogeneity. Besides, these enzyme preparations have already proven to be suitable for protein 3D crystallization, further evidence of high enzyme stability. The purified QFR samples appear in the SDS-PAGE gel as three subunit bands with very minor contaminations and with roughly correct stoichiometric ratios<sup>m</sup>. The quality of the enzyme purification procedure can also be assessed by examination of the purification table (Table 3-II). As the enzymatic activity measured by “MB assay” in the cytosolic fraction after ultracentrifugation of the solubilized membranes was negligible, it can be inferred that the QFRs were stably attached to the membrane and the enzyme integrity was maintained during mechanical disruption of the cells. Interestingly, when the *H. pylori* QFR sample was subjected to gel filtration, the total QFR enzymatic activity measured with the “DMNH<sub>2</sub> assay” decreased dramatically. This may reflect, for instance, the loss of tightly bound phospholipids, which may affect the catalytic efficiency of subunit C. This last hypothesis arises from two main observations: the protein appears as a unique and homogeneous peak in the gel filtration chromatogram, proving that the enzyme is still assembled as a complex; and the partial activity measured with the “MB assay” ensure that the hydrophilic subunits are not affected by gel filtration. Further discussions on the role of lipids in the QFR from *H. pylori* are given below.

#### 4.1.4. A full protein characterization of the produced enzymes

To prove that the hemes have been correctly inserted into the transmembrane subunit C at the correct stoichiometric ratio, the heme content has been measured spectroscopically and compared with the polypeptide concentration (BCA assay). As expected from a dihemic protein complex, the protein-to-heme ratio was confirmed to be equal to 1:2. Another confirmation was given by the fact that, during the heme titration, the distal and the proximal hemes contributed equally to the total change in absorbance.

The fluorescence associated with QFR subunit A on an SDS-PAGE gel illuminated with UV light (Figure 3-9) ascertained that the prosthetic group FAD of the both produced QFRs is covalently linked to this subunit, in analogy to *W. succinogenes* QFR. This data is also

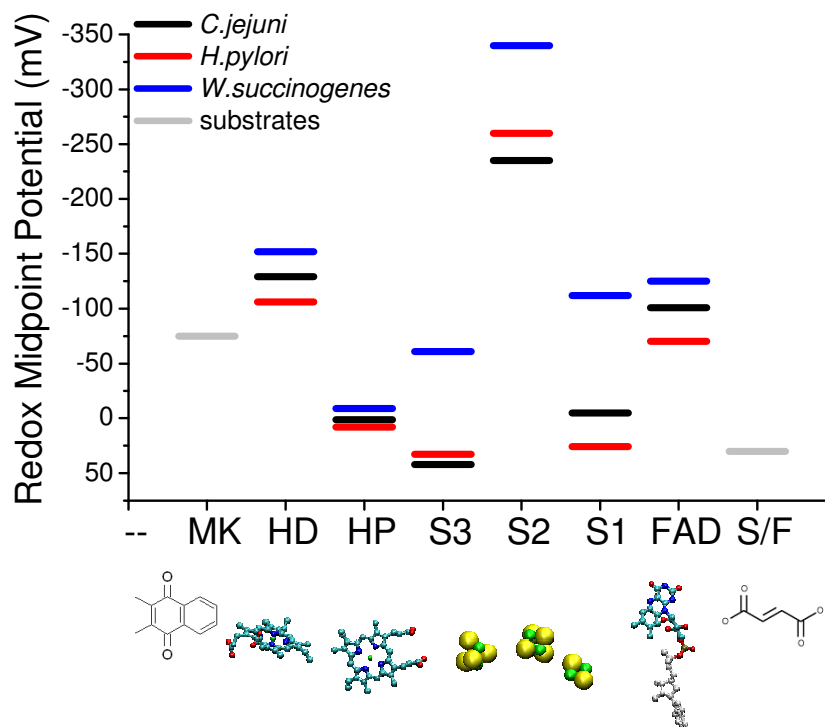
---

<sup>m</sup> The thickness of the bands from the SDS-PAGE can be roughly estimated and reflects the molar mass.

confirmed in the *C. jejuni* QFR thanks to the determination of its 3D-crystal structure (Figure 3-29).

#### 4.1.4.1. Redox midpoint potentials of QFR cofactors and correlation to enzymatic activities

The redox midpoint potentials of the QFR cofactors from the species *W. succinogenes*, *C. jejuni* and *H. pylori*, have been measured and are presented graphically in the figure below (Figure 4-1).



**Figure 4-1:** Redox midpoint potentials of the QFR cofactors from *C. jejuni* (black), *H. pylori* (red) and *W. succinogenes* (blue). Abbreviations: MK, menaquinone/menaquinol redox couple; HD, distal heme; HP, proximal heme; S3, iron-sulfur cluster S3; S2, iron-sulfur cluster S2; S1, iron-sulfur cluster S1; FAD, flavin adenosine dinucleotide prosthetic group; S/F, succinate/fumarate redox couple. The substrates menaquinone and fumarate, and all the cofactors are represented graphically.

Similar measurements were carried out previously in the *W. succinogenes* QFR (Uden, *et al.*, 1984). However, although the data obtained for the Fe-S centers in this last reference are in reasonable agreement with the data obtained in this work, the calculated redox midpoint potential of the *W. succinogenes* FAD was rather questionable. Thus, the signal assigned to the flavin semiquinone by Uden *et al.* could only be detected and measured as



'characteristic shoulders' at both sides of a major peak arising from the redox mediators. Most importantly, instead of the bell-shaped titration curve, the signal persisted and even increased at low potentials, giving a maximal yield of 19%<sup>n</sup> and half-maximal amplitude at -120 mV. A similarly shaped titration curve was obtained by poisoning the enzyme with the succinate/fumarate couple, in this case giving a redox midpoint potential of -20 mV (41% yield). In contrast to these quoted experiments, the titrations of the FAD prosthetic group of all the three QFRs that were performed here resulted in clear bell-shaped curves (n=2), which could then be correctly fitted with a double Nernst equation for redox midpoint potential determination. Since molecules of native quinone are known to co-purify together substoichiometrically with the membrane proteins in general (Luna-Chavez, *et al.*, 2000, Xia, *et al.*, 1997, Simon, *et al.*, 2000b, Gast, *et al.*, 1985) and with  $\epsilon$ -proteobacterial QFR specifically (Mileni, *et al.*, 2005a) at a ratio of about 0.2 molecules per monomer (see chapter 3.2.2) and since the EPR signal signature from FAD<sup>•-</sup> is quite similar to that generated by a naphthosemiquinone, any possible misinterpretation of the obtained signals was avoided by re-performing the redox titration in the presence of a 10-fold molar concentration of the menaquinone MK<sub>4</sub><sup>o</sup>. Since the yield of radical obtained did not change, it was concluded that the signal assignment to FAD is correct.

As it is possible to notice from the EPR signal yield of the measured flavins (around 10%), the radical stability constant of these prosthetic groups was very low. The low stability of the semiquinone species has also been annotated for most of the other flavin-containing enzyme like the *E. coli* fumarate reductase and succinate dehydrogenase (Heering, *et al.*, 1997, Leger, *et al.*, 2001), the *Shewanella frigidimarina* flavocytochrome *c*<sub>3</sub> (Turner, *et al.*, 1999), the *Nocardia corallina* alkene mono-oxygenase (AMO) complex (Gallagher, *et al.*, 1999), etc. Although this view is in contrast with the model which describes separate one-electron transfer processes as determinants of the course of catalytic electron transfer (Heering, *et al.*, 1997), most of the results available in the literature, which were obtained also by using other techniques such as protein film voltammetry (PFV) or UV/VIS spectroscopy, favor a model where the two one-electron transfer processes through this center occur almost concertedly and are defined as cooperative (Leger, *et al.*, 2001). This conception agrees well with the mechanism of fumarate reduction by a hydride transfer, thus the transfer of one proton, and two electrons from the FAD prosthetic group.

---

<sup>n</sup> The plateau represented 19% of radical signal compared to the enzyme concentration.

<sup>o</sup> The native menaquinone is MK<sub>6</sub>, thus, only two isoprenoid chains longer than the one supplied.

Apart from the iron-sulfur clusters of the *W. succinogenes* QFR, whose redox midpoint potentials are about 100 mV lower, only relatively small differences are noticed<sup>p</sup> between the cofactors of the QFRs from *H. pylori* and *C. jejuni*. More precisely, the FAD, the S1 cluster and the distal heme of the *H. pylori* QFR were higher than those of the *C. jejuni* QFR of about 25 mV. However, the overall midpoint potential difference between the first (at the distal heme) and the last reduction stage (at the FAD) of the electron transfer ( $\Delta E_{\text{FAD}}^{\text{HD}}$ ), and hence the free energy difference<sup>q</sup> (overall  $\Delta G$ ), were very similar:  $\Delta E_{\text{FAD}}^{\text{HD}}$ : 27 mV, 28 mV, and 36 mV, for the *W. succinogenes*, *C. jejuni*, and *H. pylori* QFR, respectively.

However, it must be borne in mind that the experimentally calculated redox midpoint potentials are relative to an oxidizing environment at pH 7.0 or pH 7.3. Since these bacteria inhabit quite different niches, which are all different from the aforementioned experimental *in vitro* conditions, the indicated differences may reflect differences in their physiological behaviors *in vivo*. For instance, the *H. pylori*'s habitat has an extremely low pH, albeit the cytoplasmic pH is close to neutrality (Tomb, *et al.*, 1997). Hence, the midpoint potential of the cofactors, and especially those in proximity of the periplasm, would be most likely increased because they are affected by a lower pH (this behavior is called redox-Bohr effect). It is in fact calculated that an increase of 1 pH unit leads to a theoretical  $E_m$  decrease of 60 mV<sup>r</sup>. Therefore, the  $\Delta E$  value of 36 mV obtained *in vitro* could be only apparently larger as the real (*in vivo*) midpoint potential of the *H. pylori* QFR distal heme could be somewhat higher since it could be influenced by the lower pH. On the other hand, as this bacterium can also adopt a positive-inside membrane potential by concentrating cations on the cytoplasmic side of the membrane (Marais, *et al.*, 1999a), the electron transfer from the periplasm to the cytoplasm *in vivo* would anyway be electrostatically more favorable.

The *W. succinogenes* species inhabits bovine rumen, which provides a very low environmental redox potential (Waghorn, 1991, Marounek, *et al.*, 1982) and a pH close to neutrality (Annamalai, *et al.*, 2004). The low values of the midpoint potentials of the *W. succinogenes* QFR cofactors, and especially of the iron-sulfur clusters, might hence be ascribed to this highly reducing environment. Thus, the functionality of the cofactors is evidently optimal when their redox midpoint potentials are tuned and balanced with the environmental potential found in the rumen. Otherwise, re-oxidation of the cofactors, or

<sup>p</sup> The error in the determination of the midpoint potentials can be estimated to be  $\pm 10$  mV.

<sup>q</sup> The correlation between  $\Delta G$  and  $\Delta E$  is given by the equation:  $\Delta G = -zF\Delta E$

<sup>r</sup> This value is relative to a redox reaction where one electron is involved. Thus, the value has to be halved when two electrons are taking part in the redox reaction.

more in general the enzymatic electron transfer would be more difficult or even energetically unfavorable in such a low potential environment.

Over the experimental conditions adopted for the “DMNH<sub>2</sub> assay”, the enzymatic activity of the *W. succinogenes* QFR may gain an advantage due to the lower potential of the cofactors (especially the iron-sulfur clusters). Indeed, given that the rate-limiting step of this catalytic reaction was the delivery of the electrons between the iron-sulfur clusters and the fumarate (Unden, *et al.*, 1984, see Figure 1-4), such lower potentials at this stages would probably accelerate the electron transfer, therefore resulting in a higher turnover rate compared to the other QFR species. On the other hand, the enzymatic activity of the *H. pylori* QFR ( $V_{\text{MAX}}$ : 12.2 U mg<sup>-1</sup>) was faster than the *C. jejuni* QFR ( $V_{\text{MAX}}$ : 9.3 U mg<sup>-1</sup>) probably because of the steeper course of its cofactor's redox midpoint potentials (Figure 4-1,  $\Delta E$ : 36 mV).

In any case, because of the unpredictable changes caused by the environmental conditions *in vivo*, this effort to interpret the obtained redox midpoint potential values is rather speculative. Moreover, it must necessarily be considered that the redox midpoint potentials have been measured in a situation where the induced artificial reduction by dithionite of one cofactor species with a certain midpoint potential is occurring only when all other species with higher midpoint potentials are already reduced. For instance, the determined low potential for the [4Fe-4S] iron-sulfur clusters may be an artifact due to anti-cooperative electrostatic interactions between adjacent redox centers (Cammack, 1995, Salerno, 1991). Hence, like any titration of this kind, the values presented herein are not representing a real physiological situation where the reduction of one species is occurring when the adjacent (or preceding) ones are in the oxidized form.

#### 4.1.4.2. Identification of lipids bound to the QFR

Several biochemical and structural analysis have already shown that respiratory membrane proteins, including SQORs, contain phospholipids (for recent reviews see ref. (Lee, 2004, Palsdottir & Hunte, 2004). For instance, the phospholipids oleoyl-palmitoyl-phosphatidylethanolamine and cardiolipin have been assigned to electron densities found in the *E. coli* SQR structure (PDB code 1NEK, Yankovskaya, *et al.*, 2003). Similarly, the *W. succinogenes* QFR (PDBs 1QLA and 1E7P) and *E. coli* QFR (PDBs 1KF6, 1KFY, 1LOV) have been found to bind hydrophobic compounds (assigned as LM, glycols, etc.) which may mimic, during crystallization, the presence of lipid molecules. Because of the blurred density and high B-factors, modeling of lipids or detergents into electronic densities is always very

difficult, and the identification of the correct compound is often questionable, these findings are strongly supporting for the presence of lipid molecules within SQOR proteins.

It is believed that lipids may sustain the conformational stability and rigidity of protein complexes and therefore improve their crystallization properties. In the past it was already shown that addition of a small amount of synthetic non-native phospholipid (DOPC) to a purified protein complex resulted in a dramatic improvement in crystallization efficiency (Zhang, *et al.*, 2003).

The two-dimensional thin layer chromatography performed in the *H. pylori* and *C. jejuni* QFR supports the hypothesis that a number of hydrophobic compounds interact and co-purify with these membrane protein complexes. Identification of all or some of these compounds, eventually lipids, would be helpful to understand the molecular set up of the membrane-associated portions of the enzyme, and most importantly this would be a step forward for finding the best crystallization conditions. As inferred from the TLC plate staining results, all of these compounds are phosphorous-containing molecules, indication that some of them could very likely be phospholipids. Curiously, it could be noticed that whereas the TLC spot-patterns of the *C. jejuni* QFR sample before and after the gel filtration were the similar, the *H. pylori* QFR sample had lost, after the gel filtration, almost any spot with retention factor similar to those of the phospholipids, as measured in the standard calibration TLC plate. On the whole, even though staining procedures and standard calibrations were adopted, it was not possible to identify any lipid type<sup>s</sup>. Nonetheless, these results strongly suggest that during gel filtration of the *H. pylori* QFR, marked lipid depletion was occurring, and this was *de facto* confirmed by the deterioration of crystallization success. MALDI TOF mass spectrometry has already been shown to be a successful method for lipid determination (Distler, *et al.*, 2004) in purified membrane proteins. The *H. pylori* QFR sample after isoelectric focusing has been analyzed with this technique in order to reveal the molecular structure of the compounds detected by TLC. Although identification of synthetic lipids added to the protein solution (as a sort of positive control) was relatively easy, native lipids or other co-purified compounds were not detected with this strategy. An explanation for the failure of this attempt is probably given by the fact that the bound native lipids were present in a substoichiometric amount, and hence less than two molecules per monomer<sup>t</sup>. This amount of lipids was likely too low to be detected. Furthermore, together with a possible difficulty in detaching of the bound lipid molecules from the natural protein-

---

<sup>s</sup> Defined by the type of polar head.

<sup>t</sup> For the positive control, two molecules of synthetic lipid per monomer were added.

binding site, the detection of lipids may suffer from the presence of such a large amount of protein which has a much larger molecular weight.

Lipid depletion probably also occurred at an early stage of the purification (i.e. anion exchange chromatography). The identification by MALDI TOF mass spectrometry of the low lipid amount that can be co-purified was challenged by the presence of contaminants. Even after elimination of the polypeptide milieu by methanol-chloroform extraction or after TLC isolation, it was neither possible to avoid contaminations nor to identify any compound. A solution to the problem may be obtained with the development of an extraction procedure that does not lead to accumulation of contaminants in the sample, so that a higher concentration of lipids in the extracts would increase the chances of gaining more signal intensity.

High-pressure liquid chromatography permitted the identification of the cardiolipin polar head contained in the *H. pylori* QFR sample. Another peak corresponding to the retention time of phosphatidylethanolamine was observed, though its concentration was extremely low. From integration of the peaks of the HPLC chromatogram, it was clear that the concentration of the detergents in the sample was, as expected, almost two orders of magnitude higher than the concentration of cardiolipin. Because of their partial depletion during purification, other lipidic compounds may not be seen, especially those having longer retention times, since the corresponding signal peak would be even more broadened. Nevertheless, the presence of very low concentrations of lipids might be ascribed to other contaminating proteins and not to the QFR.

However, specific functional studies on the *H. pylori* QFR based on enzymatic activity have proven that cardiolipin has a beneficial effect, whereas this was not the case for phosphatidylethanolamine. Similarly, the stability of the lipid-supplied protein sample observed in the crystallization trials is consistent with this view: only after addition of cardiolipin the *H. pylori* QFR sample was far more suitable for crystallization (Figure 3-24) and far less prone to forming gel phases or amorphous precipitates.

Whether cardiolipin was the only lipid present in this enzyme or it coexisted with other lipidic species is not yet known, although experimental evidences demonstrated that this was a lipid of crucial importance for enzymatic activity, stability, and crystallization.

#### 4.1.4.3. Ultracentrifugation experiments identify a homogeneous and homodimeric form of the QFR in other two $\epsilon$ -proteobacteria

From the available crystal structure of the *W. succinogenes* QFR it was found that this membrane protein complex crystallized as a homodimer. In more details, a QFR monomer surface corresponding approximately to  $3665 \text{ \AA}^2$  (8 %) is buried upon dimer formation (Lancaster, *et al.*, 1999). As it was described earlier in this thesis, also the crystal structure of the *C. jejuni* QFR showed a formation of a homodimer with a largely buried surface area. In order to unequivocally determine whether the dimer formation of these  $\epsilon$ -proteobacteria corresponds to the real physiological conformation of the complex or simply represents a crystallization artifact, the detergent solubilized complexes from *W. succinogenes*, *C. jejuni* and *H. pylori* were analyzed by analytical ultracentrifugation.

According to the procedure described in (Tziatzios, *et al.*, 2003), the oligomeric state of QFR was determined by evaluating the main peak in the  $c(s)$ -distribution. Assuming that QFR from *C. jejuni* is in a monomeric state with  $M_1=132,400 \text{ g/mol}$ , the calculated amount of protein-bound detergent, was 1.75 g per g of protein, using the  $\bar{v}$ - and  $M_{\text{eff},c}$ -values given above. The corresponding amounts for QFR from *H. pylori* and from *W. succinogenes* were found to be 1.82 and 2.0 g/g, respectively. Such high amounts of detergent bound by the enzyme are certainly not reasonable (Gennis, 1989, Moeller & Le Maire, 1993). In addition it has to be considered that, according to the structural properties of the enzyme (Uden, *et al.*, 1980, Lancaster, *et al.*, 1999), only one of the three protein subunits (subunit C with  $M_r = 30 \text{ kDa}$ ) corresponding to less than one quarter of the molecular mass is membrane-embedded. Thus, the amounts of the bound detergent given above, which refer to the whole molecule, should be multiplied by a factor of approx. 4, to correspond to that part of the dimeric QFR which is integrated into the membrane. Consequently the assumption that QFR is in a monomeric state cannot be correct. Under the assumption that the main fraction of the enzyme is a dimer, the protein-bound detergent was calculated to be 0.21, 0.25 and 0.34 g/g of protein for QFR from the three organisms. These values are relatively low; nevertheless they are consistent with the range of values observed for other membrane proteins (Gennis, 1989, Moeller & Le Maire, 1993). On the other hand, a trimeric or higher oligomeric state of QFR can be ruled out, since, even in absence of bound detergent, the calculated  $M_{\text{eff},c}$ -value was much higher than the figure calculated from  $s$  and  $D$ . It is concluded that the homooligomeric state of the detergent solubilized QFRs from *C. jejuni*, from *H. pylori* and from *W. succinogenes* is dimeric.

#### 4.1.5. Enzyme preparations producing X-ray diffracting 3D-crystals

Homogeneity and purity of a membrane protein preparation can also be tested by “crystallizability”: the expression and purification procedures presented here are able to produce reproducible and highly stable 3D-crystals. The QFR from *C. jejuni* can produce crystals up to a size of the order of millimeters, which diffract up to about 3.0 Å. So far, the QFR from *H. pylori* produced rather smaller crystals that diffract up to 8 Å. The production procedure established in this work makes itself conspicuous for the optimum output in terms of yield (quantity) and quality. This is not only advantageous for screening of new crystallization conditions and co-crystallization attempts of this enzymes as well as eventual mutant enzymes, but greatly increases the reproducibility, and therefore enforces reliability when comparing crystallization results.

##### 4.1.5.1. The 3D-crystal structure of the *C. jejuni* QFR

The 3D-crystal structure of the QFR from the *C. jejuni* species has been solved at 3.24 Å resolution. The crystallographic statistics (Table 3-X) obtained for data processing and refinement are very good for a structure solved at this resolution, but it mostly depends from the fact that the calculated phases derive from a structure that has a much higher resolution, and hence the quality of the initial phases was much better than expected for the observed resolution of the data.

Thanks to clear definition and sharpness of the electron density maps, the model structure was unambiguously assigned for most parts of the protein. However, some very important regions, such as the quinone binding site in the subunit C and the capping domain in the subunit A, are very blurred and model building was prevented. The weak intensities of the reflections ( $I/\sigma(I)$ ), the high B-factors, and especially the structural heterogeneity in certain areas of the protein have caused weaknesses in the electron density maps and consequently resulted in heavy uncertainties on interpretation. In fact, the slightly high percentages of amino acids falling into the generously allowed and disallowed regions of the Ramachandran plot are an explicit sign of these weaknesses. At the present state, an interpretation of fine structural details that are crucial for an understanding of the functional aspects in this enzyme cannot be pursued.

On the whole, it has been found that the structure of the *C. jejuni* QFR has a high level of structural homology to that of the *W. succinogenes* QFR<sup>u</sup>. Although slight differences between the two species cannot be ruled out at the present stage of analysis, the positions and the orientations of the cofactors, as well as many other features, appear to be conserved. This finding was somewhat surprising as the primary structure identity of the QFRs from *W. succinogenes* and *C. jejuni* ranges from 50% to 70% amongst the three subunits (Table 4-I).

#### 4.1.6. Functional characterization

Although QFR activity from *C. jejuni* and *H. pylori* bacterial lysates was detected in several works (Olbe, *et al.*, 2003, Chen, *et al.*, 2002, Pitson, *et al.*, 1999, Chen, *et al.*, 1999, Smith, *et al.*, 1999, Ge, *et al.*, 1997, Hoffman, *et al.*, 1996, Mendz, *et al.*, 1995, Mendz & Hazell, 1993, Grivennikova & Vinogradov, 1982), these enzymatic activity measurements of the homologously produced QFR performed on cell homogenates or scarcely purified samples (Birkholz, *et al.*, 1994), were characterized by a very low enzymatic activity and stability (reviewed by Lancaster & Simon, 2002).

In this work, an extensive enzymatic characterization has been carried out through the activity measurement with different enzymatic assays (Table 3-VII) on pure, highly stable enzymes.

The first apparent peculiarity of the *W. succinogenes* QFR is that its partial activities were marked by much higher values compared to the other two species. Besides, this enzyme and the one from *C. jejuni* show that the “BV assay” enzymatic activity, where the electrons are delivered from the reduced BV to fumarate, was far higher than the “MB assay” activity, where the electrons are delivered from succinate to methylene blue (opposite direction than the physiological fumarate reduction). Differently, the *H. pylori* QFR does not have the same properties, being activity values obtained with the “BV assay” and “MB assay” rather similar. However it should be taken into consideration that, in contrast to the other two species, the *H. pylori* genome (Tomb, *et al.*, 1997) contains a QFR operon, but not a SQR operon. Furthermore, it should also be considered that the ability of *H. pylori* to establish a positive inside membrane potential (Matin, *et al.*, 1996) may, in physiological conditions, influence this ratio.

Nevertheless, this kind of assays cannot be accurately compared amongst the species due to the fact that, since BV and MB are not natural substrates and do not bind to specific catalytic

---

<sup>u</sup> A detailed description of the structure can be retrieved in Lancaster, *et al.*, 1999 or Lancaster, 2003.



sites, these two compounds may have different binding site accessibility in the different enzymes. Hence one may conclude, for instance, that the *W. succinogenes* QFR has higher activities because it simply displays higher accessibility to the BV and MB.

Instead, a more reliable way of comparing the enzymes is to consider the total enzymatic activity measured with the “DMNH<sub>2</sub> assay”. In this view, the three enzymes do not show remarkable differences, being the QFR enzymatic activities ( $V_{\max}$ ) from *C. jejuni*, *H. pylori*, and *W. succinogenes* equal to 9.3 U mg<sup>-1</sup>, 12.3 U mg<sup>-1</sup>, and 14.7 U mg<sup>-1</sup>, respectively. As pointed out earlier, these activity values were achieved using the “DT-DMNH<sub>2</sub> assay”, a method that increases their values by a factor of two if compared to the “BH<sub>4</sub>-DMN assay”. Very interestingly, the values obtained with the “DT-DMNH<sub>2</sub> assay” are perfectly similar to the values obtained with the alternative procedure “low-sensitivity-BH<sub>4</sub>-DMN assay”, thus by monitoring the fumarate reduction in the presence of excess NaBH<sub>4</sub>. Likely, the increasing amount of oxidized DMN in the assay mixture during catalysis slows down the reaction, thereby explaining the shorter linearity and the lower  $V_{\max}$  values obtained with the “BH<sub>4</sub>-DMN assay”.

Overall, previous determinations of *W. succinogenes* QFR activities corresponding to 28.8 U mg<sup>-1</sup>, 7.4 U mg<sup>-1</sup>, and 180 U mg<sup>-1</sup> with the “MB assay”, “BH<sub>4</sub>-DMNH<sub>2</sub> assay” (Lancaster, *et al.*, 2000), and “BV assay” (Unden & Kröger, 1986), respectively, agree perfectly with the results shown here. Nevertheless,  $K_M$  values for fumarate in the *C. jejuni* QFR and *H. pylori* QFR (Table 3-VII) are much smaller than previous measurements (1.9 mM and 0.83 mM, respectively) reviewed in ref. Lancaster & Simon, 2002. The  $K_M$  values obtained here (in the order of one tenth of mM) appear more reasonable for efficient catalysis of QFRs.

#### 4.1.6.1. An accurate inhibitor characterization

In the past years, a number of compounds have already been suggested as inhibitors of QFR from *C. jejuni* and *H. pylori* species (Chen, *et al.*, 2002, Mendz, *et al.*, 1995, Smith, *et al.*, 1999, Olbe, *et al.*, 2003, Hoffman, *et al.*, 1996, Chen, *et al.*, 1999, Grivennikova & Vinogradov, 1982). Although some of these, such as metronidazole, nizatidine, morantel and TTFA, could not be assayed with the available assay methods due to the (prohibitive) high absorbance at the monitored wavelength, the QFR inhibitors omeprazole, oxantel, and thiabendazole could be tested and characterized. In contrast to the previous measurements, where  $K_i$  values were estimated in non-purified samples and/or by NMR spectroscopy, in this work we assign precise  $K_i$  values based on UV/VIS-spectroscopy activity measurement of the pure enzyme.

The  $K_i$  values listed in Table 3-VII reveal that the order of inhibition effect was oxantel>thiabendazole>omeprazole, albeit this latter inhibitor had no effect in *H. pylori* QFR. With the use of Lineweaver-Burk plots, we could also assign the type of inhibition exerted by these three compounds. Omeprazole, which has no effect on the *H. pylori* QFR, has a competitive inhibitory effect on the *C. jejuni* QFR, thus it binds to the quinol-binding site. Curiously, the thiabendazole exerts a non-competitive (or allosteric) inhibition effect in the *C. jejuni* QFR, while in the *H. pylori* QFR the type of inhibition is competitive. In the “BV assay”, this compound does not affect either of the two enzymes, thus this inhibitor is supposed to bind to the hydrophobic transmembrane subunit C of the QFR, seemingly close to the quinone-binding site. Oxantel was formerly analyzed on *H. pylori* broken cells by monitoring fumarate concentration with NMR spectroscopy (Mendz, *et al.*, 1995) and it was predicted to bind competitively at the fumarate binding site with an inhibition constant equal to about 60  $\mu$ M. The results obtained here about the QFR inhibition by oxantel show that it exerts an un-competitive inhibition (with respect to the quinone substrate), thus the inhibitor binds to a site other than the active site (for quinone), but only when the substrate is bound. Inhibition by oxantel is also observed in the partial activity assays, proving that it is binding or affecting the hydrophilic subunits of the enzyme. In other words, although it is considered to bind at the fumarate binding site (Mendz, *et al.*, 1995), i.e. rather far from the quinone site, it is assumed that the binding of the oxantel is able to decrease its affinity for the quinone, plausibly by imposing a structural change that is perceived by the quinol oxidation site. Alternatively, multiple binding sites (i.e. one located in the subunit C and a second in the hydrophilic domain) would also explain the observed effects. Whilst the binding location found in these results does not contradict the previous characterization, experiments performed on the isolated enzyme show a markedly lower inhibition effect. Earlier studies on the *C. jejuni* QFRs activity in the presence of oxantel and thiabendazole have shown a much lower inhibition ( $IC_{50}$  of 6 and 70 mM, respectively) (Smith, *et al.*, 1999). In conclusion, despite the fact that these compounds had perceivable inhibitory effects, they are rather modest inhibitors, and are probably not useful even as drug leads. As pointed out earlier, the QFR from *H. pylori*, *S. typhimurium*, and likely also *C. jejuni* can be considered as potential targets for the eradication of these species, as current therapies often produce severe side effects, they are aspecific, and occasionally ineffective due to acquired antibiotic resistances (Ge, 2002, Marais, *et al.*, 1999b). The screening for new and highly effective inhibitors is now made possible with the use of the isolated active enzymes.

## 4.2. <sup>13</sup>C-Labeling of QFR Heme Propionates

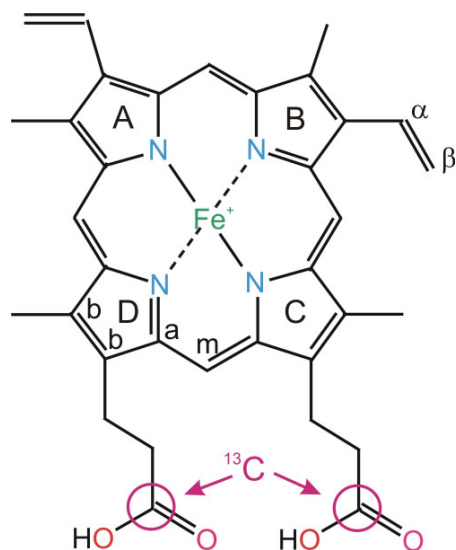
### 4.2.1. Construction of the $\Delta$ *hemL* deletion strain

In anaerobic bacteria, the glutamate-1-semialdehyde-2,1-amino-mutase (encoded by the *hemL* gene) is responsible for the synthesis of 5-aminolevulinate, a precursor of the heme biosynthesis (Michal, 1999). The deletion of the *hemL* gene in the WT *W. succinogenes* resulted in an auxotrophic strain that was therefore able to grow in minimal medium only with the addition of exogenous ALA. Further characterization of the mutant genome was performed by PCR, which showed an unequivocal replacement of the *hemL* gene with the kanamycin resistance gene. These two data clearly show that the mutant strains do not possess a functional glutamate-1-semialdehyde-2,1-amino-mutase, and are forced to make use of the exogenous ALA.

The low cell density reached in the large culture was partly due to the use of minimal medium, and partly because of the low concentration of the (labeled) ALA. Since it was observed that longer degassing time of the medium often reduced the growth irreproducibility, this problem might be due to hypersensitivity of the mutant cells to oxygen. Due to the fact that this problem was overcome by increasing the amount of inoculated cells, a speculative explanation to the hypersensitivity phenomenon could be that the cells may require readily available heme groups and functional heme proteins to scavenge oxygen or reactive oxygen species (ROS) present in the medium prior to start growing. If this holds true, the oxygen scavenger may originate from an archaic remains of aerobic respiratory chain found in the genome of *W. succinogenes* (Baar, *et al.*, 2003), and could be represented by the cytochrome *cbb<sub>3</sub>* and *bd* terminal oxidases.

### 4.2.2. A <sup>13</sup>C-labeled QFR suitable for FTIR spectroscopy analysis and comparison

MALDI TOF analysis ascertained that the full labeling (nearly 100%) of the heme propionates indeed occurred, thus confirming the results of the genetic work and providing a solid basis for the discussion of the spectroscopic results. The mutant strain N2 of *W. succinogenes* was therefore able to produce a QFR specifically <sup>13</sup>C-labeled at the carboxyl carbon atoms of the heme propionates (Figure 4-2).



**Figure 4-2: The chemical structure of a heme *b* group and indication of the isotopically labeled propionates (magenta).** The porphyrin ring consists of four pyrrole units named from A to D (green letters). The respective carbons that connect the pyrrole units are named by Greek letters from  $\alpha$  to  $\delta$ .

Enzymatic activities of the purified  $^{13}\text{C}$ -labeled QFR were very similar to the unlabeled QFR, ensuring that the former enzyme is correctly folded and functional. Since both hemes are involved in the total enzymatic activity (Lancaster, *et al.*, 2000), the full functionality indicates that the QFR contains all cofactors, including the labeled hemes. Further proof was given spectrophotometrically, as the heme-to-protein ratio resulted to be 2:1 (as expected for a di-hemic QFR), and as the characteristic “two steps” in the heme redox titration curve had equal intensity. The high specific activity together with the SDS-PAGE pattern of the isolated labeled QFR after isoelectric focusing allow to conclude that the enzyme functionality and purity was comparable to the usual WT QFR preparation.

To further exclude any major difference in the physicochemical properties between the two proteins, the redox midpoint potentials of the labeled QFR hemes have been measured by visible spectroscopy. Any differences were found to be insignificant within the context of this study.

Hydrophobic substrates such as menaquinone, which tightly bind to the transmembrane region of the protein, are found to co-purify in substoichiometric ratios of about 0.1 or 0.2 molecules of menaquinone per enzyme monomer. To rule out the possibility of major quinone-occupancy differences, determination of bound quinone was performed in the labeled and unlabeled preparations, and resulted in quinone contents of  $0.23 \pm 0.025$  per

monomer. Considering only the signal generated from one propionate per monomer, less than 5% of the double difference FTIR signal would be ascribed to differences in native menaquinone concentration. The expected signal shifts in the frequencies around  $1400\text{ cm}^{-1}$  and  $1550\text{ cm}^{-1}$  upon potential changes would thus be undoubtedly due to heme propionate(s) protonation/deprotonation events.

### 4.2.3. FTIR Spectroscopy analysis of the labeled and unlabeled enzymes

The obtained FTIR spectroscopic results based on  $^{13}\text{C}$ -labeling of the QFR heme propionates clearly indicate an involvement of at least one of the two propionate groups of the low potential distal heme  $b_D$  of QFR in the electrochemically induced redox reaction. This is reflected in contributions of the protonated and deprotonated forms of the respective group(s) to the computed “unlabeled-minus-labeled” QFR double-difference spectra.

#### 4.2.3.1. Tentative vibrations of protonated heme propionates

Above  $1700\text{ cm}^{-1}$ , similar and rather broad contributions were observed in the FTIR difference spectra for the full potential, and for the “reduced-minus-intermediate” potential step, which might be assigned to vibrations of protonated heme propionate(s) of  $b_D$  and which are shifted to lower wavenumbers where they are heavily obscured by other vibrations (i.e., the amide I and the strong water absorbance, which are both centered around  $1650\text{ cm}^{-1}$ ) upon  $^{13}\text{C}$ -labeling. Based on observations from multiple independent experiments on the unlabeled QFR WT enzyme, the signal around  $1718\text{ cm}^{-1}$  appears to be more susceptible for amplitude variations. Although frequencies above  $1710\text{ cm}^{-1}$  would be very high for a  $\nu(\text{COOH})$  heme propionate vibration (Behr, *et al.*, 1998), the results obtained in this study indicate a frequency for a propionate carboxyl group vibration which is in the range of Glu or Asp  $\nu(\text{COOH})$  modes. Yet, this is conceivable if the local environment of the specific propionate is very hydrophobic so that it is not hydrogen-bonded, enabling the observed high frequency for the  $\nu(\text{COOH})$  mode. If experimental errors such as insufficient equilibration or pH effects can be excluded, the apparent differences between the specifically labeled and unlabeled QFR in this range are very likely related to the  $^{13}\text{C}$ -labeling of the heme propionates. In principle, such a scenario is covered by the particular position and environment of the ring C propionate of  $b_D$  as it is oriented parallel to the membrane plane inside the hydrophobic subunit and not along the membrane normal as the other

propionates. Thus, it is feasible that the observed difference signals above  $1710\text{ cm}^{-1}$  contain ring C heme propionate contributions, which indicates a redox-coupled protonation change and/or an environmental change of a propionate group of  $b_D$ . Yet, it remains difficult to explain the entire spectral features in terms of heme propionate vibrations, and additional effects arising from scaling errors cannot be excluded presently.

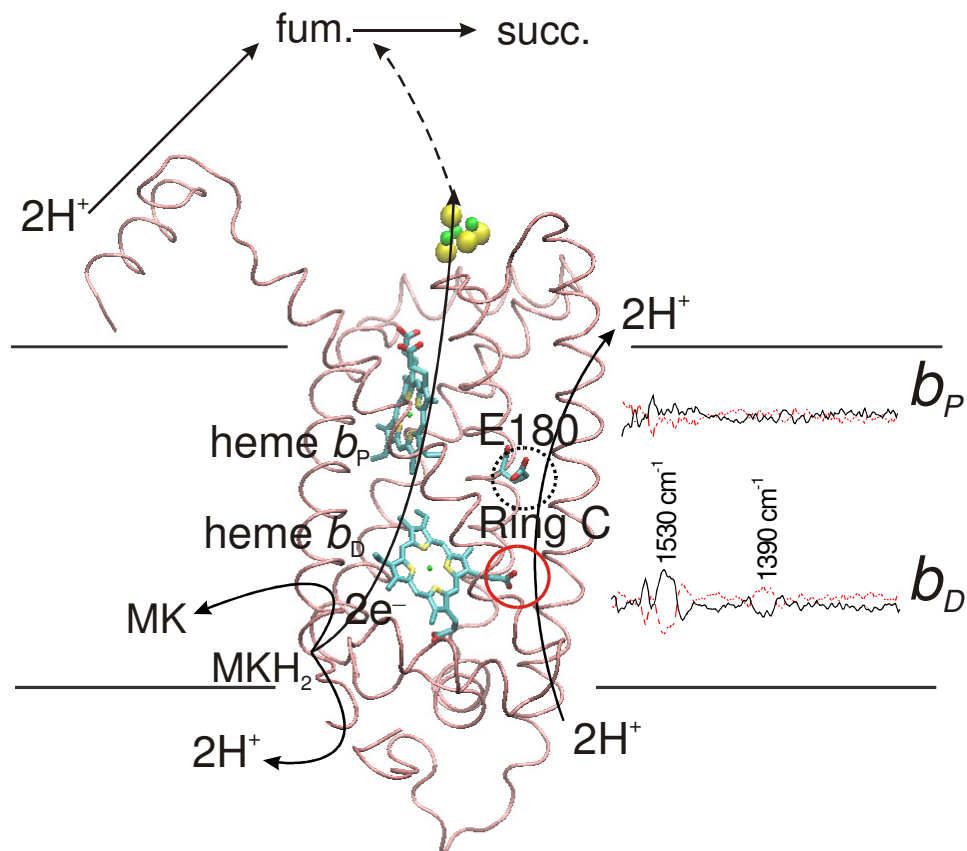
#### 4.2.3.2. Tentative anti- and symmetric vibrations of deprotonated heme propionates

The distinct series of positive and negative double-difference bands in the frequency range between  $1560\text{ cm}^{-1}$  and  $1500\text{ cm}^{-1}$  are more reliable to discuss, and they are indicative of antisymmetric  $\nu_{\text{as}}(\text{COO}^-)$  vibrations of deprotonated heme propionates and/or environmental changes (e.g., due to a redox-coupled conformational change of the propionate group resulting in a different coordination of the oxygen atoms) of the respective groups. The band pattern cannot be ascribed to a simple downshift of a single deprotonated heme propionate mode upon  $^{13}\text{C}$ -labeling, and hence the observed pattern points out combined redox effects. As inferred from the crystal structure of QFR and rationalized by previous electrostatic calculations (Haas & Lancaster, 2004), the ring D propionate of the distal heme  $b_D$  is engaged in a salt bridge with the positively charged FrdC-R162. Thus, the only reasonable candidate for a (de)protonation event and/or environmental changes is the ring C propionate of the low-potential distal heme  $b_D$ , and an environmental change of the ring D propionate, which might reflect a variation in the strength of the salt bridge, for instance. Corresponding mandatory signals for the symmetric  $\nu_{\text{s}}(\text{COO}^-)$  vibrations are present in the double-difference spectra in the frequency range between  $1410\text{ cm}^{-1}$  and  $1360\text{ cm}^{-1}$ , although they are less pronounced. At least for the acidic side chains of Asp and Glu, this is in line with smaller extinction coefficients for symmetric  $\nu_{\text{s}}(\text{COO}^-)$  modes compared to the antisymmetric ones (Mileni, *et al.*, 2005a).

#### 4.2.3.3. Differences between the full and partial potential steps at the distal heme

It is inferred that the spectral features in the double-difference spectra of the full and the low-potential step arise from the (low-potential) heme  $b_D$  propionates. The observed discrepancies that are visible for the two steps could be due to the different reference potentials “intermediate” and “oxidized”, respectively. At the intermediate potential, the

(high-potential) proximal heme  $b_p$  is reduced, and heme  $b_D$  is oxidized. At the oxidizing potential, *both* hemes are fully oxidized. Hence, it is feasible that the redox state of the proximal heme influences the redox transition of the distal heme  $b_D$ . In the electrostatic calculations presented by Haas *et al.* (Haas & Lancaster, 2004), the two oxidized hemes destabilize each other by 0.6  $\Delta pK$  units, whereas the interactions with and among the reduced heme species are negligible. Thus, it is conceivable that the different redox state of the proximal heme  $b_p$  has a noticeable influence (minor frequency shifts and/or intensity variations, as can be seen in Figure 4-3) on the vibrations of the ionized propionates of the oxidized distal heme  $b_D$ . The absence of significant contributions from the propionates of the high-potential proximal heme  $b_p$  is in line with the results from both the structure and the electrostatic calculations that both propionates are involved in stable salt bridges and consequently not available for redox-driven proton transfer (Haas & Lancaster, 2004). For the distal heme  $b_D$ , it is inferred that the ring C propionate is the dominating source for the observed double-difference bands, as any effect at the ring D propionate of  $b_D$  would be restricted to an environmental change due to the salt bridge, which was identified in the crystal structures and MCCE calculations. The interpretation of the obtained experimental data associated with the distal heme  $b_D$ , and particularly with the ring C propionate, in terms of a (de)protonation event possibly accompanied by an environmental effect, which could well be a conformational change, agrees very well with the suggested role of this propionate in the proposed “E-pathway” hypothesis of coupled transmembrane electron and proton transfer (Lancaster, 2002b).



**Figure 4-3: A representation of the E-pathway hypothesis.** The transmembrane subunit FrdC, depicted in pink, contains the proximal heme (heme  $b_P$ ) and the distal heme (heme  $b_D$ ). The electron and proton transfers are indicated as black arrows. The abbreviations “fum.” and “succ.” stand for fumarate and succinate, respectively. The proposed key components of the pathway are highlighted: the side chain residue E180 (black dotted circle) and the ring C propionate of the distal heme (red circle). At the right side the FTIR double-difference spectra relative to the proximal ( $b_P$ ) and distal ( $b_D$ ) hemes are shown.

### 4.3. Concluding remarks and perspectives

A broad range of methods and techniques were employed in order to reach the different goals of this thesis. In the first part, a heterologous gene expression in *W. succinogenes* for large-scale membrane protein production has been developed. Future genetic work will aim at the optimization of vector-based expression of genes encoding other metalloproteins from pathogenic  $\epsilon$ -proteobacteria that may become realistic anti-microbial targets. The QFRs from



the pathogenic bacteria *H. pylori* and *C. jejuni* have been produced and purified. Consequently, large amounts of stable and active purified protein permitted to extensively characterize these two enzymes, and to solve the 3D-crystal structure of the *C. jejuni* QFR at 3.24 Å. This work provides the basis for further functional and structural studies of these membrane protein complexes that can be especially used to achieve new inhibitors and new drugs for eradication of *H. pylori* and *C. jejuni*. Since the inhibitors here characterized have different effects on these QFRs (e.g. the omeprazole does not exert any inhibitory effect on the *H. pylori* QFR), the inhibitor development (e.g. inhibitor screening by enzymatic assay, structure-based drug design, etc.) is far more reliable when using the target enzymes themselves, and not surrogate enzymes like the *W. succinogenes* QFR, whose high-resolution structure is already available.

However, a crystal structure of the *C. jejuni* QFR that diffracts at higher resolution is necessary for further structure-based mechanistic or inhibitor studies. Therefore, the first perspective is to achieve a better crystal structure with higher resolution and without discontinuities in the electron density maps, especially in the crucial regions, like the active sites. For instance, co-crystallization of the protein with oxantel or other fumarate-competitive inhibitors might help to tighten the capping domain, which would improve the electron density in this region as well as increase the overall structure resolution. Similarly, the achievement of QFR crystal structures containing efficient inhibitors such as menaquinone-analogues, i.e. binding at the Q-site, could aid improving the structure but also unveiling important structural insights into the enzyme mechanism.

Furthermore, site-directed mutagenesis on the *C. jejuni* and *H. pylori* QFRs is now a straight forward tool to selectively investigate the function of specific residues in these enzymes. For example, the glutamate residues FrdC-E66 and FrdC-E180 from the *W. succinogenes* QFR were replaced with glutamines in order to prove their ability to provide a basis for proton transfer during catalysis. Experiments performed on the respective variant enzymes enabled to propose that the former residue (E66) is an essential constituent of the menaquinol oxidation site by accepting protons from quinol during oxidation, whereas the latter residue (E180) is one of the key components of the proposed E-pathway (Haas, *et al.*, 2005). Amino acid substitutions at the homologous residues of the *H. pylori* and *C. jejuni* QFRs are required so that the previous functional characterizations can be verified and confirmed. Furthermore, due to the position of the FrdC-M163 in the structure of the *W. succinogenes* QFR, substitution of this residue with either an arginine or a lysine has been carried out in order to promote the formation of a salt bridge with the ring C heme propionate and

therefore to prevent proton transfer through this proposed key component of the E-pathway. Although the FrdC-M163 mutants in the *W. succinogenes* QFR were unstable and could not be produced (Juhnke & Lancaster, unpublished), homologous mutations on the *C. jejuni* and *H. pylori* QFRs may result in more stable mutants that can be characterized. At present, the plasmids containing the eight mentioned mutations (four in the *C. jejuni* QFR and four in the *H. pylori* QFR, Table 2-IX) have been produced, sequenced, and are hence ready to be inserted into the genome of the *W. succinogenes*  $\Delta$ frdCAB strain by transformation.

The *W. succinogenes* mutant strain N2 was able to produce large amounts of QFR which was specifically  $^{13}\text{C}$ -labeled at the carboxyl carbon atoms of the heme propionates. The purified labeled enzyme have been successfully characterized by electrochemically-induced FTIR difference spectroscopy and compared to the unlabeled enzyme. The absence of significant signal differences relative to the propionates of the (high-potential) proximal heme *b* is in line with the results from both the structure (7) and the electrostatic calculations that both propionates are involved in stable salt bridges and consequently not available for redox-driven proton transfer. Concerning the (low-potential) distal heme *b*, it is inferred that the ring C propionate is the dominating source for the observed double-difference bands. The interpretation of the obtained experimental data associated with the distal heme *b*, and particularly with the ring C propionate, in terms of a (de)protonation event possibly accompanied by an environmental effect, which could well be a conformational change, agrees very well with the suggested role of this propionate in the proposed “E-pathway” hypothesis of coupled transmembrane electron and proton transfer.

In future works the *W. succinogenes* mutant N2 can be employed for efficiently producing QFR, or other proteins, which have  $^{13}\text{C}$ - or  $^{15}\text{N}$ -labeled hemes at one or more positions by supplying the medium with isotopically labeled ALA. FTIR or NMR spectroscopy may then be employed to analyze the labeled proteins for further studies.

## 5. REFERENCES

- Ackrell, B.A., Kearney, E.B., Mims, W.B., Peisach, J. and Beinert, H. (1984) Iron-sulfur cluster 3 of beef heart succinate-ubiquinone oxidoreductase is a 3-iron cluster. *J Biol Chem*, **259**:4015-8
- Albracht, S.P., Uden, G. and Kroger, A. (1981) Iron-sulphur clusters in fumarate reductase from *Vibrio succinogenes*. *Biochim Biophys Acta*, **661**:295-302
- Annamalai, T., Mohan Nair, M.K., Marek, P., Vasudevan, P., Schreiber, D., Knight, R., Hoagland, T. and Venkitanarayanan, K. (2004) In vitro inactivation of *Escherichia coli* O157:H7 in bovine rumen fluid by caprylic acid. *J Food Prot*, **67**:884-8
- Baar, C., Eppinger, M., Raddatz, G., Simon, J., Lanz, C., Klimmek, O., Nandakumar, R., Gross, R., Rosinus, A., Keller, H., Jagtap, P., Linke, B., Meyer, F., Lederer, H. and Schuster, S.C. (2003) Complete genome sequence and analysis of *Wolinella succinogenes*. *Proc Natl Acad Sci U S A*, **100**:11690-5
- Bardhan, P.K. (1997) Epidemiological features of *Helicobacter pylori* infection in developing countries. *Clin Infect Dis*, **25**:973-8
- Baymann, F., Robertson, D.E., Dutton, P.L. and Mäntele, W. (1999) Electrochemical and spectroscopic investigations of the cytochrome *bc*<sub>1</sub> complex from *Rhodobacter capsulatus*. *Biochemistry*, **38**:13188-99
- Behr, J., Hellwig, P., Mäntele, W. and Michel, H. (1998) Redox dependent changes at the heme propionates in cytochrome *c* oxidase from *Paracoccus denitrificans*: direct evidence from FTIR difference spectroscopy in combination with heme propionate <sup>13</sup>C labeling. *Biochemistry*, **37**:7400-6
- Behr, J., Michel, H., Mäntele, W. and Hellwig, P. (2000) Functional properties of the heme propionates in cytochrome *c* oxidase from *Paracoccus denitrificans*. Evidence from FTIR difference spectroscopy and site-directed mutagenesis. *Biochemistry*, **39**:1356-63
- Beinert, H. (2002) Spectroscopy of succinate dehydrogenases, a historical perspective. *Biochim Biophys Acta*, **1553**:7-22
- Berks, B.C., Page, M.D., Richardson, D.J., Reilly, A., Cavill, A., Outen, F. and Ferguson, S.J. (1995) Sequence analysis of subunits of the membrane-bound nitrate reductase from a denitrifying bacterium: the integral membrane subunit provides a prototype for the dihaem electron-carrying arm of a redox loop. *Mol Microbiol*, **15**:319-31
- Bertero, M.G., Rothery, R.A., Palak, M., Hou, C., Lim, D., Blasco, F., Weiner, J.H. and Strynadka, N.C. (2003) Insights into the respiratory electron transfer pathway from the structure of nitrate reductase A. *Nat Struct Biol*, **10**:681-7
- Biel, S., Simon, J., Gross, R., Ruiz, T., Ruitenber, M. and Kroger, A. (2002) Reconstitution of coupled fumarate respiration in liposomes by incorporating the electron transport enzymes isolated from *Wolinella succinogenes*. *Eur J Biochem*, **269**:1974-83
- Birkholz, S., Knipp, U., Lemma, E., Kroger, A. and Opferkuch, W. (1994) Fumarate reductase of *Helicobacter pylori*--an immunogenic protein. *J Med Microbiol*, **41**:56-62
- Blaser, M.J. (1997) Epidemiologic and clinical features of *Campylobacter jejuni* infections. *J Infect Dis*, **176 Suppl 2**:S103-5
- Bokranz, M., Morschel, E. and Kröger, A. (1985) Phosphorylation and phosphate-ATP exchange catalyzed by the ATP synthase isolated from *Wolinella succinogenes*. *Biochim Biophys Acta*, **810**:332-9
- Bolivar, F., Rodriguez, R.L., Greene, P.J., Betlach, M.C., Heyneker, H.L. and Boyer, H.W. (1977) Construction and characterization of new cloning vehicles. II. A multipurpose cloning system. *Gene*, **2**:95-113

- Bronder, M., Mell, H., Stupperich, E. and Kröger, A. (1982)** Biosynthetic Pathways of *Vibrio succinogenes* growing with fumarate as terminal electron acceptor and sole carbon source. *Arch Microbiol*, **131**:216-23
- Brunger, A.T., Adams, P.D., Clore, G.M., Delano, W.L., Gros, P., Grosse-Kunstleve, R.W., Jiang, J.S., Kuszewski, J., Nilges, M., Pannu, N.S., Read, R.J., Rice, L.M., Simonson, T. and Warren, G.L. (1998)** Crystallography & NMR system: A new software suite for macromolecular structure determination. *Acta Crystallogr D Biol Crystallogr*, **54 ( Pt 5)**:905-21
- Butzler, J.P. (2004)** Campylobacter, from obscurity to celebrity. *Clin Microbiol Infect*, **10**:868-76
- Cammack, R. (1995)** Redox states and potentials. In: *Bioenergetics: a practical approach*. (Brown, G. C. and Cooper, C. E., Eds.) IRL Press, Oxford, UK, pp. 85-109
- Cantor, C.R. and Schimmel, P.R. (1980)** Ultracentrifugation In: *Biophysical Chemistry", Part II* ((Eds.) Freeman, New York, pp. 591-641
- Cecchini, G. (2003)** Function and structure of complex II of the respiratory chain. *Annu Rev Biochem*, **72**:77-109
- Cecchini, G., Ackrell, B.A., Deshler, J.O. and Gunsalus, R.P. (1986)** Reconstitution of quinone reduction and characterization of *Escherichia coli* fumarate reductase activity. *J Biol Chem*, **261**:1808-14
- Cecchini, G., Maklashina, E., Yankovskaya, V., Iverson, T.M. and Iwata, S. (2003)** Variation in proton donor/acceptor pathways in succinate:quinone oxidoreductases. *FEBS Lett*, **545**:31-8
- Chen, M., Andersen, L.P., Zhai, L. and Kharazmi, A. (1999)** Characterization of the respiratory chain of *Helicobacter pylori*. *FEMS Immunol Med Microbiol*, **24**:169-74
- Chen, M., Jensen, B., Zhai, L., Colding, H., Kharazmi, A., Kristiansen, J.E. and Andersen, L.P. (2002)** Nizatidine and omeprazole enhance the effect of metronidazole on *Helicobacter pylori* in vitro. *Int J Antimicrob Agents*, **19**:195-200
- Chowdhury, D. and Arora, A. (2001)** Axonal Guillain-Barre syndrome: a critical review. *Acta Neurol Scand*, **103**:267-77
- Clark, W.M. (1960)** In: *Oxidation-reduction potentiality of organic systems*. (-, Eds.) Tindal & Cox Ltd., London, pp. 125,507
- Correa, P. (1996)** *Helicobacter pylori* and gastric cancer: state of the art. *Cancer Epidemiol Biomarkers Prev*, **5**:477-81
- Correa, P. (2003a)** *Helicobacter pylori* infection and gastric cancer. *Cancer Epidemiol Biomarkers Prev*, **12**:238s-41s
- Correa, P. (2003b)** Bacterial infections as a cause of cancer. *J Natl Cancer Inst*, **95**:E3
- Covacci, A., Telford, J.L., Del Giudice, G., Parsonnet, J. and Rappuoli, R. (1999)** *Helicobacter pylori* virulence and genetic geography. *Science*, **284**:1328-33
- Cover, T.L. and Blaser, M.J. (1999)** *Helicobacter pylori* factors associated with disease. *Gastroenterology*, **117**:257-61
- Dietrich, W. and Klimmek, O. (2002)** The function of methyl-menaquinone-6 and polysulfide reductase membrane anchor (PsrC) in polysulfide respiration of *Wolinella succinogenes*. *Eur J Biochem*, **269**:1086-95
- Distler, A.M., Hiser, C., Ling, Q., Hilmi, Y., Ferguson-Miller, S. and Allison, J. (2004)** Mass spectrometric detection of protein, lipid and heme components of cytochrome *c* oxidase from *R. sphaeroides* and the stabilization of non-covalent complexes from the enzyme. *European Journal of Mass Spectrometry*, **10**:295-308
- Dunn, B.E., Cohen, H. and Blaser, M.J. (1997)** *Helicobacter pylori*. *Clin Microbiol Rev*, **10**:720-41
- Dutton, P.L. (1978)** Redox potentiometry: determination of midpoint potentials of oxidation-reduction components of biological electron-transfer systems. *Methods Enzymol.*, **54**:411-35

- Folch, J., Lees, M. and Sloane Stanley, G.H. (1957)** A simple method for the isolation and purification of total lipides from animal tissues. *J Biol Chem*, **226**:497-509
- Fujimori, K., Shimodaira, S., Akamatsu, T., Furihata, K., Katsuyama, T. and Hosaka, S. (2005)** Effect of *Helicobacter pylori* eradication on ongoing mutation of immunoglobulin genes in gastric MALT lymphoma. *Br J Cancer*, **92**:312-9
- Gaby, A.R. (2001)** *Helicobacter pylori* eradication: are there alternatives to antibiotics? *Altern Med Rev*, **6**:355-66
- Gallagher, S.C., Cammack, R. and Dalton, H. (1999)** Electron transfer reactions in the alkene mono-oxygenase complex from *Nocardia corallina* B-276. *Biochem. J.*, **339**:79-85
- Gast, P., Michalski, T.J., Hunt, J.E. and R., N.J. (1985)** Determination of the amount and the type of quinones present in single crystals from reaction center protein from the photosynthetic bacterium *Rhodospseudomonas viridis*. *FEBS Letters*, **179**:325-8
- Ge, Z. (2002)** Potential of fumarate reductase as a novel therapeutic target in *Helicobacter pylori* infection. *Expert Opin Ther Targets*, **6**:135-46
- Ge, Z., Jiang, Q., Kalisiak, M.S. and Taylor, D.E. (1997)** Cloning and functional characterization of *Helicobacter pylori* fumarate reductase operon comprising three structural genes coding for subunits C, A and B. *Gene*, **204**:227-34
- Ge, Z., Feng, Y., Dangler, C.A., Xu, S., Taylor, N.S. and Fox, J.G. (2000)** Fumarate reductase is essential for *Helicobacter pylori* colonization of the mouse stomach. *Microb Pathog*, **29**:279-87
- Geisler, V., Ullmann, R. and Kröger, A. (1994)** The direction of the proton exchange associated with the redox reactions of menaquinone during electron transport in *Wolinella succinogenes*. *Biochim. Biophys. Acta*, **1184**:219-26
- Gennis, R.B. (1989)** Biomembranes: molecular structure and function. Springer-Verlag, Berlin, Heidelberg, New York pp. 85-137
- Graf, M., Bokranz, M., Böcher, R., Friedl, P. and Kröger, A. (1985)** Electron transport driven phosphorylation catalyzed by proteoliposomes containing hydrogenase, fumarate reductase and ATP synthase. *FEBS Letters*, **184**:100-03
- Grivennikova, V.G. and Vinogradov, A.D. (1982)** Kinetics of ubiquinone reduction by the resolved succinate: ubiquinone reductase. *Biochim Biophys Acta*, **682**:491-5
- Grivennikova, V.G., Gavrikova, E.V., Timoshin, A.A. and Vinogradov, A.D. (1993)** Fumarate reductase activity of bovine heart succinate-ubiquinone reductase. New assay system and overall properties of the reaction. *Biochim Biophys Acta*, **1140**:282-92
- Gross, R., Simon, J., Theis, F. and Kröger, A. (1998)** Two membrane anchors of *Wolinella succinogenes* hydrogenase and their function in fumarate and polysulfide respiration. *Arch Microbiol*, **170**:50-8
- Haas, A.H. (2004)** Doctoral thesis.
- Haas, A.H. and Lancaster, C.R.D. (2004)** Calculated coupling of transmembrane electron and proton transfer in dihemic quinol:fumarate reductase. *Biophysical Journal*, **87**:4298-315
- Haas, A.H., Sauer, U.S., Groß, R., Simon, J., Mäntele, W. and Lancaster, C.R.D. (2005)** FTIR difference spectra of quinol:fumarate reductase from *Wolinella succinogenes* support the "E-pathway" hypothesis. *Manuscript submitted*,
- Hägerhall, C., Magnitsky, S., Sled, V.D., Schroder, I., Gunsalus, R.P., Cecchini, G. and Ohnishi, T. (1999)** An *Escherichia coli* mutant quinol:fumarate reductase contains an EPR-detectable semiquinone stabilized at the proximal quinone-binding site. *J Biol Chem*, **274**:26157-64
- Hansson, L.E. (2000)** Risk of stomach cancer in patients with peptic ulcer disease. *World J Surg*, **24**:315-20

- Heering, H.A., Weiner, J.H. and Armstrong, F.A. (1997)** Direct detection and measurement of electron relays in a multicentered enzyme: voltammetry of electrode-surface films of *E. coli* fumarate reductase, an iron-sulfur flavoprotein. *J. Am. Chem. Soc.*, **119**:11628 - 38
- Hellwig, P., Soulimane, T., Buse, G. and Mäntele, W. (1999)** Electrochemical, FTIR, and UV/VIS spectroscopic properties of the *ba<sub>3</sub>* oxidase from *Thermus thermophilus*. *Biochemistry*, **38**:9648-58
- Hellwig, P., Rost, B., Kaiser, U., Ostermeier, C., Michel, H. and Mäntele, W. (1996)** Carboxyl group protonation upon reduction of the *Paracoccus denitrificans* cytochrome *c* oxidase: direct evidence by FTIR spectroscopy. *FEBS Lett.*, **385**:53
- Hodel, A., Kim, S.-H. and Brünger, A.T. (1992)** Model bias in macromolecular crystal structures. *Acta Cryst. A*, **48**:851-58
- Hoffman, P.S., Goodwin, A., Johnsen, J., Magee, K. and Veldhuyzen Van Zanten, S.J. (1996)** Metabolic activities of metronidazole-sensitive and -resistant strains of *Helicobacter pylori*: repression of pyruvate oxidoreductase and expression of isocitrate lyase activity correlate with resistance. *J Bacteriol*, **178**:4822-9
- Horsefield, R., Yankovskaya, V., Tornroth, S., Luna-Chavez, C., Stambouli, E., Barber, J., Byrne, B., Cecchini, G. and Iwata, S. (2003)** Using rational screening and electron microscopy to optimize the crystallization of succinate:ubiquinone oxidoreductase from *Escherichia coli*. *Acta Crystallogr D Biol Crystallogr*, **59**:600-2
- Hussell, T., Isaacson, P.G., Crabtree, J.E. and Spencer, J. (1993)** The response of cells from low-grade B-cell gastric lymphomas of mucosa-associated lymphoid tissue to *Helicobacter pylori*. *Lancet*, **342**:571-4
- Iverson, T.M., Luna-Chavez, C., Cecchini, G. and Rees, D.C. (1999)** Structure of the *Escherichia coli* fumarate reductase respiratory complex. *Science*, **284**:1961-6
- Janausch, I.G., Zientz, E., Tran, Q.H., Kroger, A. and Unden, G. (2002)** C4-dicarboxylate carriers and sensors in bacteria. *Biochim Biophys Acta*, **1553**:39-56
- Johnson, M.K., Morningstar, J.E., Bennett, D.E., Ackrell, B.A. and Kearney, E.B. (1985)** Magnetic circular dichroism studies of succinate dehydrogenase. Evidence for [2Fe-2S], [3Fe-xS], and [4Fe-4S] centers in reconstitutively active enzyme. *J Biol Chem*, **260**:7368-78
- Jones, T.A., Zou, J.Y., Cowan, S.W. and Kjeldgaard (1991)** Improved methods for building protein models in electron density maps and the location of errors in these models. *Acta Crystallogr A*, **47** ( Pt 2):110-9
- Jormakka, M., Byrne, B. and Iwata, S. (2003a)** Protonmotive force generation by a redox loop mechanism. *FEBS Lett*, **545**:25-30
- Jormakka, M., Byrne, B. and Iwata, S. (2003b)** Formate dehydrogenase--a versatile enzyme in changing environments. *Curr Opin Struct Biol*, **13**:418-23
- Jormakka, M., Tornroth, S., Byrne, B. and Iwata, S. (2002)** Molecular basis of proton motive force generation: structure of formate dehydrogenase-N. *Science*, **295**:1863-8
- Kannangara, C.G., Gough, S.P., Bruyant, P., Hooper, J.K., Kahn, A. and Von Wettstein, D. (1988)** tRNA(Glu) as a cofactor in delta-aminolevulinic acid biosynthesis: steps that regulate chlorophyll synthesis. *Trends Biochem Sci*, **13**:139-43
- Kelly, D.J. (1998)** The physiology and metabolism of the human gastric pathogen *Helicobacter pylori*. *Adv Microb Physiol*, **40**:137-89
- Kelly, D.J. (2001)** The physiology and metabolism of *Campylobacter jejuni* and *Helicobacter pylori*. *Symp Ser Soc Appl Microbiol*, **30**:16S-24S
- Kenney, W.C. and Kroger, A. (1977)** The covalently bound flavin of *Vibrio succinogenes* succinate dehydrogenase. *FEBS Lett*, **73**:239-43
- Körtner, C., Lauterbach, F., Tripier, D., Unden, G. and Kröger, A. (1990)** *Wolinella succinogenes* fumarate reductase contains a dihaem cytochrome *b*. *Mol Microbiol*, **4**:855-60

- Kröger, A. (1978)** Fumarate as terminal acceptor of phosphorylative electron transport. *Biochim. Biophys. Acta*, **505**:129-45
- Kröger, A. and Klingenberg, M. (1973)** The kinetics of the redox reactions of ubiquinone related to the electron-transport activity in the respiratory chain. *Eur J Biochem*, **34**:358-68
- Kröger, A. and Innerhofer, A. (1976a)** The function of the *b* cytochromes in the electron transport from formate to fumarate of *Vibrio succinogenes*. *European Journal of Biochemistry*, **69**:497-506
- Kröger, A. and Innerhofer, A. (1976b)** The function of menaquinone, covalently bound FAD and iron-sulfur protein in the electron transport from formate to fumarate of *Vibrio succinogenes*. *European Journal of Biochemistry*, **69**:487-95
- Kröger, A., Dorrer, E. and Winkler, E. (1980)** The orientation of the substrate sites of formate dehydrogenase and fumarate reductase in the membrane of *Vibrio succinogenes*. *Biochim Biophys Acta*, **589**:118-36
- Kröger, A., Winkler, E., Innerhofer, A., Hackenberg, H. and Schägger, H. (1979)** The formate dehydrogenase involved in electron transport from formate to fumarate in *Vibrio succinogenes*. *Eur J Biochem*, **94**:465-75
- Kröger, A., Geisler, V., Lemma, E., Theis, F. and Lenger, R. (1992)** Bacterial fumarate respiration. *Archives of Microbiology*, **158**:311-14
- Kröger, A., Biel, S., Simon, J., Gross, R., Uden, G. and Lancaster, C.R.D. (2002)** Fumarate respiration of *Wolinella succinogenes*: enzymology, energetics and coupling mechanism. *Biochim. Biophys. Acta*, **1553**:23-38
- Kuniyasu, H., Yasui, W., Yokozaki, H. and Tahara, E. (2000)** *Helicobacter pylori* infection and carcinogenesis of the stomach. *Langenbecks Arch Surg*, **385**:69-74
- Laemmli, U.K. (1970)** Cleavage of structural proteins during the assembly of the head of bacteriophage T4. *Nature*, **227**:680-5
- Lancaster, C.R. (2003a)** The structure of *Wolinella succinogenes* quinol: fumarate reductase and its relevance to the superfamily of succinate: quinone oxidoreductases. *Adv Protein Chem*, **63**:131-49
- Lancaster, C.R.D. Ed., 2002, BBA 1553, pp. 1-176.**
- Lancaster, C.R.D. (2001a)** Succinate:quinone oxidoreductases--what can we learn from *Wolinella succinogenes* quinol:fumarate reductase? *FEBS Lett*, **504**:133-41
- Lancaster, C.R.D. (2001b)** Succinate:quinone oxidoreductases. In: *Handbook of Metalloproteins (vol. 1)* (Messerschmidt, A., Huber, R., Poulous, T. and Wieghardt, K., Eds.) Wiley, Chichester, UK, pp. 379-401
- Lancaster, C.R.D. (2002a)** Succinate:quinone oxidoreductases: an overview. *Biochimica et Biophysica Acta*, **1553**:1-6
- Lancaster, C.R.D. (2002b)** *Wolinella succinogenes* quinol:fumarate reductase-2.2-A resolution crystal structure and the E-pathway hypothesis of coupled transmembrane proton and electron transfer. *Biochim Biophys Acta*, **1565**:215-31
- Lancaster, C.R.D. (2003b)** Crystallization of *Wolinella succinogenes* quinol:fumarate reductase. In: *Membrane Protein Purification and Crystallization: A Practical Guide (2nd ed.)*. (Hunte, C., Schägger, H. and von Jagow, G., Eds.) Academic Press, San Diego, pp. 219-28
- Lancaster, C.R.D. (2004a)** Structure and function of succinate:quinone oxidoreductases and the role of quinol:fumarate reductases in fumarate respiration. In: *Respiration in Archaea and Bacteria Volume 1: Diversity of Prokaryotic Electron Transport Carriers*. (Zannoni, D., Eds.) Kluwer Scientific, Dordrecht, The Netherlands, pp. 57-85
- Lancaster, C.R.D. (2004b)** Respiratory chain complex II and succinate:quinone oxidoreductases. *Encyclopedia of Biological Chemistry*, **3**:681-7

- Lancaster, C.R.D. and Simon, J. (2002)** Succinate:quinone oxidoreductases from epsilon-proteobacteria. *Biochim Biophys Acta*, **1553**:84-101
- Lancaster, C.R.D., Gross, R. and Simon, J. (2001)** A third crystal form of *Wolinella succinogenes* quinol:fumarate reductase reveals domain closure at the site of fumarate reduction. *Eur J Biochem*, **268**:1820-7
- Lancaster, C.R.D., Kröger, A., Auer, M. and Michel, H. (1999)** Structure of fumarate reductase from *Wolinella succinogenes* at 2.2 Å resolution. *Nature*, **402**:377-85
- Lancaster, C.R.D., Gross, R., Haas, A.H., Ritter, M., Mäntele, W., Simon, J. and Kröger, A. (2000)** Essential role of Glu-C66 for menaquinol oxidation indicates transmembrane electrochemical potential generation by *Wolinella succinogenes* fumarate reductase. *Proc Natl Acad Sci U S A*, **97**:13051-6
- Lancaster, C.R.D., Sauer, U.S., Groß, R., Haas, A.H., Graf, J., Schwalbe, H., Mäntele, W., Simon, J. and Madej, G. (2005)** *Manuscript submitted*,
- Lange, C., Nett, J.H., Trumpower, B.L. and Hunte, C. (2001)** Specific roles of protein-phospholipid interactions in the yeast cytochrome bc<sub>1</sub> complex structure. *Embo J*, **20**:6591-600
- Lauterbach, F., Kortner, C., Tripier, D. and Unden, G. (1987)** Cloning and expression of the genes of two fumarate reductase subunits from *Wolinella succinogenes*. *Eur J Biochem*, **166**:447-52
- Lauterbach, F., Kortner, C., Albracht, S.P., Unden, G. and Kröger, A. (1990)** The fumarate reductase operon of *Wolinella succinogenes*. Sequence and expression of the *frdA* and *frdB* genes. *Arch Microbiol*, **154**:386-93
- Lecuit, M., Abachin, E., Martin, A., Poyart, C., Pochart, P., Suarez, F., Bengoufa, D., Feuillard, J., Lavergne, A., Gordon, J.I., Berche, P., Guillevin, L. and Lortholary, O. (2004)** Immunoproliferative small intestinal disease associated with *Campylobacter jejuni*. *N Engl J Med*, **350**:239-48
- Lee, A.G. (2004)** How lipids affect the activities of integral membrane proteins. *Biochim Biophys Acta*, **1666**:62-87
- Leger, C., Heffron, K., Pershad, H.R., Maklashina, E., Luna-Chavez, C., Cecchini, G., Ackrell, B.A. and Armstrong, F.A. (2001)** Enzyme electrokinetics: energetics of succinate oxidation by fumarate reductase and succinate dehydrogenase. *Biochemistry*, **40**:11234-45
- Lemma, E., Unden, G. and Kröger, A. (1990)** Menaquinone is an obligatory component of the chain catalyzing succinate respiration in *Bacillus subtilis*. *Arch Microbiol*, **155**:62-7
- Ljungdahl, L.G. and Wood, H.G. (1969)** Total synthesis of acetate from CO<sub>2</sub> by heterotrophic bacteria. *Annual Review of Microbiology*, **23**:515-38
- Lodish, H., Berk, A., Zipursky, S.L., Baltimore, D. and Darnell, J. (1999)** *Molecular Cell Biology*. W.H. Freeman & Company
- Lorenzen, J.P., Kröger, A. and Unden, G. (1993)** Regulation of anaerobic respiratory pathways in *Wolinella succinogenes* by the presence of electron acceptors. *Archives of Microbiology*, **159**:477-83
- Lubben, M. and Morand, K. (1994)** Novel prenylated hemes as cofactors of cytochrome oxidases. Archaea have modified hemes A and O. *J Biol Chem*, **269**:21473-9
- Luna-Chavez, C., Iverson, T.M., Rees, D.C. and Cecchini, G. (2000)** Overexpression, purification, and crystallization of the membrane-bound fumarate reductase from *Escherichia coli*. *Protein Expr Purif*, **19**:188-96
- Maguire, J.J., Johnson, M.K., Morningstar, J.E., Ackrell, B.A. and Kearney, E.B. (1985)** Electron paramagnetic resonance studies of mammalian succinate dehydrogenase. Detection of the tetranuclear cluster S<sub>2</sub>. *J Biol Chem*, **260**:10909-12
- Maklashina, E. and Cecchini, G. (1999)** Comparison of catalytic activity and inhibitors of quinone reactions of succinate dehydrogenase (Succinate-ubiquinone oxidoreductase) and fumarate reductase (Menaquinol-fumarate oxidoreductase) from *Escherichia coli*. *Arch Biochem Biophys*, **369**:223-32



- Marais, A., Mendz, G.L., Hazell, S.L. and Megraud, F. (1999a)** Metabolism and genetics of *Helicobacter pylori*: the genome era. *Microbiology and Molecular Biology Reviews*, **63**:642-74
- Marais, A., Monteiro, L., Occhialini, A., Pina, M., Lamouliatte, H. and Megraud, F. (1999b)** Direct detection of *Helicobacter pylori* resistance to macrolides by a polymerase chain reaction/DNA enzyme immunoassay in gastric biopsy specimens. *Gut*, **44**:463-7
- Marounek, M., Bartos, S. and Kalachnyuk, G.I. (1982)** Dynamics of the redox potential and rh of the rumen fluid of goats. *Physiol Bohemoslov*, **31**:369-74
- Matin, A., Zychlinsky, E., Keyhan, M. and Sachs, G. (1996)** Capacity of *Helicobacter pylori* to generate ionic gradients at low pH is similar to that of bacteria which grow under strongly acidic conditions. *Infect Immun*, **64**:1434-6
- Matsson, M., Tolstoy, D., Aasa, R. and Hederstedt, L. (2000)** The distal heme center in *Bacillus subtilis* succinate:quinone reductase is crucial for electron transfer to menaquinone. *Biochemistry*, **39**:8617-24
- Mead, P.S., Slutsker, L., Dietz, V., Mccaig, L.F., Bresee, J.S., Shapiro, C., Griffin, P.M. and Tauxe, R.V. (1999)** Food-related illness and death in the United States. *Emerg Infect Dis*, **5**:607-25
- Mell, H., Wellnitz, C. and Kröger, A. (1986)** The electrochemical proton potential and the proton/electron ratio of the electron transport with fumarate in *Wolinella succinogenes*. *Biochim. Biophys. Acta*, **852**:212-21
- Mendz, G.L. and Hazell, S.L. (1993)** Fumarate catabolism in *Helicobacter pylori*. *Biochem Mol Biol Int*, **31**:325-32
- Mendz, G.L., Hazell, S.L. and Srinivasan, S. (1995)** Fumarate reductase: a target for therapeutic intervention against *Helicobacter pylori*. *Arch Biochem Biophys*, **321**:153-9
- Michal, G. (1999)** Tetrapyrroles. In: *Biochemical Pathways: An Atlas of Biochemistry and Molecular Biology* (Michal, G., Eds.) John Wiley & Sons, Inc., New York, USA, pp. 68-74
- Mileni, M., Haas, A.H., Mäntele, W., Simon, J. and Lancaster, C.R.D. (2005a)** Probing heme propionate involvement in transmembrane proton transfer coupled to electron transfer in dihemic quinol:fumarate reductase by <sup>13</sup>C-labeling and FTIR difference spectroscopy. *Manuscript submitted*,
- Mileni, M., Macmillan, F., Tziatzios, C., Zwicker, K., Haas, A.H., Mäntele, W., Simon, J. and Lancaster, C.R.D. (2005b)** Heterologous production in *Wolinella succinogenes* and characterization of the quinol:fumarate reductases from *Helicobacter pylori* and *Campylobacter jejuni*. *Manuscript submitted*,
- Mitchell, P. (1979)** Keilin's respiratory chain concept and its chemiosmotic consequences. *Science*, **206**:1148-59
- Moeller, J.V. and Le Maire, M. (1993)** Detergent binding as a measure of hydrophobic surface area of integral membrane proteins. *Journal of Biological Chemistry*, **268**:18659-72
- Olbe, L., Carlsson, E. and Lindberg, P. (2003)** A proton-pump inhibitor expedition: the case histories of omeprazole and esomeprazole. *Nat Rev Drug Discov*, **2**:132-9
- Otwinowski, Z. and Minor, W. (1997)** Processing of X-ray Diffraction Data Collected in Oscillation Mode. *Methods in Enzymology*, **276**:307-26
- Page, C.C., Moser, C.C., Chen, X. and Dutton, P.L. (1999)** Natural engineering principles of electron tunnelling in biological oxidation-reduction. *Nature*, **402**:47-52
- Palsdottir, H. and Hunte, C. (2004)** Lipids in membrane protein structures. *Biochim Biophys Acta*, **1666**:2-18
- Parkhill, J., Wren, B.W., Mungall, K., Ketley, J.M., Churcher, C., Basham, D., Chillingworth, T., Davies, R.M., Feltwell, T., Holroyd, S., Jagels, K., Karlyshev, A.V., Moule, S., Pallen, M.J., Penn, C.W., Quail, M.A., Rajandream, M.A., Rutherford, K.M., Van Vliet, A.H., Whitehead, S. and Barrell, B.G. (2000)** The genome sequence of the food-borne pathogen *Campylobacter jejuni* reveals hypervariable sequences. *Nature*, **403**:665-8

- Parsonnet, J., Hansen, S., Rodriguez, L., Gelb, A.B., Warnke, R.A., Jellum, E., Orentreich, N., Vogelman, J.H. and Friedman, G.D. (1994) *Helicobacter pylori* infection and gastric lymphoma. *N Engl J Med*, **330**:1267-71
- Patton, G.M. and Robins, S.J. (1998) Separation and quantitation of phospholipid classes by HPLC. *Methods Mol Biol*, **110**:193-215
- Peek, R.M., Jr. and Blaser, M.J. (2002) *Helicobacter pylori* and gastrointestinal tract adenocarcinomas. *Nat Rev Cancer*, **2**:28-37
- Pitson, S.M., Mendz, G.L., Srinivasan, S. and Hazell, S.L. (1999) The tricarboxylic acid cycle of *Helicobacter pylori*. *Eur J Biochem*, **260**:258-67
- Richter, O.M. and Ludwig, B. (2003) Cytochrome *c* oxidase--structure, function, and physiology of a redox-driven molecular machine. *Rev Physiol Biochem Pharmacol*, **147**:47-74
- Salerno, J.C. (1991) Electron transfer in succinate:ubiquinone reductase and quinol:fumarate reductase. *Biochem Soc Trans*, **19**:599-605
- Sambrook, J., Fritsch, F.E. and Maniatis, T. (1989) *Molecular Cloning: A Laboratory Manual*, 2nd ed. Cold Spring Harbor, NY
- Sanger, F., Nicklen, S. and Coulson, A.R. (1977) DNA sequencing with chain-terminating inhibitors. *Proc Natl Acad Sci U S A*, **74**:5463-7
- Sato-Watanabe, M., Itoh, S., Mogi, T., Matsuura, K., Miyoshi, H. and Anraku, Y. (1995) Stabilization of a semiquinone radical at the high-affinity quinone-binding site (Q<sub>H</sub>) of the *Escherichia coli* bo-type ubiquinol oxidase. *FEBS Lett*, **374**:265-9
- Schägger, H. and Pfeiffer, K. (2000) Supercomplexes in the respiratory chains of yeast and mammalian mitochondria. *Embo J*, **19**:1777-83
- Schnorpfel, M., Janausch, I.G., Biel, S., Kröger, A. and Unden, G. (2001) Generation of a proton potential by succinate dehydrogenase of *Bacillus subtilis* functioning as a fumarate reductase. *Eur J Biochem*, **268**:3069-74
- Schuck, P. (1998) Sedimentation analysis of noninteracting and self-associating solutes using numerical solutions to the Lamm equation. *Biophysical Journal*, **75**:1-10
- Schuck, P. (2000) Size-distribution analysis of macromolecules by sedimentation velocity ultracentrifugation and Lamm equation modeling. *Biophysical Journal*, **78**:1606-19
- Simon, J., Gross, R., Klimmek, O. and Kröger, A. (2000a) The Genus *Wolinella*. The Prokaryotes: An Evolving Electronic Resource for the Microbiological Community, 3rd edition (Dworkin, M. *et al.* eds.) New York, Springer-Verlag
- Simon, J., Gross, R., Ringel, M., Schmidt, E. and Kröger, A. (1998) Deletion and site-directed mutagenesis of the *Wolinella succinogenes* fumarate reductase operon. *European Journal of Biochemistry*, **251**:418-26
- Simon, J., Gross, R., Einsle, O., Kroneck, P.M., Kröger, A. and Klimmek, O. (2000b) A NapC/NirT-type cytochrome *c* (NrfH) is the mediator between the quinone pool and the cytochrome *c* nitrite reductase of *Wolinella succinogenes*. *Mol Microbiol*, **35**:686-96
- Smith, M.A., Mendz, G.L., Jorgensen, M.A. and Hazell, S.L. (1999) Fumarate metabolism and the microaerophily of *Campylobacter* species. *The International Journal of Biochemistry & Cell Biology*, **31**:961-75
- Smith, P.K., Krohn, R.I., Hermanson, G.T., Mallia, A.K., Gartner, F.H., Provenzano, M.D., Fujimoto, E.K., Goeke, N.M., Olson, B.J. and Klenk, D.C. (1985) Measurement of protein using bicinchoninic acid. *Anal Biochem*, **150**:76-85
- Solnick, J.V., O'Rourke, J.L., Vandamme, P. and Lee, A. (2003) The Genus *Helicobacter*. The Prokaryotes: An Evolving Electronic Resource for the Microbiological Community, 3rd edition (Dworkin, M. *et al.* eds.) New York, Springer-Verlag

- Southern, E.M. (1975)** Detection of specific sequences among DNA fragments separated by gel electrophoresis. *Journal of Molecular Biology*, **98**:503-17
- Thauer, R.K. and Morris, J.G. (1984)** Metabolism of chemotrophic anaerobes: old views and new aspects. In: *The microbe 1984, part II. Prokaryotes and eukaryotes.* (Kelly, D. P. et al., Eds.) Cambridge University Press, Cambridge, pp. 123-68
- Thauer, R.K., Jungermann, K. and Decker, K. (1977)** Energy conservation in chemotrophic anaerobic bacteria. *Bacteriol Rev*, **41**:100-80
- Tomb, J.F., White, O., Kerlavage, A.R., Clayton, R.A., Sutton, G.G., Fleischmann, R.D., Ketchum, K.A., Klenk, H.P., Gill, S., Dougherty, B.A., Nelson, K., Quackenbush, J., Zhou, L., Kirkness, E.F., Peterson, S., Loftus, B., Richardson, D., Dodson, R., Khalak, H.G., Glodek, A., Mckenney, K., Fitzgerald, L.M., Lee, N., Adams, M.D., Venter, J.C. and Et Al. (1997)** The complete genome sequence of the gastric pathogen *Helicobacter pylori*. *Nature*, **388**:539-47
- Turner, K.L., Doherty, M.K., Heering, H.A., Armstrong, F.A., Reid, G.A. and Chapman, S.K. (1999)** Redox properties of flavocytochrome  $c_3$  from *Shewanella frigidimarina* NCIMB400. *Biochemistry*, **38**:3302-9
- Tziatzios, C., Schubert, D., Schuck, P., Lancaster, C.R.D., Gennis, R.B. and Barquera, B. (2003)** The state of association of the  $\text{Na}^+$  - translocating NADH : quinone oxidoreductase in detergent solution. An ultracentrifugation study. *Prog Colloid Polym Sci*, *in press*:
- Uemura, N., Okamoto, S., Yamamoto, S., Matsumura, N., Yamaguchi, S., Yamakido, M., Taniyama, K., Sasaki, N. and Schlemper, R.J. (2001)** *Helicobacter pylori* infection and the development of gastric cancer. *N Engl J Med*, **345**:784-9
- Unden, G. (1988)** Differential roles for menaquinone and demethylmenaquinone in anaerobic electron transport of *E. coli* and their *fnr*-independent expression. *Arch Microbiol*, **150**:499-503
- Unden, G. and Kröger, A. (1982)** Reconstitution in liposomes of the electron-transport chain catalyzing fumarate reduction by formate. *Biochim. Biophys. Acta*, **682**:258-63
- Unden, G. and Kröger, A. (1986)** Reconstitution of a functional electron-transfer chain from purified formate dehydrogenase and fumarate reductase complexes. *Methods Enzymol*, **126**:387-99
- Unden, G., Hackenberg, H. and Kröger, A. (1980)** Isolation and functional aspects of the fumarate reductase involved in the phosphorylative electron transport of *Vibrio succinogenes*. *Biochim Biophys Acta*, **591**:275-88
- Unden, G., Albracht, S.P.J. and Kröger, A. (1984)** Redox potentials and kinetic properties of fumarate reductase complex from *Vibrio succinogenes*. *Biochimica et Biophysica Acta*, **767**:460-69
- Unden, G., Morschel, E., Bokranz, M. and Kröger, A. (1983)** Structural properties of the proteoliposomes catalyzing electron transport from formate to fumarate. *Biochim Biophys Acta*, **725**:41-8
- Vanaken, T., Foxall-Vanaken, S., Castleman, S. and Ferguson-Miller, S. (1986)** Alkyl glycoside detergents: synthesis and applications to the study of membrane proteins. *Methods Enzymol*, **125**:27-35
- Venyaminov, S.Y. and Kalnin, N.N. (1990)** Quantitative IR spectrophotometry of peptide compounds in water ( $\text{H}_2\text{O}$ ) solutions. I. Spectral parameters of amino acid residue absorption bands. *Biopolymers*, **30**:1243-57
- Waghorn, G.C. (1991)** Electronegativity and redox potential of rumen digesta in-situ In cows eating fresh lucerne. *New Zealand Journal of Agricultural Research*, **34**:359-62
- Wagner, G.C., Kassner, R.J. and Kamen, M.D. (1974)** Redox potentials of certain vitamins K: implications for a role in sulfite reduction by obligately anaerobic bacteria. *Proc Natl Acad Sci U S A*, **71**:253-6
- Warren, M.J. and Scott, A.I. (1990)** Tetrapyrrole assembly and modification into the ligands of biologically functional cofactors. *Trends Biochem Sci*, **15**:486-91

- Wassenaar, T.M. and Newell, D.G. (2001)** The Genus *Campylobacter*. The Prokaryotes: An Evolving Electronic Resource for the Microbiological Community, 3rd edition (Dworkin, M. *et al.* eds.) New York, Springer-Verlag
- Westenberg, D.J., Gunsalus, R.P., Ackrell, B.A. and Cecchini, G. (1990)** Electron transfer from menaquinol to fumarate. Fumarate reductase anchor polypeptide mutants of *Escherichia coli*. *J Biol Chem*, **265**:19560-7
- Wotherspoon, A.C., Doglioni, C., Diss, T.C., Pan, L., Moschini, A., De Boni, M. and Isaacson, P.G. (1993)** Regression of primary low-grade B-cell gastric lymphoma of mucosa-associated lymphoid tissue type after eradication of *Helicobacter pylori*. *Lancet*, **342**:575-7
- Xia, D., Yu, C.A., Kim, H., Xia, J.Z., Kachurin, A.M., Zhang, L., Yu, L. and Deisenhofer, J. (1997)** Crystal structure of the cytochrome *bc*<sub>1</sub> complex from bovine heart mitochondria. *Science*, **277**:60-6
- Yankovskaya, V., Horsefield, R., Tornroth, S., Luna-Chavez, C., Miyoshi, H., Leger, C., Byrne, B., Cecchini, G. and Iwata, S. (2003)** Architecture of succinate dehydrogenase and reactive oxygen species generation. *Science*, **299**:700-4
- Zhang, H., Kurisu, G., Smith, J.L. and Cramer, W.A. (2003)** A defined protein-detergent-lipid complex for crystallization of integral membrane proteins: The cytochrome *b<sub>f</sub>* complex of oxygenic photosynthesis. *Proc Natl Acad Sci U S A*, **100**:5160-3
- Zhang, Z., Huang, L., Shulmeister, V.M., Chi, Y.I., Kim, K.K., Hung, L.W., Crofts, A.R., Berry, E.A. and Kim, S.H. (1998)** Electron transfer by domain movement in cytochrome *bc*<sub>1</sub>. *Nature*, **392**:677-84

# Appendixes

## Appendix A

Nucleotidic alignment of the *C. jejuni frdCAB* operons from the NCTC11168 strain and the clinically isolated (C.I.) strain.

Cj NCTC11168	1	atgcgtgagcttatcgaaggttatttgggtaagagcattgagggcaaaaa
Cj C.I.	1	atgcgtgagcttatcgaaggttatttgggtaagagcattgagggcaaaaa
Cj NCTC11168	51	aagtaaaatgcctgcgaaattagactttatccaaagtgcctcagggcttt
Cj C.I.	51	aagtaaaatgcctgcgaaattagactttatccaaagtgcctcagggcttt
Cj NCTC11168	101	ttttaggtccttttatgtgggtgcatatgctttttgtttctacaatttta
Cj C.I.	101	ttttaggtccttttatgtgggtgcatatgctttttgtttctacaatttta
Cj NCTC11168	151	gtcagtgaggatTTTTTtaattctgtagtgcattttttagaattaaatt
Cj C.I.	151	gtcagtgaggatTTTTTtaattctgtggtacattttttagaattaaatt
Cj NCTC11168	201	tgtttacgataatcctggtatgagttatcttacttcatttttagccgcct
Cj C.I.	201	tgtttacgataatcctggtatgagttatcttacttcatttttagccgcct
Cj NCTC11168	251	gtgttttagtggttttttctgtcatgctttacttgcaatgagaaaaatt
Cj C.I.	251	gtgttttagtggttttttctgtcatgctttacttgcaatgagaaaaatt
Cj NCTC11168	301	cctattaattaccgtcagtatcaaatactaagaacacacagtaaaaaat
Cj C.I.	301	cctattaattaccgtcagtatcaaatactaagaacacacagtaaaaaat
Cj NCTC11168	351	gaatcacagcgatacttcggttatgggtgggtcaagcttttacaggtttta
Cj C.I.	351	gaatcacagcgatacttcggttatgggtgggtcaagcttttacaggtttta
Cj NCTC11168	401	ttatgttttcttaggttctgctcatcttatttttattgtaaccaatgca
Cj C.I.	401	ttatgttttcttaggttctgctcatcttatttttattgtaaccaatgca
Cj NCTC11168	451	gataaaatcagcggcgatgatgtcaggagatagggttgtaagtcattttat
Cj C.I.	451	gataaaatcagcggcgatgatgtcaggagatagggttgtaagtcattttat
Cj NCTC11168	501	gtggcttttttatgctgttcttttagtctgtgttgaacttcaggaagta
Cj C.I.	501	gtggcttttttatgctgttcttttagtctgtgttgaacttcaggaagta
Cj NCTC11168	551	tagggctttatagactttgtgttaaattggggttggtttgaggaaaaat
Cj C.I.	551	tagggctttatagactttgtgttaaattggggttggtttgaggaaaaat
Cj NCTC11168	601	gtaaaagaaagtcgcaaaaagcttaaaactgctaaatggataatcagtat
Cj C.I.	601	gtaaaagaaagtcgcaaaaagcttaaaactgctaaatggataatcagtat
Cj NCTC11168	651	tttcttcctagttttaggtgtgttaagtcttgagcattttataaaaaatag
Cj C.I.	651	tttcttcctagttttaggtgtgttaagtcttgagcattttataaaaaatag
Cj NCTC11168	701	gttatgaaaactaccaaaatcaaaccctactgcatgataaaaaaac
Cj C.I.	701	gttatgaaaactaccaaaatcaaaccctactgcatgataaaaaaac
Cj NCTC11168	751	tacaatggagcaaattatgaatatacaatatagtgatgctttagtaaatag
Cj C.I.	751	tacaatggagcaaattatgaatatacaatatagtgatgctttagtaaatag

Cj NCTC11168	801	gcgaggattagcaggtcttagagcggctattgaagtagcaaagagtggc
Cj C.I.	801	gcgaggattagcaggtcttagagcggctattgaagtagcaaagagtggc
Cj NCTC11168	851	caaagtgtaacacttttaagtatttgtccagtgaagcgttctcactctgc
Cj C.I.	851	caaagtgtaacacttttaagtatttgtccagtgaagcgttctcactctgc
Cj NCTC11168	901	agcggtgcaaggaggtatgcaggcaagtttagcaaatggggc <sup>a</sup> aaaggtg
Cj C.I.	901	agcggtgcaaggaggtatgcaggcaagtttagcaaatggggc <sup>a</sup> aaaggtg
Cj NCTC11168	951	agggtgataatgaagatcttcactt <sup>t</sup> gcagatacagtaaaaggaagtgat
Cj C.I.	951	agggtgataatgaagatcttcactt <sup>t</sup> gcagatacagtaaaaggaagtgat
Cj NCTC11168	1001	tggggctgtgatcaagaagtagcaagaatg <sup>t</sup> ttgctcaaactgc <sup>c</sup> ccaaa
Cj C.I.	1001	tggggctgtgatcaagaagtagcaagaatg <sup>t</sup> ttgctcaaactgc <sup>c</sup> ccaaa
Cj NCTC11168	1051	agcagtgcgtag <sup>a</sup> cttgcggcttgggggtg <sup>c</sup> cttggactag <sup>a</sup> gttacta
Cj C.I.	1051	agcagtgcgtag <sup>a</sup> cttgcggcttgggggtg <sup>c</sup> cttggactag <sup>a</sup> gttacta
Cj NCTC11168	1101	aaggtccaagaactgtt <sup>t</sup> gtaatcaatgc <sup>a</sup> caaaaaactgtgattgaagaa
Cj C.I.	1101	aaggtccaagaactgtt <sup>t</sup> gtaatcaatgc <sup>a</sup> caaaaaactgtgattgaagaa
Cj NCTC11168	1151	aaagaagaagcgcac <sup>g</sup> ggg <sup>c</sup> ttatt <sup>a</sup> atgct <sup>a</sup> gagattttgg <sup>t</sup> ggaact <sup>a</sup> aa
Cj C.I.	1151	aaagaagaagcgcac <sup>g</sup> ggg <sup>c</sup> ttatt <sup>a</sup> atgct <sup>a</sup> gagattttgg <sup>t</sup> ggaac <sup>a</sup> aa
Cj NCTC11168	1201	aaaatggagaacttg <sup>t</sup> tatat <sup>c</sup> gcagatgcaacagg <sup>g</sup> cattgtatgcttt
Cj C.I.	1201	aaaatggagaacttg <sup>t</sup> tatat <sup>c</sup> gcagatgcaacagg <sup>g</sup> cattgtatgcttt
Cj NCTC11168	1251	atgggtgtagcaaatgaagc <sup>t</sup> attaaacatcaagtaaaaaatt <sup>t</sup> attgataga
Cj C.I.	1251	atgggtgtagcaaatgaagc <sup>t</sup> attaaacatcaagtaaaaaatt <sup>t</sup> attgataga
Cj NCTC11168	1301	atggaagcagtaagaattatcca <sup>t</sup> gatggtaaaaaatg <sup>c</sup> tttaggtgtgat
Cj C.I.	1301	atggaagcagtaagaattatcca <sup>t</sup> gatggtaaaaaatg <sup>c</sup> tttaggtgtgat
Cj NCTC11168	1351	<sup>c</sup> gctagagatttaact <sup>a</sup> aatggacaact <sup>c</sup> att <sup>t</sup> gcttatattgca <sup>a</sup> agaggaa
Cj C.I.	1351	<sup>c</sup> gctagagatttaact <sup>a</sup> aatggacaact <sup>c</sup> att <sup>t</sup> gcttatattgca <sup>a</sup> agaggaa
Cj NCTC11168	1401	ccatgatagcaacaggggg <sup>c</sup> tatggtagaatttataaacaactacaat
Cj C.I.	1401	ccatgatagcaacaggggg <sup>c</sup> tatggtagaatttataaacaactacaat
Cj NCTC11168	1451	g <sup>c</sup> ggtaattt <sup>t</sup> gtgaaggaacaggtgc <sup>a</sup> gc <sup>a</sup> atcgctcttgaaac <sup>a</sup> ggg <sup>c</sup> ct
Cj C.I.	1451	g <sup>c</sup> agtaattt <sup>t</sup> gtgaaggaacaggtgc <sup>a</sup> gg <sup>c</sup> tatcgctcttgaaac <sup>a</sup> ggg <sup>a</sup> ct
Cj NCTC11168	1501	ttgcagactttcaaat <sup>a</sup> tatggaagcagtgcaatttca <sup>t</sup> ccaactcctattg
Cj C.I.	1501	ttgcagactttcaaa <sup>c</sup> atggaagcagtgcaatttca <sup>c</sup> ccaactcctattg
Cj NCTC11168	1551	tgccaagcggat <sup>t</sup> ttt <sup>t</sup> gcttact <sup>g</sup> aggg <sup>c</sup> tgtcg <sup>t</sup> gg <sup>t</sup> gatgg <sup>t</sup> ggaatt
Cj C.I.	1551	tgccaagcggat <sup>t</sup> ttt <sup>t</sup> gcttacc <sup>g</sup> aagg <sup>t</sup> tgtcg <sup>t</sup> gg <sup>t</sup> gatgg <sup>c</sup> ggaatt
Cj NCTC11168	1601	tt <sup>a</sup> cg <sup>c</sup> gatgtggatggat <sup>a</sup> t <sup>c</sup> gtttt <sup>t</sup> atgcctgattatgaaccagagaa
Cj C.I.	1601	tt <sup>a</sup> cg <sup>t</sup> gatgtggatggat <sup>a</sup> t <sup>c</sup> gtttt <sup>t</sup> atgcctgattatgaaccagagaa
Cj NCTC11168	1651	aaaagaacttgcaagccgtgatgtg <sup>t</sup> gtaagtcgtagaatgatgga <sup>a</sup> cata
Cj C.I.	1651	aaaagaacttgcaagccgtgatgtg <sup>t</sup> gtaagtcgtagaatgatgga <sup>a</sup> cata
Cj NCTC11168	1701	ttcgtaaagg <sup>a</sup> aa <sup>a</sup> gg <sup>t</sup> gtaaaaag <sup>c</sup> ccttatgg <sup>g</sup> gatcatttatggc <sup>t</sup> t
Cj C.I.	1701	ttcgtaaagg <sup>t</sup> aa <sup>a</sup> gg <sup>t</sup> gtaaaaag <sup>c</sup> ccttatgg <sup>a</sup> gatcatttatggc <sup>t</sup> t
Cj NCTC11168	1751	gatatttctatact <sup>t</sup> gg <sup>a</sup> agag <sup>c</sup> tcatgtggaaaaaaatct <sup>c</sup> cg <sup>c</sup> gatgt
Cj C.I.	1751	gatatttctatact <sup>a</sup> gg <sup>t</sup> cg <sup>t</sup> gc <sup>c</sup> atgtggaaaaaaatct <sup>t</sup> cg <sup>t</sup> gatgt

Cj NCTC11168	1801	a	caagatattt	g	taaaactttt	a	atggtatt	g	atcc	a	gcagatga	g	ggtc	
Cj C.I.	1801	g	caagatattt	g	taaaactttt	a	atggtatt	g	atcc	g	gcagatga	a	ggtc	
Cj NCTC11168	1851	c	aaaaggtt	g	ggcgccag	t	tcttcca	a	tgca	g	cattatt	t	ctatgggtgga	
Cj C.I.	1851	c	aaaaggtt	g	ggcgccag	t	tcttcca	a	tgca	a	cattatt	t	ctatgggtgga	
Cj NCTC11168	1901	a	ttagaact	a	aaccaac	g	gggtgaa	a	gtcaat	g	ggttaa	a	cggactttttgc	
Cj C.I.	1901	a	ttagaact	a	aaccaac	a	gggtgaa	a	gtcaat	g	ggttaa	a	cggactttttgc	
Cj NCTC11168	1951	t	tgtggaga	a	gcagctt	g	ctgctgg	g	gatatg	c	a	ggattt	a	atcgtttaggtg
Cj C.I.	1951	t	tgtggaga	a	gcagctt	g	ctgctgg	g	gatatg	c	a	ggattt	a	atcgtttaggtg
Cj NCTC11168	2001	g	gaattc	a	tgtgctg	a	aaactgt	t	gtagc	a	ggat	a	tatgatagtg	
Cj C.I.	2001	g	gaattc	a	tgtgctg	a	aaactgt	t	gtagc	a	ggat	a	tatgatagtg	
Cj NCTC11168	2051	t	ttgcag	a	tattt	g	t	taaaata	a	a	atggtg	a	agtaattgacacaaatgtagt	
Cj C.I.	2051	t	ttgcag	a	tattt	g	t	taaaata	a	a	atggtg	a	agtaattgacacaaatgtagt	
Cj NCTC11168	2101	a	aaagact	t	cttaact	a	aagagt	a	tcaat	a	t	t	taaaatc	
Cj C.I.	2101	a	aaagact	t	cttaact	a	aagagt	a	tcaat	a	t	t	taaaatc	
Cj NCTC11168	2151	a	agaaggt	a	aaacata	a	atg	t	t	t	t	t	t	
Cj C.I.	2151	a	agaaggt	a	aaacata	a	atg	t	t	t	t	t	t	
Cj NCTC11168	2201	a	tgtggg	a	taaggt	g	ccatct	t	t	t	t	a	acaggtga	
Cj C.I.	2201	a	tgtggg	a	taaggt	g	ccatct	t	t	t	t	a	acaggtga	
Cj NCTC11168	2251	a	gtagat	g	aactt	g	aaaaact	t	t	t	a	aagatt	c	
Cj C.I.	2251	a	gtagat	g	aactt	g	aaaaact	t	t	t	a	aagatt	c	
Cj NCTC11168	2301	a	ttgtaa	a	gaactt	g	attgtg	c	aaatc	c	a	gagctt	g	
Cj C.I.	2301	a	ttgtaa	a	gaactt	g	attgtg	c	aaatc	c	a	gagctt	g	
Cj NCTC11168	2351	g	tgcca	a	gaatg	t	taaaaa	a	tagc	a	ctt	t	g	
Cj C.I.	2351	g	tgcca	a	gaatg	t	taaaaa	a	tagc	a	ctt	t	g	
Cj NCTC11168	2401	a	agaac	a	gaaagt	c	gtgggg	c	gcatt	a	t	a	gggaagattat	
Cj C.I.	2401	a	agaac	a	gaaagt	c	gtgggg	c	gcatt	a	t	a	gggaagattat	
Cj NCTC11168	2451	a	tgattt	a	aattg	g	atgaa	a	gaac	a	a	a	actttt	
Cj C.I.	2451	a	tgattt	a	aattg	g	atgaa	a	gaac	a	a	a	actttt	
Cj NCTC11168	2501	a	ctta	a	ccacg	a	cataga	a	at	a	c	gaagag	c	
Cj C.I.	2501	a	cttt	g	ccacg	a	cataga	a	at	a	c	gaagag	c	
Cj NCTC11168	2551	t	ccacc	a	gattc	c	ggtg	a	tac	g	ggtg	c	taag	
Cj C.I.	2551	t	ccacc	a	gattc	c	ggtg	a	tac	g	ggtg	c	taag	
Cj NCTC11168	2601	c	ttta	a	agt	g	aaaa	a	c	g	cca	a	gctga	
Cj C.I.	2601	c	ttta	a	agt	g	aaaa	a	c	g	cca	a	gctga	
Cj NCTC11168	2651	g	aagct	g	aagg	c	aaagg	t	cg	t	t	a	gaaatt	
Cj C.I.	2651	g	aagct	g	aagg	c	aaagg	t	cg	t	t	a	gaaatt	
Cj NCTC11168	2701	t	gaatt	g	caag	c	t	aaat	a	a	a	a	g	
Cj C.I.	2701	t	gaatt	g	caag	c	t	aaat	a	a	a	a	g	
Cj NCTC11168	2751	a	tgagt	a	g	aaaa	a	t	g	a	c	a	a	
Cj C.I.	2751	a	tgagt	a	g	aaaa	a	t	g	a	c	a	a	

Cj NCTC11168	2801	aatttctaaccacatTTTgtgacttatgagcttgaagaaactcctTTta
Cj C.I.	2801	aatttctaaccacatTTTgtgacttatgagcttgaagaaactcctTTta
Cj NCTC11168	2851	tgacggTTTTgtatgTTTgactTTTgatccgtgaaaaaatggatgcagat
Cj C.I.	2851	tgacggTTTTgtatgTTTgactTTTgatccgtgaaaaaatggatgcgat
Cj NCTC11168	2901	ctgagTTTTgactTTTgTTTgtcgtgcagggattTgcggatcTTgtgcaat
Cj C.I.	2901	ctgagTTTTgactTTTgTTTgtcgtgcagggattTgcggatcTTgtgcaat
Cj NCTC11168	2951	gatgattaatggagtgccaaaactTgctTgTaaaactTTTgactaaagatt
Cj C.I.	2951	gatgattaatggagtgccaaaactTgctTgTaaaactTTTgactaaagatt
Cj NCTC11168	3001	atcctgatggagtgatagagcttatgcctatgcctgcatttaggcatatt
Cj C.I.	3001	atcttgatggagtgatagagcttatgcctatgcctgcatttagacatatt
Cj NCTC11168	3051	aaagatttaagcgtgaatacagggcagtggtTgaagacatgtgtaagcg
Cj C.I.	3051	aaagatttaagcgtgaatacagggcagtggtTgaagacacgtgtaaacg
Cj NCTC11168	3101	tgttgaaagctgggtgcataatgaaaaagaaactgatatttctaactTg
Cj C.I.	3101	tgttgaaagctgggtgcataatgaaaaagaaactgatatttctaactTg
Cj NCTC11168	3151	aagaacgcattgagccagaagTtgcgatgaaactTTTgaacttgatcgt
Cj C.I.	3151	aagaacgtattgagccagaagTtgcgatgaaactTTTgaacttgatcgt
Cj NCTC11168	3201	tgtatagagtTggaattTgtgtagcttctTgtgcaactaaacttatgcg
Cj C.I.	3201	tgtatagagtTggaattTgtgtagcttctTgtgcaactaaacttatgcg
Cj NCTC11168	3251	cccaaatttcatagctgctacagggctTTtaagaacagctagatatttac
Cj C.I.	3251	cccaaatttcatagctgctacagggctTTtaagaacggctagatatttac
Cj NCTC11168	3301	aagatccgcatgaccatagaagTgtggaagattTTTtatgaattagtaggc
Cj C.I.	3301	aagatccgcatgaccatagaagTgtggaagattTTTtatgaattagtaggc
Cj NCTC11168	3351	gatgatgatggTgtTTTTggTTgtatgtcattgctTgctTgtgaagataa
Cj C.I.	3351	gatgatgatggTgtTTTTggTTgtatgtcattgctTgctTgtgaagataa
Cj NCTC11168	3401	ttgccctaagaattacTTTtacaagTaaaatcgcttatatgagaagac
Cj C.I.	3401	ttgccctaagaattacTTTtacaagTaaaatcgcttatatgagaagac
Cj NCTC11168	3451	aactTgtcgctcaaagaaataaataa
Cj C.I.	3451	aactTgtcgctcaaagaaataaataa



## Appendix B

Amino acid alignment of the FrdA, -B, and -C polipeptide chains from different strains of the  $\epsilon$ -proteobacteria species *W. succinogenes*, *C. jejuni*, and *H. pylori*:

*Wolinella succinogenes* DSM1740 (Ws DSM1740)

*Campylobacter jejuni* NCTC11168 (Cj 11168)

*C. jejuni* clinically isolated strain (Cj C.I.)

*C. jejuni* RM1221 (Cj RM1221)

*Helicobacter pylori* 26695 (Hp 26695)

*H. pylori* J99 (Hp J99).

### FrdA

Ws DSM1740	1	mseqftrreflqsacitmgalavstsgvdrafassslpintsgipscdvl
Cj 11168	1	mninqs-----dal
Cj C.I.	1	mninqs-----dal
Cj RM1221	1	mninqs-----dal
Hp 26695	1	mkityc-----dal
Hp J99	1	mkityc-----dal
Ws DSM1740	51	iigsgaaglaavaarkkdpslnvivskvmptrsattmaeggingvidf
Cj 11168	10	viggglaglaaaievaksgqsvtllsicpv--krshsaavqggmqaslan
Cj C.I.	10	viggglaglaaaievaksgqsvtllsicpv--krshsaavqggmqaslan
Cj RM1221	10	viggglaglaaaievaksgqsvtllsicpv--krshsaavqggmqaslan
Hp 26695	10	iiggglaglrasiackqkglntivlslvvp--rrshsaaqggmqaslan
Hp J99	10	iiggglaglrasiackqkglntivlslvvp--rrshsaaqggmqaslan
Ws DSM1740	101	s---egdsfalhaydtvkvgdflvdqdtamkfaehageaihelldyigmpf
Cj 11168	58	gakgegdnedlhfadvtkgsdwgcdqevarmfaqtapkavrelaawgvpw
Cj C.I.	58	gakgegdnedlhfadvtkgsdwgcdqevarmfaqtapkavrelaawgvpw
Cj RM1221	58	gakgegdnedlhfadvtkgsdwgcdqevarmfaqtapkavrelaawgvpw
Hp 26695	58	akkssegdnedlhfladtvkgsdwgcdqvarmfvtapkairelaswgvpw
Hp J99	58	akkssegdnedlhfladtvkgsdwgcdqvarmfvtapkairelaswgvpw
Ws DSM1740	148	sr-----dkngkvdkryaggaskircnfsadktg
Cj 11168	108	trvtkgprtvinvaqktvieekeeahglinardfggtkkwrctciadatg
Cj C.I.	108	trvtkgprtvinvaqktvieekeeahglinardfggtkkwrctciadatg
Cj RM1221	108	trvtkgprtvinvaqktvieekeeahglinardfggtkkwrctciadatg
Hp 26695	108	trikkgdrpavvnghevhtiterddrhgyilsrdfggtkkwrctftadatg
Hp J99	108	trikkgdrpavvnghevhtiterddrhgyilsrdfggtkkwrctftadatg
Ws DSM1740	177	hilthtclddalkngvklmldhqlldigvdngrccegvvlrdirtgtiapv
Cj 11168	158	hcmllygvaneai khqvkiidrmeavriihdgkkclgviardltngqliay
Cj C.I.	158	hcmllygvaneai khqvkiidrmeavriihdgkkclgviardltngqliay
Cj RM1221	158	hcmllygvaneai khqvkiidrmeavriihdgkkclgviardltngqliay
Hp 26695	158	htmlyavanealhhkvdiqdrkdmlafihhdkncygavvrlditgeisay
Hp J99	158	htmlyavanealhhkvdiqdrkdmlafihhdkncygavvrlditgeisay

Ws DSM1740 227 raksvvlatggytrvfwnrststpyiatgdgaasamragva-fkdpemlqf  
Cj 11168 208 iargtmiatggygriy-kqttnavicegtgaaialetglcrlnsmeavqf  
Cj C.I. 208 iargtmiatggygriy-kqttnavicegtgaaialetglcrlnsmeavqf  
Cj RM1221 208 iargtmiatggygriy-kqttnavicegtgaaialetglcrlnsmeavqf  
Hp 26695 208 vskgtllatggygrvy-khttnavicdgagaasaletgvaklgnmeavqf  
Hp J99 208 vskgtllatggygrvy-khttnavicdgagaasaletgvaklgnmeavqf

Ws DSM1740 276 hptgvchggvlliteaargeggillnnqgerfmknya-kkmelaprdivsr  
Cj 11168 257 hptpivpsgilltegcrgdggilrdvdgyrfmpdyepekkelasrdvvsr  
Cj C.I. 257 hptpivpsgilltegcrgdggilrdvdgyrfmpdyepekkelasrdvvsr  
Cj RM1221 257 hptpivpsgilltegcrgdggilrdvdgyrfmpdyepekkelasrdvvsr  
Hp 26695 257 hptalvpsgilmtegcrgdggvldrdfgrfmpayepekkelasrdvvsr  
Hp J99 257 hptalvpsgilmtegcrgdggvldrdfgrfmpayepekkelasrdvvsr

Ws DSM1740 325 sietairegrafgkmeayvlldvthlgkekimrnlpqirhigllfenmd  
Cj 11168 307 rmmehirkkgvkspygdhlwldisilgrahveknlrdrvqdictfngid  
Cj C.I. 307 rmmehirkkgvkspygdhlwldisilgrahveknlrdrvqdictfngid  
Cj RM1221 307 rmmehirkkgvkspygdhlwldisilgrahveknlrdrvqdictfngid  
Hp 26695 307 rilehiqkgygakspygdhvwldiaailgrnhveknlrdrvrdiamtfagid  
Hp J99 307 rilehiqkgygakspygdhvwldiaailgrnhveknlrdrvrdiamtfagid

Ws DSM1740 375 lvekp-----iairptahysmggidvmg  
Cj 11168 357 padegp-----kgwapvlpmqhysmggirtkp  
Cj C.I. 357 padegp-----kgwapvlpmqhysmggirtkp  
Cj RM1221 357 padegp-----kgwapvlpmqhysmggirtkp  
Hp 26695 357 padskeqtkdnmqgvpanepeyggamakkgwipikpmqhysmggvrtnp  
Hp J99 357 padseeqtkdnmqgaptnepeyggamakkgwipikpmqhysmggvrtnp

Ws DSM1740 398 lesmstaipglfaageaacvsihganrlggnslcdtvvtgkiagtnaasf  
Cj 11168 384 -tgesqwlnglfaageaacwdmhgfnrlggnscaetvvagmivgdyfady  
Cj C.I. 384 -tgesqwlnglfaageaacwdmhgfnrlggnscaetvvagmivgayfady  
Cj RM1221 384 -tgesqwlnglfaageaacwdmhgfnrlggnscaetvvagmivgdyfady  
Hp 26695 407 -kgeth-lkglfcaageaacwdlhgfnrlggnsvseavvagmiigdyfash  
Hp J99 407 -kgeth-lkglfcaageaacwdlhgfnrlggnsvsepvvagmiigdyfash

Ws DSM1740 448 assagfgsgthl-hdltlkwmsrfkevankgevnemyaireelgavnwd  
Cj 11168 433 cknngavidtnvkdfltkyqylkslvdkegkhn-vfeiknrmkeimwd  
Cj C.I. 433 cknngavidtnvkdfltkyqylkslvdkegkyn-vfeiknrmkeimwd  
Cj RM1221 433 cknngavidtnvkdfltkyqylkslvdkegkyn-vfeiknrmkeimwd  
Hp 26695 455 cleaqieintkveafikesqdymhflhlnegked-vyeirermkevmd  
Hp J99 455 cleaqieintkveafikesqdymhflhlnegked-vyeirermkevmd

Ws DSM1740 497 nmgvfrtesrlvaledkhnell-----qarydalripntnpvfntaftey  
Cj 11168 482 kvairftgeglkeavdeleklykdsqdvkvhckeldcanpeleey----  
Cj C.I. 482 kvairftgeglkeavdeleklykdsqdvkvhckeldcanpeleey----  
Cj RM1221 482 kvairftgeglkeavdeleklykdsqdvkvhckeldcanpeleey----  
Hp 26695 504 kvgvfregkrleaelkelqelyarsknicvknkvlh-nnpeleday----  
Hp J99 504 kvgvfregkkleaelkelqelyarsknicvknkvlh-nnpeleday----

Ws DSM1740 542 elgnillasraarmgaearkesrgshyredyikrddanflkhsmv-----  
Cj 11168 528 rvprmlkialcvaygallrtesrgahyredypkrddlnwmkrtntfwveg  
Cj C.I. 528 rvprmlkialcvaygallrtesrgahyredypkrddlnwmkrtntfwveg  
Cj RM1221 528 rvprmlkialcvaygallrtesrgahyredypkrddlnwmkrtntfwveg  
Hp 26695 549 rtkkmlklalcitqgallrtesrgahtridyprkrdkwlntlaswpsa  
Hp J99 549 rtkkmlklalcitqgallrtesrgahtridyprkrdkwlntlaswpsa

```

Ws DSM1740 -----
Cj 11168 578 et-lprieyeeldimkmeippafrgygakgniienplsekrqaevdaire
Cj C.I. 578 et-lprieyeeldimkmeippafrgygakgniienplsekrqaevdaire
Cj RM1221 578 et-lprieyeeldimkmeippafrgygakgniienplsekrqaevdaire
Hp 26695 599 eqdmptieyeeldvmkmeispdfrgygkkgnfiphpkkeerdeailktil
Hp J99 599 eqdmptieyeeldvmkmeispdfrgygkkgnfiphpkkeerdeailktil

Ws DSM1740 587 tmdsngklhlgwkdvvv-----tqfkieerky-----
Cj 11168 627 kmeaegkgryeiqnalmpyelqakykapnqri-----
Cj C.I. 627 kmeaegkgryeiqnalmpyelqakykapnqri-----
Cj RM1221 627 kmeaegkgryeiqnalmpyelqakykapnqri-----
Hp 26695 649 eleklgkdrieqvhalmpfelqekykarnmrledeevrargehlysfvnh
Hp J99 649 eleklgkdrieqvhalmpfelqekykarnmrledeevrargehlysfvnh

Ws DSM1740 -----
Cj 11168 659 -----gvdye
Cj C.I. 659 -----gvdye
Cj RM1221 659 -----gvdye
Hp 26695 699 elldqhnankgehhe
Hp J99 699 dlldqhnankgehhe

```

## FrdB

```

Ws DSM1740 1 ---mgrmltirvfkypqsavskphfkeykieeapsmtifivlnmirety
C. jejuni 11 1 ms---rkltikafkynplskiskphfvtyeleetpfmtvfvcltlirekm
Cj C.I. 1 ms---rkltikafkynplskiskphfvtyeleetpfmtvfvcltlirekm
Cj RM1221 1 ms---rkltikafkynplskiskphfvtyeleetpfmtvfvcltlirekm
Hp 26695 1 msdnertivrvlkdqpsavskphfkeyqlketpsmtlfialnlirehq
Hp J99 1 msdnertivrvlkdqpsavskphfkeyqlketpsmtlfialnlirehq

Ws DSM1740 48 dpdlndfdvcragicgscgmmingrpslactlttkdfedgvitllplpaf
C. jejuni 11 48 dadlsfdfvcragicgscammingvpklacktltkdypdgvielmpmpaf
Cj C.I. 48 dadlsfdfvcragicgscammingvpklacktltkdylgdgvielmpmpaf
Cj RM1221 48 dadlsfdfvcragicgscammingvpklacktltkdypdgvielmpmpaf
Hp 26695 51 dpdlsfdfvcragicgscammvngprlactltssfesgvitlmpmpsf
Hp J99 51 dpdlsfdfvcragicgscammvngprlactltssfengvitlmpmpsf

Ws DSM1740 98 klikdlsvdtgnwfnngsqrveswihaqkehdiskleeriepevaqevfe
C. jejuni 11 98 rhikdlsvntgewfedmckrveswhneketdiskleeriepevadetfe
Cj C.I. 98 rhikdlsvntgewfedtckrveswhneketdiskleeriepevadetfe
Cj RM1221 98 rhikdlsvntgewfedmckrveswhneketdiskleeriepevadetfe
Hp 26695 101 tlikdlsvntgdwflmtkrveswahskeevditrpekrvpepdeaqevfe
Hp J99 101 tlikdlsvntgdwfsdmtkrveswahskeevditkpekrvpepdeaqevfe

Ws DSM1740 148 ldraciegcciiaacgtkimredfvgaaglnrvvrfmidphdertdedyfe
C. jejuni 11 148 ldraciegicvascatklmrpnfiaatgllrtarylqdpdhhrsvedfye
Cj C.I. 148 ldraciegicvascatklmrpnfiaatgllrtarylqdpdhhrsvedfye
Cj RM1221 148 ldraciegicvascatklmrpnfiaatgllrtarylqdpdhhrsvedfye
Hp 26695 151 ldraciegcciiascgtklmrpnfigaagmnrarmrfmidshderndddfye
Hp J99 151 ldraciegcciiascgtklmrpnfigaagmnrarmrfmidshdersdddfye

```

Ws DSM1740	198	ligdddgvfgcmtllachdvcpknlplqskiy	lrrk	mvsvn---
C. jejuni 11	198	lvgdddgvfgcmsllacedncpkelplqskiy	mr-rql	vaqrnk
Cj C.I.	198	lvgdddgvfgcmsllacedncpkelplqskiy	mr-rql	vaqrnk
Cj RM1221	198	lvgdddgvfgcmsllacedncpkelplqskiy	mr-rql	vaqrnk
Hp 26695	201	lvgdddgvfgcmsliachdhtcpkelplqssiat	tlrnrmlk	vgksr
Hp J99	201	lvgdddgvfgcmsliachdhtcpkelplqssiat	tlrnrmlk	vgksr

## FrdC

Ws DSM1740	1	mtnesilesy	gvtp	perkksrmpakldww	qsatg	lflglflm	ighm	ffvst
FrdC11168	1	--mreliegy	lgksie	gkkskmpakldfi	qsasg	lflglflm	wvhl	mfvst
Cj C.I.	1	--mreliegy	lgksie	gkkskmpakldfi	qsasg	lflglflm	wvhl	mfvst
Cj RM1221	1	--mreliegy	lgksie	gkkskmpakldfi	qsasg	lflglflm	wvhl	mfvst
Hp 26695	1	mqqeeiiegy	ygaskgl	kksgiyakldfl	qsatg	lilalfmia	hmfl	vss
Hp J99	1	mqqeeiiegy	ygaskgl	kksgiyakldfl	qsatg	lilalfmia	hmfl	vss

Ws DSM1740	51	illgdnvmlwvtkkfeldfifeggkpi---	vvsflaafv	favfia	hafla
FrdC11168	145	ilvsedffnsvvhfle--lkfvynpvmsylts	sflaacvl	vvfv	halla
Cj C.I.	49	ilvsedffnsvvhfle--lkfvynpvmsylts	sflaacvl	vvfv	halla
Cj RM1221	49	ilvsedffnsvvhfle--lkfvynpvmsylts	sflaacvl	vvfv	halla
Hp 26695	51	ilisdeamykvakffegslflkagepa---	ivsvvaagi	ililva	hafla
Hp J99	51	ilisdeamykvakffegslflkagepa---	ivsvvaagi	ililva	hafla

Ws DSM1740	98	mrkfpinyrqyltfkthkdlmrhgdttlwwi	qamtg	famfflgs	vhl	ym
FrdC11168	289	mrkfpinyrqyqilrthskkmnhsdtslww	vqaftg	fmfflgs	ahlifi	
Cj C.I.	97	mrkfpinyrqyqilrthskkmnhsdtslww	vqaftg	fmfflgs	ahlifi	
Cj RM1221	97	mrkfpinyrqyqilrthskkmnhsdtslww	vqaftg	fmfflgs	ahlifi	
Hp 26695	98	lrkfpinyrqykvfkthkhlmkhgdtslw	fiqaltg	famfflas	ihl	fvm
Hp J99	98	lrkfpinyrqykvfkthkhlmkhgdtslw	fiqaltg	famfflas	ihl	fvm

Ws DSM1740	148	mtqpqtigpvs	ssfrmv	sewwply	lvll	favelhgs	vglyrl	avkwgwf
FrdC11168	439	vtnadkisgdm	sgdrvvsh	fmwlfyavll	vcvelhgs	siglyrl	cvkwgwf	
Cj C.I.	147	vtnadkisgdm	sgdrvvsh	fmwlfyavll	vcvelhgs	siglyrl	cvkwgwf	
Cj RM1221	147	vtnadkisgdm	sgdrvvsh	fmwlfyavll	vcvelhgs	siglyrl	cvkwgwf	
Hp 26695	148	ltepesigphg	ssyrfvt	qnflllyifll	favelhgs	siglyrl	ai	kwgwf
Hp J99	148	ltepesigphg	ssyrfvt	qnflllyifll	favelhgs	siglyrl	ai	kwgwf

Ws DSM1740	198	dgetpdktranlkkklktlmsaflivlgllt	fgayvkk	gleqtd	pnid--y			
FrdC11168	589	egknvkesrkkklktakwiisiffllvlgv	lslaafik	igyeny	qntqtta			
Cj C.I.	197	egknvkesrkkklktakwiisiffllvlgv	lslaafik	igyeny	qntqtta			
Cj RM1221	197	egknvkesrkkklktakwiisiffllvlgv	lslaafik	igyeny	qntqtta			
Hp 26695	198	----knvsiqglrk	kwamsvffivlg	lcty	gayikk	glenkeng	ikt	mq
Hp J99	198	----knvsiqglrk	kwamsvffivlg	lcty	gayikk	glenkdn	gikt	mq

Ws DSM1740	246	kyfdykrthhr---
FrdC11168	739	miknynganyeyti*
Cj C.I.	247	miknynganyeyti-
Cj RM1221	247	miknynganyeyti-
Hp 26695	244	eaieadgkfhke---
Hp J99	244	eaieadgkfhke---

## Appendix C

Validation of the solved *C. jejuni* QFR crystal structure performed with the program PROCHECK (by Roman A Laskowski, Malcolm W MacArthur, David K Smith, David T Jones, E Gail Hutchinson, A Louise Morris, David S Moss & Janet M Thornton): Ramachandran plots and residue properties of the three polipeptide chains FrdA (CjQFR2304 – ChainA), FrdB (Chain B), and FrdC (Chain C).



## Acknowledgements

I am extremely grateful to Dr. Roy Lancaster for the excellent supervision, valuable suggestions, and in particular for teaching me so much in these last years in the lab.

I am very thankful to Prof. Hartmut Michel for giving me the opportunity to work in his department, for the continuous stimulation in proceeding my work, and for providing excellent working facilities, equipments, and for funding the labeled 5-aminolevulinate.

I am grateful to Prof. Bernd Ludwig of the Johann Wolfgang Goethe University for his academic support and for taking the responsibility of external supervision.

I would also like to thank:

Dr. Fraser MacMillan and Dr. Klaus Zwicker for helping me to carry out numerous EPR experiments and for the fruitful discussions;

Prof. Klaus Fendler and particularly Christian Bamann for the friendship, the patience and the active collaboration on the electrometric and spectrophotometric measurement on proteoliposomes;

Dr. Stefan Bereswill for providing *C. jejuni* cells and *H. pylori* genomic DNA;

Dr. Ute Bahr and Prof. Michael Karas for carrying out the mass spectrometric measurements;

Dr. Alexander Haas for carrying out the heme titrations and FTIR spectroscopy measurements;

Ms. Nicole Hilgendorff for providing *W. succinogenes* wild type QFR samples;

Dr. Christos Tziatzios, for performing the ultracentrifugation experiments.

I am also thankful to Ms. Nicole Hilgendorff, Ms. Hanne Müller, and Ms. Conny Münke for excellent technical assistance.

I very much thank Mrs. Barbara Schiller and Dr. Lutz Kampmann for helping with computational hardware, software and for nice discussions.

I am very grateful to Dr. Alexander Haas, Paolo Lastrico, Dr. Fraser MacMillan, Dr. Stephen Marino, and Ulrike Wedemeyer for giving valuable suggestions about this thesis

manuscript; Dr. Alexander Haas and Dr. Tina Stumpp for the German version of the summary.

I thank all members of the Lancaster's group, in particular Hanno Juhnke for the nice 'spanish' atmosphere in the lab and Heiko Hiltcher for helping with the *C. jejuni* and *H. pylori* QFR mutant plasmids, and all the department of Molecular Membrane Biology for their interest and their support, in particular Sebastian Richers for helping with the lipid analysis by HPLC.

I am very grateful to Prof. Achim Kröger, Dr. Jörg Simon, Dr. Simone Biel, Dr. Oliver Klimmek, Mrs. Monica Sanger, Mr. Oliver Schurmann, Dr. Roland Gross, Mrs. Diana Schnella, Marco Polidori, Dr. René Pisa, and Dr. Vicky Dietrich who welcomed me in their department and introduced me into the "*Wolinella* world".

I especially would like to thank my parents, for giving me their unlimited and inestimable support, when we were near or far, at present and in the past, throughout all my life.

I wish to thank those members of my family who support me, and especially my grandparents, who are greatly taking care of me from up there.

Very special thanks go to Alexander Haas, Tomaso Frigato, Emiliano Feresin, Matteo Lamborghini, René and Nadine Staritzbichler, Fraser MacMillan, Stephen Marino, Antonio e Rita Zanfino, Francesco Acquaviva, and especially Nicole Hilgendorff for their moral support and truly friendship demonstrated inside and outside the institute.

I heartily thank my other "Italian-connection" friends: Paolo Lastrico, Antonio Caldarelli, Miro Venturi, Alessandra Ambruosi, Gianni Zifarelli, Luana Licata, and particularly Paolo's Kaliffa for making a great super-strong coffee; Giuseppe Montalto and all my friends from Corigliano for the company and cheerfulness inside the institute; Dr. Luigi Matteuzzi and his wife Hilde for taking care of me and for always being there.

A special thank goes to all my precious friends who are living in Italy, for being close to me and who are able to make me feel like I would still live there: Mirco Anselmi, Alessandro Brunori, Francesco Brunori, Simone Casavecchia, Paolo Cerioni, Angelo Ciavattini,



Francesca Giaccaglia and Lorenzo Coacci, Mirco Dangelantonio, Giada Farinelli, the “fratellini” Claudio e Graziano Marchegiani, Samuele Miglio, Marco Morroni, Eleonora Pesaresi, Francesco Pieroni, Maurizio Rossi, Mauro Vignoni, all my university mates, and so many others that would be impossible to list them all. They are the real “The Incredibles”!

This thesis is dedicated to my late friend Simone Concettoni, to whom a cursed fate has hampered finding solace in this life, but who left to us his splendid wealth and his contagious laugh that neither time nor space distances will ever wipe out.

This work was made possible thanks to the generous financial support of the International Max Planck Research School and the Max Planck Society.



# Curriculum Vitae



**Name:** Mauro Mileni

**Birth:** 17th December 1976,  
Corridonia (MC), Italy

**Address in Italy:** via Emilia, 9  
60015, Falconara Marittima (Ancona)  
E-mail: milenim@yahoo.it

## EDUCATION

**6<sup>th</sup> September 2001-1<sup>st</sup> August 2005:** **Doctoral thesis**

Title: "Biochemical, Structural and Functional Characterization of Diheme-Containing Quinol:Fumarate Reductases: the Role of Heme Propionates and the Enzymes from Pathogenic  $\epsilon$ -Proteobacteria".

Doctoral thesis accomplished under the supervision of P.D. Dr. C. Roy D. Lancaster, in the department of Molecular Membrane Biology (directed by Prof. Dr. Hartmut Michel), Max Planck Institute of Biophysics (Frankfurt am Main).

Supervision at the Johann Wolfgang Goethe University (Frankfurt am Main) by Prof. Dr. Bernd Ludwig, director of the Molecular Genetics department.

Degree received at the faculty of Chemical and Pharmaceutical Sciences, Johann Wolfgang Goethe University (Frankfurt am Main).

**October 1995- July 2001:**

**1st Degree and specialization**

Course of Biological Sciences (3 years) followed by a specialization in Biotechnology (2 years) at the Mathematical-Natural-Physical Sciences faculty, "Universita' degli Studi di Ancona" (now renamed "Università Politecnica delle Marche"), Ancona, Italy.

May 1998: Begin of the experimental work for the degree thesis within the Microbial Genetics Laboratory.

1998-1999: Part of the thesis was accomplished with biochemical and molecular biological experiments at the University of Wolverhampton, England.

July 2001: Graduation with the experimental degree thesis: "Comprehension of sodium chloride tolerance in yeast: a genetic approach". Grade of 110/110, summa cum laude.

**September 1990- June 1995:**

**High school**

I.T.I.S. "Vito Volterra" high school in Torrette (Ancona) with specialization in chemistry.

June 1995: Diploma of chemist.

**TEACHING**

- 2005: assistant for the BPC (Biophysical Chemistry) course, held by Dr. Roy Lancaster at the J.W. Goethe University
- 2004: assistant for the BX (Biological X-ray Crystallography) course, held by Dr. Roy Lancaster at the Max Planck Institute of Biophysics
- 2004: assistant for the BPC (Biophysical Chemistry) course, held by Dr. Roy Lancaster at the J.W. Goethe University
- 2000/2001: responsible instructor for "Laboratory of Microbial Genetics", a practical training in molecular biology and microbiology at the University of Ancona
- 2000/2001: assistant for the "Laboratory of Biology II", at the University of Ancona